INFORMATION TO USERS

This manuscript has been reproduced from the microfilm master. UMI films the text directly from the original or copy submitted. Thus, some thesis and dissertation copies are in typewriter face, while others may be from any type of computer printer.

The quality of this reproduction is dependent upon the quality of the copy submitted. Broken or indistinct print, colored or poor quality illustrations and photographs, print bleedthrough, substandard margins, and improper alignment can adversely affect reproduction.

In the unlikely event that the author did not send UMI a complete manuscript and there are missing pages, these will be noted. Also, if unauthorized copyright material had to be removed, a note will indicate the deletion.

Oversize materials (e.g., maps, drawings, charts) are reproduced by sectioning the original, beginning at the upper left-hand corner and continuing from left to right in equal sections with small overlaps. Each original is also photographed in one exposure and is included in reduced form at the back of the book.

Photographs included in the original manuscript have been reproduced xerographically in this copy. Higher quality 6" x 9" black and white photographic prints are available for any photographs or illustrations appearing in this copy for an additional charge. Contact UMI directly to order.

UMI

A Bell & Howell Information Company
300 North Zeeb Road, Ann Arbor MI 48106-1346 USA
313/761-4700 800/521-0600

Université d'Ottawa · University of Ottawa

Dedication

To Lea and Seeiso...thank you.

CONTENTS

Dedication		i
Contents		ii
Abstract		v
Acknowledgements		vii

CHAPTER 1 INTRODUCTION

1.1	Surface Chemistry and Spectroscopy	1
1.2	Infrared Properties of Oxides	3
	1.2.1 Silica	3
	1.2.2 Alumina	8
	1.2.3 Titania	13
	1.2.4 Zirconia	14
	1.2.5 Silica-Alumina	16
1.3	Thin Films	18
1.4	Spectroscopic Characterization of Solid Acid Catalysts	23
1.5	Acidic Solids	26
	References	29

CHAPTER 2 EXPERIMENTAL

2.1	Instrumentation	38
2.2	IR Cells	39
2.3	Vacuum Manifold	43
2.4	Sample Preparations	43
	References	45

CHAPTER 3 YTTRIA-SILICA-ALUMINA CATALYSTS

3.1	Introduction	46
3.2	Ammonia (NH_3) Adsorption	48
3.3	Pyridine (C_5H_5N) Adsorption	65
3.4	Acetonitrile-d_3 (CD_3CN) Adsorption	81
3.5	^{31}P NMR of Adsorbed Trimethylphosphine	93
	3.5.1 Introduction	93
	3.5.2 Experimental	94

	3.5.3 Results	94
3.6	Discussion	99
	3.6.1 Brønsted Acidity	99
	3.6.2 Lewis Acidity	100
	References	102

CHAPTER 4 FLUORIDED ALUMINA CATALYSTS

4.1	Introduction	106
4.2	Acetonitrile-d_3 (CD_3CN) Adsorption	107
4.3	Ammonia (NH_3) Adsorption	113
4.4	Discussion	116
	References	118

CHAPTER 5 CATALYST PERFORMANCE

5.1	Introduction	120
5.2	Isomerization of 2-Methyl-2-Pentene (2M2P)	121
5.3	Experimental	123
	5.3.1 Flow System	123
	5.3.2 Gas Chromatograph	126
5.4	Selected Results	131
5.5	Discussion	132
	References	134

CHAPTER 6 THIN FILMS

6.1	Introduction	136
6.2	Low Wavenumber OH Modes	142
6.3	Hexamethyldisilazane (HMDS) Adsorption	145
6.4	Trimethylgallium (TMG) Adsorption	149
6.5	Titanium Tetrachloride ($TiCl_4$) Adsorption	154
6.6	Other Probes	164
	6.6.1 Vanadyl Trichloride ($VOCl_3$)	164
	6.6.2 Boron Trichloride (BCl_3)	167
	6.6.3 Germanium Tetrachloride ($GeCl_4$)	170
6.7	Discussion	170
	6.7.1 Methyl Containing HS Agents	170
	6.7.2 Chlorine Containing HS Agents	171
	6.7.3 Spectral Artefacts	174

References 178

GENERAL CONCLUSIONS 181

APPENDICES
I. List of Hexene Isomers 186
II. $TiCl_x$ Stretching Mode Calculations 187

ABSTRACT

This thesis focuses on the characterization of various oxide based materials, some of which are potential industrial catalysts. The major instrumental technique used in this work is infrared (IR) spectroscopy. To a lesser extent nuclear magnetic resonance (NMR) spectroscopy was used. Also, attempts were made to correlate spectroscopic results with those from a standard test reaction which would allow us to rank moderate strength catalysts, based on their acidity. This test involved the isomerization of 2-methyl-2-pentene (2M2P). The isomerization of 2M2P is a particularly useful reaction since the olefin can convert into a large number of products, the relative rates of formation of which reflect the acid strength of the catalyst.

Halide containing solid acids are common catalysts, however the availability and use of halogen containing treatment gases in their preparation has come under increasing environmental scrutiny. As a result there is interest in developing alternative environmentally compatible halide free catalysts as replacements. Silica-aluminas are too acidic for this purpose. However, by adding weakly basic rare earth oxides to silica-alumina catalysts their overall acidity can be lowered to degrees comparable to halide containing acids. Yttria behaves in a manner similar to the rare earth oxides and was used for this purpose. Olefin model reactions, in particular the isomerization of 2M2P, show that the acid strength of silica-aluminas can be adjusted to that of halided, chlorided or fluorided, aluminas with the addition of rare earth oxides in the 4-20 wt. % range. In this work changes in the surface acidity of 4, 8, 12 and 16 wt. % Y_2O_3 doped SiO_2-Al_2O_3 catalysts were investigated as well as those of fluorided aluminas using probe molecules.

IR spectroscopy has been used for many years to characterize the acidity of oxides. This technique makes use of probe molecules. These molecules are expected to interact, *i.e.* H-bond, physically adsorb or chemically adsorb, with surface active sites. These active sites,

commonly referred to as acid sites, contribute to acid catalysis in a host of reactions. The probe molecules which will be discussed in this thesis vary in size and basicity and include: ammonia (NH_3), pyridine (C_5H_5N) and deuterated acetonitrile (CD_3CN). Absorption coefficients of probe molecules at gas-solid interfaces are generally not known hence absolute numbers for acid sites cannot be obtained using IR spectroscopy. The advantage of NMR over IR spectroscopy is that in the former the signal intensity is directly proportional to the number of probe nuclei present at a particular acid site. Trimethylphosphine, $(CH_3)_3P$, was used as an NMR probe in order to obtain the concentrations of acid sites.

Thin film (TF) experiments were performed on the pure oxides of silica, alumina, titania and zirconia. By performing TF experiments the samples used weighed about 0.1-0.5 mg/cm^2 as opposed to the 2.5-10 mg/cm^2 common for self supporting discs. This allowed us to probe the far IR region, down to 200 cm^{-1}, for the first time, as there was less interference from bulk modes.

ACKNOWLEDGEMENTS

There are several people I would like to thank. Firstly, my supervisor, Professor Barry A. Morrow. Thank you for your guidance, patience and willingness to share your expertise throughout the course of my graduate work.

To my *mentors*, Stephen Lang and Yaohua Wang. Thanks for showing me the ropes and for the pleasant company over the years. I would also like to thank my present co-worker, Zhongyuan Dang, for all the fruitful discussions we have had with respect to various aspects of this thesis during its write up.

Thank you Dr. Ian Gay for the NMR results, and Dr. Yoshimitsu Amenomiya for sharing your time and knowledge in helping to develop our 2M2P probe test.

To Lise Maisonneuve and the entire Chemistry Department support staff. Your work does not go unnoticed or unappreciated. Thank you.

To my colleagues, Sham Syal, Steve V. De Cliff and Diann Denning, thanks for the help and good company.

Lastly, I would like to thank my family: Jonathan, Ntseke, Leabiloe, mangoane Mateboho, mangoane Lipalesa, as well as my parents, for your unselfish and unwavering support which made this work possible.

CHAPTER 1

INTRODUCTION

1.1 SURFACE CHEMISTRY AND SPECTROSCOPY

Surface science has proven to be an extremely important field of study as it plays a major role in a host of processes which include catalysis, chromatography and corrosion to name but a few [1-6]. All of these processes depend on the nature of the interactions which occur when sorbate species come into contact with solid surfaces. The primary goal of surface chemistry is to investigate these interactions which occur on specific sites, commonly referred to as the active sites, of solid surfaces. The most important active sites on oxides are generally acidic sites and are responsible for acid catalysis, *e.g.* in hydrocarbon cracking, isomerization or polymerization. With the aid of spectroscopy one can probe the surface of solids and gain information on the nature of the active sites, *i.e.* their chemical properties and concentrations.

At present there is a plethora of techniques to choose from to *characterize* solid surfaces [1-14]. Infrared (IR) absorption spectroscopy is undoubtedly the single most useful technique for this task [10]. The technique is of great importance in the determination of molecular structure, and its extension to surface chemistry has lead to the direct observation of interactions and perturbations that occur at the surface of a catalyst during adsorption; this in turn can provide information on the composition and structure of surface compounds as well as the type of bonding involved between adsorbate molecules and the surface, thus contributing to a better understanding of catalysis [11]. IR spectroscopy was among the first instrumental techniques to be applied to the characterization of catalysts in the 1950s [12] and over the past three decades it has developed into the premier physical method in catalysis

research [13]. Unlike some other spectroscopic techniques which, for example, involve electron or ion bombardment, IR spectroscopy is non-destructive, hence it will not cause changes in the surface chemistry of the system under investigation, and it works at all pressures.

IR spectra arise from transitions between vibrational energy levels with corresponding absorption or emission of energy at discrete frequencies. These correspond to specific normal modes of vibration of molecules or surface groups which undergo a change in dipole moment during vibration. Sometimes, however, due to surface interactions, band frequencies alone are not sufficient to permit unambiguous assignments to specific adsorbed species. In these cases other approaches may have to be followed, *e.g.* isotope exchange experiments [15].

The major purpose of this thesis was to apply IR spectroscopy to some problems in surface chemistry. The research performed revolved around the use of oxide based materials which are relevant to catalysis. The thesis is divided into four major parts:

Chapter 3 involves the study of yttria doped silica-alumina catalysts. These are industrially important isomerization catalysts. By varying the yttria loading on these catalysts, one can vary their surface acidity and hence their catalytic properties.

Chapter 4 involves the study of fluorided-alumina catalysts. In this case the temperature of calcination was varied; consequently this too can lead to a change in surface acidity and catalytic properties of this material.

Chapter 5 discusses a method in which catalytic activity can be quantified. By choosing a suitable test reaction one can analyze the products formed; a scale of catalytic acidity can be devised based upon the results. Different reactions require catalysts with different surface acidity characteristics, hence this scale has been shown to be of great significance. The particular test reaction chosen was that of the isomerization of 2-methyl-2-pentene.

Chapter 6 deals with an IR method (thin film technique) for studying oxides in the low wavenumber spectral region (1000-200 cm^{-1}). This technique has the advantage of allowing one to investigate the far infrared region; this was not possible using the more common self supporting disc approach, as was used in this work described in Chapters 3 and 4. From a pure research perspective this chapter tries to tackle some of the difficulties involved in attempting to characterize an oxide surface.

The details of the work required are given as needed in the above mentioned chapters. However, the remainder of Chapter 1 gives the general background of the main features of the thesis.

1.2 INFRARED PROPERTIES OF OXIDES

A comprehensive review of the infrared spectra of various oxides already exists [16] as do several texts [17-21]. Hence the purpose of this section is not to provide an extensive account of a similar nature, but rather to introduce and highlight the main spectral features of the oxides used in this work, in particular those of silica (SiO_2) and alumina (Al_2O_3), and the mixed oxide silica-alumina (SiO_2-Al_2O_3). A brief discussion on titania (TiO_2) and zirconia (ZrO_2), which were used in thin film work (Chapter 6), will also be given in this section.

1.2.1 Silica

High surface area silica is amorphous and can be manufactured in one of several ways [16,20,21]. The type of silica used in this work was *pyrogenic* or *fumed* silica (sold under the trade names *Cabosil* or *Aerosil*). This is produced by the flame hydrolysis of tetrachlorosilane, $SiCl_4$, reaction (1.1); hydrogen and oxygen combine to form water prior to reacting with $SiCl_4$

at 1000-1100°C which results in the formation of minute finely divided non-porous silica particles 5-40 nm in diameter, with surface areas ranging from 50-400 m^2/g.

$$SiCl_4 + 2H_2 + O_2 \rightarrow SiO_2 + 4HCl \qquad (1.1)$$

Other forms of SiO_2 include precipitated SiO_2 and silica gels which are synthesized in solution via the reaction of an alkali metasilicate with an acid [16,20,21]. *Cabosil M-5* was used in this work and was obtained from Cabot Inc. and had a B.E.T. surface area of 200 m^2/g.

The infrared spectra of *Cabosil M-5* self supporting discs (10 mg/cm^2) which have been evacuated at room temperature (RT), 450 and 900°C for an hour are shown in Figure 1.1. The sharp peak at 3747 cm^{-1} is due to isolated non-interacting silanol groups. The slight tailing of this peak to lower wavenumbers is due to residual H-bonded silanol pairs and these diminished as the temperature of activation was increased. For the RT activated sample, centered at about 3530 cm^{-1} are bands due to H-bonded pairs or chains of silanol groups [17,20,21]. At about 3720 cm^{-1} is a small peak which appears as a shoulder on the 3747 cm^{-1} peak and this is due to the free SiOH of an H-bonded pair or chain [22-24]. Lastly the small peak at about 3660 cm^{-1} are silanols which are perturbed due to interparticle contact [19] and become more inaccessible to probe molecules as the size of the probe increases [25-27]. These silanols may be present in bulk silica or regions where silica particles are in close contact and their numbers increase as the pressure used to prepare the self supporting discs increases [26,29]. They are fairly unreactive, *e.g.* they do not completely dehydroxylate at 450°C and do not react with hydrogen sequestering (HS) reagents such as $Al(CH_3)_3$ or $TiCl_4$ [30]. HS reagents react with surface hydroxyl groups to cleave the O-H bond.

The small peaks in the 2000-1600 cm^{-1} range correspond to various overtone and combination modes belonging to the bulk phase of SiO_2. Hence they are not surface modes and do not undergo any interaction with adsorbed species. Silica discs are opaque in the ranges: 1300-1000 cm^{-1}, 850-750 cm^{-1} and 600-380 cm^{-1}; these regions of total absorbance, *i.e.*

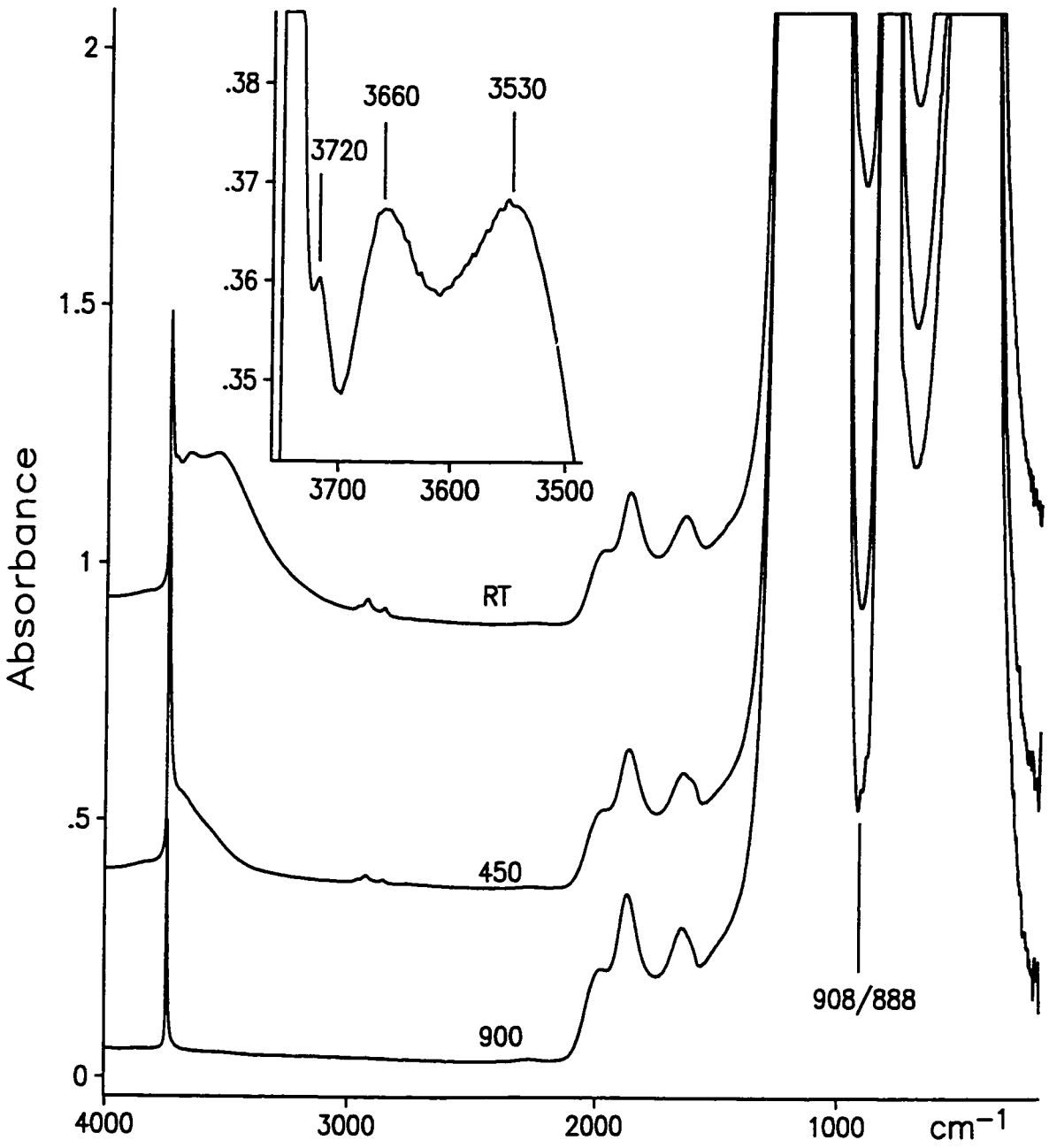

Figure 1.1 Infrared spectra for room temperature (RT), 450 and 900°C activated silica self supporting discs (10 mg/cm^2); 908 and 888 cm^{-1} peaks in 900°C SiO_2 are also noted. The inset shows an expanded view of the OH region of RT activated silica.

absorbance greater than 2, are due to SiOSi bulk modes [16].

The small peaks at about 2930 and 2868 cm^{-1} can be attributed to adsorbed hydrocarbons.

As can be seen from Figure 1.1, increasing the temperature of activation from RT to 450°C eliminates most of the H-bonding interactions and the peak intensity of the 3747 cm^{-1} band increases. This increase in intensity during dehydroxylation is probably due to the condensation of vicinal silanols in a chain containing an odd number of silanols:

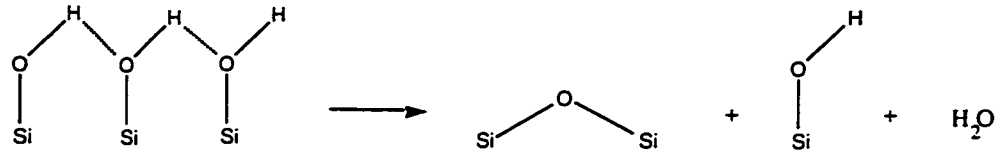

(1.2)

Upon going from 450 to 900°C activation all H-bonded and perturbed species are eliminated and the isolated non-interacting silanol peak decreases in intensity and becomes more symmetric. The weak peaks at about 2900 cm^{-1} are also eliminated and new bands at 908 and 888 cm^{-1} appear in one of the window regions of the spectrum which are assigned to Lewis acid surface defects [22,28,31,32]. These are highly strained four membered siloxane rings [33-37]; the four atom rings, cyclodisiloxanes or edge shared tetrahedral surface defects, are due to the elimination of water from a pair of vicinal hydroxyls and is a reversible reaction [34,36]. Strained surface defects in SiO_2 are more reactive than unstrained SiO_2 because:

1. They act as strong acid-base sites which can readily adsorb probe molecules;
2. The Si-O bond in strained defects is more susceptible to reactions with adsorbed species which result in bond rupture.

During adsorption, the spectral features associated with strained defects disappear whilst new IR bands appear thus suggesting that dissociative chemisorption takes place. The adsorbates (probe molecules) which have been used in various studies include: boron halides, water and ammonia to name but a few [22,28,31,33,36,37].

Some of the silicon based structures which may be present of the surface of silica are depicted in Figure 1.2.

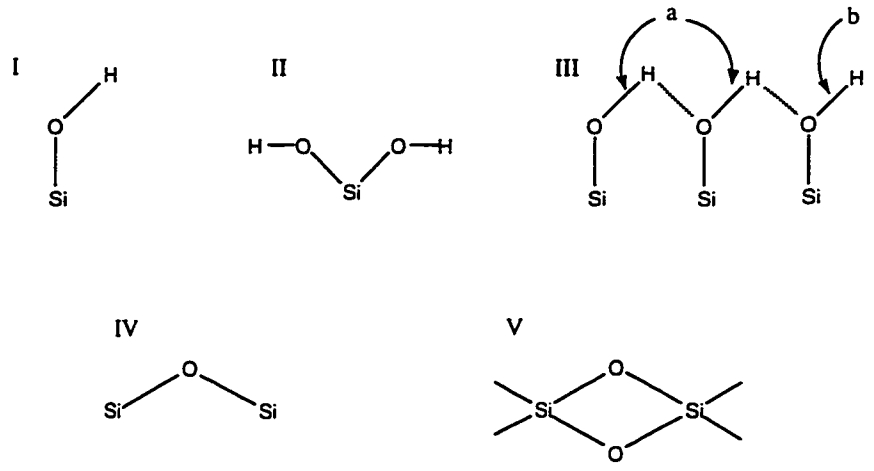

Figure 1.2 Possible silanol and siloxane configurations for surface silica:

I	Single isolated non-interacting silanols, ≈ 3747 cm^{-1};
II	Geminal silanols, ≈ 3747 cm^{-1};
III_a	Vicinal H-bonded pairs or chains of silanol groups, 3600-3400 cm^{-1};
III_b	Terminal free silanol of an H-bonded pair or chain, 3720-3715 cm^{-1};
IV	Surface siloxane bridge sites, < 1300 cm^{-1};
V	Strained four membered siloxane rings, 908 and 888 cm^{-1}.

It is important to note that Figure 1.2 does not account for all possible types of silanol structures, however it does highlight those which are most common. Other structures are possible since:

1. The number of silanols in a chain or ring may vary;
2. Different orientations of silanols may arise due to the irregular surface of SiO_2;
3. Both single and geminal silanols may partake in H-bonding [20].

1.2.2 Alumina

Alumina (Al_2O_3) exists in several forms all of which differ in their crystalline structure. It is the most widely used catalyst support and takes part in numerous processes such as hydrotreatment and catalytic reforming [38,39]. What makes alumina so attractive is that it is structurally stable, it can be prepared in a wide variety of ways having different pore sizes or surface areas and, most importantly, it is inexpensive [16,21,38-40]. Aluminas are manufactured via the thermal dehydration of various aluminium hydroxides: the trihydroxides, $Al(OH)_3$, of which Gibbsite and Bayerite are the common crystalline forms; and the oxyhydroxides, AlO(OH): (crystalline) boehmite, pseudo (or gelatinous) boehmite and diaspore which differ in their crystalline arrangement. Equations 1.3-1.7 show the relationship between the various forms of alumina and the temperatures (in degrees Celsius) necessary to cause a phase transition:

$$\text{pseudo Boehmite} \xrightarrow{250} \gamma\text{-}Al_2O_3 \tag{1.3}$$

$$\text{Gibbsite} \xrightarrow{300} \chi\text{-}Al_2O_3 \xrightarrow{800} \kappa\text{-}Al_2O_3 \xrightarrow{1150} \alpha\text{-}Al_2O_3 \tag{1.4}$$

$\downarrow 180$

$$\text{Boehmite} \xrightarrow{475} \gamma\text{-}Al_2O_3 \xrightarrow{790} \delta\text{-}Al_2O_3 \xrightarrow{1150} \theta + \alpha\text{-}Al_2O_3 \xrightarrow{1200} \alpha\text{-}Al_2O_3 \tag{1.5}$$

$\uparrow 180$

$$\text{Bayerite} \xrightarrow{250} \eta\text{-}Al_2O_3 \xrightarrow{850} \theta\text{-}Al_2O_3 \xrightarrow{1150} \alpha\text{-}Al_2O_3 \qquad (1.6)$$

$$\text{Diaspore} \xrightarrow{500} \alpha\text{-}Al_2O_3 \qquad (1.7)$$

The transitional aluminas, in particular the η and γ phases are the most common catalyst supports [21,38,39,41-44]. γ-Al_2O_3 has a high surface area and is relatively stable at the temperatures at which catalytic reactions take place; η-Al_2O_3 is more acidic than γ-Al_2O_3, however doping γ-Al_2O_3 with halides leads to an increase in acidity [19,38]. The transition aluminas in equation 1.4 (χ and κ-Al_2O_3) are amorphous and hexagonal type aluminas and are less common than the crystalline cubic transition phase aluminas of equations 1.5 and 1.6 which all have defect spinel structures. Spinels are mixed oxides of Al^{3+} cations with divalent cations which have the general formula MAl_2O_4. The M^{2+} cations occupy 1/8 of tetrahedral sites in the cubic closed packing array of oxide ions, whereas Al^{3+} occupy 1/2 of the octahedral sites, hence $M_8^{IV}[Al_{16}^{VI}O_{32}]$ per unit cell [50]. Consequently the differences between the *low temperature* transition phases (γ and η-Al_2O_3) and the *high temperature* transition phases (δ and θ-Al_2O_3) are relatively small.

Phase transformations are a continuous process and it is very difficult to have a pure phase, especially in the case of powders; as a result a mixture of phases is usually present [41,51]. *Aluminoxid C* alumina from Degussa A.G. Frankfurt with a surface area of 105 m^2/g was used in this work. Degussa's alumina is often a mixture of γ and δ-phase, however in this case X-ray diffraction (XRD) showed that the δ-phase was predominant.

The infrared spectrum of a self supporting disc (10 mg/cm^2) of Degussa alumina at RT is shown in Figure 1.3. There is a large asymmetric peak at about 3500 cm^{-1} in the OH region which is due to H-bonded AlOH groups and coordinated molecular water; degassing at 450°C

eliminated these species whilst 900°C degassing eliminated most of the AlOH species. Alumina discs are totally absorbing between 1000 and 300 cm^{-1} and the small peaks in the range 1400-1600 cm^{-1} are due to surface carbonate impurities which can be removed by calcining the sample in excess oxygen (50 Torr) at 450°C for an hour.

The OH region (for the 450°C sample) exhibits three peaks at 3790, 3675 and 3725 cm^{-1} with a small shoulder at 3773 cm^{-1}. According to Knözinger and Ratnasamy [41] there is a maximum of five different OH configurations possible which can occur on the surface of transition aluminas (Figure 1.4). The occurrence and concentration of these bands, however, depends of the relative contributions of the different crystal faces. The terminations of aluminas crystallites occurs along a limited number of low index crystal planes: (111), (110) and (100). All of the possible OH configurations are expected on (111) whereas only I_a, I_b and II_b are found on (110) faces and the (100) face consists of I_b type OH groups. The OH groups possess slightly different net electrical charges which result in varying properties.

Table 1.1 Hydroxyl Assignments of Degussa Al_2O_3*.

OH Type	# Al_o	# Al_t	wavenumber OH/cm^{-1}	net charge (Q) at OH
I_a	0	1	3773	-0.25
I_b	1	0	3790	-0.5
II_a	1	1	3725	0.25
II_b	2	0	-	0
III	3	0	3675	0.5

*where the subscripts "o" and "t" refer to octahedral and tetrahedral.

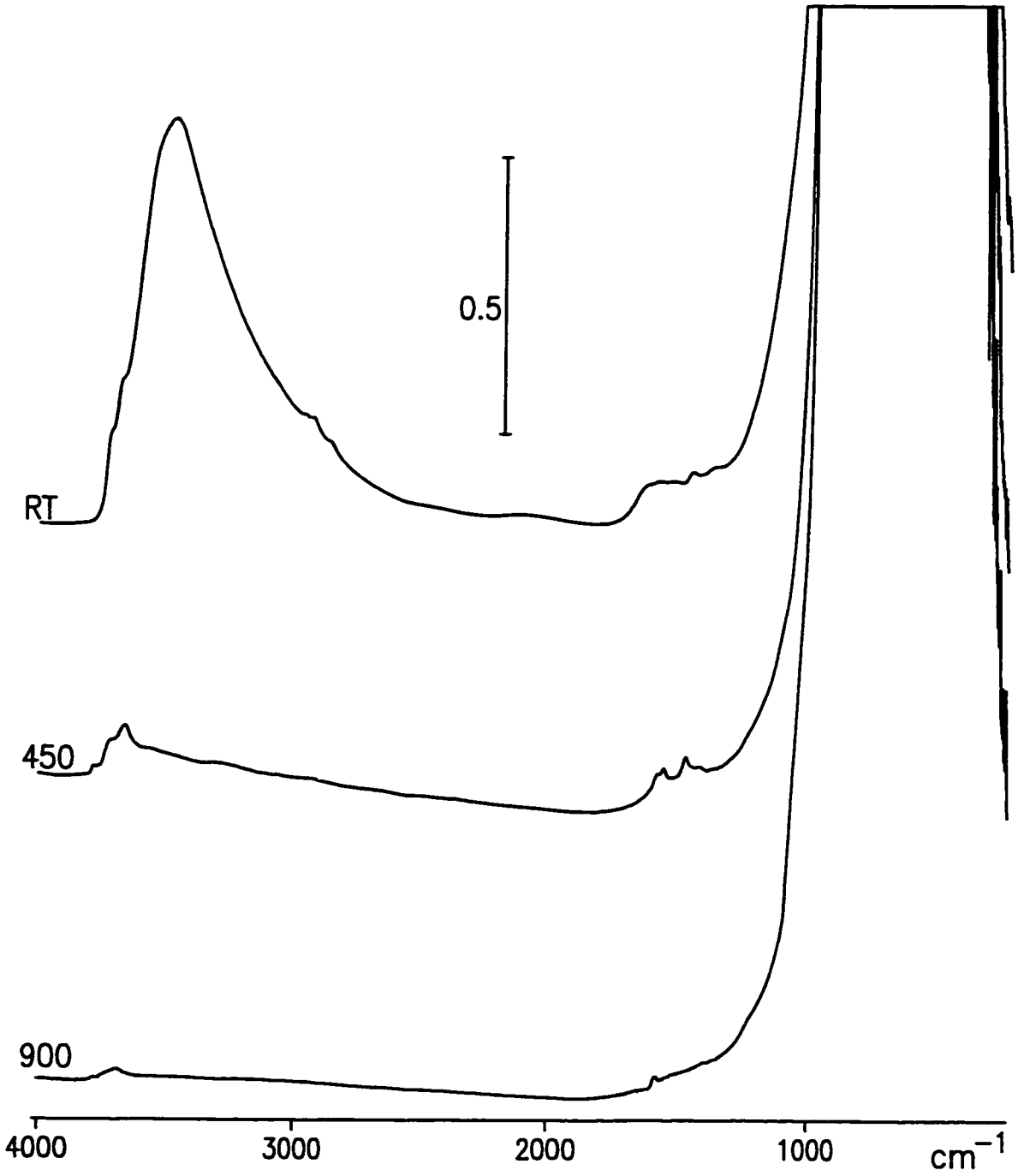

Figure 1.3 Infrared spectra of room temperature (RT), 450 and 900°C activated alumina self supporting disc (10 mg/cm^2).

Species II_b which would normally fall in the range 3740-3745 cm^{-1} [16,19] was not present on this particular sample. The five hydroxyl species which may be present on the surface of alumina are depicted in Figure 1.4.

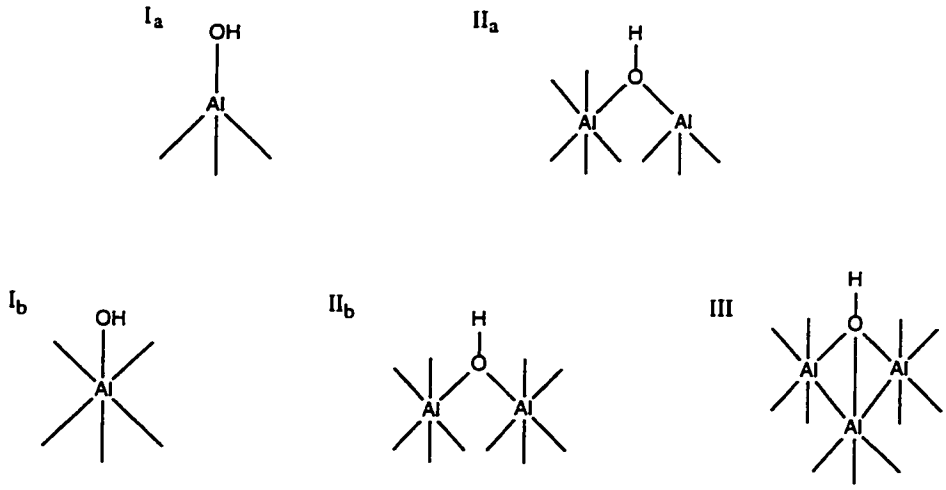

Figure 1.4 The five possible OH configurations for surface transition aluminas.

As the net charge of the hydroxyl group decreases their basicity increases; and protonic acidity decreases making it more labile and easier to remove. Brønsted acidity, thus decreases in the order: $III > II_a > II_b > I_a > I_b$. The "a" and "b" subscripts refer to the OH layer on top of the A and B surface layers parallel to the (111) plane of the spinel lattice [41].

The net charge, Q, at OH is the sum of the negative charge of an anion and of the strengths of the electrostatic bonds. The latter term is provided by Pauling's *electrostatic valence rule* [43] and according to this rule the net charge in a stable ionic structure would be equal or nearly equal to zero. The strength of an electrostatic bond, s, is given by:

$$s = z/\nu \qquad (1.8)$$

where z = electric charge of a cation

ν = coordination number of the cation

In the case of Al_2O_3, Al^{3+} cations exist in octahedral, Al_o, and tetrahedral, Al_t, sites at the centers of polyhedra of which an oxygen anion forms a corner. The net charge is thus given as:

$$\mathbf{Q = \zeta + q} \tag{1.9}$$

where ζ = sum of cation electrostatic bond strength

q = negative charge of anion/surface ligand

Hence

$$\mathbf{Q = 1/2\ Al_o + 3/4\ Al_t - 1} \tag{1.10}$$

1.2.3 Titania

Titania exists in three crystalline forms: anatase, rutile and brookite, of which the first two are the most common. Both anatase and rutile have Ti^{4+} ions octahedrally coordinated by oxygen O^{2-} ions, each of which have three Ti^{4+} neighbours. The differences in the two structures lies in the different packing of TiO_6 octahedral structural units [44]. The type of TiO_2 produced depends on the preparation; typically, TiO_2 used in catalysis can be prepared via the hydrolysis of titanium salts such as $TiOSO_4$ or $TiCl_4$ in acid solution or via the flame hydrolysis of $TiCl_4$ [16,21].

The TiO_2 used in this work was *Titania P 25* from Degussa A.G. Frankfurt which was produced via the flame hydrolysis of $TiCl_4$; it contained 15% rutile and 85% anatase, and had a B.E.T. surface area of 55 m^2/g. Anatase (which can be converted to rutile by heating above 700°C) is more stable at low temperatures and has a higher surface area than rutile [16,21].

Hence from a catalysis perspective it is a much better phase. Busca *et al.* have performed a considerable amount of work involving the IR characterization of TiO_2 surfaces to which the reader is referred [45]; also an account of the IR spectra of surface hydroxyl groups was presented by Tsyganenko and Filiminov [46] and an excellent review on the surface of TiO_2 has been provided by Parfitt [47]. The oxide is characterized by bands in the OH spectral region. Figure 1.5 shows the IR spectra of 450°C activated TiO_2 (and ZrO_2) self supporting discs (10 mg/cm^2); the titania was further calcined in excess oxygen at 500°C for an hour. In the case of TiO_2 the number and frequencies of OH bands depend on several factors such as phase, extent of dehydroxylation and the presence of impurities.

1.2.4 Zirconia

Zirconia exists in three polymorphic phases: monoclinic (at low temperatures), tetragonal (stable between 1100-2400°C) and cubic (at high temperatures) [48]. Also, at high pressures, a fourth phase, orthorhombic, has been identified [49].

The ZrO_2 used in this work was *Experimental Product Zirconium Dioxide* from Degussa A.G. Frankfurt prepared by the flame hydrolysis of $ZrCl_4$. This contained an equal mixture of monoclinic and tetragonal phases and had a B.E.T. surface area of 45 m^2/g.

For a discussion on the IR surface properties of this oxide the reader is referred to the work of Jacob *et al.* [48] as well as the work of Tanabe on the surface and catalytic properties of ZrO_2 [52]. Briefly, the IR spectrum of ZrO_2 is characterized by two sharp bands in the OH stretching region (Figure 1.5); the higher frequency band, 3781 cm^{-1}, is assigned to singly coordinated OH whilst the lower frequency band, 3671 cm^{-1}, is assigned to multiple coordinated OH groups [16,46,48].

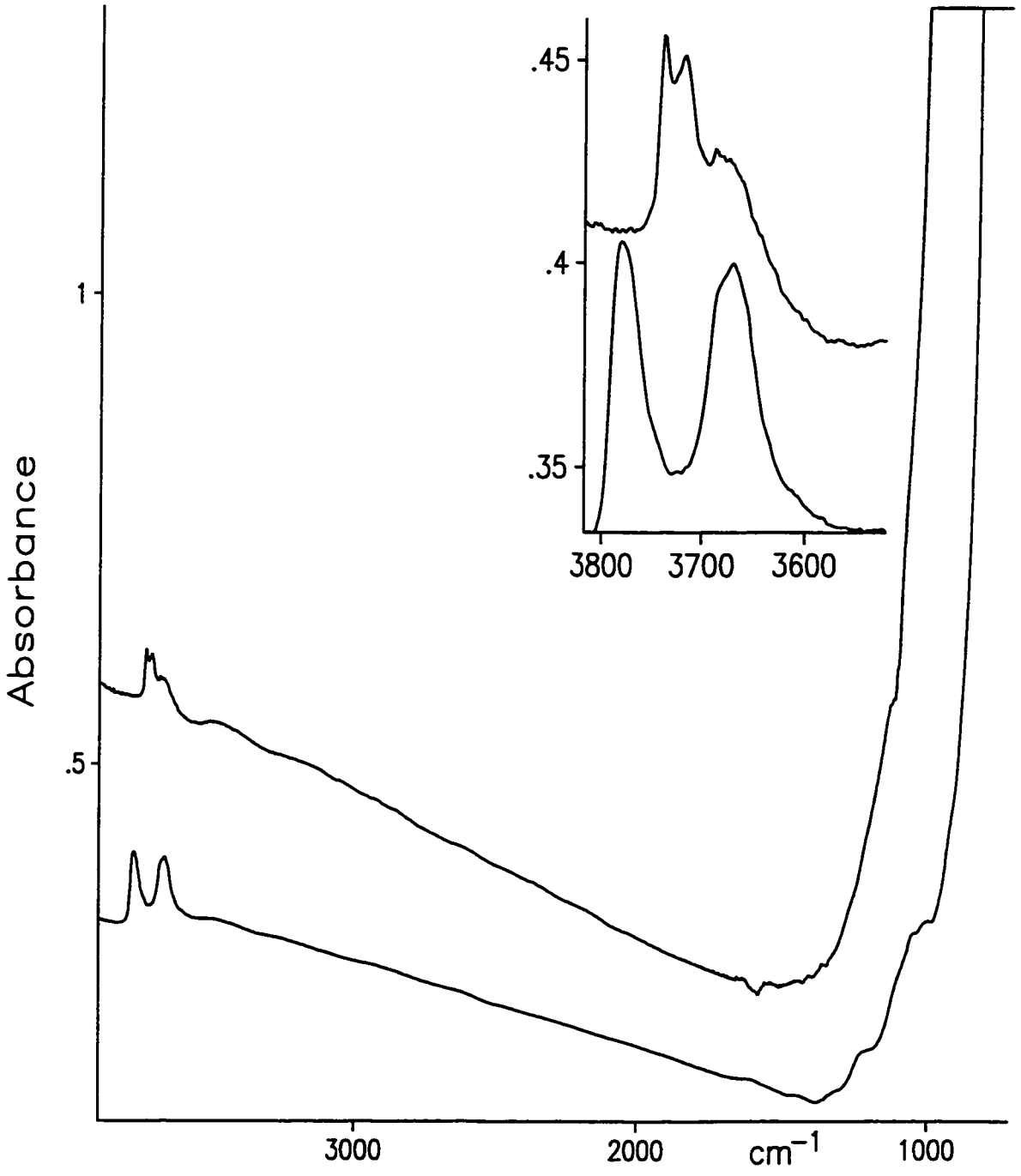

Figure 1.5 Infrared spectra of 450°C activated titania (top) and zirconia (bottom) self supporting discs (10 mg/cm^2).

1.2.5 Silica-Alumina

Silica-alumina (SA) is prepared by the coprecipitation of silicates and aluminum salts which eventually yields a homogeneous mixed oxide gel. After drying, an amorphous mixed oxide of relatively high surface area can be obtained [18,19,53]. The IR spectrum (Figure 1.6) is virtually identical to that of silica for the same temperature of activation; the principal features are a sharp SiOH vibration at 3747 cm^{-1} due to isolated single or geminal OH groups, and for lower temperatures of activation, there is a broad feature near 3550 cm^{-1} due to hydrogen bonded OH groups.

As catalytic materials, the optimum percentage of Al_2O_3 is usually in the 12 to 25% range because such materials have an optimum concentration of Brønsted and Lewis acid sites for a variety of catalytic processes [18]. Insertion of trivalent aluminum into the silica lattice results in tetravalent aluminum having a net negative charge. This is counterbalanced by protonic centres which give rise to the Brønsted acidity. Little is known about the structure of the Lewis acid sites, although these are presumably associated with electron deficient Al sites [54]. The number of Lewis sites increases steadily with percent Al_2O_3 to about 75% and thereafter decreases [53]. The stronger Lewis sites are associated with lower percentages of Al_2O_3 and an additional weak Lewis acid site is created when the percent Al_2O_3 exceeds about 50%. The number of Brønsted sites peaks at about 25-35%, but the greater activity for acid catalysis seems, none the less, to be associated with SA's in the 12 to 25% Al_2O_3 range. Far less research has been carried out on SA than on SiO_2 or on Al_2O_3 although there has been a revival of interest in studying SA catalysts which are prepared by chemical vapor deposition of volatile silicon based materials on to Al_2O_3 with the aim of carefully controlling the number of Lewis and Brønsted sites [55-58].

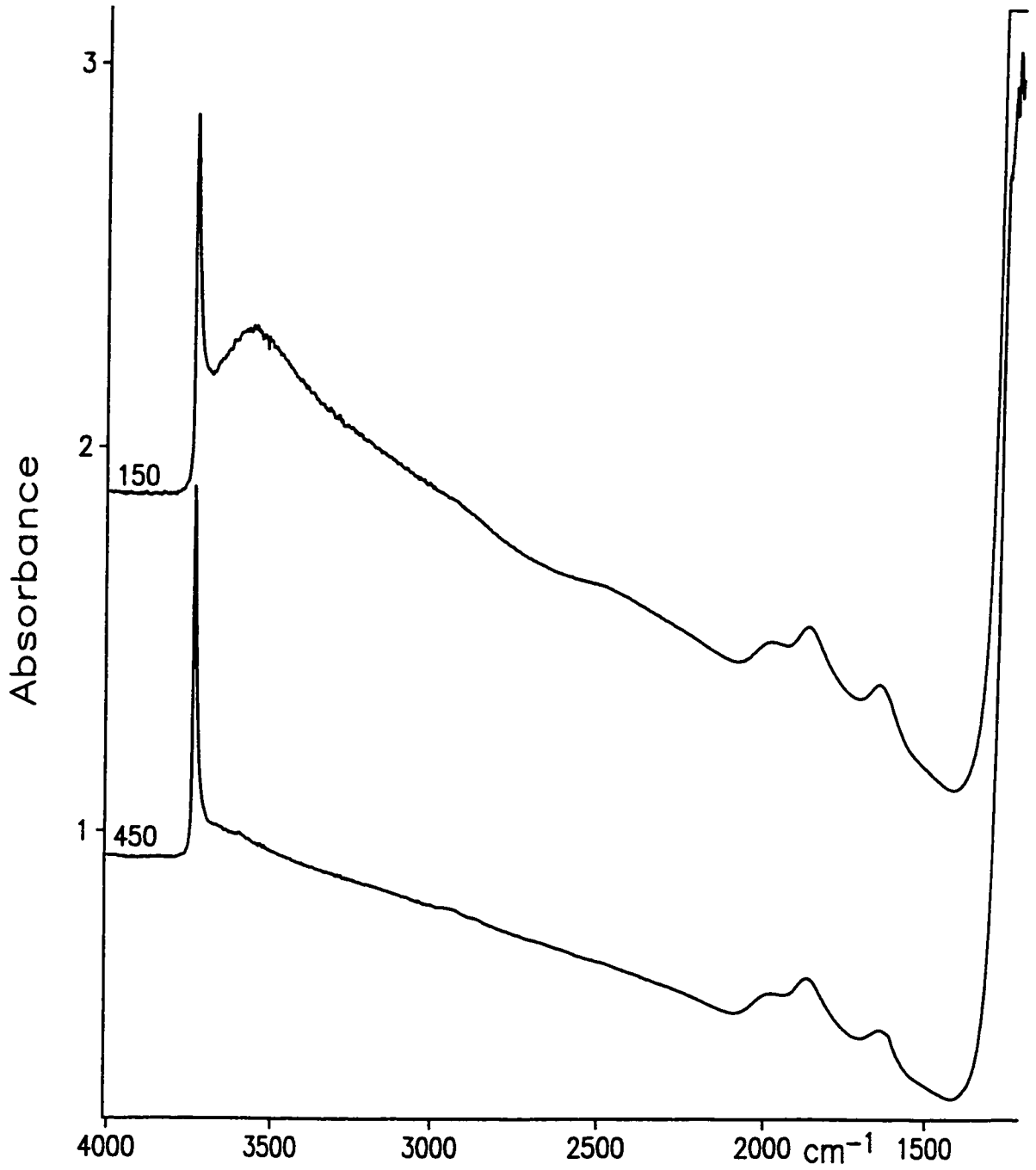

Figure 1.6 Infrared spectra of 150 and 450°C activated silica-alumina self supporting disc (10 mg/cm^2).

1.3 THIN FILMS

Self supporting discs of the oxides discussed in section 1.2 are opaque in the low wavenumber region due to the absorption of IR radiation by oxide lattice modes. Discs of silica are opaque between 1300-1000 cm^{-1} and from 850-750 cm^{-1}, while discs of Al_2O_3, TiO_2 and ZrO_2 are completely opaque below 1000, 900 and 800 cm^{-1} respectively. The thin film (TF) technique, which was developed in this laboratory [59], is an alternative method for obtaining infrared spectra of adsorbed species in the low wavenumber spectral region. In this method, the amount of oxide is greatly reduced to about 0.1-0.5 mg/cm^2 from 2.5-10 mg/cm^2 generally required for a self supporting disc. This is done by dispersing a thin layer of the oxide on an optically transparent substrate (see below). Typical thin film background spectra for all of the oxides are shown in Figures 1.7 and 1.8 for room temperature activation. This is the first time that thin film spectra of Al_2O_3, TiO_2 and ZrO_2 have been published. As can be seen from these spectra, the lattice modes of vibration are not totally absorbing and the adsorption bands of adsorbed species in this spectral region can now be followed. The spectra of adsorbed species in these regions are obtained by subtracting the background from the spectrum obtained after adsorption. It is essential that the entire experiment be carried out *in situ*, *i.e.* without moving the sample out of the infrared beam in order to avoid spectral artefacts due to inhomogeneities in film thickness when the subtraction is carried out.

In the standard IR experiments with oxides, in which the far IR region is not investigated, self supporting discs are preferable over thin films. The transmission of IR radiation in low frequency work is greatly increased in thin films at the expense of a reduction in the number of surface species being sampled. In view of the high residual background absorption for thin films below about 1000 cm^{-1}, the S/N ratio is, none the less, poor after spectral subtraction. Hence up to 400 scans were required in thin film experiments as opposed to 25 scans for self supporting discs. Also, self supporting discs may be subjected to high temperature activation (up to 1200°C if necessary) whereas thin films are limited by the thermal stability of the support window. Common thin film support windows include ZnSe,

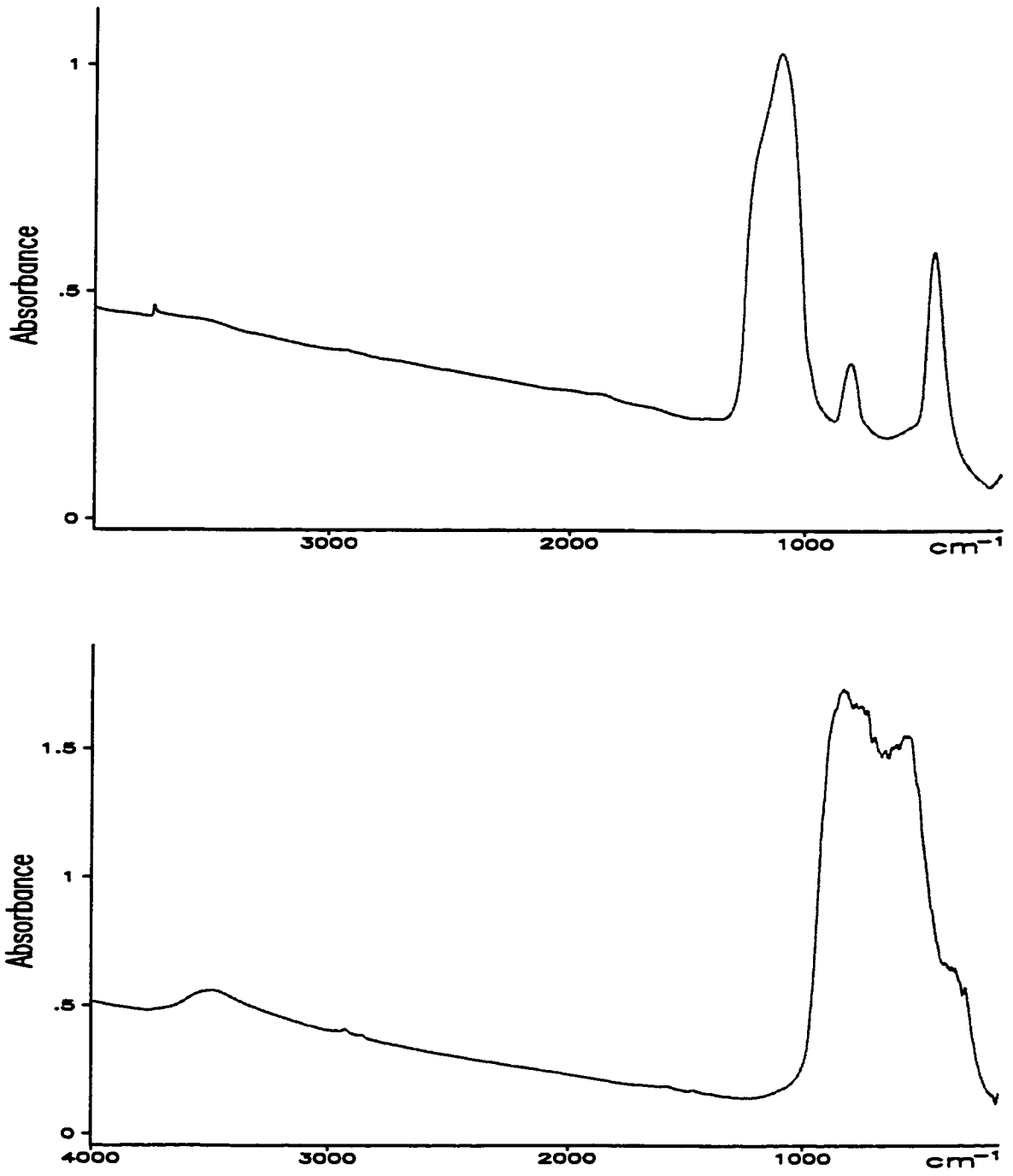

Figure 1.7 Infrared spectra of room temperature activated silica (top) and alumina (bottom) thin films.

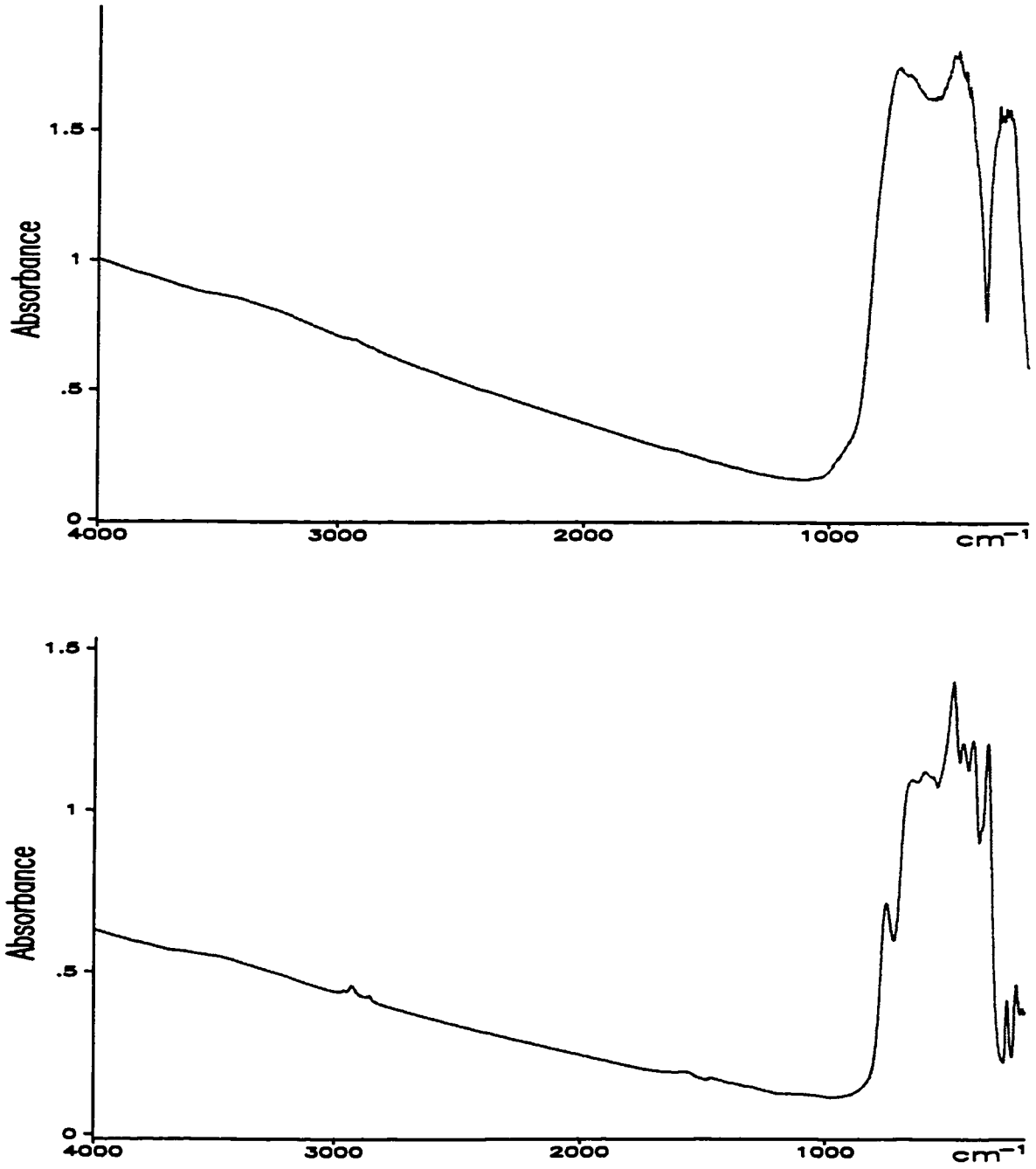

Figure 1.8 Infrared spectra of room temperature activated titania (top) and zirconia (bottom) thin films.

KCl and CsI, the upper temperature limits of which are approximately 500, 450 and 400°C, respectively. Furthermore self supporting discs avoid any problems that may arise due to chemical reactivity or thermal instability of the support. In the final analysis, the choice of thin films or self supporting discs depends on the particular type of experiment being performed.

An example of the usage of the TF technique is illustrated in Figure 1.9 for a system previously studied in our laboratory [15]. In this study dimethylchorophosphine, PMe_2Cl, chemisorbed on SiO_2 resulted in the formation of $SiOP{=}O(Me_2)$. Figure 1.9A and 1.9B show the spectra of silica before and after the reaction, respectively. Figure 1.9C shows the difference spectrum, B minus A, at almost 10 times the original scale. All the peaks in spectrum C are better resolved and the peaks at 1244 and 1045 cm^{-1}, labeled a and b, and which do not appear in spectrum B, are characteristic of P=O and an SiOP vibrational modes, respectively. In this study ^{18}O shifts for these vibrational modes were also investigated. This example serves to illustrate the utility and methodology behind the TF technique.

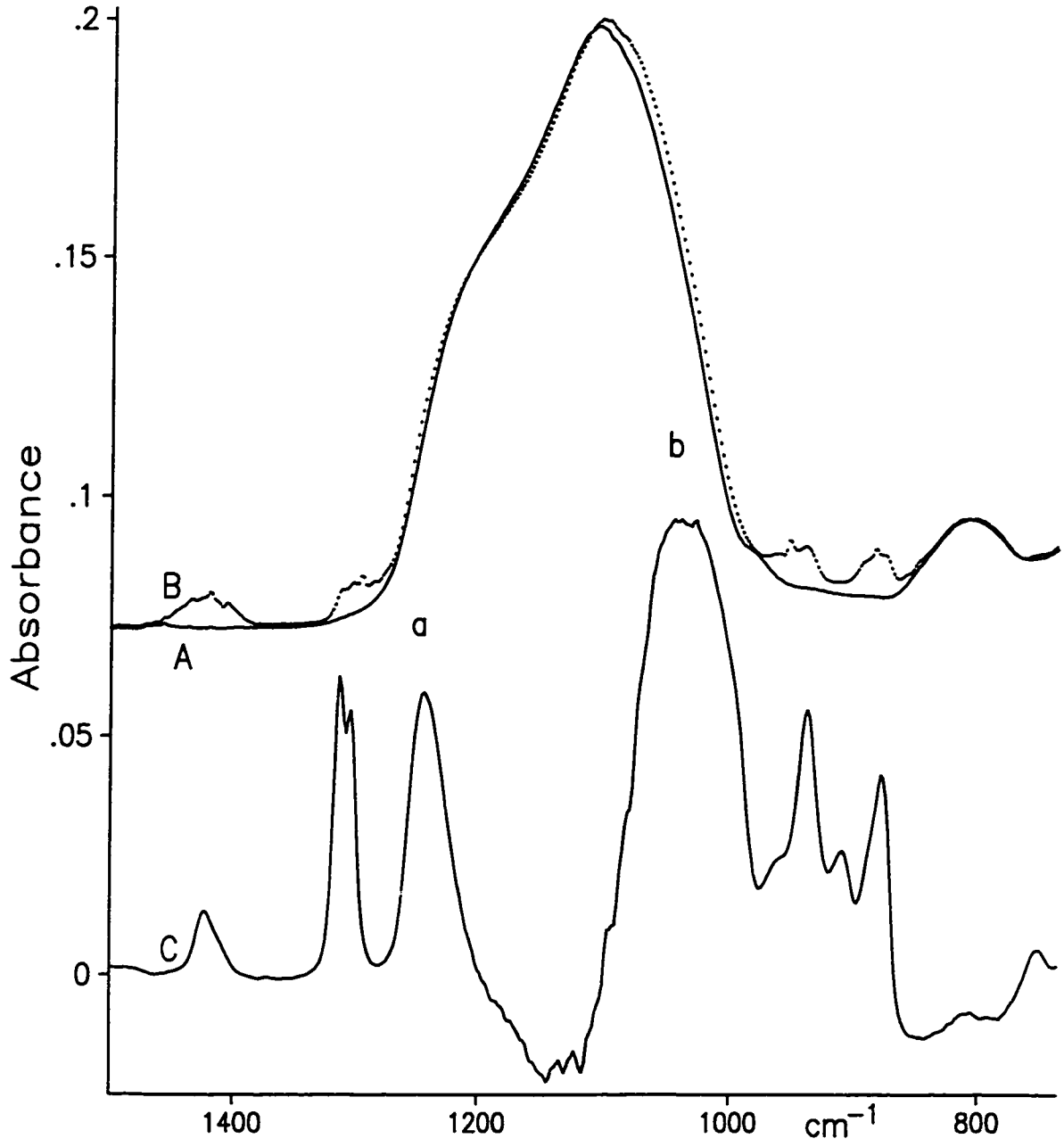

Figure 1.9 Thin film spectra of: **A** silica, **B** silica with chemisorbed PMe_2Cl, and **C** the difference spectrum (B minus A); peaks **a** and **b** are discussed in the text. The absorbance scale refers to spectrum C.

1.4 SPECTROSCOPIC CHARACTERIZATION OF SOLID ACID CATALYSTS

Infrared spectroscopy has been used for many years to characterize the acidity of acid oxide catalysts. In this procedure, a probe molecule which usually contains an electron donor pair (usually on nitrogen or phosphorus) is expected to coordinate to Lewis acid centres on a catalyst. Conversely, the molecule may act as a proton acceptor and become protonated by interaction with a Brønsted acid site. A suitable probe will be chosen to have an acceptable degree of acidity, and to be useful, it should have vibrational modes which are unique for coordinated or protonated forms. If the vibrational spectra of the physically adsorbed, coordinated and protonated forms were all similar, one could not distinguish between the various forms and such a probe would be unsuitable.

For studying adsorption at the gas solid interface, the most commonly used IR probes are ammonia and pyridine and, to a lesser extent, trimethyl phosphine. The pK_a values in aqueous solution for these molecules are 9.24 for NH_3, 8.65 for $P(CH_3)_3$ and 5.24 for C_5H_5N where K_a is the equilibrium constant for the reaction:

$$BH^+ \rightleftarrows B + H^+ \qquad (1.11)$$

BH^+ being the conjugate acid of the conjugate base B. Although these are experimental values for these bases in solution, they do however provide a rough scale which is expected to be approximately applicable to protonation at the solid gas interface [60]. Therefore, it is generally considered that ammonia and trimethyl phosphine have approximately the same base strength and that of pyridine is considerably less. Finally, we recognize that these values are a guide only to the proton accepting ability, and tell us nothing of the relative electron pair donation ability when B is a Lewis base.

The details of the use of IR spectroscopy for distinguishing between the various adsorbed forms of each of the above bases, whether protonated or coordinated, will be discussed later. However, as useful as IR spectroscopy is for characterizing acid and base sites, the method is not quantitative because extinction coefficients are generally not known at gas solid interfaces, although relative quantitative information can sometimes be obtained. The major advantage of the IR experiment is that it is easy to perform and results can be obtained rapidly.

Solid state NMR spectroscopy has been recognized for many years as being a powerful tool for investigating the structure and dynamic behaviour of molecules [61]. In recent times it has developed to the extent to which it sees widespread use in many fields including catalysis [62]. For studying acid sites on oxides, NMR can be used to study the coordination or protonation of various basic probe molecules [63-79].

In liquids dipole-dipole interactions and chemical shift anisotropy (CSA) are averaged out to zero due to rapid isotropic rotational and translational diffusion. In solids the restriction of molecular re-orientation is preserved and these motions are inhibited. Hence the dipole-dipole and CSA interactions become a source of spectral broadening resulting in anisotropic powder patterns in amorphous and polycrystalline samples. These problems can be overcome by the use of various NMR spectroscopic techniques such as high power decoupling and magic angle spinning (MAS), and in cases where signal intensity is also a problem, cross polarization (CP) [80].

The main advantage of NMR over IR spectroscopy is that in the former there is a direct correlation between peak intensities and the total amount of species present; in NMR the intensity of a signal is directly proportional to the total number of nuclear spins. For nuclei other than ^1H, signal averaging of thousands of scans usually is required in order to obtain a good S/N ratio. The observed signal is proportional to $[1-\exp(-t/T_1)]$ where t is the repolarization time and T_1 is the longitudinal relaxation time. In a sample with several NMR

lines, different resonances may have different T_1 values. A short t relative to T_1 would result in spectra where the quickly relaxing lines appear intensified compared with the slow relaxing species. Therefore T_1 values must be measured to ensure a sufficiently long t.

Considering the type of probe molecules frequently used in IR characterization of catalysts, *e.g.* NH_3 and pyridine, NMR of the spin 1/2 nuclei ^{13}C and ^{15}N of such species, isotopically labeled, would be of primary interest in solid acid characterization. Indeed ^{13}C and ^{15}N solid state NMR have been used in catalysis studies [63-66]. However ^{13}C has relatively small chemical shifts for bound species which make it difficult to distinguish between various adsorbed forms. In the case of ^{15}N, its low gyromagnetic ratio renders it low in sensitivity even with isotopically enriched samples [66-68].

^{31}P is a spin 1/2 nucleus of high sensitivity, 100% natural abundance and its short relaxation times allow for quantitative analyses of surface acid sites [67,68,70-73]. Also the ^{31}P nucleus gives rise to chemical shifts which extend over a wide range, the measurement of which provides a means for the determination of molecular structures on P containing compounds [68,69,75,80,81].

Alkyl phosphines have proven to be very useful molecular probes for investigating surface acid sites. In particular trimethyl phosphine (TMP), PMe_3 (where Me = CH_3), has become, primarily through the work of Lunsford [68,71,74] and Maciel [67], a standard NMR probe for measuring the nature, number and strength of acid sites on catalysts. As a result of its higher basicity (TMP strength is about 1000 times greater than that of pyridine) and its relatively smaller size, TMP can adsorb onto a greater number of acid sites.

The ^{31}P resonance of $[(CH_3)_3P\text{-}H]^+$ is well separated from the Lewis bound and physisorbed moieties [71,72], the latter two not being well separated from each other. Additionally, the spectrum of the proton adduct, $[(CH_3)_3P\text{-}H]^+$, can exhibit $J_{P\text{-}H}$ coupling which in essence verifies the presence of the Brønsted acid moiety [63,68,71,74,75,77]. Partially

resolved $J_{P\text{-}Al}$ couplings for PMe_3 adsorbed on Al_2O_3 have been observed and these confirm the observation of Lewis acid-base pairs present in the spectrum [72,75,77,78].

Due to the high natural abundance, high NMR sensitivity and short relaxation times of ^{31}P, TMP has become a very attractive NMR probe molecule for studying solid acid sites of catalysts. Hence TMP was chosen as a probe molecule in the NMR analysis of this work.

1.5 ACIDIC SOLIDS

Acidic solids are widely used as catalysts in the petrochemical industry for hydrocarbon conversion in processes such as fluid catalytic cracking, hydrocracking and naphtha isomerization for making higher valued products. Typically, strong acids as found in zeolites such as faujasites or ZSM-5 are used in these applications.

Hydroprocessing technologies such as ring opening and hydroisomerization are used in the production of branched hydrocarbon species which in turn can be used as feedstocks in other applications. The isomerization catalysts used in this type of work tend to be less acidic than the typical zeolite catalysts common in this field thus minimizing cracking reactions. They are required to be of similar acid strength to halide containing acids and to be effective over a narrow acidity range.

In view of the narrow acidity range requirements imposed on the isomerization catalysts a tool was necessary which would allow one to *fine tune* solid acidity in order to optimize catalyst performance on petroleum feeds. Such a tool was developed by Kramer *et al.* [82] and involved the usage of 2-methyl-2-pentene (2M2P). The 2M2P catalytic probe test is responsive to changes in moderate acidity and provides a scale of acidity that can distinguish various catalysts and the types of reactions they may be used in (see Figure 1.10). Reaction products are formed over sites of varying acidity. For example, in the case of a weak acid site

on a solid catalyst, 2M2P can be readily converted to 4-methyl-2-pentene (4M2P) via a double bond shift, whereas stronger acid sites are required to induce a skeletal shift of the methyl group to form 3-methyl-2-pentene (3M2P).

For a given series of solid acids, the ratio of 3M2P to 4M2P, normalized with respect to surface area, reflects the strength of the acid sites for skeletal isomerization (see Chapter 5). The greater the ratio the greater is the acid strength.

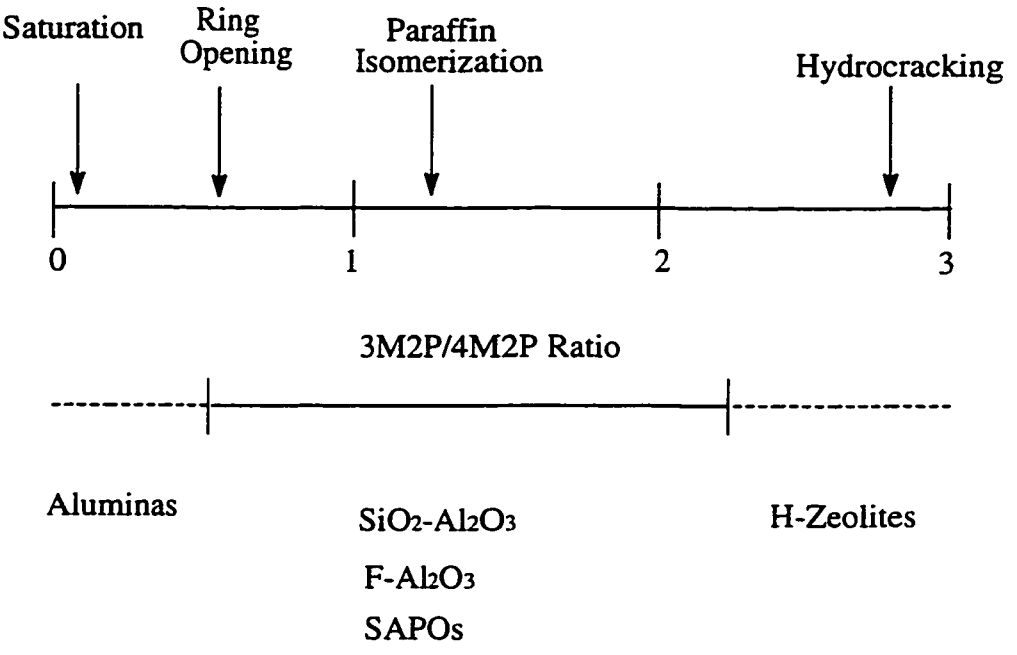

Figure 1.10 Possible reactions on solid acids and the 2M2P scale.

In order to fine tune or optimize catalyst performance, the acid strengths of various catalysts can be altered by the addition of various species or dopants. For example, the acid strength of alumina can be increased by doping with fluoride (see Chapter 4). Also, the addition of well dispersed weakly basic rare earth oxides *neutralizes* the stronger acid sites of

SiO_2-Al_2O_3 leading to an overall decrease in acid strength to levels shown by halided aluminas [83,84]. Yttria, Y_2O_3, which behaves similarly to rare earth oxides was used in this work for this purpose (see Chapter 3).

The 2M2P test alone does not provide information about the acid site population *vs.* site strength or define the type of sites that contribute to catalyst performance. However, by combining this test with spectroscopic techniques one can further define the characteristics of useful catalysts for a particular reaction from a broad set of moderate materials. The main spectroscopic technique used in this research was IR vibrational spectroscopy which was performed not only on Y_2O_3-SiO_2-Al_2O_3 and F-Al_2O_3 catalysts, but also on the pure oxides, from which they were derived, by using various basic probe molecules which were capable of reacting with the surface of the catalysts.

REFERENCES

1. Walls J.M. and Smith R. *eds.*
   "Surface Science Technologies", Elsevier Science Ltd., Oxford 1994

2. Hudson J.B.
   "Surface Science: An Introduction", Butterworth-Heinemann, Boston 1992

3. Woodruff D.P. and Delchar T.A.
   "Modern Techniques of Surface Science", 2^{nd} *ed.*, Cambridge University Press, Cambridge 1994

4. Bamford C.H., Tipper C.F.H. and Compton R.G. *eds.*
   "Simple Processes at the Gas-Solid Interface", ***19***, Elsevier Science Publishers B.V., Amsterdam 1984

5. Niemantsverdrict J.W.
   "Spectroscopy in Catalysis: An Introduction", Weinheim, N.Y. 1995

6. Somarjai G.A.
   "Introduction to Surface Chemistry and Catalysis", John Wiley & Sons, Inc., N.Y. 1994

7. Thomas J.M. and Lambert R.M. *eds.*
   "Characterization of Catalysts", John Wiley & Sons, Inc., Chichester 1980

8. Gasser R.P.H.
   "An Introduction to Chemisorption and Catalysis by Metals", Oxford University Press, Oxford 1985

9. Srivastava R.D.
   "Heterogeneous Catalytic Science", CRC Press, Inc., Boca Raton 1988

10. Davydov A.A.
"Infrared spectroscopy of Adsorbed Species on the Surface of Transition Metal Oxides", John Wiley & Sons Ltd., N.Y. 1990

11. Imelik B. and Vedrine J.C. *eds.*
"Catalysyts Characterization: Physical techniques for Solid Materials", Plenum Press, N.Y. 1994

12. Delgass W.N., Haller G.L., Kellerman R. and Lunsford J.H.
"Spectroscopy in Heterogeneous Catalysis", Academic Press Inc., N.Y. 1975

13. Yates J.T. and Madey T.E.
"Vibrational Spectroscopy of Molecules on Surfaces", Plenum Press, N.Y. 1987

14. Anderson J.R. and Pratt K.C.
"Introduction to Characterization and Testing of Catalysts", Academic Press, Sydney 1985

15. Morrow B.A. and Lang S.J.
J. Phys. Chem., 98, 13319 (1994)

16. Morrow B.A.
"Studies in Surface Science and Catalysis", 57A, A161-A224 (1990)

17. Little L.H.
"Infrared Spectra of Adsorbed Species", Academic Press Inc., London 1966

18. Hair M.L.
"Infrared Spectroscopy in Surface Chemistry", Marcel Dekker, N.Y. 1967

19. Kiselev A.V. and Lygin V.I.
"Infrared Spectra of Surface Compounds", Keter Publishing House Jerusalem Ltd., 1975

20. McFarlan A.J.
Ph. D. Thesis, University of Ottawa, 1991

21. Augustine R.L.
"Heterogeneous Catalysis for the Synthetic Chemist", Marcel Dekker, Inc., N.Y. 1996

22. Morrow B.A., Cody I.A. and Lee L.S.M.
J. Phys. Chem., ***80*** *(25), 2761 (1976)*

23. Ghiotti G., Garrone E., Morterra C. and Boccuzzi F.
J. Phys. Chem., ***83****, 2863 (1979)*

24. Zhdanov S.P., Kosheleva L.S. and Titova T.I.
Langmuir, 3, 960 (1987)

25. Morrow B.A. and McFarlan A.J.
Langmuir, 7, 1695 (1991)

26. Morrow B.A. and McFarlan A.J.
Amer. Chem. Soc. Adv. Chem. Ser., ***234****, 183 (1994)*

27. Armistead C.G., Taylor A.J., Hambleton F.H., Mitchell S.A. and Hockey J.A.
J. Phys. Chem., 73 (11), 3947 (1969)

28. Morrow B.A. and Cody I.A.
J. Phys. Chem., ***80*** *(18), 1995 (1976)*

29. Hambleton F.H., Hockey J.A. and Taylor J.A.G.
Nature, ***208****, 138 (1965)*

30. Kinney J.B. and Staley R.H.
*J. Phys. Chem., **87**, 3735-3740 (1983)*

31. Morrow B.A. and Cody I.A.
*J. Phys. Chem., **80** (18), 1998 (1976)*

32. Morrow B.A. and Devi A.
*J. Chem. Soc., Faraday Trans. 1, **68**, 403 (1972)*

33. Michalske T.A. and Bunker B.C.
*J. Appl. Phys., **56** (10), 2628 (1984)*

34. Ferrari A.M., Garrone E., Spoto G., Ugliengo P. and Zecchina A.
*Surf. Sci., **323**, 151-162 (1995)*

35. Grabbe A., Michalske T.A. and Smith W.L.
*J. Phys. Chem., **99**, 4648-4654 (1995)*

36. Bunker B.C., Haaland D.M., Ward K.J., Michalske T.A., Smith W.L., Binkley J.S., Melius C.F. and Balfe C.A.
*Surf. Sci., **210**, 406-428 (1989)*

37. Bunker B.C., Haaland D.M., Michalske T.A., and Smith W.L
*Surf. Sci., **222**, 95-118 (1989)*

38. Knözinger H.
*"Studies in Surface Science and Catalysis", **20**, 111-125 (1985)*

39. Satterfield C.N.
"Heterogeneous Catalysis in Industrial Practice", 2nd ed., McGraw-Hill, Inc., N.Y. 1991

40. Lippens B.C. and De Boer J.H.
*Acta Cryst., **17**, 1312 (1964)*

41. Knözinger H. and Ratnasamy P.
*Catal. Rev.-Sci. Eng., **17** (1), 31-70 (1978)*

42. Busca G., Lorenzelli V., Gianguido R. and Willey R.J.
*Langmuir, **9**, 1492-1499 (1993)*

43. Pauling L.
"The Nature of the Chemical Bond", 3rd ed., Cornel University Press, Ithaca, N.Y. 1960

44. Knözinger H.
*Adv. Cat., **25**, 184 (1976)*

45. Busca G., Saussey H., Saur O., Lavalley J.C. and Lorenzelli V.
*App. Cat., **14**, 245-260 (1985)*

46. Tsyganenko A.A. and Filimonov V.N.
Spect. Lett., 5 (12), 477-487 (1972)

47. Parfitt G.D.
*Progr. Surf. Membr. Sci., **11**, 181-226 (1976)*

48. Jacob K-H., Knözinger E. and Benfer S.
J. Mat. Chem., 3 (6), 651-657 (1993)

49. *"Kirk-Othmer Encyclopedia of Chemical Technology", 3rd ed., **24***, John Wiley and Sons, N.Y. 1984

50. Morterra C. and Magnacca G.
Cat. Today, 27, 497-532 (1996)

51. Baraton M.I. and Quintard P.
*J. Mol. Struct., **79**, 337-340 (1982)*

52. Tanabe K.
*Mat. Chem. Phys., **13**, 347-364 (1985)*

53. Scokart P.O., Declerck F.D., Sempels R.E. and Rouxhet P.G.
*J. Chem. Soc. Faraday Trans. 1, **73**, 359 (1977)*

54. Murrell L.L. and Dispenziere Jr., N.C.
*Cat. Lett., **2**, 329 (1989)*

55. Sheng T.C., Lang S.J., Morrow B.A. and Gay I.D.
*J. Cat., **148**, 10 (1994)*

56. Niwa M., Katada N. and Murakami Y.
*J. Phys. Chem., **94**, 6441 (1991)*

57. Sato S., Sodesawa T., Nozaki F. and Shoj H.
*J. Molec. Cat., **66**, 343 (1991)*

58. Katada N. Toyama T. and Niwa M.
*J. Phys. Chem., **98**, 7647 (1994)*

59. Morrow B.A., Tripp C.P. and McFarlane R.A.
J. Chem. Soc. Chem. Commun., 1282 (1984)

60. Tanabe K.
*"Studies in Surface Science and Catalysis", **50**,* Elsevier, Amsterdam 1989

61. Fyfe C.A.
"Solid State NMR for Chemists", C.F.C. Press, Guelph 1983

62. Bell A.T. and Pines A. *eds.*
"NMR Techniques in Catalysis", Marcel Dekker, Inc., N.Y. 1994

63. Earl W.L., Fritz P.O., Gibson A.A.V. and Lunsford J.H.
*J. Phys. Chem., **91**, 2091-2095 (1987)*

64. Maciel G.E., Haw J.F., Chuang I-S., Hawkins B.L., Early T.A., McKay D.R. and Petrakis L.
*J. Am. Chem. Soc., **105** (17), 5529 (1983)*

65. Haw J.F., Chuang I-S., Hawkins B.L. and Maciel G.E.
*J. Am. Chem. Soc., **105**, 7206-7207 (1983)*

66. Ripmeester, J.A.
*J. Am. Chem. Soc., **105** (9), 2925-2927 (1983)*

67. Baltusis L., Fryre J.S. and Maciel G.E.
*J. Am. Chem. Soc., **109**, 40-46 (1987)*

68. Lunsford J.H., Tutunjian P.N., Chu P., Yeh E.B. and Zalewski D.J.
*J. Phys. Chem., **93**, 2590-2595 (1989)*

69. Guillaume D., Gautier S., Despujol I., Alario F. and Beccat P.
*Cat. Lett., **43**, 213-218 (1997)*

70. Gay I.D., McFarlan A.J. and Morrow B.A.
*J. Phys. Chem., **95**, 1360 (1991)*

71. Lunsford J.H., Rothwell W.P. and Shen W.
*J. Am. Chem. Soc., **107**, 1540-1547 (1985)*

72. Sheng T.C. and Gay I.D.
*J. Catal., **145**, 10-15 (1994)*

73. Bendada A., DeRose E.F. and Fripiat J.J.
*J. Phys. Chem., **98**, 3838-3842 (1994)*

74. Rothwell W.P., Shen W.X. and Lunsford J.H.
*J. Am. Chem. Soc., **106**, 2452-2453 (1984)*

75. Sang H., Chu H.Y. and Lunsford J.H.
*Cat. Lett., **26**, 235-246 (1994)*

76. Sheng T.C., Kirszenstejn P. and Gay I.D.
*Cat. Lett., **23**, 119-126 (1994)*

77. Chu P-J., de Mallmann A. and Lunsford J.H.
*J. Phys. Chem., **95**, 7362-7368 (1991)*

78. Chu P-J., Lunsford J.H. and Zalewski D.J.
*J. Mag. Res., **87**, 68-79 (1990)*

79. Coster D.J., Bendada A., Chen F.R. and Fripiat J.J.
*J. Cat., **140**, 497-509 (1993)*

80. Pines A., Gibby M.G. and Waugh J.S.
*J. Chem. Phys., **59**, 569 (1973)*

81. Emsley J.W., Feeney J. and Sutcliffe L.H.
"High Resolution NMR Spectroscopy", Pergamon Press Ltd., Oxford 1966

82. Kramer G.M., McVivker G.B. and Ziemiak J.J.
*J. Cat., **92**, 355 (1985)*

83. Soled S.L., McVicker G.B. and Gates W.E.
U.S. Patents 5,208,200 (1993), 5,248,409 (1993) and 5,254,518 (1993)

84. Soled S.L., McVicker G.B., Misco S., Gates W.E. and Baumgartner J.
*"Studies in Surface Science and Catalysis", **101,*** 563-572, Elsevier Science B.V., Amsterdam 1996

CHAPTER 2

EXPERIMENTAL

2.1 INSTRUMENTATION

The infrared spectra recorded in this work were obtained using a Bomem Michelson MB-100 Fourier transform infrared (FTIR) spectrometer. In the early work this instrument was equipped with a KBr beam splitter which limited its spectral range to the mid infrared region, *i.e.* 5000-400 cm^{-1}. In the latter part of the work the KBr beam splitter was replaced with a CsI beam splitter which allowed us for the first time to probe the far infrared region, thus increasing the spectral range down to 200 cm^{-1}.

The MB-100 was also equipped with a ceramic glow bar source which emits in the infrared, as well as an ambient temperature deuterated triglycerine sulphate (DTGS) detector. The maximum resolution of the instrument was 1 cm^{-1}, however all spectra were recorded using 4 cm^{-1} resolution. A routine spectrum with *self supporting discs* consisted of acquiring 25 scans, which were signal averaged, over an acquisition time of about 40 s. Experiments in which *thin films* were used required greater signal averaging and as a result anywhere between 200-400 scans were obtained.

These spectra which were acquired on the MB-100 were processed using *Spectra Calc* software on an IBM compatible 386 computer. All the infrared spectra presented in this work are plotted in units of absorbance ($\log_{10} I_o/I$) *vs.* wavenumber (cm^{-1}).

2.2 *IR CELLS*

Two types of infrared cells were used in this work. The first was the *standard* type of cell used in this laboratory which has been previously described by Morrow and Ramamurthy [1] and is shown in Figure 2.1.

The main body of the cell, that is the lower section, can be made of either Pyrex, which has an upper temperature limit of 500°C, or quartz, which has an upper temperature limit of 1200°C, depending on the type of work being carried out.

The lower section consisted of two regions: a furnace region and a window region which is about 20 cm from the furnace. The furnace consisted of Kanthal wire windings having a resistance of 0.09 Ω/cm which were insulated with glass wool matting. Cell temperatures were measured by a Chromel-Alumel thermocouple encased within a thin quartz tube which resided between the heating wire and insulation matting. It has been determined that between room temperature and 450°C the temperatures measured inside such an IR cell and at the furnace do not differ by more than 2°C [2].

The window region consists of two 2.5 cm diameter IR transparent windows, chosen according to usage, which were attached with epoxy resin. In this work KBr and CsI windows were primarily used. Upon heating at temperatures above 300°C external air cooling of the windows had to be implemented.

The upper section, including the stopcock, was constructed of Pyrex. The sample was placed in a forked quartz sample holder. If need be the sample was either sandwiched with quartz discs or placed on a quartz ring prior to placement in the sample holder for stability. The top of the sample holder consisted of two sealed compartments one of which was empty

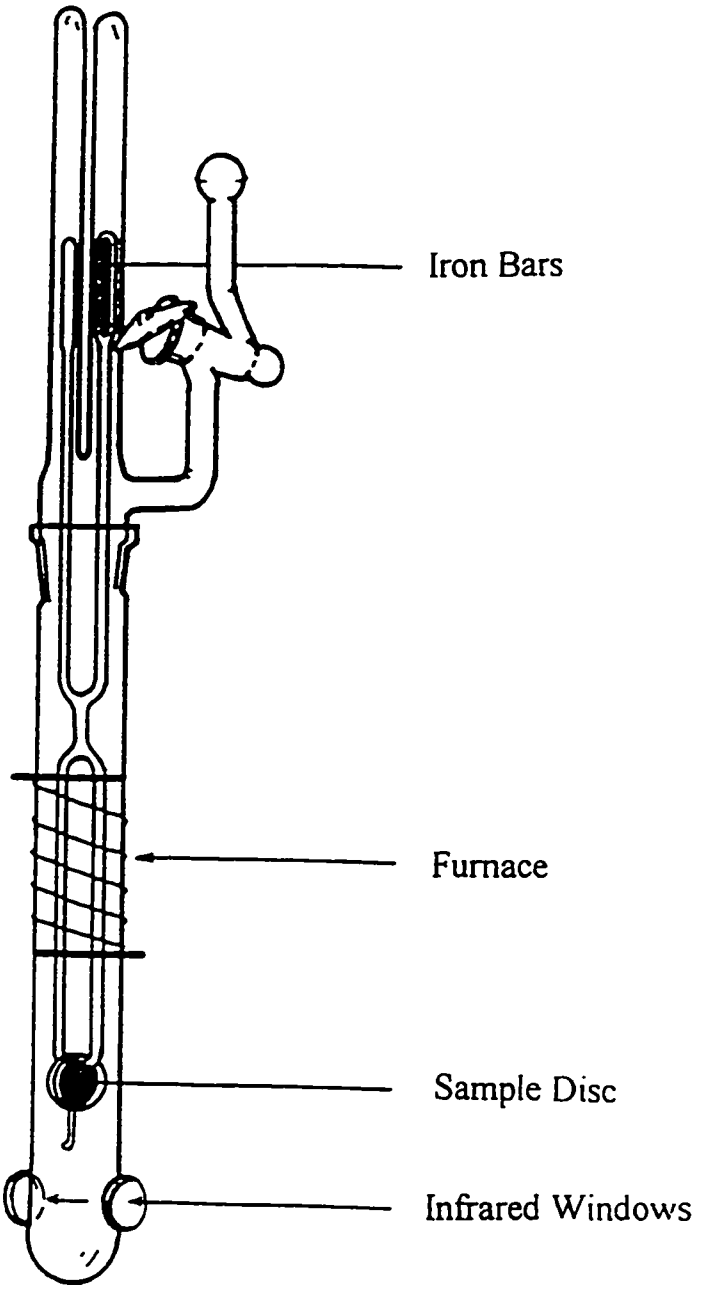

Figure 2.1 Standard infrared cell.

and the other of which was filled with iron bars. Hence the sample could be lowered and raised, moving between the heating and window regions, by externally placing a magnet on the Pyrex top directly over the iron bars.

The large 34/45 ground glass taper connecting the top and the bottom sections of the cell was lubricated with Apiezon H grease. Apiezon N grease was used for the vacuum stopcock and ground glass ball/swivel joint which connected the cell to the vacuum line. The total cell volume was about 300 cm^3.

The second type of IR cell which was used is illustrated in Figure 2.2 and has been described previously by McFarlan [2]. It was used in this work to perform *in situ* (inside the IR spectrometer) IR temperature programmed desorption (TPD) type experiments.

The cell body was made of quartz and was 14 cm in length and about 2.5 cm o.d. (2.2 cm i.d.). A 2.5 cm diameter ZnSe window was sealed with epoxy resin to one end. At the other end a 5.0 cm diameter KBr or KCl window formed a vacuum seal over the quartz flange when lightly greased with Apiezon H. The sample holder, which had a slot for sample discs, was made of quartz. The total cell volume was about 90 cm^3.

Sample heating was achieved by placing a movable 7.0 cm in length 3.3 cm o.d. (3.1 cm i.d.) tube furnace over the region of the cell where the sample resided. The maximum *in situ* temperature used was about 350°C. Until recently heating at temperatures higher than this was achieved *ex situ* and this required external air cooling on both infrared windows; now samples have been heated *in situ* to temperatures of 400°C whilst dry air was used to cool the window.

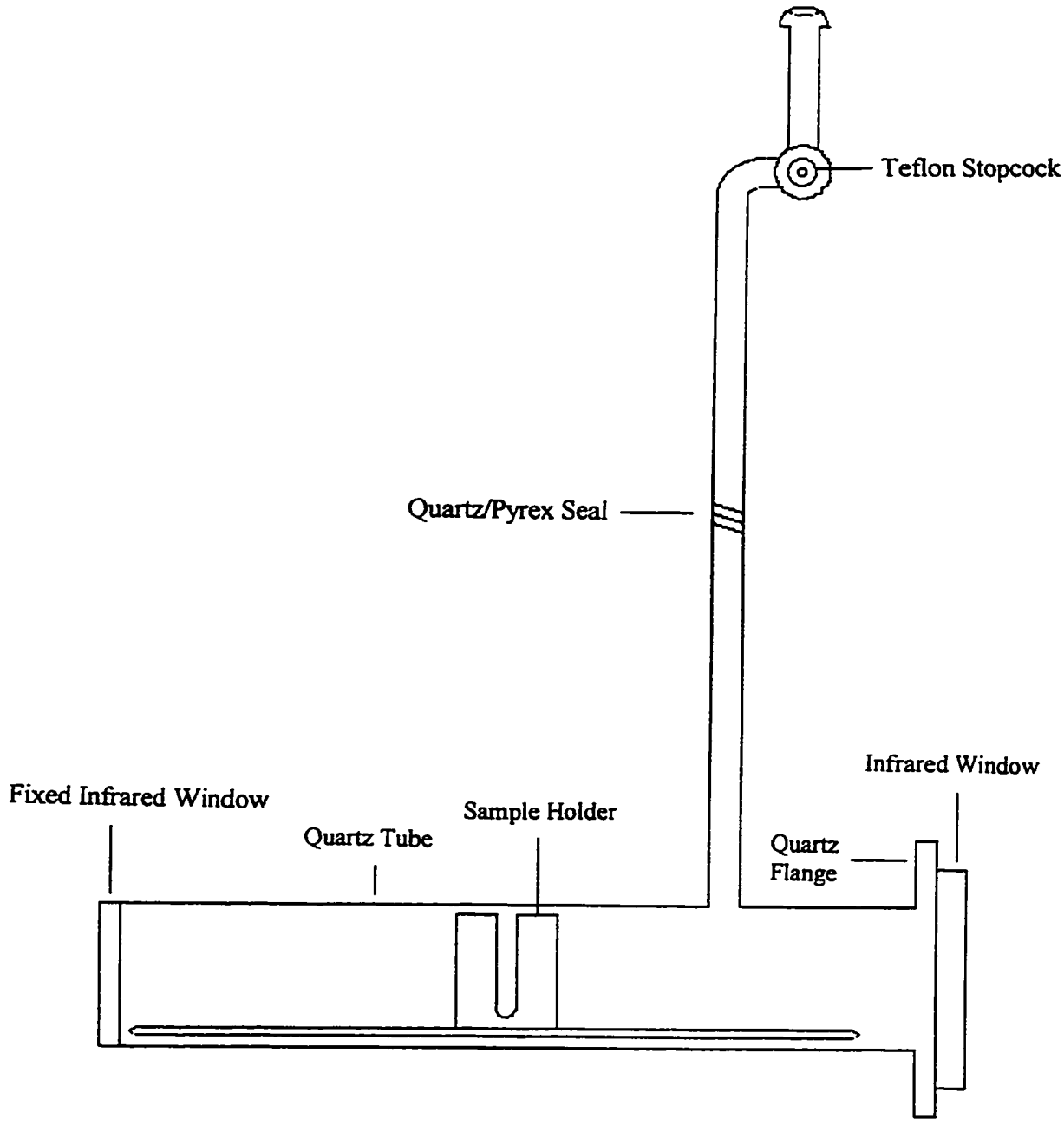

Figure 2.2 Infrared cell used in temperature programmed desorption experiments.

2.3 *VACUUM MANIFOLD*

The vacuum line in use was a portable Pyrex vacuum manifold, 300 cm^3 in volume, equipped with 6 inlets. These inlets or 14/23 ground glass taper joints were connected to the manifold via 8 mm diameter Teflon stopcocks. A 15 mm diameter Pyrex/Teflon stopcock separated the main part of the manifold from the vacuum pumps. The vacuum line was equipped with two pumps: an air cooled oil diffusion pump in series with a two stage rotary vane roughing pump. These pumps, in particular the oil in the diffusion pump, had to be protected from the reactive gaseous reagents which were commonly used. This was achieved by placing a liquid nitrogen cold trap between the manifold and the vacuum pumps. Ideally a base pressure of about 10^{-6} Torr is obtainable. However, a base pressure of about 10^{-5} Torr was obtainable after evacuating an infrared cell for about 30 min.

The absolute pressures of the gaseous reagents in the manifold were measured using digital capacitance manometers of which three were available with ranges of 10^{-3}-10, 10^{-2}-100 and 10^{-1}-1000 Torr depending on the experiment. An analogue thermocouple gauge was always used which allowed one to check for leaks within the system.

2.4 *SAMPLE PREPARATIONS*

For infrared studies two types of samples were prepared: self supporting discs and thin films. Self supporting discs were prepared by pre-weighing an amount of oxide to one hundredth of a milligram, usually anywhere between 10.00-50.00 mg depending on the experiment. The weighed amount was then evenly spread across the face of a 2.5 cm diameter stainless steel die which was then pressed under pressure, 10^6-10^8 Pa depending on the type of oxide being used. For example, SiO_2 required very little pressure 10^6 Pa or less whereas the yttria impregnated SiO_2-Al_2O_3 catalysts required an extremely high pressure of 10^8 Pa.

In the case of catalysts such as Al_2O_3, TiO_2 and ZrO_2 lens paper or mica discs or weighing paper had to be placed between the die faces. These measures prevented the adherence of the oxides to the die. The mica discs and weighing paper could be easily removed from the oxide disc; lens paper on the other hand had to be impregnated with the oxide which was achieved over the course of pressing several discs.

Thin films were prepared in one of the three following ways:

1. Evenly spread a small quantity of oxide on to a transparent support window (ZnSe, CsI) then using a spatula lightly wipe the surface. The oxide adheres to the surface of the window.

2. Evenly spread a small quantity of oxide on to a stainless steel die or a quartz window then place a support window on to the oxide and press firmly whilst rotating so that the oxide adheres to the support window.

3. Place a small quantity of oxide in a small tube or flask to which chloroform was added. Secure a nozzle top to the tube or flask and pass nitrogen through the oxide suspension in order to spray the oxide/chloroform mixture on to a support window. Evaporation of the chloroform leaves a film of the oxide.

Method 1 always worked for SiO_2 and method 2 sometimes worked for Al_2O_3 and TiO_2; method 3 was used when the second method did not work and was always reliable. The support window was then mounted in the sample holder as in the case of self supporting discs.

REFERENCES

1. Morrow B.A. and Ramamurthy P.
   J. Phys. Chem., 77 (26), 3052 (1973)

2. McFarlan A.J.
   Ph. D. Thesis, University of Ottawa, 1991

CHAPTER 3

YTTRIA-SILICA-ALUMINA CATALYSTS

3.1 INTRODUCTION

When work was started on the ytrria (Y_2O_3, Y) doped silica-alumina (SiO_2-Al_2O_3, SA) catalysts, herein after referred to as **xYSA** (where **x** is the weight percentage of Y_2O_3 doped on to the SiO_2-Al_2O_3 support), it was with the intention of characterizing a potential isomerization catalyst. Due to the basic nature of Y_2O_3 the acidity of SA catalysts would be decreased upon such doping. The objective of this work was to characterize the acidity or changes in acidity of SiO_2-Al_2O_3 catalysts as a function of increasing levels of surface deposited Y_2O_3 via infrared (IR) and solid state magic angle spinning (MAS) nuclear magnetic resonance (NMR) spectroscopy.

The catalysts were prepared from yttrium nitrate hexahydrate, $Y(NO_3)_3.6H_2O$, by Dr. Stewart Soled of Exxon, via incipient wetness impregnation. The catalysts provided were 0, 4, 8, 12 and 16% YSA; the 0% YSA being reserved for the undoped catalyst or pure SA (87% SiO_2 : 13% Al_2O_3). Table 3.1 shows the B.E.T. (N_2) surface areas of the YSA catalysts under study which were measured in Dr. Ian Gay's laboratory at Simon Fraser University.

Table 3.1 B.E.T. (N_2) Surface areas of YSA catalysts.

xYSA	Surface Area (m^2/g)
0	361
4	332
8	331
12	309
16	276

NMR studies on the YSA catalysts were performed using trimethylphosphine (TMP) as a basic probe molecule. As mentioned earlier (in Chapter 1) the advantage of the NMR approach is that it allows for quantitative measurements of the numbers of Lewis and Brønsted acid sites. The disadvantage, however, is that the samples are required to be vacuum sealed. Hence each measurement on a given catalyst requires a separate sample. If a series of measurements are required, this can be time consuming.

Insight was also sought into determining the strengths of acid sites in mixed oxide catalysts and to this end IR/TPD (temperature programmed desorption) type experiments were performed. This technique has the potential of giving a measure of acid strength by virtue of its ability to measure the temperature at which a probe molecule desorbs from an active site [1-3]. In the original TPD experiment there are 5 steps:

1. Catalyst pretreatment;
2. Adsorption of probe molecule;
3. Evacuation to remove physisorbed species;
4. Thermal desorption to displace chemisorbed species into carrier gas stream;
5. Detection and analysis of desorbed species.

However in this work a modified version of the TPD experiment was performed using the IR/TPD cell described previously in Chapter 2. Preliminary work was performed in order to establish a constant heating rate for the entire experiment. Ideally a slow linear heating rate is desired in TPD experiments, but given the limitations of the rather unconventional TPD cell that was used, a stepwise increment in temperature was used in which a powerstat autotransformer was set to 15 V for the first ten minutes then 20 V for the next ten minutes and finally 25 V for the last ten minutes of the experiment. Hence the *in situ* IR/TPD experiment was allowed to proceed for thirty minutes under dynamic vacuum from room temperature to about 350°C. We had previously determined that this programme gave an approximately linear increase in temperature. The same heating programme was used for every sample so that a relative measure of strength of attachment of the probe was determined, it being assumed that the longer a molecule remained attached in the 30 minutes heating programme the greater would be the acid strength.

3.2 AMMONIA (NH_3) ADSORPTION

Ammonia is a well established IR probe molecule for acid sites on oxide surfaces [4-6]. It has been shown to interact with surfaces in several ways:

1. H-bonding (via one of its H atoms) to a surface oxygen atom;
2. H-bonding (via its N atom) to a surface hydrogen atom;
3. Coordination to an electron deficient metal atom, that is a Lewis acid site;
4. Dissociation resulting in the formation of surface NH_2 and OH species;
5. Proton transfer from a Brønsted acid site to yield an ammonium ion.

In the IR context the most diagnostic spectroscopic region is that associated with the angle deformation modes from 1650-1400 cm^{-1}. Within this region band assignments can be made to confirm the presence of Lewis and Brønsted acidity at the gas solid interface.

For adsorbed NH_3, an IR band characteristic of protonated NH_3 is expected in the region 1450-1400 cm^{-1}. Generally, within this region, the lower the wavenumber the stronger the Brønsted acid site hence the greater the degree of protonation and the greater the stability of the resulting NH_4^+ ion. In ionic solids such as NH_4Cl, the antisymmetric NH_4 deformation frequency is near 1400 cm^{-1} and is a sharp band [7]. If proton transfer is not complete, for example in the case of weak Brønsted acid sites, the interaction may be depicted as MO...H...NH_3 and in this case the antisymmetric deformation mode lies near 1450 cm^{-1} [6,8].

H-bonded NH_3 has its main deformation mode in the region 1590-1580 cm^{-1}. Below this region at about 1555 cm^{-1} in the case of SiO_2, lies an Si-NH_2 band which is due to the dissociative chemisorption of NH_3 on strained siloxane sites [5,8,9]. This is characteristic of NH_3 adsorption on all SiO_2 based catalysts which have been activated at temperatures greater than 400°C [5,9-11].

Lewis acidity on the other hand is characterized by the presence of coordinated NH_3 which has distinct IR bands in the spectral region 1620-1600 cm^{-1}. On Al_2O_3 or SiO_2-Al_2O_3 this band lies closer to 1620 cm^{-1} whereas on Y_2O_3 it is at 1602 cm^{-1}.

Figure 3.1 shows IR spectra of adsorbed NH_3 on YSA catalysts which had been activated under vacuum for 1 hour at 450°C. These spectra were recorded after contacting the catalyst with a large excess, about 40 Torr, of NH_3 vapor for 15 minutes at 20°C followed by evacuation for 5 minutes. On these catalysts, evacuation for 5 minutes at room temperature is sufficient to remove all physically adsorbed and H-bonded NH_3. Further evacuation at the same temperature did not result in any additional spectral changes.

In each case there is a strong Lewis acid peak; the peak position is near 1620 cm^{-1} for 0% YSA, at 1605 cm^{-1} for 16% YSA and at intermediate values for all other YSA catalysts.

Given that the peak is near 1602 cm^{-1} for pure Y_2O_3, this shift is consistent with an increasing number of Y_2O_3 sites capable of coordinating NH_3 as the Y_2O_3 content increases.

For the 0, 4 and 8% YSA samples there is a broad Brønsted acid peak at about 1450 cm^{-1}, *i.e.* protonated ammonia. In the case of 12 and 16% YSA samples this latter band is so broad that it hardly resembles a distinct peak. This indicates that there are fewer Brønsted acid sites and that their strength probably diminishes, that is, the peak more resembles that which is more characteristic of a partially or very weakly protonated form of ammonia, as would be expected upon increased Y doping.

Finally, the $SiNH_2$ species is present in the 0-12% YSA catalysts, as is indicated by the presence of a weak peak at about 1555 cm^{-1}.

In order to assess the strength of the acid sites we have devised a modified TPD experiment. As discussed earlier, the sample is heated slowly to about 350°C with the IR cell *in situ* while continuously evacuating the sample. No quantitative data relative to the heats of adsorption can be obtained, but in a qualitative sense we endeavor to determine the relative heats of adsorption for the various species on each of the catalysts. Figures 3.2-3.6 show the IR/TPD spectra as a function of increasing temperature for 0-16% YSA. Only selected spectra have been plotted, but at equal temperature intervals, up to complete desorption in each case. That is, each plot contains seven spectra which were recorded at the same temperature for all samples.

In the case of the coordinated NH_3, 1600-1620 cm^{-1}, it can be seen that this peak disappears at about the same temperature for each loading level, including zero. In each case, it has essentially disappeared by the sixth spectrum from the top.

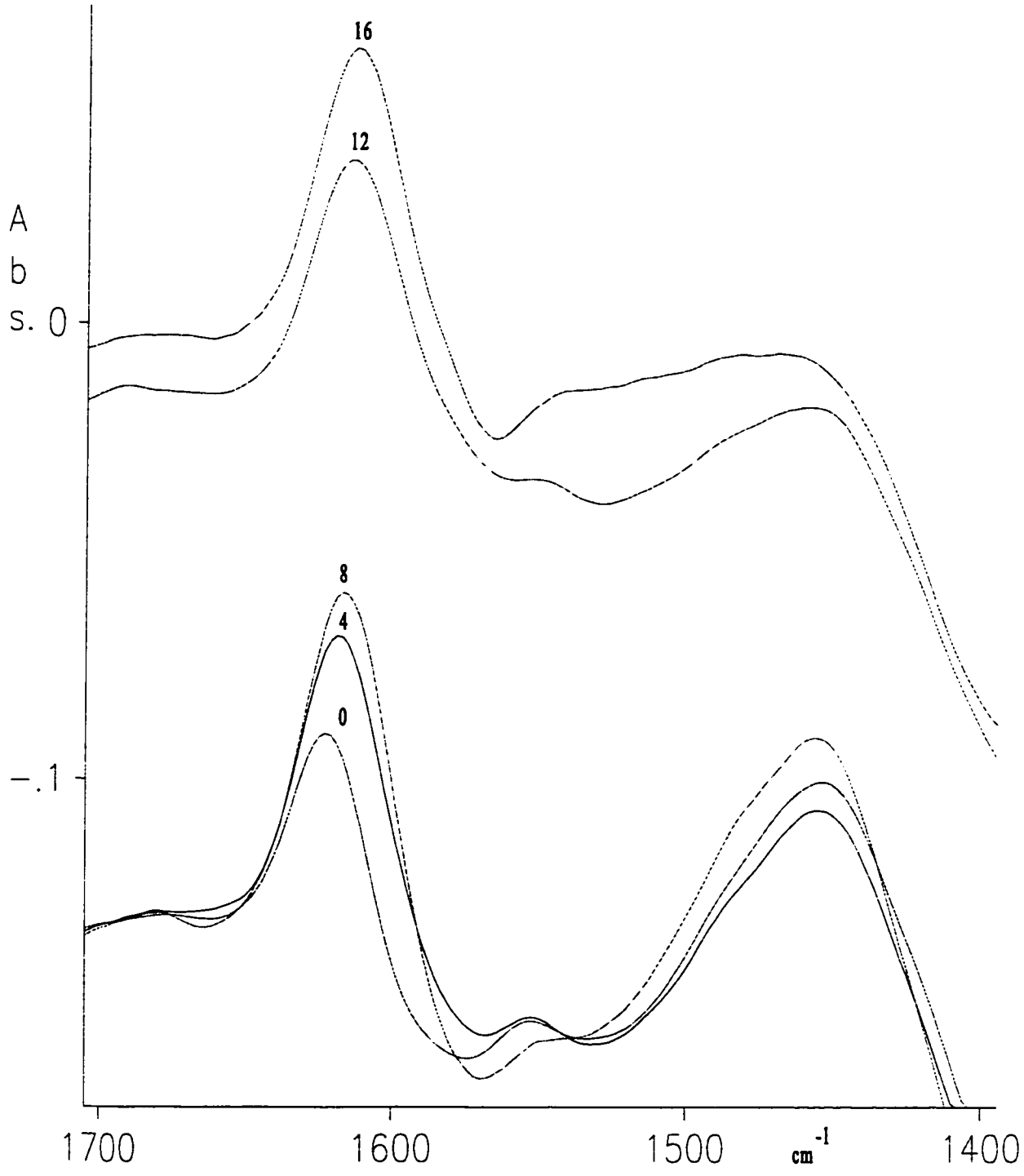

Figure 3.1 Room temperature infrared spectra of chemisorbed NH_3 on YSA catalysts, containing 0-16 wt. percent yttria activated at 450°C.

For the NH_4^+ peak (1450-1400 cm^{-1}) it is clear that as the intensity decreases the peak maximum shifts toward a lower wavenumber. This is to be expected given that the peak shift to lower wavenumber is indicative of a stronger adsorption site, hence the stronger sites desorb at the higher temperatures. Qualitatively, the Brønsted peak disappears after the Lewis peak for 0, 4 and 8% YSA catalysts, at about the same time for the 12% YSA catalyst and before the Lewis peak for the 16% YSA catalyst.

In other words, the strength of the Brønsted site appears to decrease with increasing Y_2O_3 loading, particularly at higher loadings. However, the TPD results do not show a large difference between Brønsted acid site strength of the 0, 4 and 8% YSA catalysts, at least at the temperature resolution used.

Figure 3.7 shows the results for the adsorption of ammonia on the YSA which had been activated at 150°C. These catalysts have a much higher initial OH content and are, therefore, expected to show a greater number of Brønsted acid sites. This is born out by the spectra in Figure 3.7; when compared to those shown in Figure 3.1 for the 450°C activated catalysts, the peak near 1450 cm^{-1} is much more intense (note the absorbance scale in Figures 3.1 and 3.7) although the peak near 1612 cm^{-1} is of about the same intensity in each case. However, the intensity of the 1450 cm^{-1} peak decreased with increasing yttria loading, indicating that the number of Brønsted acid sites decreased as the yttria loading increased. There was not a significant change in the intensity of the peak near 1612 cm^{-1} due to coordinated NH_3 on Lewis acid sites.

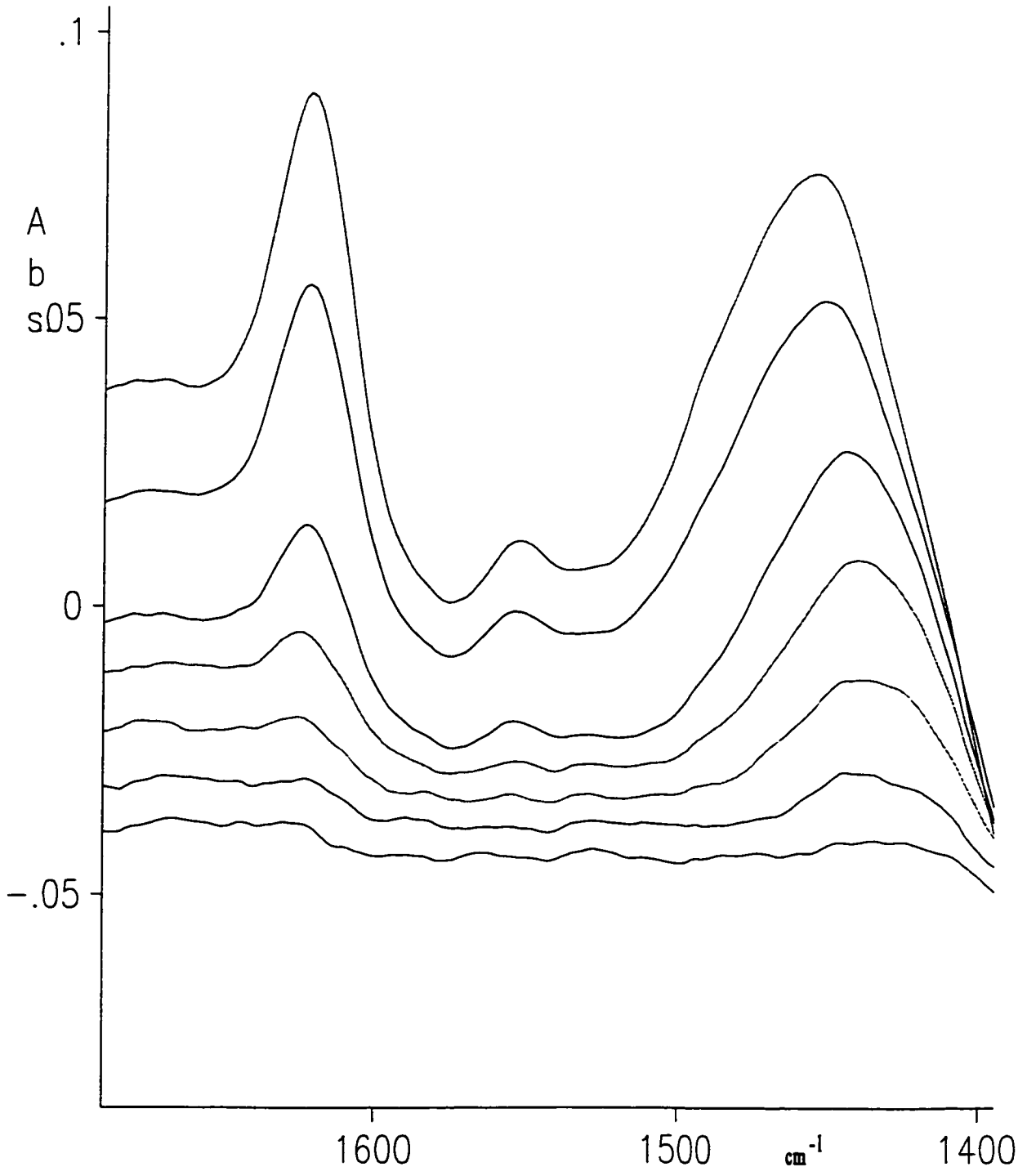

Figure 3.2 0% YSA NH_3 IR/TPD plots; the top curve is that which is shown for chemisorbed NH_3 at room temperature (Figure 3.1). The subsequent spectra, moving downwards, show the spectra observed as a function of increasing temperature while evacuating the sample.

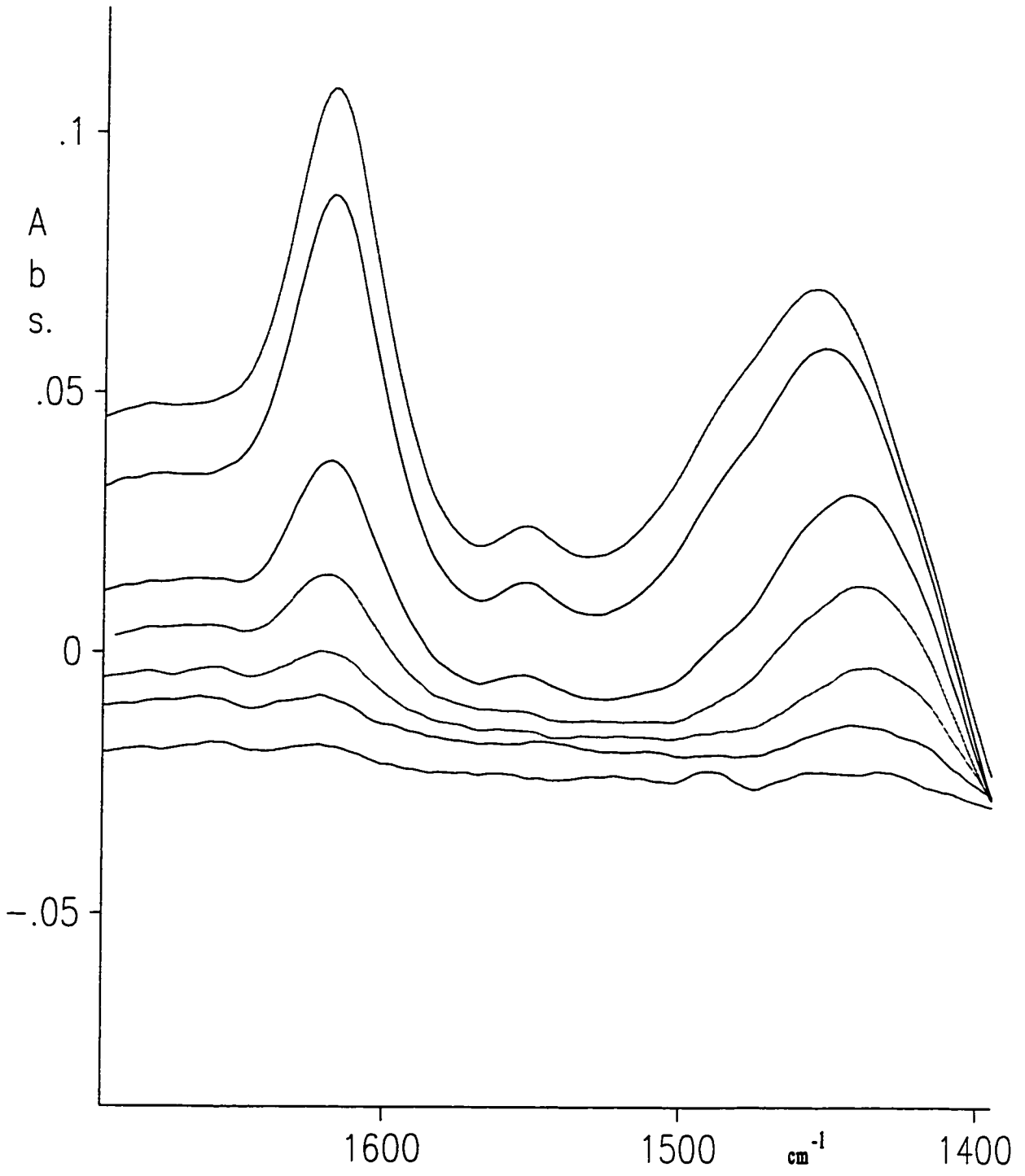

Figure 3.3 4% YSA NH_3 IR/TPD plots; the top curve is that which is shown for chemisorbed NH_3 at room temperature (Figure 3.1). The subsequent spectra, moving downward, show the spectra observed as a function of increasing temperature while evacuating the sample.

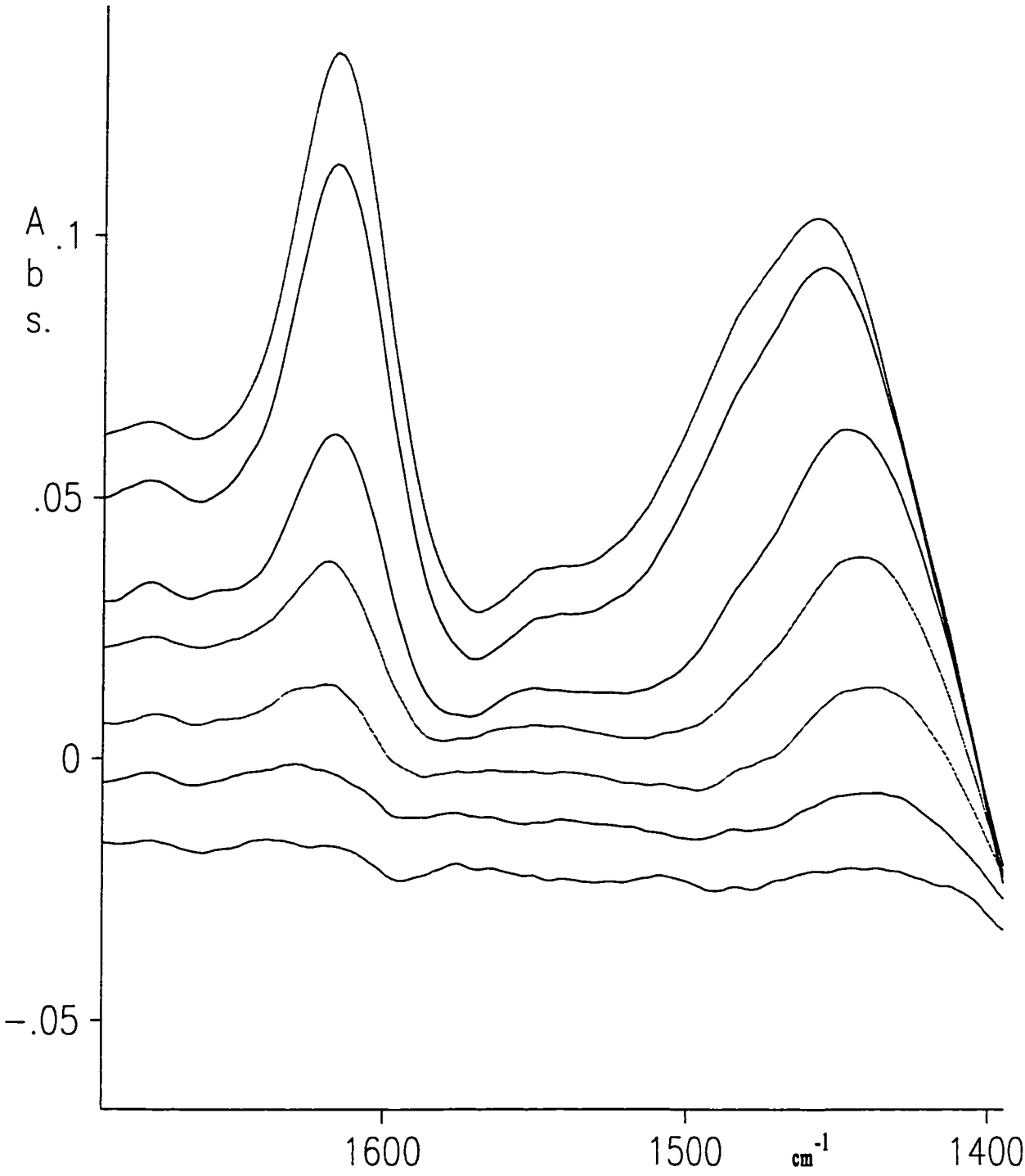

Figure 3.4 8% YSA NH_3 IR/TPD plots; the top curve is that which is shown for chemisorbed NH_3 at room temperature (Figure 3.1). The subsequent spectra, moving downward, show the spectra observed as a function of increasing temperature while evacuating the sample.

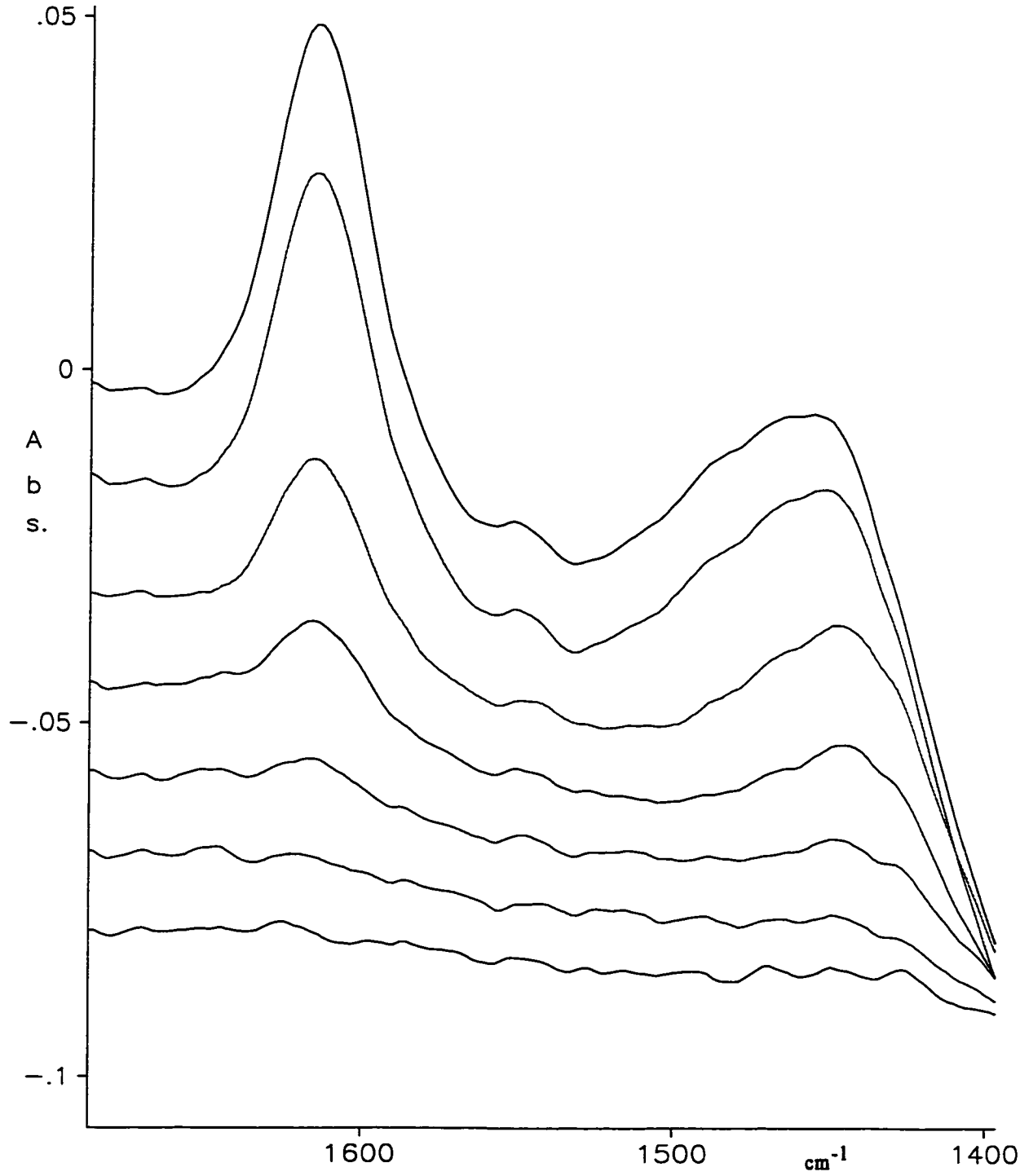

Figure 3.5 12% YSA NH_3 IR/TPD plots; the top curve is that which is shown for chemisorbed NH_3 at room temperature (Figure 3.1). The subsequent spectra, moving downward, show the spectra observed as a function of increasing temperature while evacuating the sample.

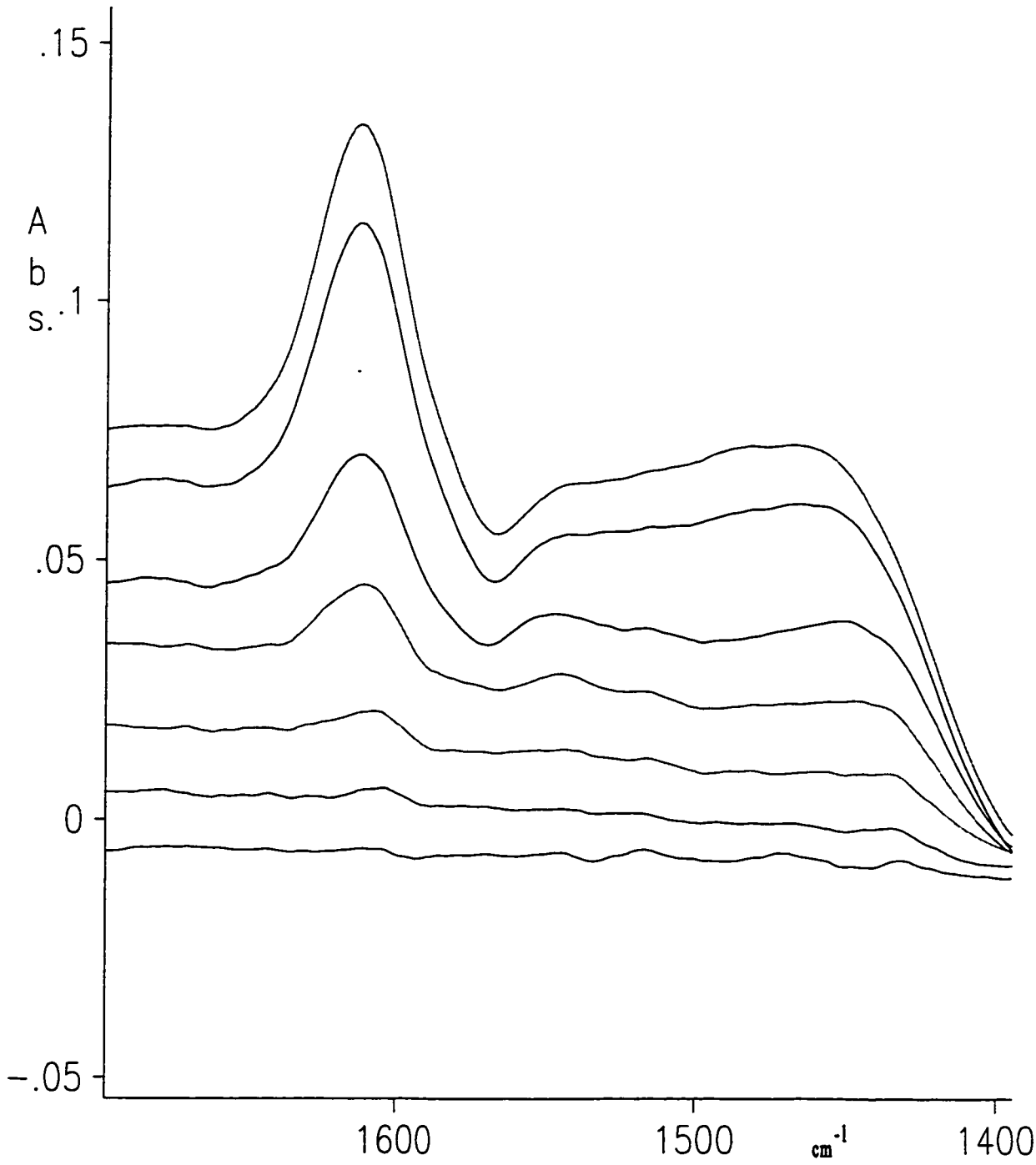

Figure 3.6 16% YSA NH_3 IR/TPD plots; the top curve is that which is shown for chemisorbed NH_3 at room temperature (Figure 3.1). The subsequent spectra, moving downward, show the spectra observed as a function of increasing temperature while evacuating the sample.

The analogous TPD spectra for each catalyst are shown in Figures 3.8-3.12 for 0 to 16% loading with yttria respectively. These show nine spectra recorded at equal time intervals during the heating from room temperature to 350°C. There is not a large difference between any of them with respect to the disappearance of the 1612 cm^{-1} peak due to coordinated ammonia. The Brønsted peak shifted, as expected, to lower wavenumber with increasing temperature, indicating that the stronger sites were liberated last as the temperature increased. It is difficult to make quantitative assumptions given that the intensity of the 1450 cm^{-1} band was stronger initially for zero loading, and weakest for the highest yttria loading. In all cases, the desorption of protonated ammonia occurred at about the same temperature for each catalyst. There is just a suggestion that the Brønsted peak disappeared slightly earlier for the 12 and 16% YSA catalysts than for the other, suggesting a slightly weaker Brønsted acidity in these cases.

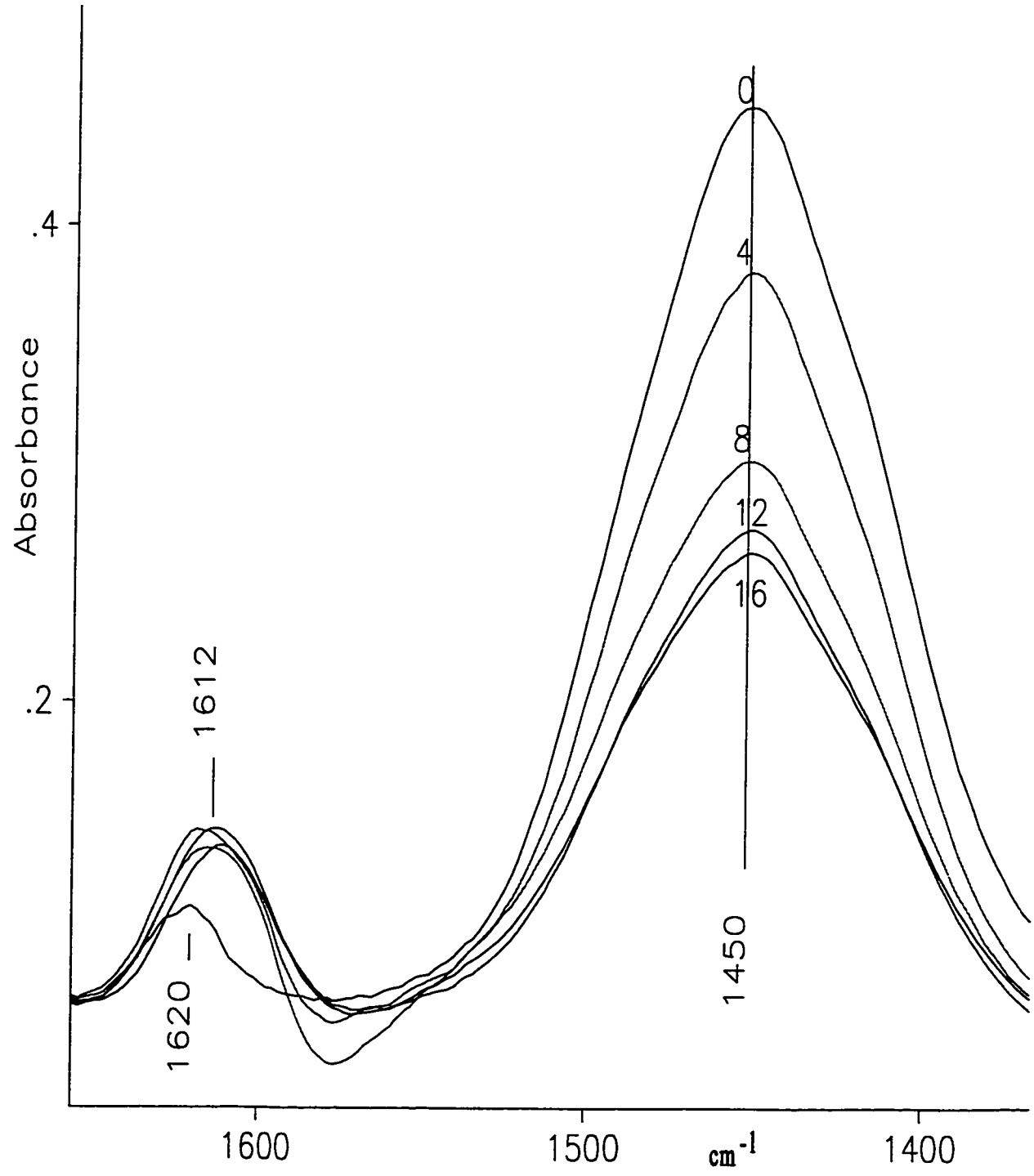

Figure 3.7 Room temperature infrared spectra of chemisorbed NH_3 on YSA catalysts containing 0-16 wt. percent yttria activated at 150°C.

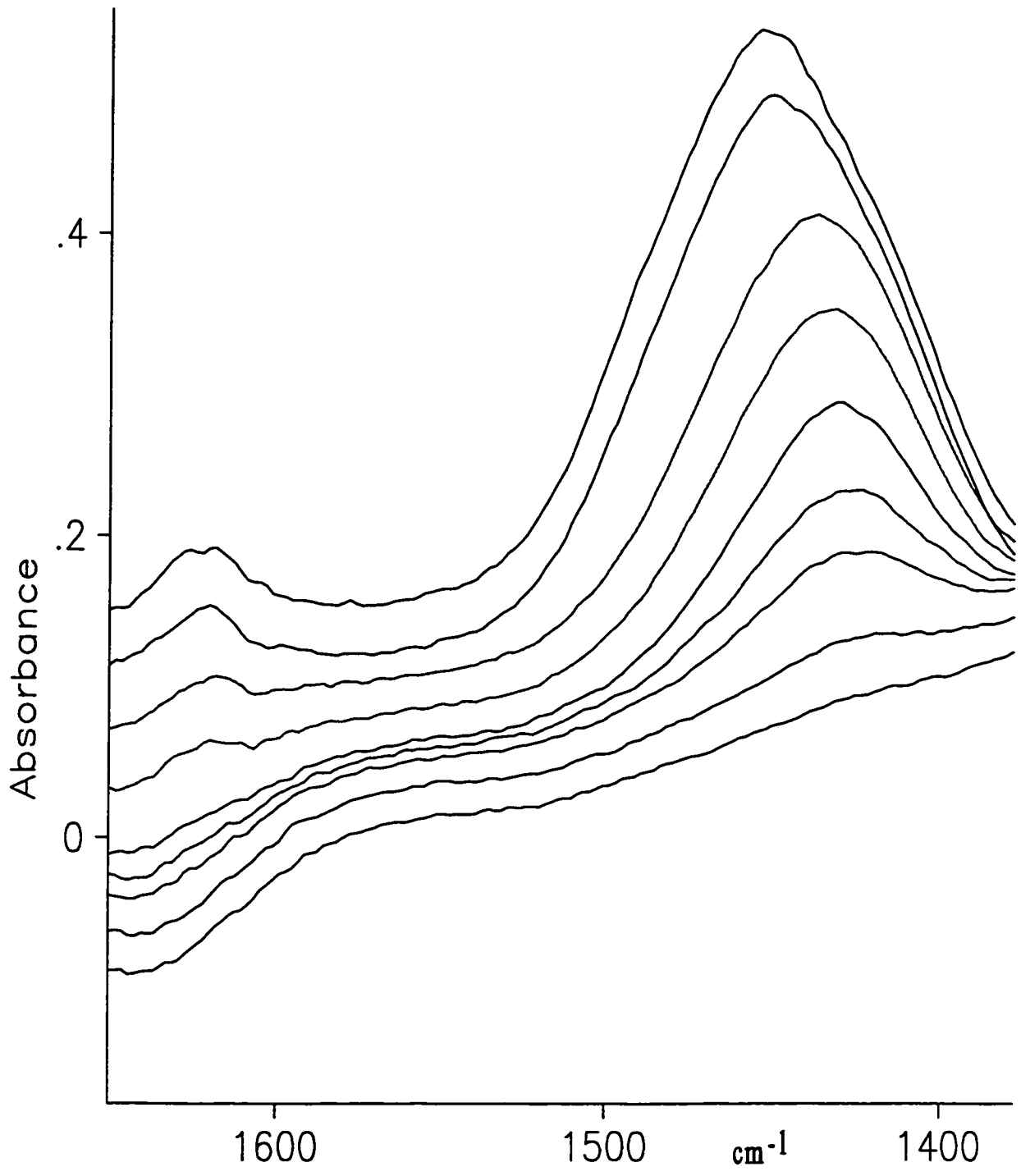

Figure 3.8 0% YSA NH_3 IR/TPD plots; the top curve is that which is shown for chemisorbed NH_3 at room temperature (Figure 3.7). The subsequent spectra, moving downward, show the spectra observed as a function of increasing temperature while evacuating the sample.

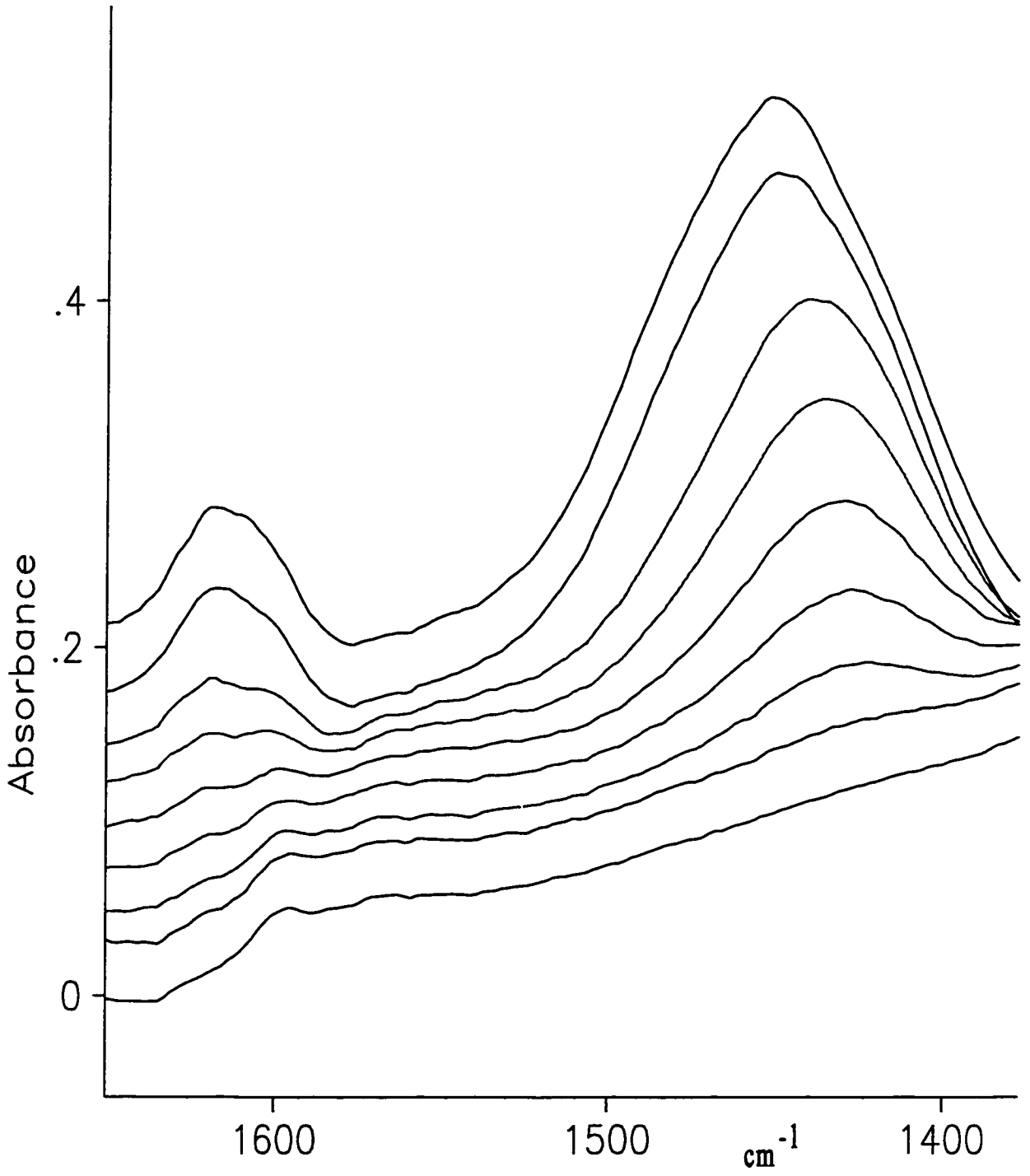

Figure 3.9 4% YSA NH_3 IR/TPD plots; the top curve is that which is shown for chemisorbed NH_3 at room temperature (Figure 3.7). The subsequent spectra, moving downward show the spectra observed as a function of increasing temperature while evacuating the sample.

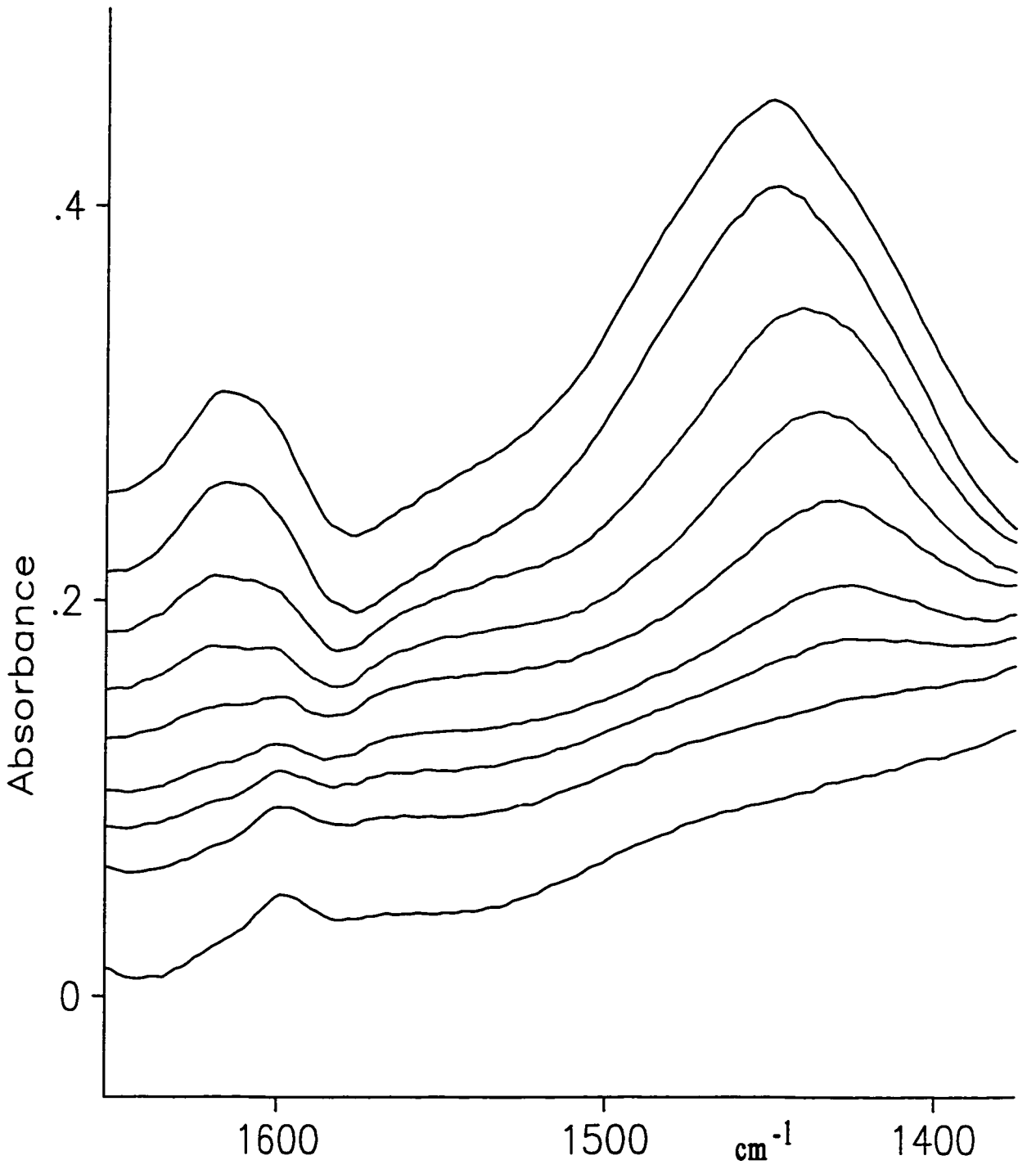

Figure 3.10 8% YSA NH_3 IR/TPD plots; the top curve is that which is shown for chemisorbed NH_3 at room temperature (Figure 3.7). The subsequent spectra, moving downward show the spectra observed as a function of increasing temperature while evacuating the sample.

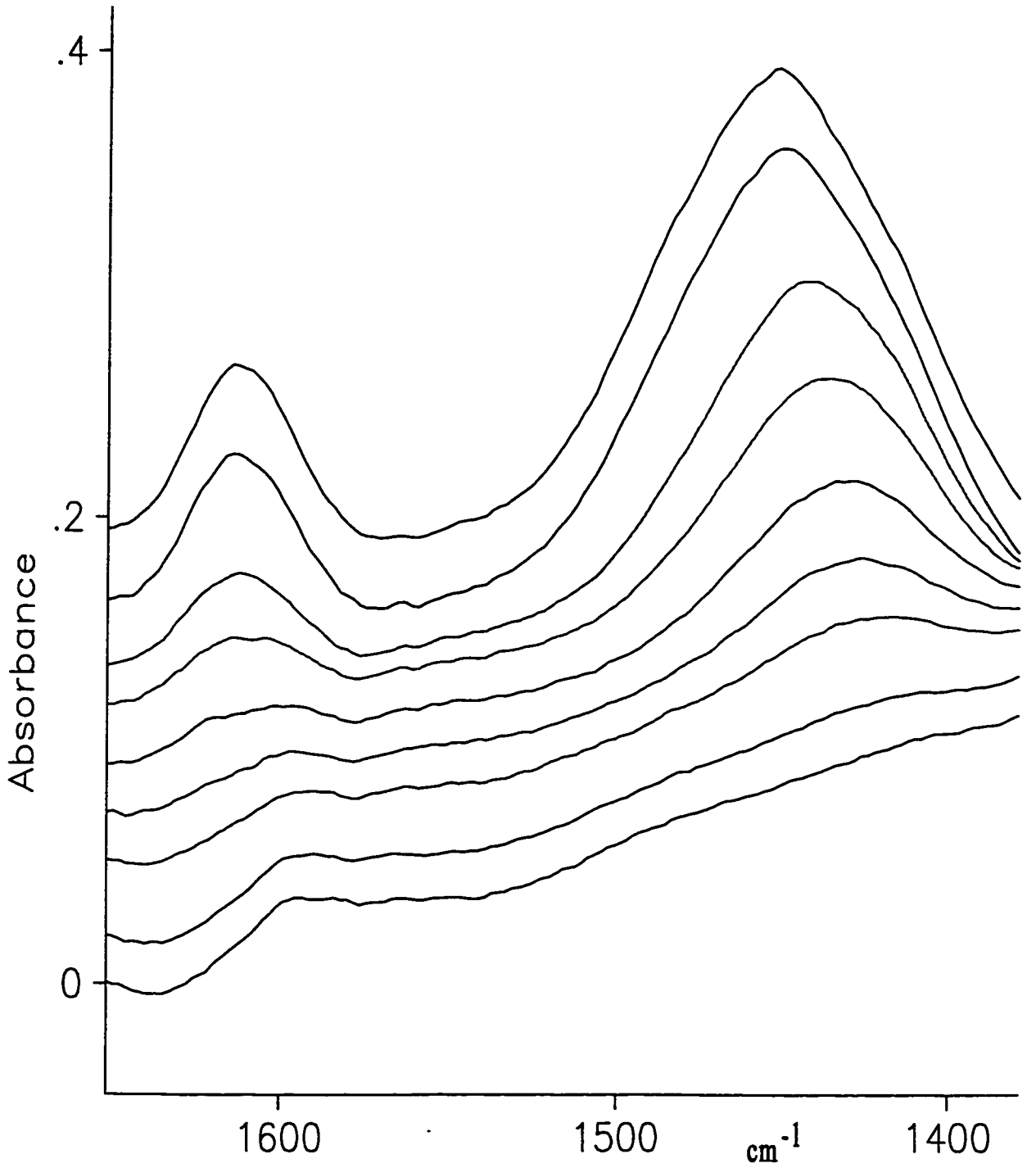

Figure 3.11 12% YSA NH_3 IR/TPD plots; the top curve is that which is shown for chemisorbed NH_3 at room temperature (Figure 3.7). The subsequent spectra, moving downward, show the spectra observed as a function of increasing temperature while evacuating the sample.

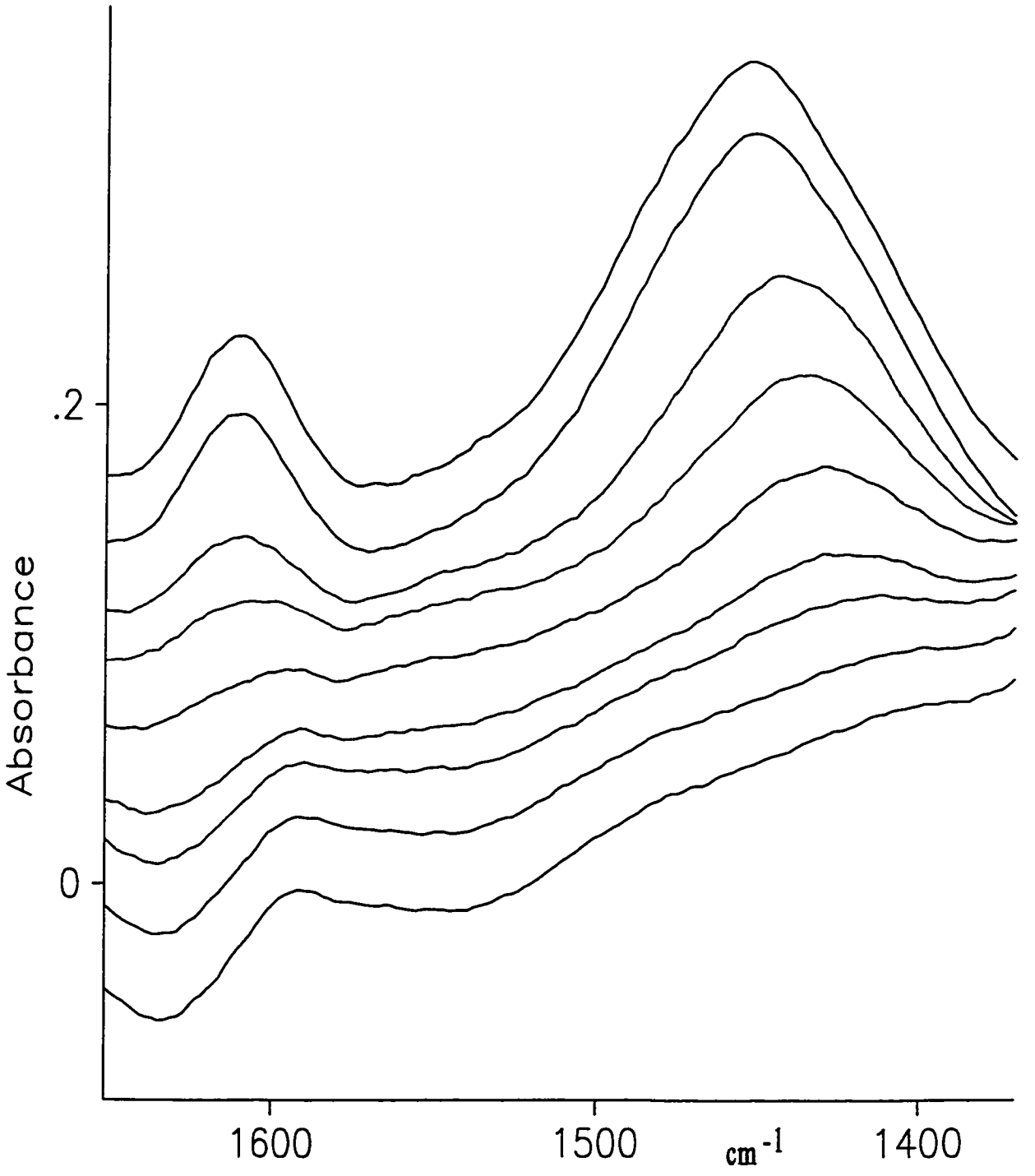

Figure 3.12 16% YSA NH_3 IR/TPD plots; the top curve is that which is shown for chemisorbed NH_3 at room temperature (Figure 3.7). The subsequent spectra, moving downward, show the spectra observed as a function of increasing temperature while evacuating the sample.

3.3 *PYRIDINE (C_5H_5N) ADSORPTION*

Pyridine (Py), like NH_3 has been widely used for studying the surface acidity for solid oxides using IR spectroscopy [12-17]. Although the two molecules have been used to probe similar surface properties, they do have their differences. The molecular cross sectional area of NH_3 is 0.127 nm^2 whereas that of Py is 0.313 nm^2. As discussed in section 1.4 the pK_a of Py is about 5 whereas that of NH_3 is about 9 [12]. Hence Py, which is both a larger molecule and a weaker base than NH_3, may not be able to access certain acidic sites due to steric hindrance, and may not be a suitable probe for weak solid acid sites that would normally react with NH_3. However, it turns out that Py can be more useful than NH_3 as a probe for Lewis acid sites.

As in the case of NH_3, Py has a lone pair of electrons on the nitrogen atom. Therefore, we expect it to coordinate to Lewis acid sites, to be protonated to Brønsted acid sites and to H-bond to OH groups; all of these forms can be easily identified [13-17] by studying the Py ring vibrations in the 1700-1400 cm^{-1} spectral region.

The ring vibrational modes ν_{19b} ($\nu_{CC(N)}$) and ν_{8a} ($\nu_{CC(N)}$) are the most sensitive vibrations with regards to the nature of intermolecular interactions via the nitrogen lone pair. These two modes are observed at 1440-1447 cm^{-1} and 1580-1600 cm^{-1} for H-bonded or physisorbed Py, at 1535-1550 cm^{-1} and near 1640 cm^{-1} for PyH^+, and at 1447-1464 cm^{-1} and 1600-1634 cm^{-1} for coordinated Py. The observation of a band at about 1540 cm^{-1} is a clear indication of the presence of the pyridinium ion and is a unique indication of Brønsted acidity on oxide catalysts. This band is due to the combined C-C stretching and in-plane C-H and N-H bending modes and, therefore, cannot be present in coordinately bound Py since the N^+-H bending motion is involved in the vibration. Hence there must be proton transfer to the nitrogen in order to observe this band [14,17]. There are two other weaker Py ring modes which absorb in this spectral region, ν_{19a} and ν_{8b} which will be discussed further below in the context of the observed spectra.

Figures 3.13 and 3.14 show a series of IR spectra for Py chemisorbed on the various YSA catalysts which have been activated at 150 and 450°C respectively. In both sets of experiments about 3 Torr of Py was added at room temperature to the activated samples prior to evacuation at 100°C for 1 h. This evacuation was used because that ensures that all physically adsorbed or hydrogen-bonded Py can be removed, as evidence by the disappearance of characteristic strong IR bands near 1580 cm^{-1} which are indicative of the presence of these species. Therefore, the observed spectra are solely due to coordinated and protonated Py on the surface. It is to be noted that there is a clear doublet in the 1445-1456 cm^{-1} spectral region and that there is the unique band due to protonated Py near 1545 cm^{-1}. There is a complex spectral profile in the region from 1640 to 1590 cm^{-1}. We will now discuss the rational for showing IR spectra after evacuation at 100°C.

As is documented in the literature, the pyridine adsorption experiment which is carried out under these circumstances is designed to probe the strong Lewis acid sites, those which are capable of retaining coordinated Py after evacuation at 100°C. The reason for using this procedure is that physically and H-bonded pyridine also have strong IR bands near 1450 cm^{-1} and near 1600-1580 cm^{-1}; these bands completely or partially overlap with those due to coordinated Py, and quantification of their relative intensities is difficult. This is a particularly serious problem in the 1450 cm^{-1} spectral region. In our case, the removal of all physically or H-bonded Py ensures that the IR bands observed in the 1450 cm^{-1} spectral region are only due to coordinated Py [protonated Py does not have a band in this spectral region].

In the spectrum of Py on pure silica-alumina, there is a band at 1456 cm^{-1} and at 1624 cm^{-1}; with increasing loading with yttria, the intensity of this band decreases as a new component appears at 1446 and 1606 cm^{-1} respectively. According to literature assignments, these bands are due to coordinated Py; the higher wavenumber band is due to coordination to Al, and lower one to Y. Table 3.3 shows the vibrational assignments for Py on the various catalysts, and includes the assignments for pure pyridine. The spectrum of pure Py is almost

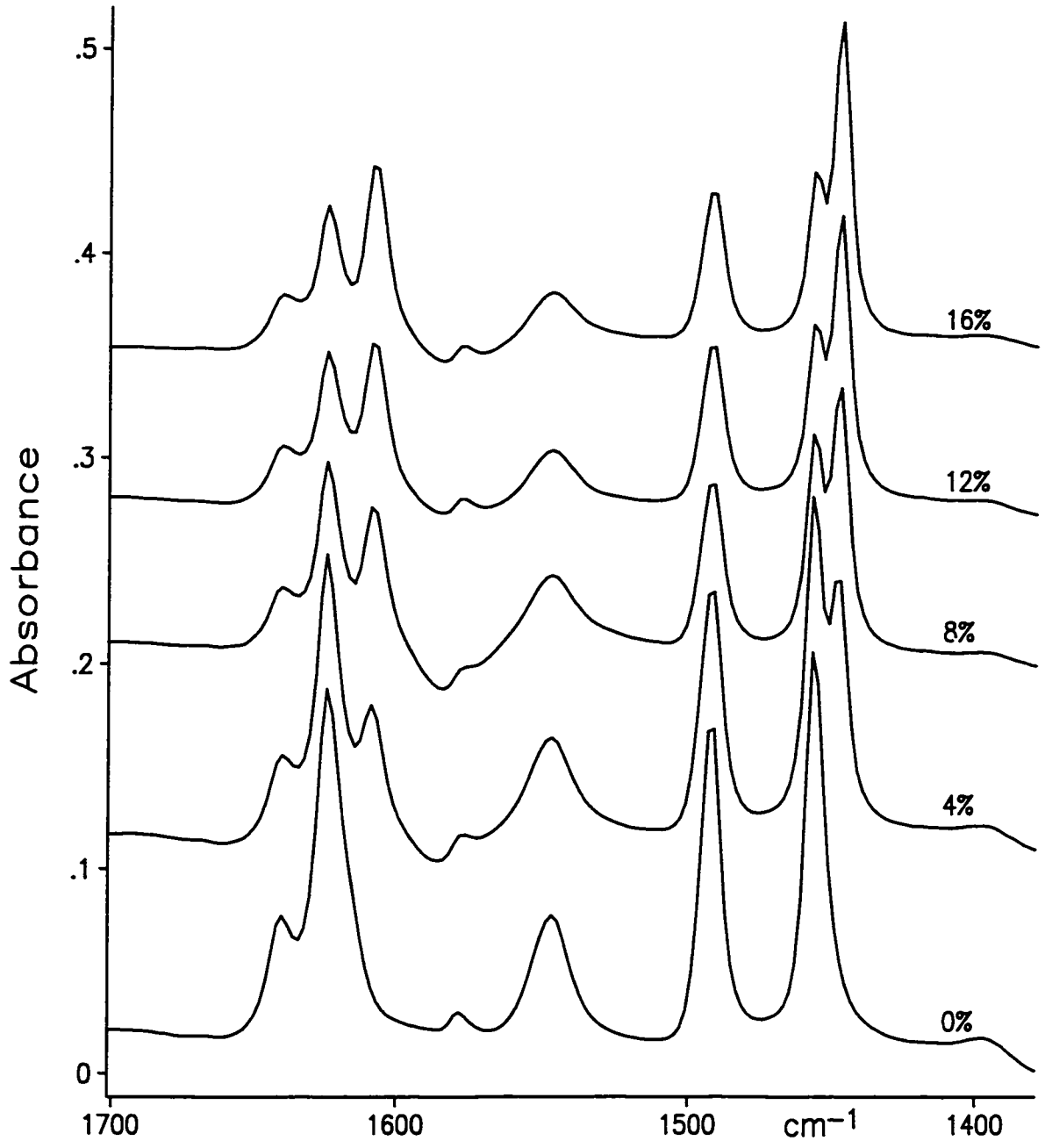

Figure 3.13 IR spectra of chemically adsorbed Py on 0-16% YSA activated at 150°C.

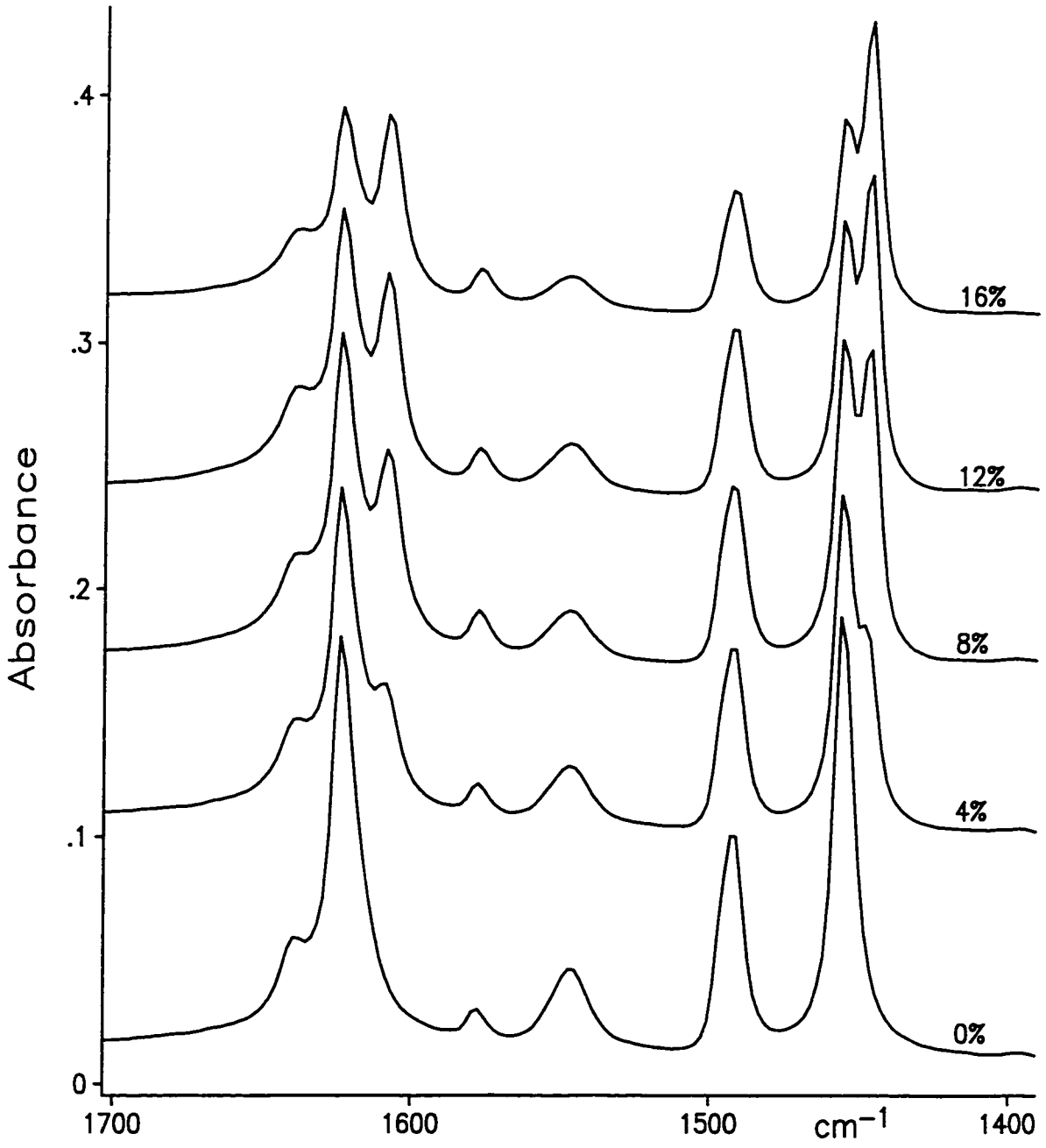

Figure 3.14 IR spectra of chemically adsorbed Py on 0-16% YSA activated at 450°C.

identical to that which results from H-bonded Py. All species give rise to a ν_{19a} band near 1490 cm^{-1}, so this band is not diagnostic of the species present. Coordinated and physisorbed or H-bonded pyridine give a very weak ν_{8b} band near 1572-1578 cm^{-1}, and again this region is not diagnostic. Between 1600 and 1640 cm^{-1} coordinated Py has its ν_{8a} mode for each form, and PyH^+ has its ν_{8a} and ν_{8b} modes. Therefore, because there are four overlapping IR bands in the 1600-1640 cm^{-1} spectral region it is difficult to extract quantitative information regarding the number of Py molecules which are coordinated to Y or Al Lewis acid sites.

Table 3.3 The assignments of Py chemically adsorbed on YSA catalysts/cm^{-1}.

$\nu_{CC(N)}$ species	*Py	BPy	LPy (Al^{3+})	LPy (Y^{3+})
8_a	1580	1640	1624	1606
8_b	1572	1610	1578	1578
19_a	1482	1490	1490	1490
19_b	1439	**1547**	**1451**	**1446**

*gas phase Py assignments [3].

This problem of overlapping of bands of various species does not occur in the region around 1450 cm^{-1} where the two observed bands are *unique* to Py coordinated to either Al or Y. It has been possible to deconvolute these bands using a mixed 70% Lorentzian 30% Gaussian sum function, deemed in many cases to be a suitable combination for IR band shapes [18]. A sample curve fit for the 12% YSA catalyst after activation at 450°C is shown in Figure 3.15. In each case, an equally good 'fit' to the experimental data was obtained. [This is an exceptional instance where curve fitting can reliably be used; physical grounds tell us that there should only be two IR bands in this region, the signal to noise ratio is very high, and a very good fit using accepted mathematical functions can be achieved].

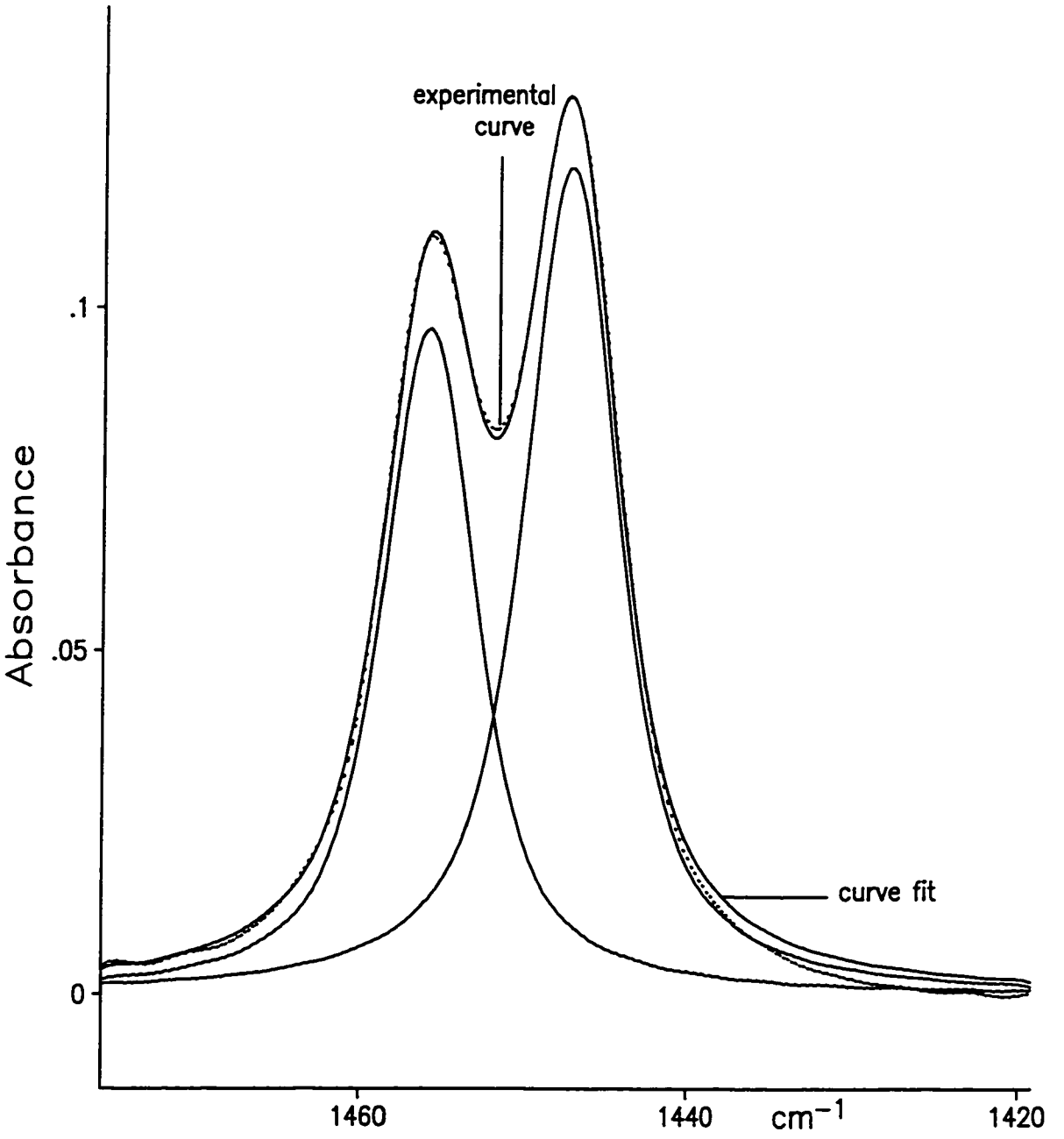

Figure 3.15 Curve fit for 12% YSA activated at 450°C for two bands characteristic of Py coordination to Al (1456 cm^{-1}) or Y (1446 cm^{-1}).

The areas of each component of the fit were obtained. These results are displayed in two ways. For the 450°C activated catalysts, Figure 3.16A shows a plot of the areas of the peaks due to Al and Y Lewis sites (that is, the intensities of the bands due to Py coordinated to Al or Y) as a function of Y loading. Figure 3.16B shows a plot of the area of the 1446 cm^{-1} peak divided by that of the 1456 cm^{-1} peak (that is, the Y:Al ratio) as a function of Y loading. Figure 3.17 shows the similar curves for 150°C activated samples. In both cases, there is a clear and obvious indication that as the yttria content increases the number of aluminum sites available for coordination decreases while those for coordination to Y increases. The near linearity of the plot in Figure 3.17B suggests a 1:1 correlation and may be coincidence. The correlation is less pronounced for the 450°C activated samples.

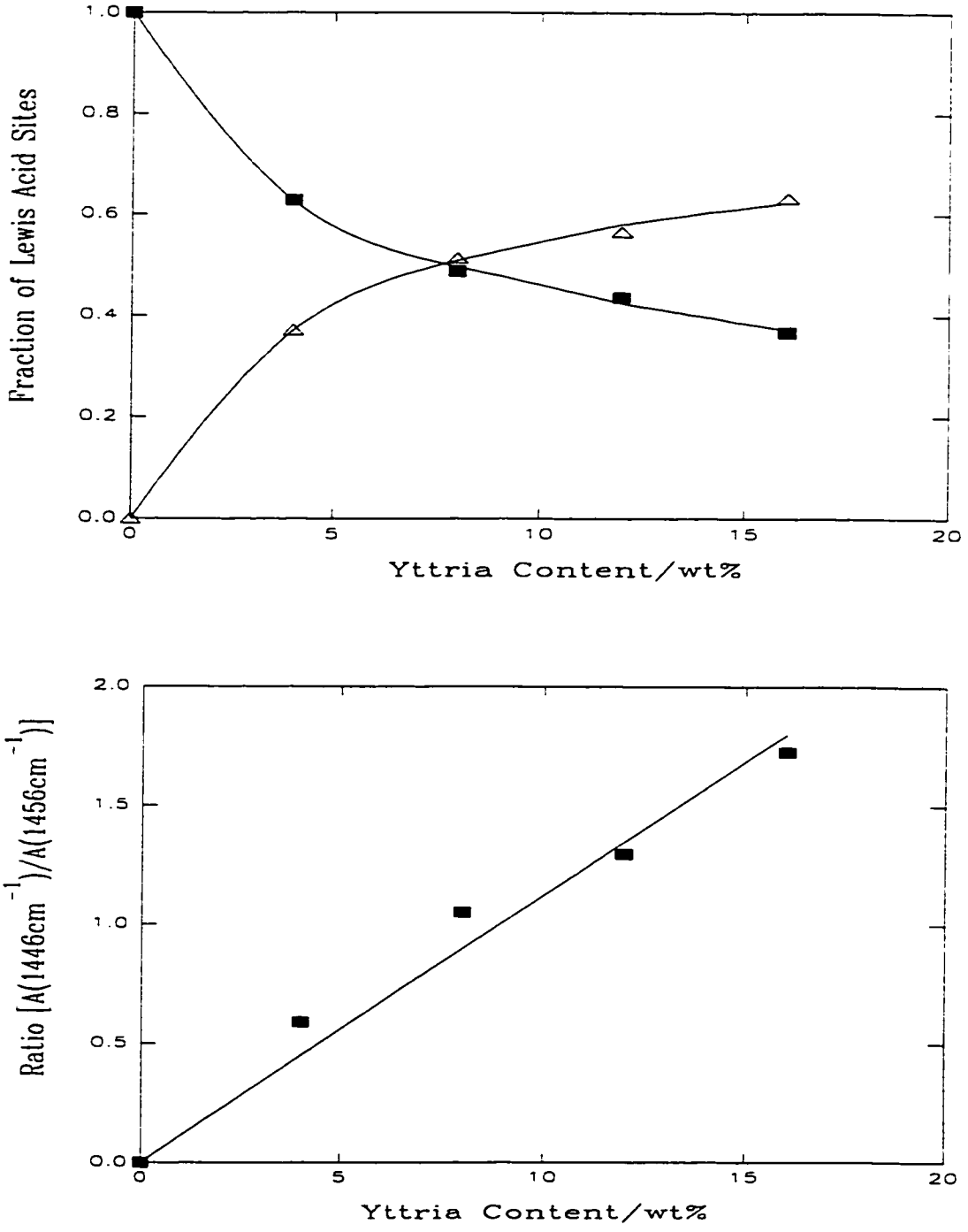

Figure 3.16 **A** *(top)* areas of the peaks due to Al(■) and Y(Δ), and **B** *(bottom)* ratio of intensity of the Lewis acid peaks, Y/Al, as a function of yttria loading on YSA activated at 450°C.

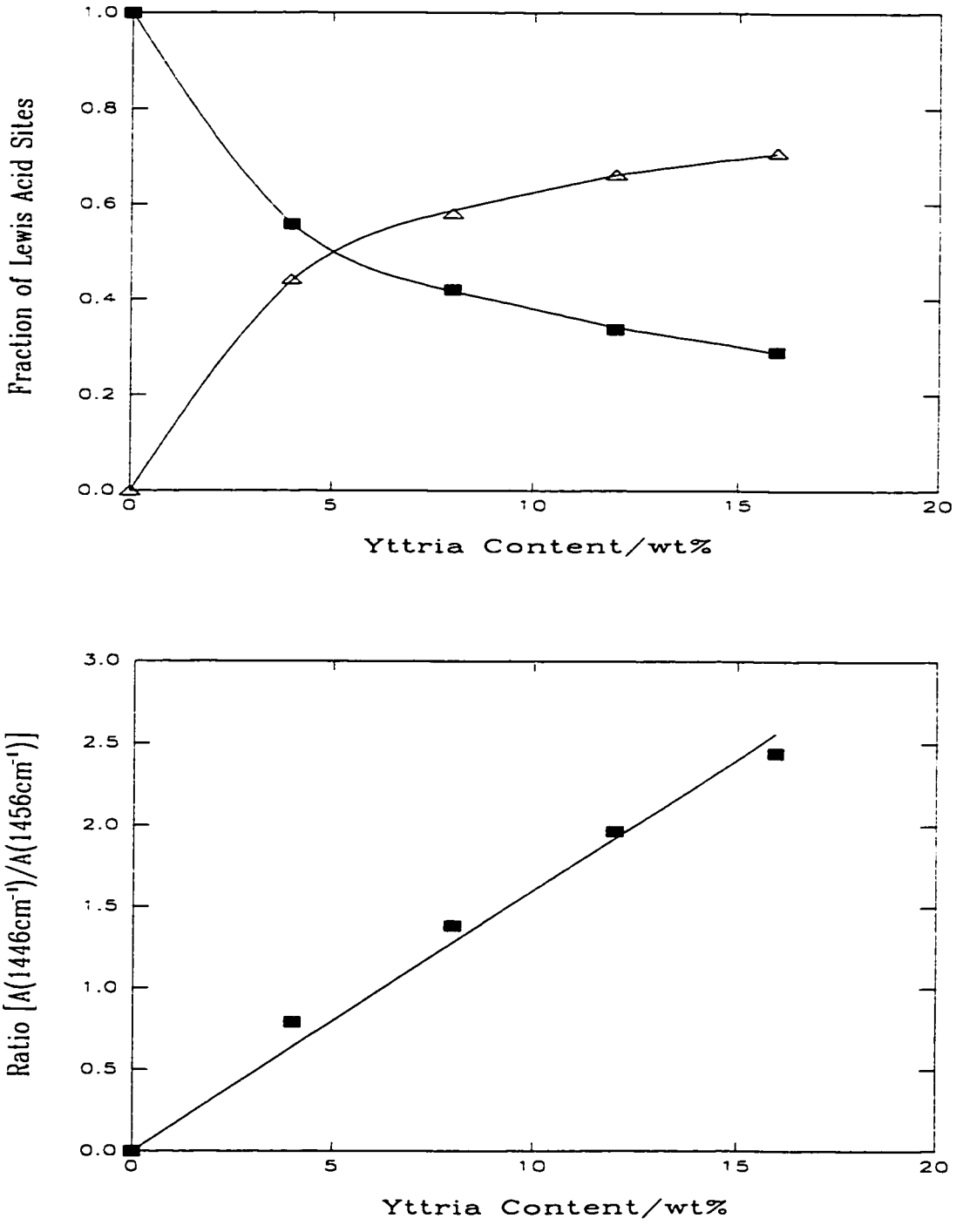

Figure 3.17 **A** *(top)* areas of the peaks due to Al(■) and Y(Δ), and **B** *(bottom)* ratio of intensity of the Lewis acid peaks, Y/Al, as a function of yttria loading on YSA activated at 150°C.

The intensity of the single peak at 1540 cm^{-1} gives a relative measure of the number of Brønsted acid sites as a function of yttria loading. It is difficult to quantify this intensity precisely because (a) the peak itself is quite weak, and (b) there is some subjectivity in the choice of the background on either side of this peak in this spectral region. An examination of Figures 3.18 and 3.19 show that as the yttria loading increases, the intensity of this peak decreases. Table 3.4 shows the relative intensities of this peak, for 450 and 150°C activation, setting the intensity for the pure SA (0% Y) to 100.

Table 3.4 The relative intensities of the 1540 cm^{-1} peak as a function of temperature at different yttria loadings.

% Y	450 °C	150 °C
0	100	100
4	74	73
8	63	54
12	59	41
16	41	36

These numbers have a considerable margin of error not only for the reasons stated above, but also because each sample, although nominally of the same mass, the optical 'thickness' is expected to be slightly inhomogeneous. Therefore, only the trend is important, and this shows a clear decrease in the number of sites capable of protonating pyridine as the yttria content increases.

The above results have demonstrated a unique ability of the use of Py as a probe of Lewis acid sites because of the splitting of the peak near 1450 cm^{-1} depending on whether Py

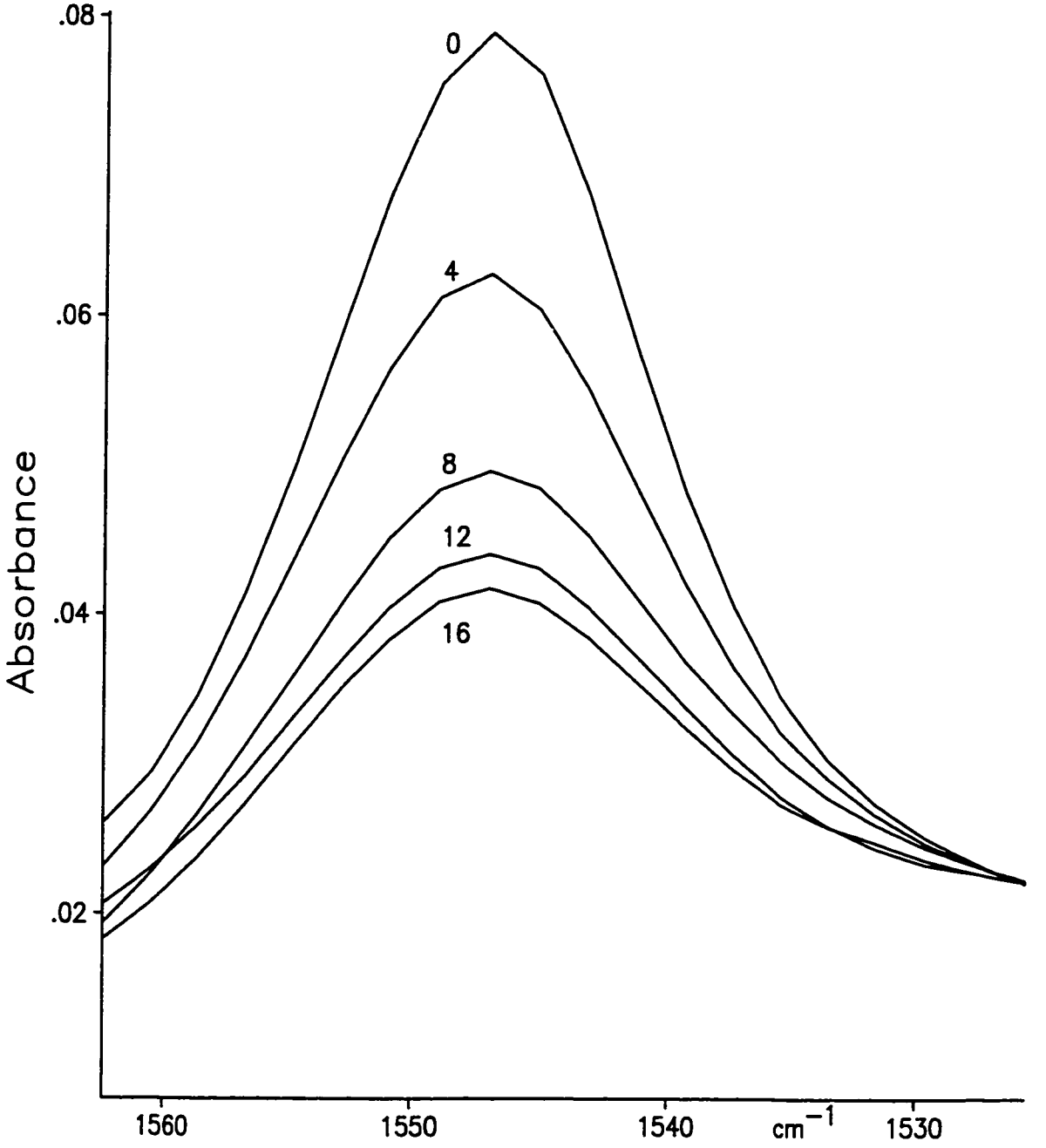

Figure 3.18 A relative measure of the number of Brønsted acid sites as a function of yttria loading (0-16%) for 150°C activated YSA catalysts.

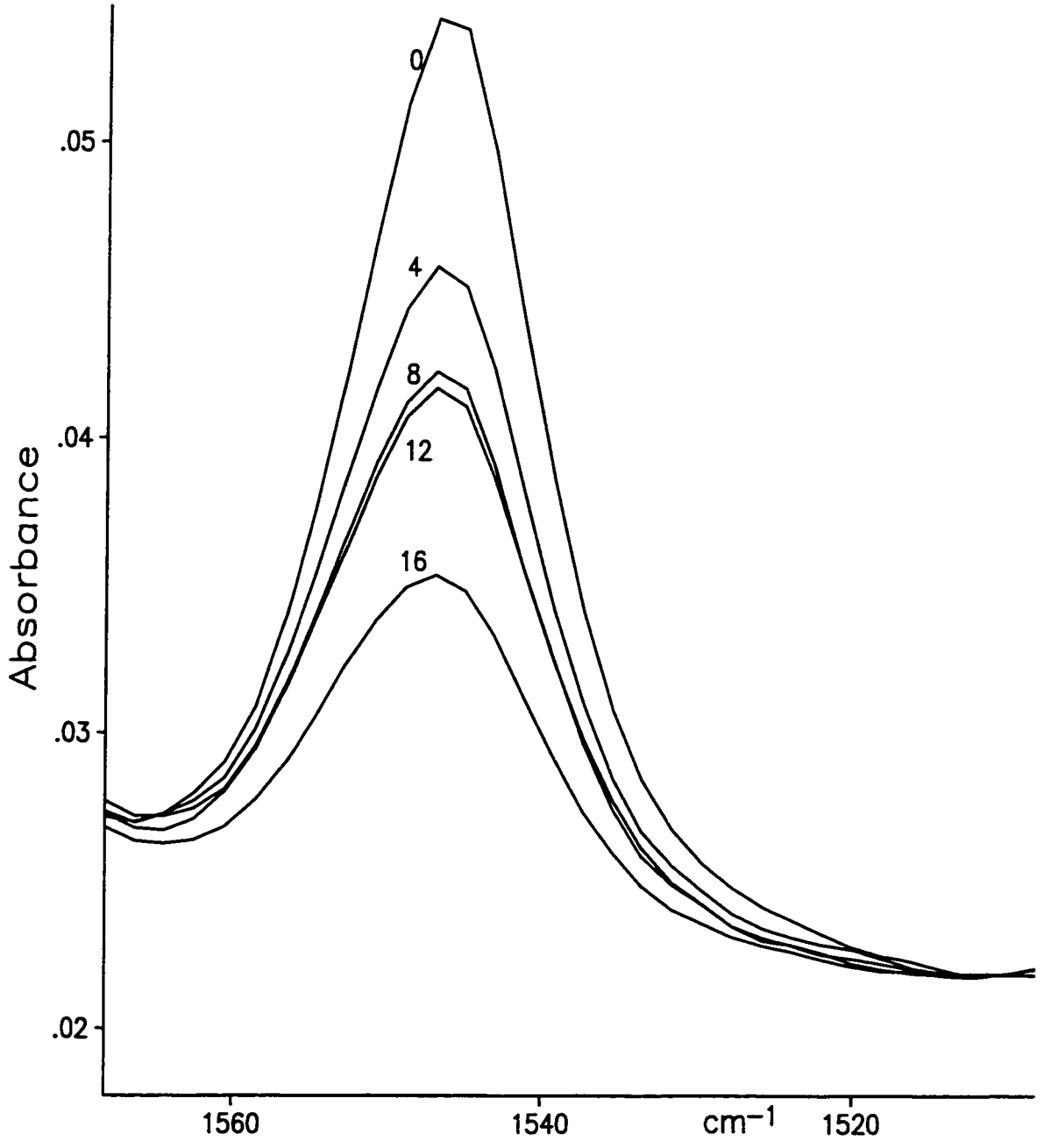

Figure 3.19 A relative measure of the number of Brønsted acid sites as a function of yttria loading (0-16%) for 450°C activated YSA catalysts.

is coordinated to Y or Al. This, to our knowledge, is the first time such data has been obtained using Py as a probe, and demonstrates a new aspect of its utility for probing mixed oxide catalysts. [The determination of the relative number of Brønsted acid sites using Py is routine]. The ability to discriminate between Y or Al Lewis acid sites can also be used to provide information regarding the dispersion of yttria over the catalyst surface as a function of the temperature of activation.

Figure 3.20 shows the IR spectra of adsorbed Py (as usual after adsorption and evacuation at 100°C) on 12% YSA as a function of the initial temperature of activation of the catalyst, this being at either 150, 300, 400, 500 and 600°C. Qualitatively, there is a decrease in the peak intensity due to protonated Py at 1547 cm^{-1} from 150 to 400°C activation and not much change thereafter. This is to be expected given that OH groups are removed from the surface as the temperature of activation increases. More significantly, however, is the striking change in the ratio of the intensities of the peaks at 1456 and 1446 cm^{-1} due to coordinated Py on Al or Y sites respectively. Figure 3.21 shows the analogous IR spectra for 4% YSA. As in the case of 12% YSA there is a decrease in the peak intensity due to protonated Py at 1547 cm^{-1} from 150 to 400°C and not much change afterwards as a result of dehydroxylating the surface at higher activation temperatures. As would be expected the peak 1446 cm^{-1} due to coordinated Py to Y sites is less intense than for 12% YSA; also this peak became less intense as activation temperature increased appearing merely as a shoulder to the 1456 cm^{-1} peak at 600°C activation. Interesting though is the fact that the 1456 cm^{-1} peak due to coordinated Py to Al sites remains more or less of the same intensity from 150 to 600°C activation. The proportion of Py coordinated to Al increases with the temperature of activation, and Figure 3.22 shows plots of the ratio of the band area of the 1446 cm^{-1} band to that of the 1456 cm^{-1} band (after deconvolution as done previously), that is, the Y/Al ratio for coordination of Py for 4 and 12% YSA.

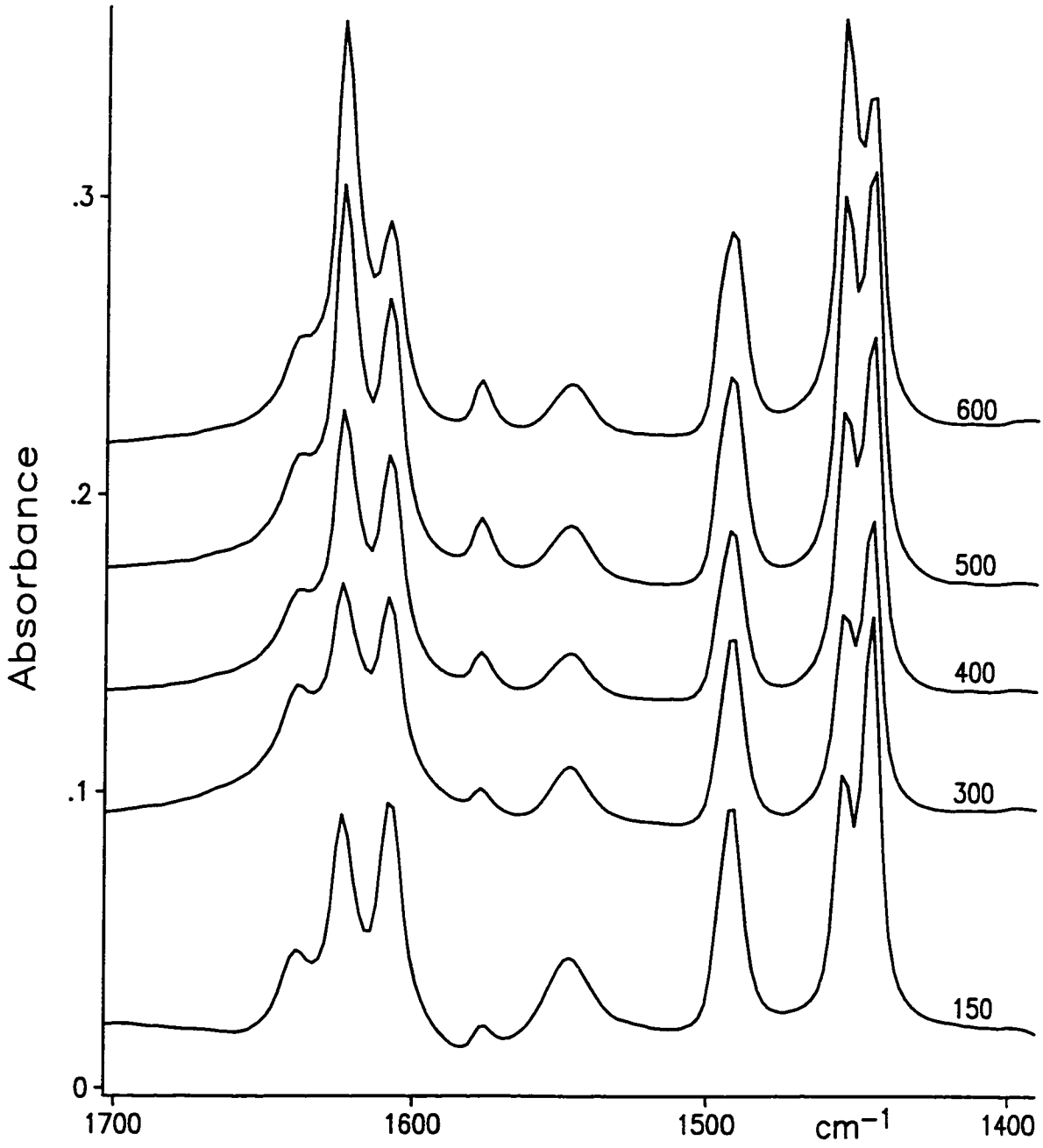

Figure 3.20 IR spectra of chemically adsorbed Py on 12% YSA as a function of initial activation temperature (shown at the side in degrees Celsius).

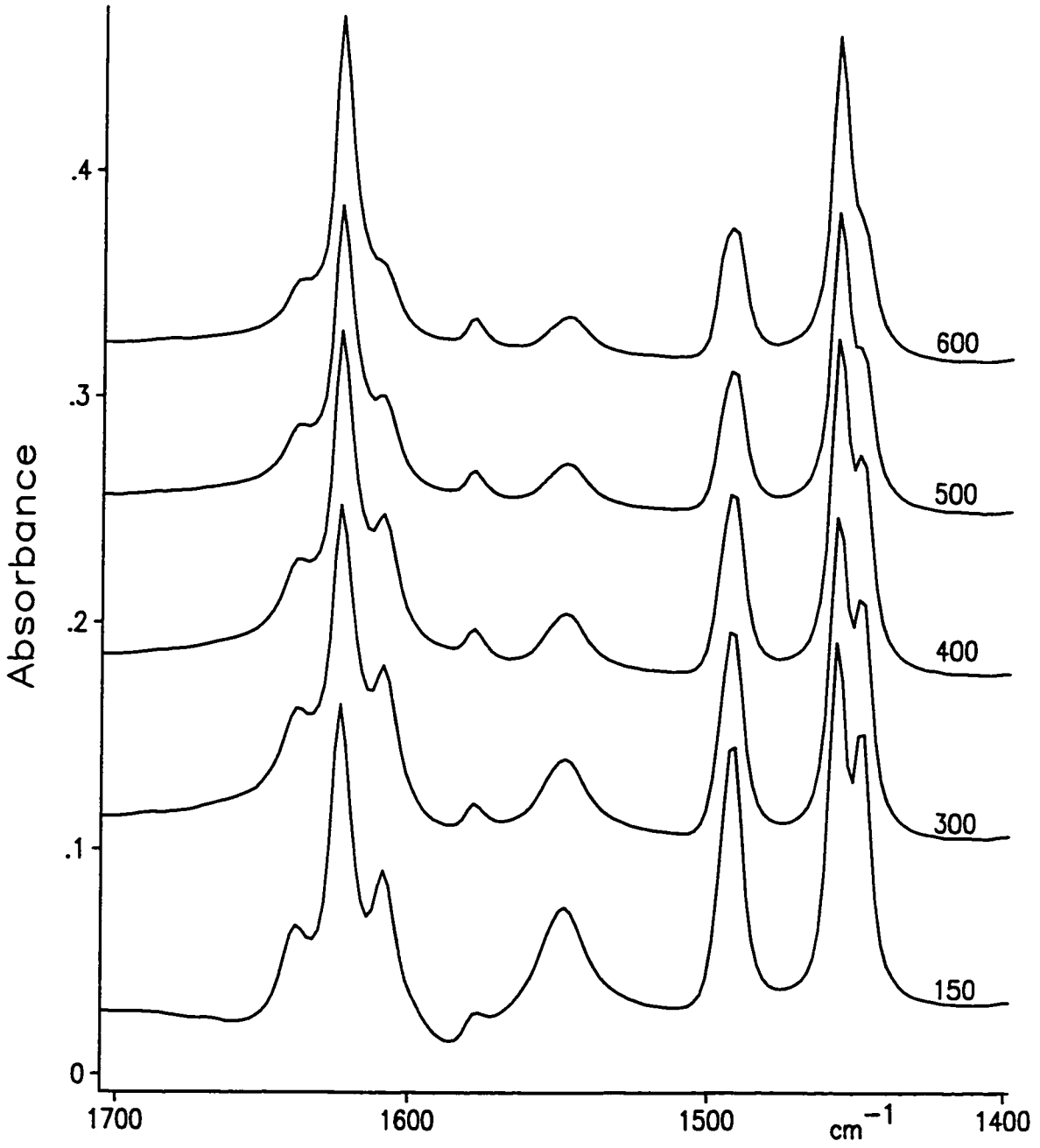

Figure 3.21 IR spectra of chemically adsorbed Py on 4% YSA as a function of initial activation temperature (shown at the side in degrees Celsius).

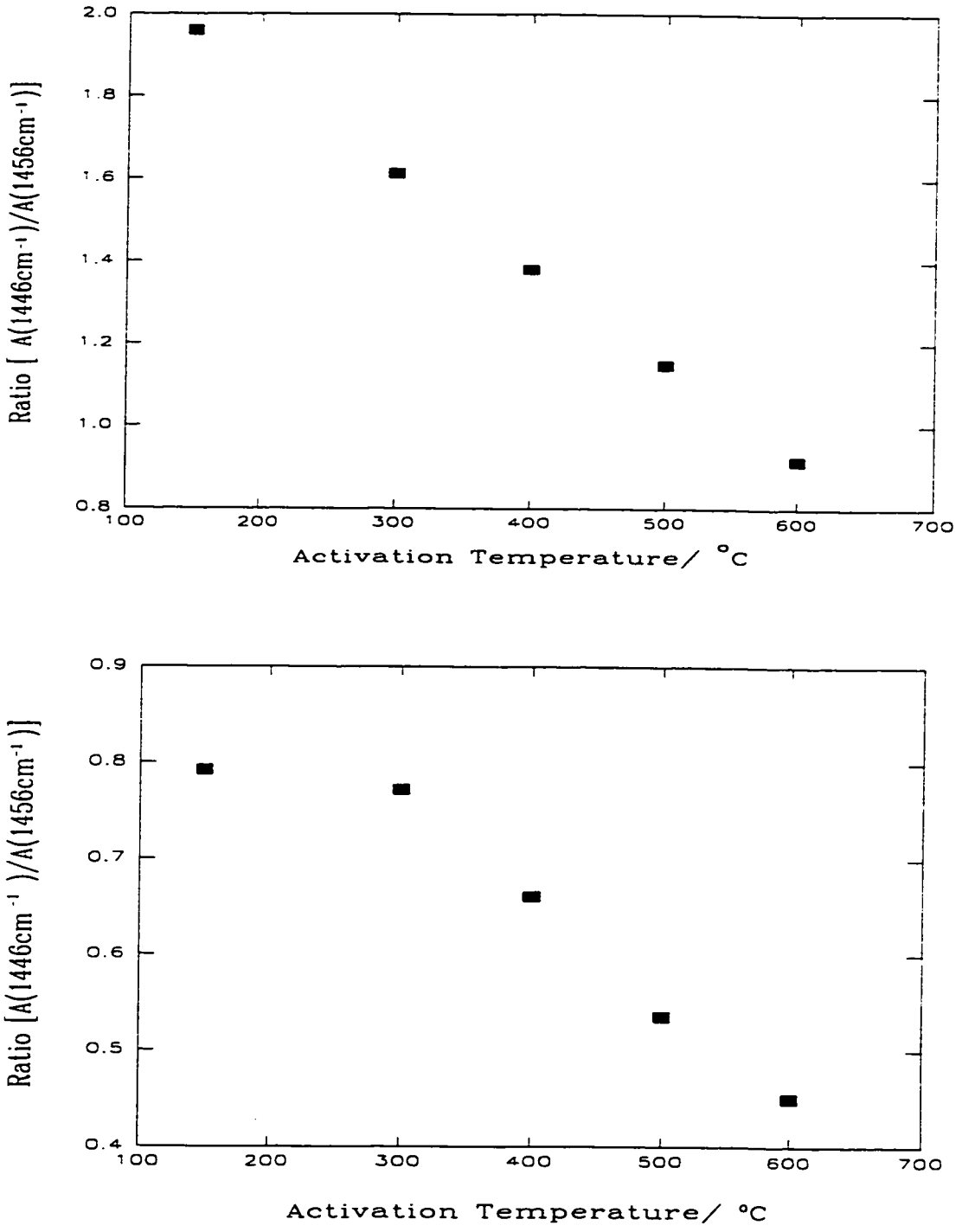

Figure 3.22 Ratio of intensity of the Lewis acid peaks, Y/Al, as a function of yttria loading on 12% YSA activated at different temperatures for **A** *(top)* 12% YSA and **B** *(bottom)* 4% YSA.

These results show that the number of Al atoms accessible to coordination of Py increases as the temperature of activation increases, and conversley, those available for coordination to Y decrease. In each experiment, a different sample was used, and the activation time at a given temperature was the same in each case. Given that the 4-16% YSA catalysts had been calcined for 2 hours at 500°C (and 0% YSA at 400°C) initially prior to activation under vacuum, the increase in the Al/Y ratio accessible to Py is probably related to diffusion of yttria into the bulk of the SA substrate during the high temperature activation. Therefore, fewer Y atoms and more Al atoms become accessible to Py as the temperature of activation increases.

It is apparent that a study of the time of activation on the ratio of Al/Y accessible to Py at a fixed temperature of activation should be carried out in order to test this hypothesis. As will be discussed in Chapter 6, there is compelling evidence that migration of surface species into the bulk of a substrate can occur even at room temperature, albeit slowly. Therefore, we have only studied this phenomonum for two samples, 4 and 12% YSA. Also, there is no compelling reason to expect the linear correlation shown in Figure 3.22A; this is probably coincidence and such a correlation was not found for the 4% YSA sample (Figure 3.22B). The diffusion of deposited Y_2O_3 into the bulk is probably entropy driven; a random mixing of Si, Al and Y is more probable than islands of yttria on a second substrate.

3.4 ACETONITRILE-d_3 (CD_3CN) ADSORPTION

Acetonitrile, CH_3CN has C_{3v} symmetry and there are 12 fundamental modes of vibration as well as various overtone and combination bands; these bands have been noted previously for CH_3CN [19-21] and its deuterated analog CD_3CN [20,22]. The nitrogen atom can coordinate to Lewis acid sites and this molecule has been used in the past as a probe for Lewis acidity. It is not a suitable probe of Bronsted acidity, pK_a for CH_3CNH^+ is -12 [23]. All

of the experiments reported below were carried out on YSA catalysts which had been activated at 450°C in vacuum.

In the C≡N spectral region, 2260-2350 cm^{-1}, the transmittance of oxides is usually high and interference from absorbate bands is thus minimized. Therefore, CH_3CN would appear to be a favourable probe for the study of Lewis acidity in oxide catalysts. However, due to Fermi resonance between the $\nu(C\equiv N)$ fundamental and $\delta_s(CH_3)$ + $\nu(C\text{-}C)$ combination bands of CH_3CN (1400 + 920 = 2320 cm^{-1}) the assignment of the bands in the C≡N spectral region is somewhat complicated [19,22,25-30]. Consequently, it is more common to use deuterated acetonitrile which does not have a combination mode in this spectral region.

The adsorption of CD_3CN on SiO_2-Al_2O_3 catalysts shows two distinct bands in the CN spectral region [22,28] (see Figure 3.23 0% YSA spectrum). There is a broad band with a maximum at 2273 cm^{-1} accompanied by a shoulder to lower wavenumber, and a second symmetrical broad band with a maximum at 2330 cm^{-1}. Liquid CD_3CN has its CN stretching mode at 2278 cm^{-1}. For CD_3CN adsorbed at the same pressure on pure silica there is a single strong IR band in this spectral region at 2276 cm^{-1}, and on alumina there are peaks at 2261 and 2334 cm^{-1}. Evacuation of the adsorbed species on SiO_2 or Al_2O_3 for 15 min. at 20°C resulted in removal of the bands near 2270-2260 cm^{-1}, but there was only a slight reduction in the intensity of the 2334 cm^{-1} peak in the case of Al_2O_3. Therefore, the doublet near 2274 cm^{-1} on 0% YSA and the shoulder to lower wavenumber is undoubtedly due to the H-bonding of CD_3CN to SiOH and AlOH groups respectively [22,31]. The peak near 2330 cm^{-1} corresponds to coordination of CD_3CN to Al Lewis acid sites on silica-alumina, which is at 2334 cm^{-1} for pure Al_2O_3 [22,28,31].

The adsorption of CD_3CN on pure yttria gave rise to IR bands at 2260 and 2284 cm^{-1}. The 2260 cm^{-1} band was readily removed by evacuation whereas that at 2284 cm^{-1} was only partially attenuated. The 2260 cm^{-1} band is due to H-bonded CD_3CN and that 2284 cm^{-1} is due to coordination. Further justification of this assignment will be given below.

The IR spectra of CD_3CN at a pressure of 5 Torr adsorbed on the various YSA catalysts is shown in Figure 3.23. Figure 3.24 shows the spectra after evacuation for 15 min. at room temperature. The unique additional feature which is not apparent in the spectrum of SA is the appearance of a new peak at 2294 cm^{-1}, the intensity of which increases as the percentage yttria increases.

In all spectra, the doublet which was observed initially at about 2275/2265 cm^{-1} was readily removed upon evacuation. These bands are apparently due to CD_3CN which is H-bonded to OH groups which are attached to either Si, Al or Y.

The band at 2330 cm^{-1} is certainly due to CD_3CN coordinated to Al. The intensity of this band decreases with increasing yttria loading. On the other hand, the band at 2294 cm^{-1} increases in intensity with the percent yttria loading and its wavenumber is close to that which was observed for coordination to pure yttria (2284 cm^{-1}); it can be assigned to CD_3CN coordinated to Y. Clearly, yttria blocks some of the Al sites previously available for coordination, and this will alter the overall acidity of the catalyst. These results are in accord with the results found from pyridine adsorption, but they are also qualitatively applicable to weak Lewis acid adsorption sites because the trends noted are applicable even in the presence of an excess of the reagent before evacuation.

When CD_3CN was adsorbed on YSA catalysts the $\nu(C\equiv N)$ mode shifted towards higher frequencies, *i.e.* from 2278 cm^{-1} (in liquid phase) to 2330 cm^{-1} when coordinated to Al or to 2294 cm^{-1} when coordinated to Y. The extent of the $\nu(C\equiv N)$ shift is said to depend on the strength of the interaction between the $C\equiv N$ fragment and the solid surface [22,25,27,32]. The CN stretching mode is sensitive to the electron withdrawing powers of metal cations to which the nitrile forms a coordination complex (adduct); thus resulting in an increase in the CN stretching frequency. With this in mind one would expect that the Lewis acid strength of

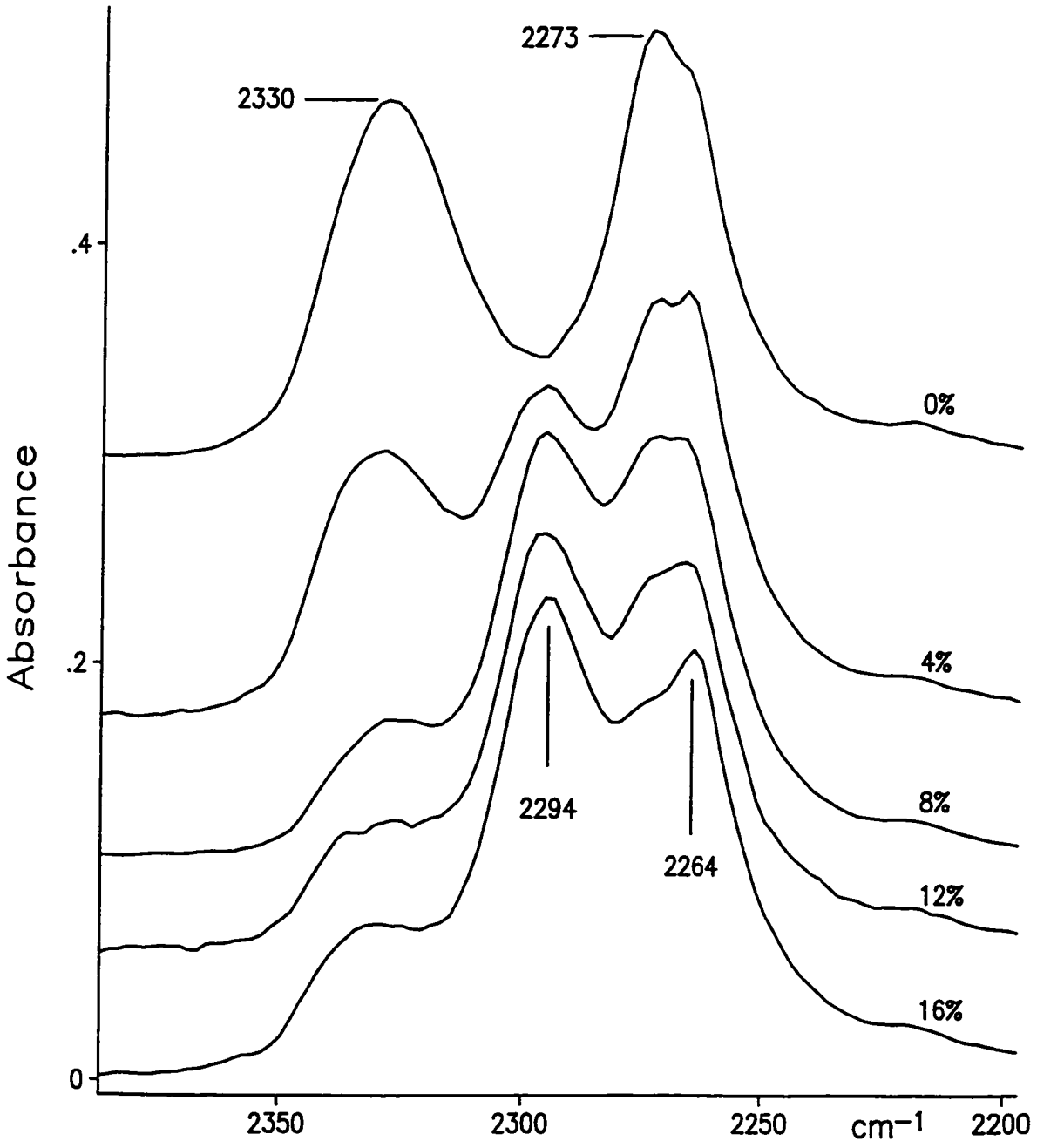

Figure 3.23 IR spectra in the CN stretching region for 5 Torr of CD_3CN in contact with the indicated YSA catalyst.

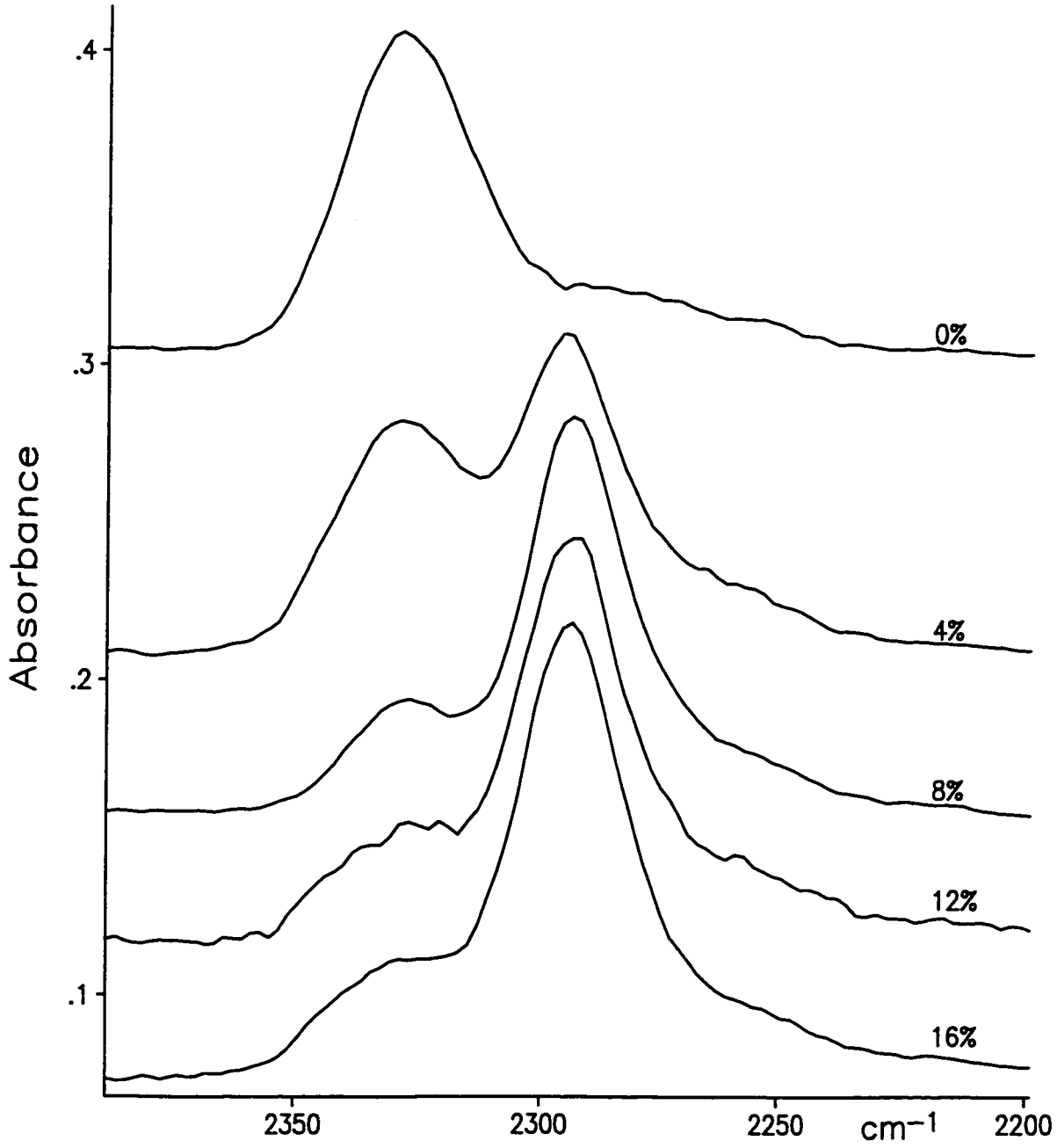

Figure 3.24 IR spectra as for Figure 3.23, but after evacuation of the adsorbed CD_3CN for 15 min. at room temperature.

the acceptors could be predicted from stretching frequency shifts. However, molecular orbital calculations have shown that *kinematic effects*, that is, the coupling of the adduct bond with the CN stretching vibration cannot be used to explain the increase in CN stretching frequency in its entirety [27]. It has been concluded that changes on coordination in the nitrogen 2s lone pair orbital (as well as nitrile interaction with OH groups) were responsible for the strengthening of the CN bond [25,27]. Further analysis of overlap energies indicated that stronger binding occurs with the CN σ system as a result of electron pair donation, and this effect, through an increase in CN force constant, explains the observed increase in $\nu(C\equiv N)$ upon coordination. The increased strength of the σ bonds arises from a greater dominant contribution from the donor atom s orbital [33] over the π orbital perturbation [34]; coordination at the more electronegative atom of the multiple bond weakens the π bonds due to an electron density shift toward the electron donor atom. Therefore, there exists π polarization of the C≡N bond and σ donation from the N lone pair. The increasing stabilization of the σ orbital offsets the increasing destabilization of the π orbitals.

In summary, it has been found that the C≡N frequency increases slightly as a result of kinematic coupling in C≡N→acid. The C≡N force constant has been shown to increase considerably upon coordination of acetonitrile and it is the major factor in the frequency increase. Molecular orbital calculations have provided further evidence to this end. Hence the N_{2s} orbital, in overlapping the C_{2s} and $C_{2p\sigma}$ orbitals, is responsible for the observed strengthening of the C≡N bond upon coordination of CD_3CN to Lewis acids [35].

The analogous IR/TPD experiments which were carried out for adsorbed NH_3 were not performed in the case of adsorbed CD_3CN. However, by heating each catalyst at 50°C intervals up to 300°C for a fixed time of 15 min. insight was gained into the thermal stability of the Al and Y coordinated species. Figures 3.25-3.29 show the resulting spectra for the YSA catalysts.

The purpose of these experiments was to determine whether the extent of Y_2O_3 loading had an effect on the thermal stability of CD_3CN coordinated to Al or Y. The results are insignificant in terms of TPD. Nevertheless the following trends were observed: (1) Heating to 250°C was sufficient to remove all adsorbed species from 8, 12 and 16% YSA catalysts, but higher temperatures of 300°C were required for 0 and 4% YSA samples. (2) The ratio of the intensity of the peaks at 2294 and 2330 cm^{-1} for CD_3CN coordinated to Y or Al decreased at higher temperatures of evacuation, which suggests that coordination to Y is weaker than to Al.

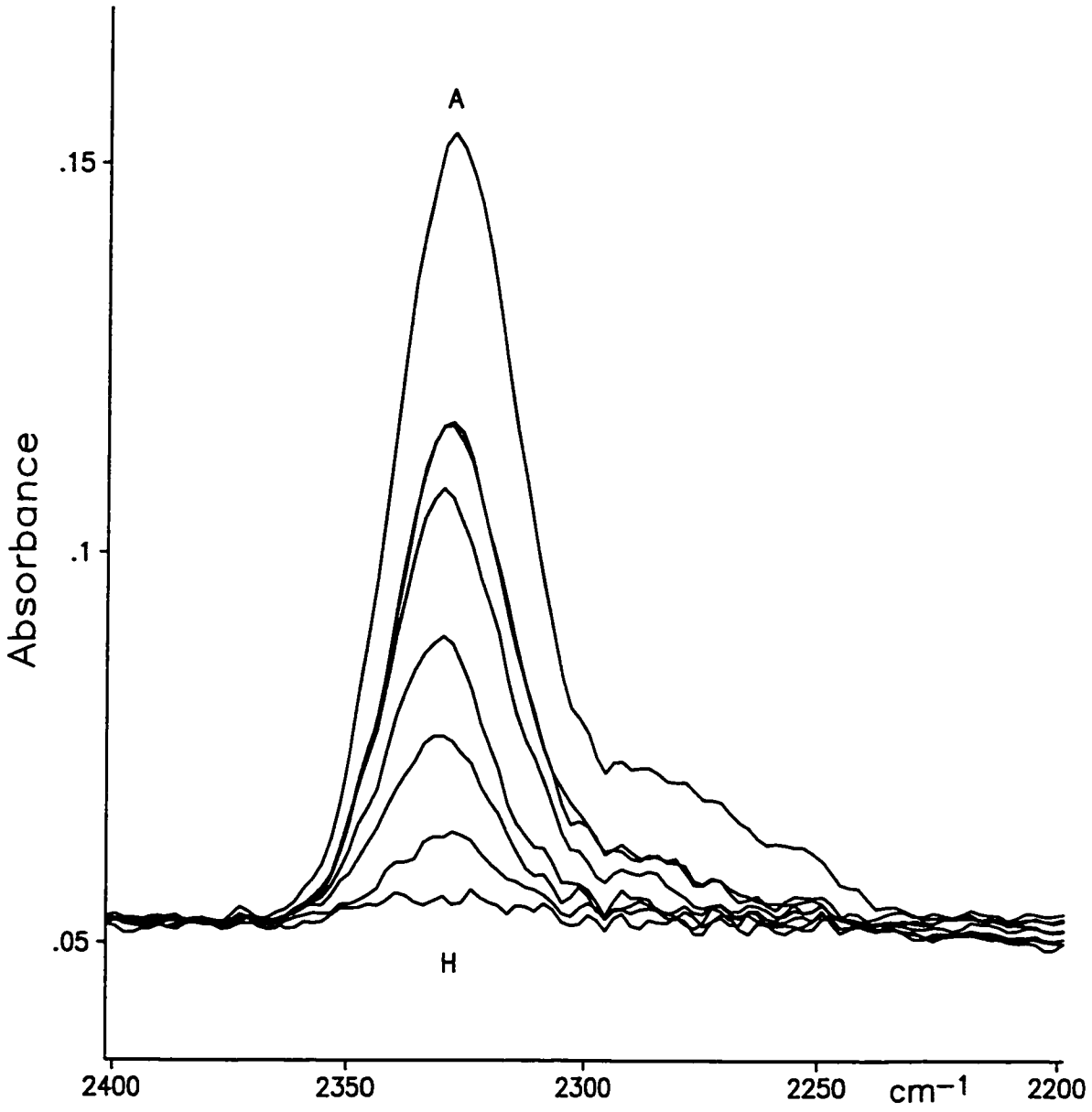

Figure 3.25 Spectrum **A** is the same IR spectrum as shown in Figure 3.24 for the 0% YSA catalyst. The subsequent spectra of decreasing intensity were observed after: **B** evacuation overnight; **C-H** evacuation 15 min. at: 50, 100, 150, 200, 250, and 300°C, respectively.

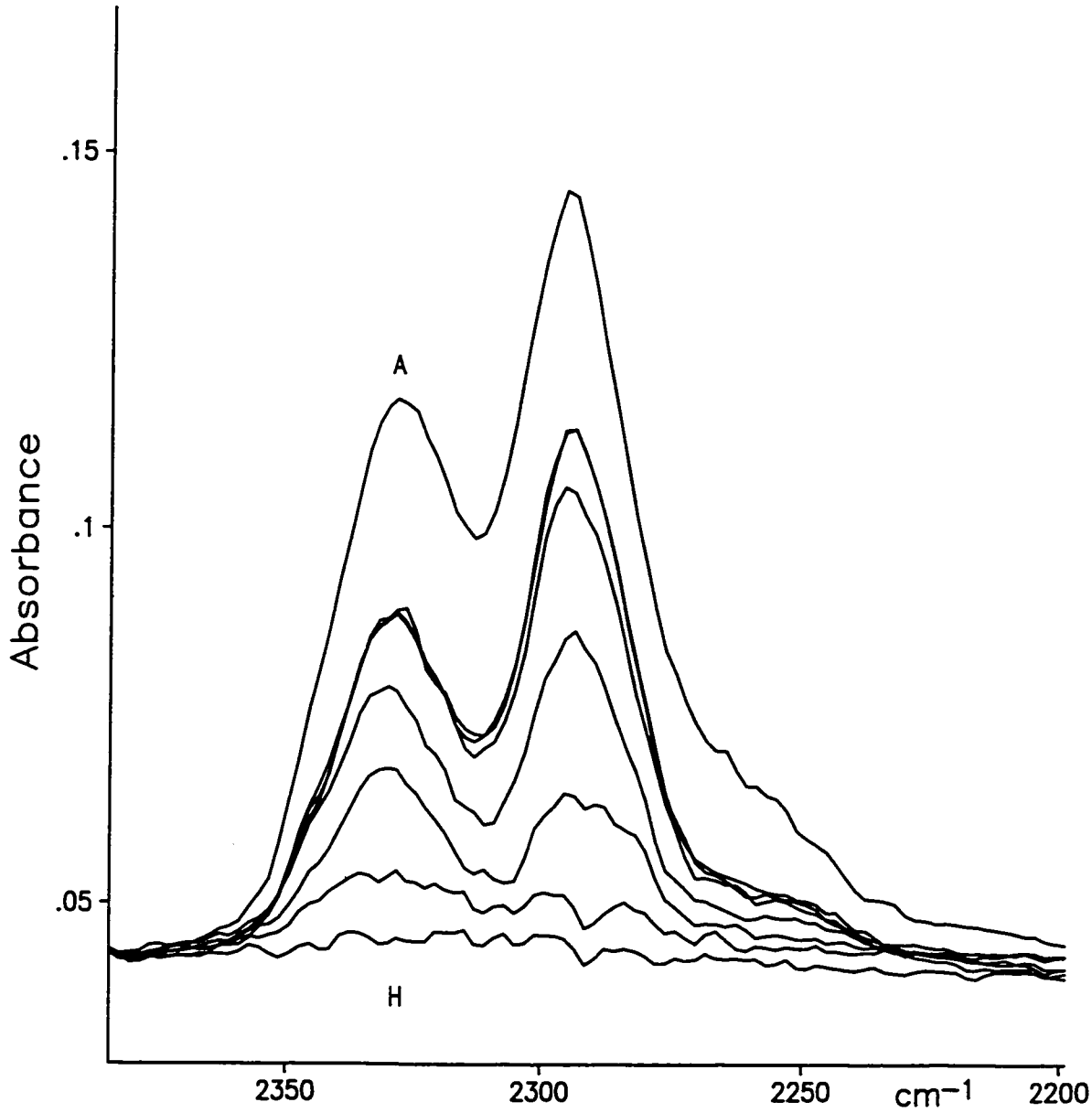

Figure 3.26 Spectrum **A** is the same IR spectrum as shown in Figure 3.24 for the 4% YSA catalyst. The subsequent spectra of decreasing intensity were observed after: **B** evacuation overnight; **C-H** evacuation 15 min. at: 50, 100, 150, 200, 250, and 300°C, respectively.

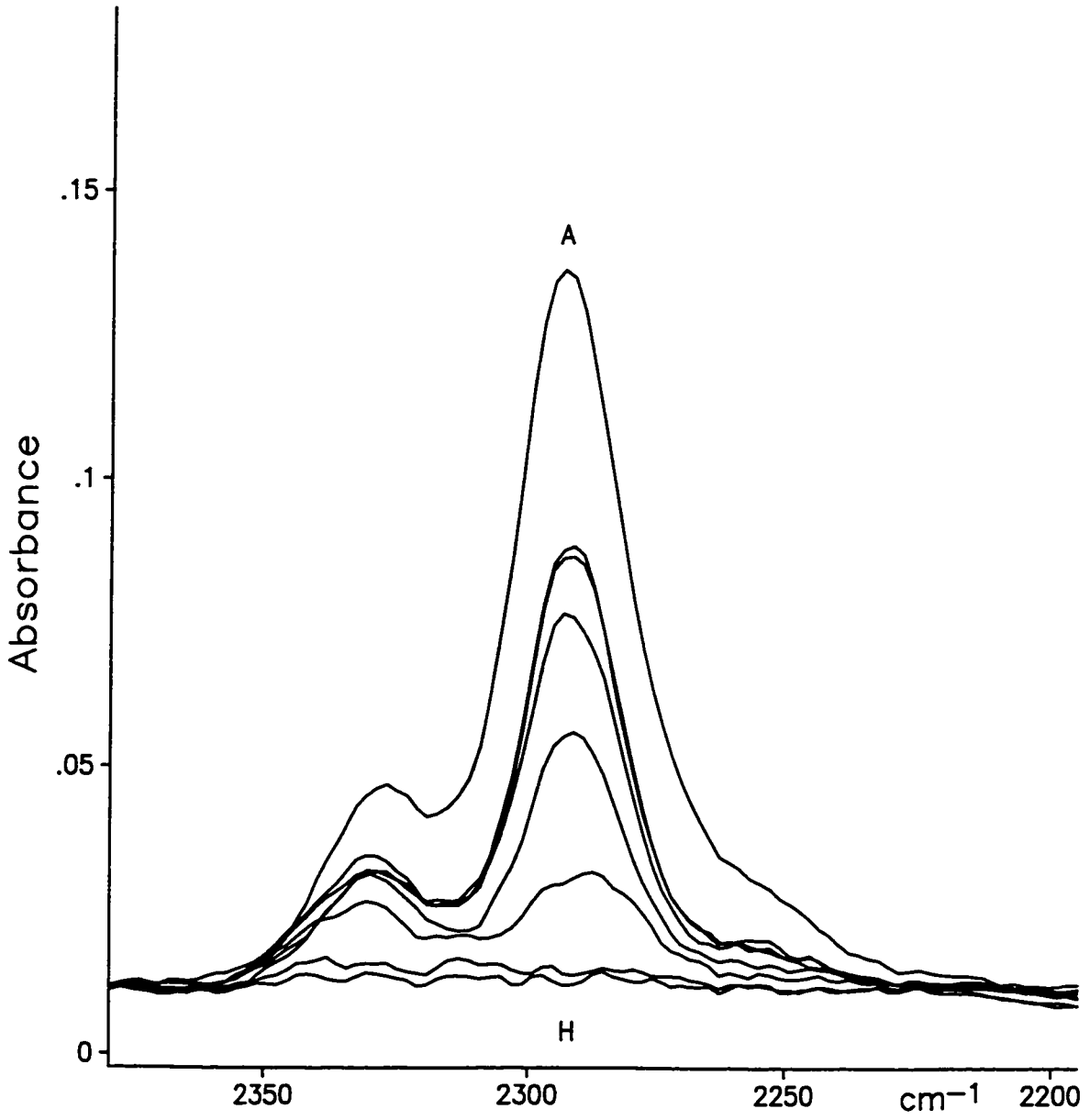

Figure 3.27 Spectrum **A** is the same IR spectrum as shown in Figure 3.24 for the 8% YSA catalyst. The subsequent spectra of decreasing intensity were observed after: **B** evacuation overnight; **C-H** evacuation 15 min. at: 50, 100, 150, 200, 250, and 300°C, respectively.

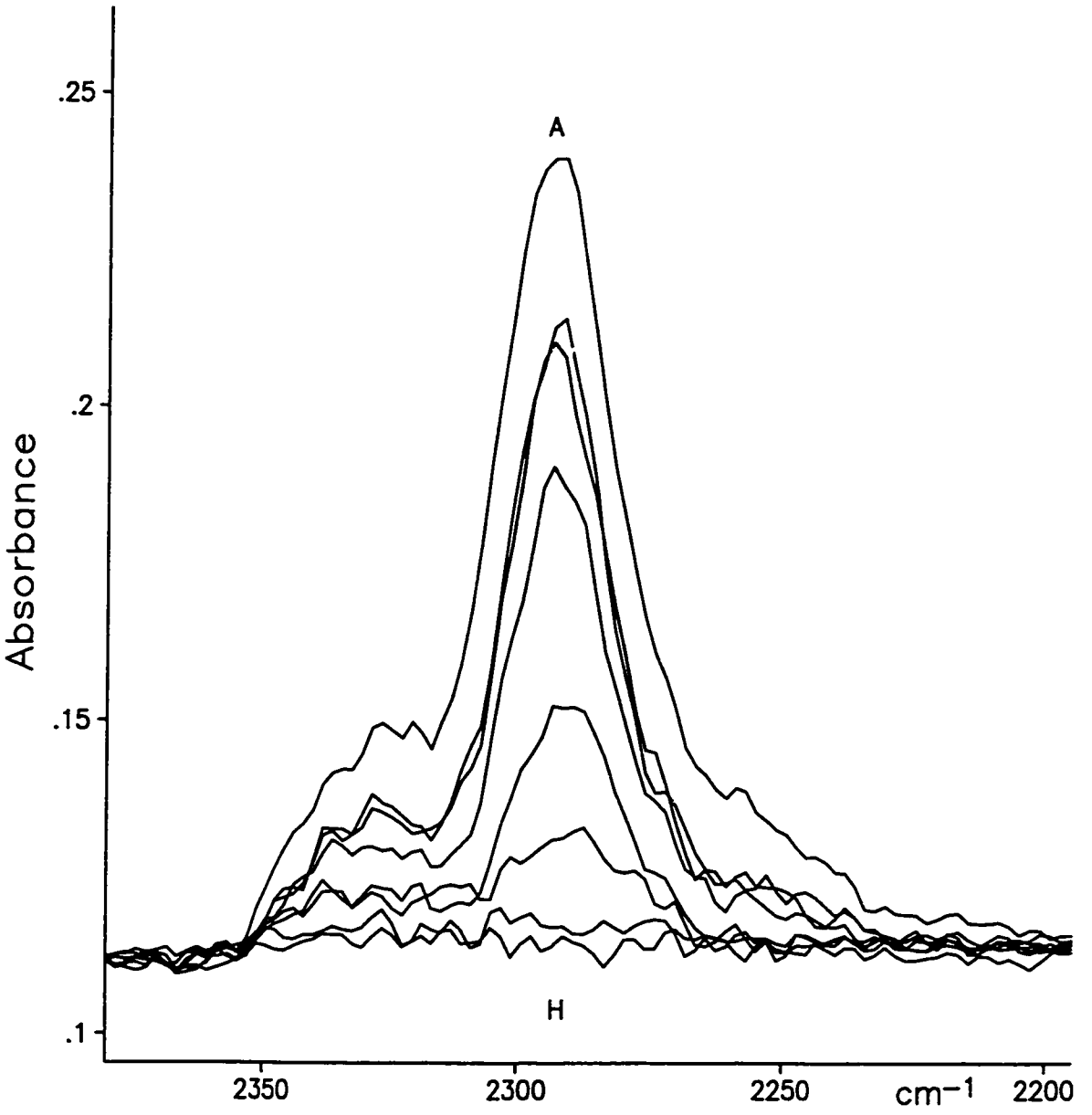

Figure 3.28 Spectrum **A** is the same IR spectrum as shown in Figure 3.24 for the 12% YSA catalyst. The subsequent spectra of decreasing intensity were observed after: **B** evacuation overnight; **C-H** evacuation 15 min. at: 50, 100, 150, 200, 250, and 300°C, respectively.

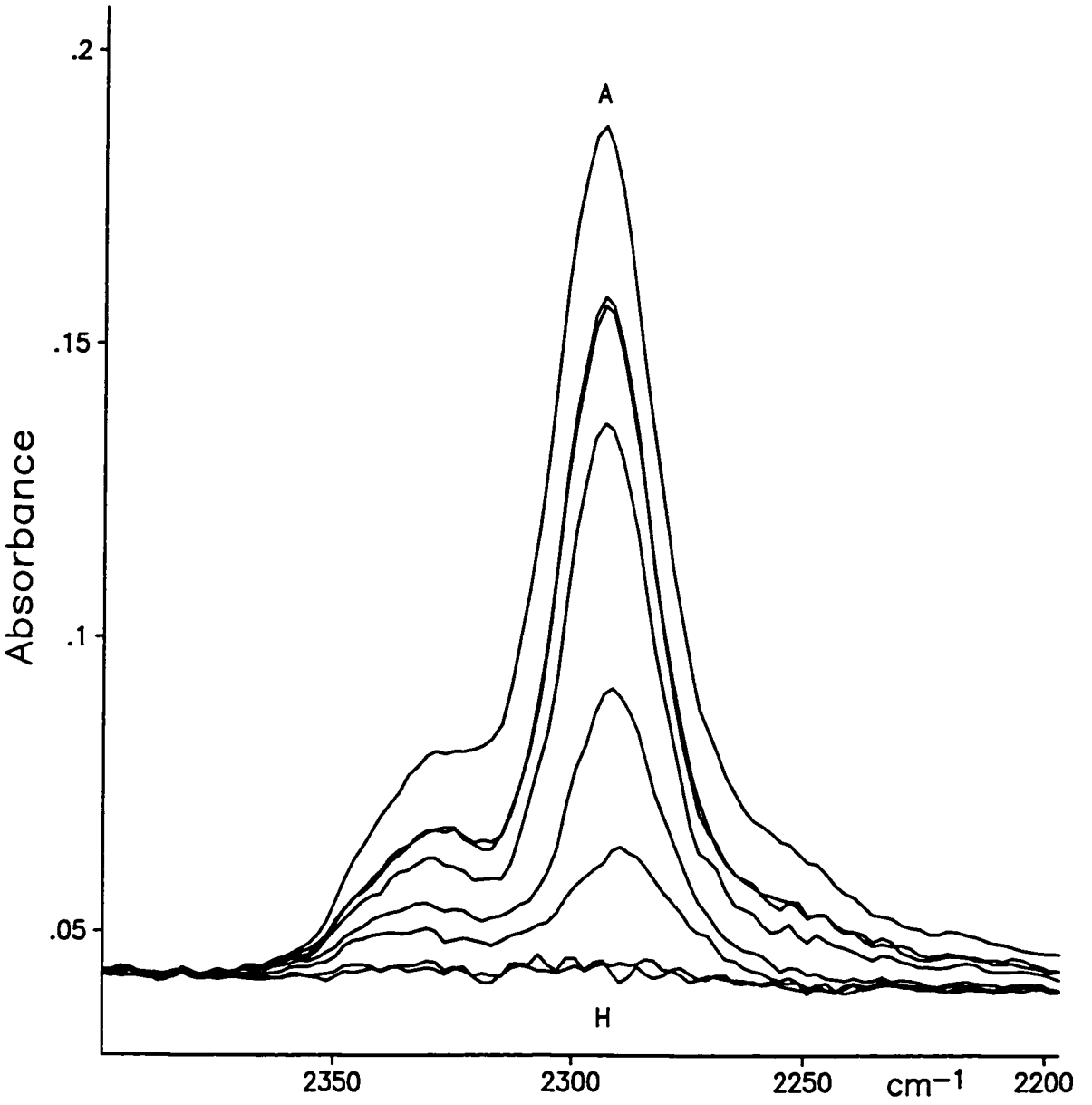

Figure 3.29 Spectrum **A** is the same IR spectrum as shown in Figure 3.24 for the 16% YSA catalyst. The subsequent spectra of decreasing intensity were observed after: **B** evacuation overnight; **C-H** evacuation 15 min. at: 50, 100, 150, 200, 250, and 300°C, respectively.

3.5 ^{31}P NMR of ADSORBED TRIMETHYLPHOSPHINE

3.5.1 Introduction

The ^{31}P resonance of pure or physically adsorbed PMe_3 occurs at about -60 ppm, that of coordinated PMe_3 occurs between -45 and -50 ppm on silica-alumina and near -51 ppm on yttria. On the other hand, protonated PMe_3, $HPMe_3^+$, gives rise to a well separated signal at about -4 ppm. Therefore, whereas the -4 ppm signal characteristic of PMe_3 interacting with Brønsted acid sites can be easily resolved, it is difficult to resolve the signals due to coordinated and physisorbed PMe_3 when both are present due to the lack of resolution and similarity in binding strengths. Accordingly, it is easy to quantify the number of Brønsted acid sites, and it is difficult to obtain an accurate measure of the number of Lewis acid sites if signals due to coordinated and physisorbed PMe_3 co-exist. In such cases, *quantitatively*, the 90° pulse experiments which give *uniform excitation* of all ^{31}P resonances are preferable over cross polarization (CP) experiments which excite ^{31}P nuclei with a significant dipolar coupling to protons, thus making it more sensitive for immobile species with short P-H distances.

According to Sheng and Gay [36] PMe_3 reacts preferentially with strong Lewis acid sites before physisorption occurs on silica-alumina catalysts. Therefore, a lower limit to the number of coordinated species can be obtained by titrating the surface with PMe_3 until a signal from physisorbed species is just detected. After this point, if there are weaker Lewis sites, both signals will intensify together and the concentration of the additional weaker Lewis acid sites cannot be determined. Consequently, although the quantitative results are reliable as applied to the number of Brønsted acid sites, they are, however, a lower limit to the number of Lewis acid sites. Baltusis *et al.* [37] have also explored the problem of discriminating between the signals due to coordinated *versus* physisorbed alkyl phosphines on silica-alumina catalysts. In their approach, as the phosphine concentration increases physisorbed and coordinated TMP *appear simultaneously*. Hence a ^{31}P NMR titration of Lewis acid sites is not a trivial matter. There exists no spectral event that signals the saturation of Lewis acid sites. For quantitative

results one must ensure that chemical exchange processes are not factors in the analysis of acid sites, *i.e.* during integration. Experimentally, this means that TMP is added until no further increase in the signal of the protonated adduct is observed. Hence, the results are a quantitative estimate of solid acidity.

3.5.2 Experimental

NMR spectra were recorded at Simon Fraser University using a home built instrument [38]. A field strength of 3.5 T which gave a ^{31}P resonance frequency of 60.5 MHz was utilized along with proton decoupling fields of 50-60 kHz. The samples were activated at 400°C for 2 hours followed by the adsorption, at room temperature, of about 0.02 mmol of TMP from gas phase at room temperature. The samples, about 0.2 g, were then vacuum sealed and spun at the magic angle at speeds of about 2 kHz and chemical shifts were referenced to 85% H_3PO_4. The ^{31}P T_1 for adsorbed species is relatively short, <1 s, and the repolarization times ranged from 1-5 s; contact times were in the order of 10^{-3} s and the number of scans per acquisition were in the thousands. Quantitative ^{31}P measurements were made using a 90° pulse sequence previously described by Duncan *et al.* [39].

3.5.3 Results

On pure Y_2O_3, no Brønsted sites were found, but Lewis sites were present. These showed a ^{31}P chemical shift of -57 ppm, compared with -48 ppm on Al_2O_3. The free shift of TMP is -62 ppm. Due to the closeness of the Lewis bound line to that of the physically adsorbed TMP, it is difficult to measure the Lewis acid concentration accurately.

Figure 3.30 shows the ^{31}P NMR spectra of TMP at low coverages adsorbed on YSA

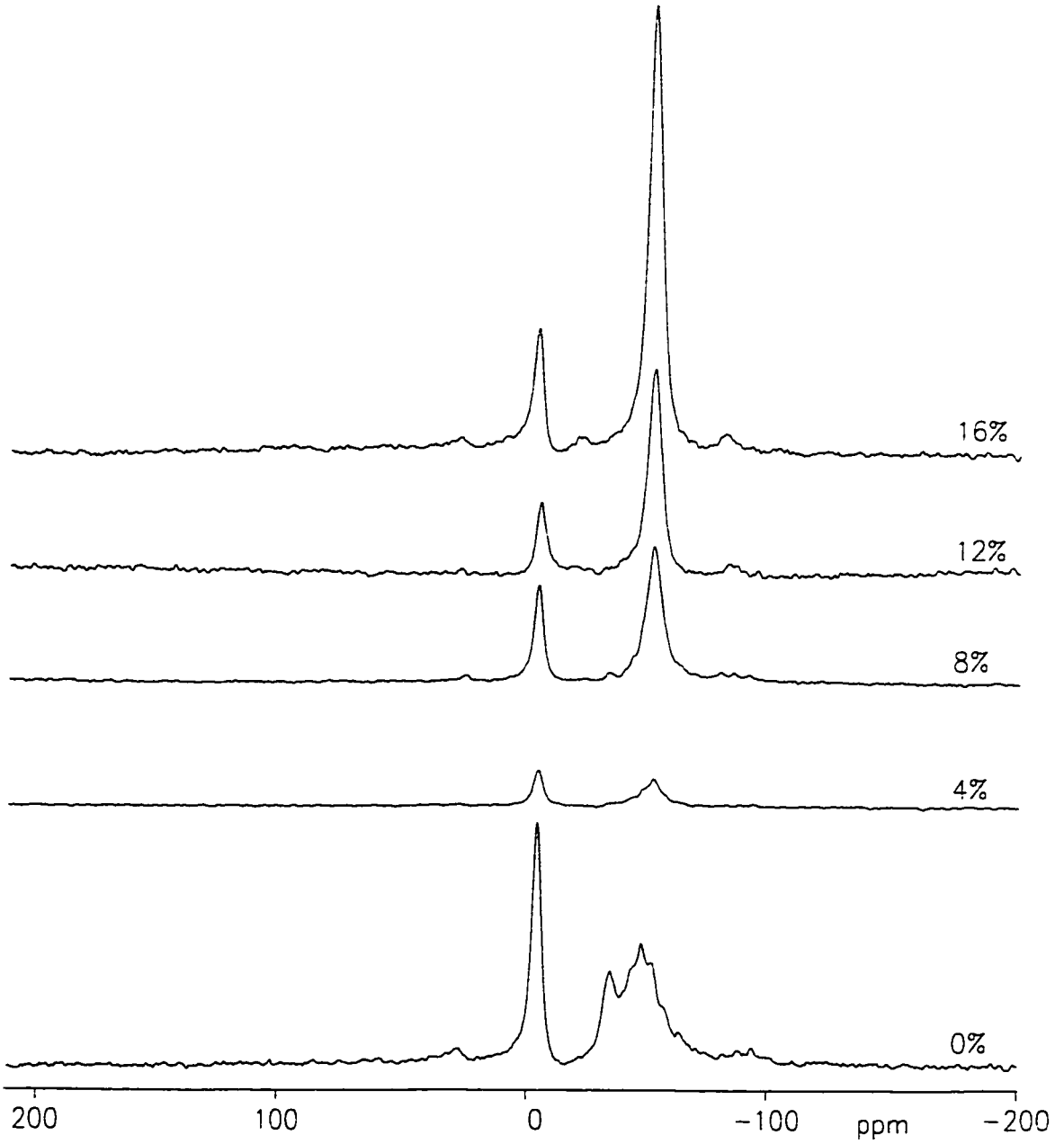

Figure 3.30 ^{31}P NMR spectra of YSA catalysts with corresponding TMP loadings: 0% YSA (0.149 mmol/g), 4% YSA (0.0920 mmol/g), 8% YSA (0.110 mmol/g), 12% YSA (0.0964 mmol/g) and 16% YSA (0.135 mmol/g).

catalysts. The pure SiO_2-Al_2O_3 sample contained, as is typical, both Brønsted and Lewis acid sites. The former showed a strong sharp peak centered at -4.5 ppm whereas the latter showed a typical multiplet due to the coupling of ^{31}P to ^{27}Al, centred at -45 ppm. Once Y_2O_3 was deposited, the Brønsted peak remained in more or less the same position, but decreased in intensity as Y_2O_3 loading increased and did not show any coupling of ^{31}P to ^{1}H (since proton decoupling was used). The Lewis peak became narrower, shifted to -51 ppm, and generally did not show a coupling pattern; however, at low TMP coverages on the 0 and 4% YSA samples, a few residual Al^{3+} Lewis sites could be detected. From these spectra the concentrations of Lewis and Brønsted sites were determined from their respective areas. The concentrations of both these acid sites vary with the amount of added Y_2O_3. In both cases there is a broad maximum centered in the range of 4 to 8% YSA. These results are shown in Table 3.5.

Table 3.5 Surface acidity measurements of YSA catalyst samples.

% YSA	Lewis (μmol/m^2)	Brønsted (μmol/m^2)
0	0.28	0.14
4	0.67	0.19
8	0.57	0.17
12	0.63	0.15
16	0.58	0.12

Figure 3.31 shows a series of ^{31}P NMR spectra at different TMP coverages for 0% YSA catalyst. These were chosen from the series of YSA catalysts to illustrate some of the difficulties that exist in determining acid site concentrations via titration. The peak centered about -4.5 ppm is due to protonated TMP, $[(CH_3)_3P\text{-}H]^+$. This peak was verified by delayed decoupling to arise from phosphorous directly bonded to a proton. As TMP loadings increase

the peak due to coordinated and physisorbed TMP increases in intensity, becomes broader and shifts upfield. The Brønsted acid peak initially increases in intensity then decreases shifting to a higher chemical shift (this shift however is insignificant compared to that of the coordinated/physisorbed peak).

There are two types of processes that take place in these titration experiments on the surface of the YSA catalysts:

1. Movement of TMP on Brønsted acid sites to coordinated/physisorbed sites;
2. Exchange between coordinated and physisorbed TMP.

The latter rapid chemical exchange mechanism results in the formation of sharp peaks (a loss of distinct peaks) [37]. The former (and quantitatively more significant) mechanism leads to a slight decrease in Brønsted acidity; hence the spectrum acquired just before this event is that which was used for quantitative analysis. The Brønsted acid concentrations listed in Table 3.5 represent a total coverage or saturation of these sites. The Lewis acid concentrations, however, are assumed to represent lower limits which are based on the size of the Lewis peak at low coverages, where exchange processes are not observed.

In determining the concentration of Lewis and Brønsted acid sites on the YSA catalysts there existed a host of variables which included: mass, surface areas and TMP concentrations. With such a scatter it is not easy to draw any firm conclusions with regards to Y_2O_3 loading and the acidity of the YSA catalysts. These results will be discussed further in the Discussion (section 3.6).

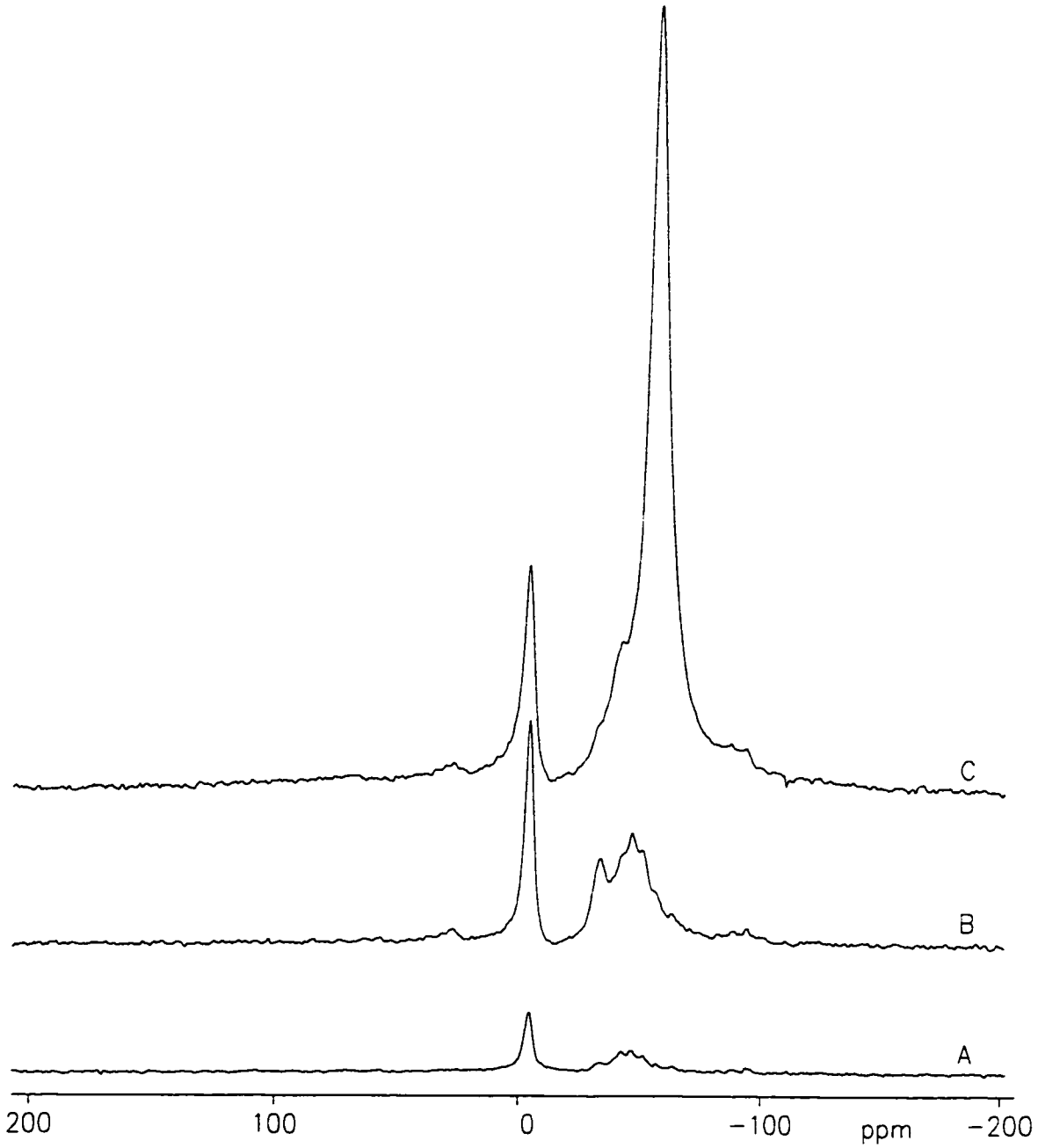

Figure 3.31 ^{31}P NMR spectra of 0% YSA catalysts at: **A** 0.0686 mmol/g, **B** 0.149 mmol/g and **C** 0.340 mmol/g TMP loadings.

3.6 DISCUSSION

The objective of this Chapter was to determine whether one could use IR and NMR methods to probe small changes in the acidity of silica-alumina (SA) catalysts by impregnating SA with varying amounts of the rare earth like base yttrium oxide (Y). Adding a base to an acidic oxide would be expected to lower the acidity. However, two effects are encountered in such a process; a change in the *number* of acid sites of a specific type, and a change in the *strength* of a given acid site.

3.6.1 Brønsted Acidity

Pyridine is the weakest base of the probes used and only probes the stronger acid sites. The results clearly showed that the number of strong Brønsted acid sites decreased with increasing loading of Y. This was true for either a 150 or 450°C activation temperature. Although the results discussed were relevant to the case where all physisorbed Py had been removed by evacuation at 100°C , the 1545 cm^{-1} band was equally intense even in the presence of physically adsorbed Py at room temperature. Therefore, protonated Py is very strongly adsorbed and evacuation at room temperature or at 100°C does not reduce their numbers significantly.

Similar results were found from the adsorption of the stronger base ammonia, although this trend was more apparent for the 150°C activated samples than for those activated at 450°C. These results again were relevant to situations where all H-bonded NH_3 had been removed by brief evacuation, although, as was found with Py, there was little difference in the intensity of the Brønsted peak even in the presence of gas phase ammonia.

The NMR results are slightly ambiguous. The number of Brønsted sites clearly decreased steadily upon going from 4 to 16% YSA (Table 3.5), but the number for 4 and 8% YSA were greater than those found for pure SA (0% YSA). However, the NMR results were

obtained without evacuation of PMe_3 and there may be differences in the number of sites capable of protonating PMe_3 without evacuation as opposed to those which can protonate NH_3 after evacuation of physisorbed species. Alternatively, it is possible that differences in the steric dimensions between PMe_3 and NH_3 play a significant role in determining the number of sites sampled, as has been found in previous studies related to probing the steric accessibility of OH groups on silica [40].

The only data relative to the *strength* of the Brønsted sites for the same probe came from the ammonia TPD experiments. These suggested that there was a small decrease in acid strength as the yttria content increased.

All things considered, it is apparent that increasing quantities of yttria on silica-alumina results in a decrease in the number and strength of Brønsted acid sites on these catalysts. The number of Brønsted acid sites (NH_3 and Py results) is greater for 150°C activation than for 450°C activation.

3.6.2 Lewis Acidity

Pyridine displayed a unique ability to quantitatively determine the ratio of Y:Al sites available for coordination on a given YSA catalyst. Not unexpectedly, that ratio increased as the yttria loading increased. There was an apparent linear increase in this ratio with yttria loading, but this may be coincidential given that other factors such as the temperature of activation also had an influence on this ratio. However, the trend was qualitatively supported by the results from the adsorption of CD_3CN.

Concerning the number of Lewis sites, the lack of a significant change in the intensity of the 1620-1605 cm^{-1} band due to coordinated NH_3 upon going from 4 to 16% YSA suggests that there is not a great change in the total number of sites available for coordination as a function of Y loading. The total intensity of the 1456/1446 cm^{-1} doublet for coordinated Py

also did not change significantly as the Y loading changed. The intensity of the 1620 cm^{-1} band due to coordinated NH_3 was lower for pure SA than for the yttria samples for either activation temperature which, ignoring any differences in the extinction coefficient for NH_3 coordinated to either Y or Al, would suggest that there are fewer coordination sites available on SA than on any of the YSA catalysts. Further speculation is unwaranted.

Finally, the NMR results are, for the reasons stated above, quite unreliable regarding the number of Lewis acid sites. However, taking the numbers in Table 3.5 to represent a lower limit to the number of Lewis acid sites, the trend is consistent with the NH_3 adsorption results; fewer Lewis sites for SA, more for the YSA catalysts and not a significant difference depending on the percent yttria added.

Regarding the strength of the Lewis acid sites, the TPD results of NH_3 desorption showed that there was an insignificant difference in the temperature at which coordinated NH_3 desorbed from any catalyst. This was also true for adsorbed CD_3CN, but these experiments did show differences in the ratio of the peak heights of CD_3CN coordinated to either Al or Y. The peak for CD_3CN coordinated to Y appeared to decrease to a greater extent than that for coordination to Al at increasing temperatures. However, this effect is difficult to assess because these were static not dynamic TPD results and, given the Py adsorption experiments and the effect of activation temperature (more Al available as T_{act} increases) the above effect may only be another manifestation of this. In future work, dynamic TPD measurements will have to be carried out. In this way, relatively rapid heating (30 min. to 350°C) would minimize the effects of slow diffusion of yttrium into the bulk.

REFERENCES

1. Amenomiya Y. and Cvetanovic R.J.
   J. Phys. Chem., 67, 144 (1963)

2. Cvetanovic R.J. and Amenomiya Y.
   Adv. Catal., 17, 103 (1967)

3. Amenomiya Y.
   Chemtech, 128 (Feb. 1976)

4. Forni L.
   Catal. Rev., 8, 103 (1973)

5. Tsyganenko A.A., Pozdgakov D.D. and Filimonov V.W.
   J. Molec. Struct., 29, 299-318 (1975)

6. Dang Z.Y., Anderson B.A., Ammenomiya Y. and Morrow B.A.
   J. Phys. Chem., 99, 14437 (1995)

7. Nakamoto K.
   "Infrared and Raman Spectra of Inorganic and Coordinaiton Compounds",
   John Wiley & Sons, N.Y. 1986

8. Blomfield G.A. and Little L.H.
   Can. J. Chem., 51, 1771 (1973)

9. Morrow B.A. and Cody I.A.
   J. Phys. Chem., 80 (18), 1995 (1976)

10. Morrow B.A. and Cody I.A.
    J. Phys. Chem., 80 (18), 1998 (1976)

11. Morrow B.A., Cody I.A. and Lee L.S.M.
*J. Phys. Chem., **80** (25), 2761 (1976)*

12. Kung M.C. and Kung H.H.
*Catal. Rev. -Sci. Eng., **27** (3), 425-460 (1985)*

13. Knozinger H.
*Adv. Catal., **25**, (1976)*

14. Basila M.P., Kantner T.R. and Rhee K.H.
*J. Phys. Chem., **68**, 3197 (1964)*

15. Morterra C. and Cerrato G.
*Langmuir, **6**, 1810-1812 (1990)*

16. Parker L.M., Bibby D.M. and Burns G.R.
*J. Chem. Soc., Faraday Trans., **87** (19), 3319-3323 (1991)*

17. Parry E.P.
*J. Catal., **2**, 371-379 (1963)*

18. Morrow B.A.
*J. Chem. Soc., Faraday Trans. 1, **70**, 1527 (1974)*

19. Knözinger H. and Krietenbrink H.
*J. Chem. Soc. Faraday Trans. 1, **71**, 2421 (1975)*

20. Sverdlov L.M., Kovner M.A. and Krainov E.P.
"Vibratioanl Spectra of Polyatomic Molecules", John Wiley & Sons, N.Y., 1970

21. Venkateswarlu P.
*J. Chem. Phys., **19** (3), 293 (1951)*

22. Chen J., Thomas J.M. and Sanker G.
*J. Chem. Soc. Faraday Trans., **90** (22), 3455 (1994)*

23. Lowry T.H. and Richardson K.S.
"Mechanism and Theory in Organic Chemistry", 3rd ed., Harper & Row, N.Y., 1987

24. Lavalley J.C.
"Trends in Physical Chemistry", ed. Menon J., **2**, 305 (1991)

25. Pelmenschikov A.G., van Santen R.A., Janchen J. and Meijer E.
*J. Phys. Chem., **97**, 11071 (1993)*

26. Pelmenschikov A.G., Morosi G. and Gamba A.; Coluccia S., Martra G., and Paukehtis E.A.
*J. Phys. Chem., **100**, 5011 (1996)*

27. Angell C.L. and Howell M.V.
*J. Phys. Chem., **73** (8), 2551 (1969)*

28. Sempels R.E. and Rouxhet P.G.
*J. Colloid and Interface Science, **55** (2), 263 (1976)*

29. Scokart P.O., Declerck F.D., Sempels R.E. and Rouxhet P.G.
*J. Chem. Soc. Faraday Trans. 1, **73**, 359 (1977)*

30. Rouxhet P.G. and Sempels R.E.
*J. Chem. Soc. Faraday Trans 1, **70**, 2021 (1974)*

31. Kinugasa M., Kishi K. and Ikeda S.
J. Phys. Chem., 77 (15), 1914 (1973)

32. Ritter G., Noller H. and Lercher J.A.
J. Chem. Soc. Faraday Trans. 1, 78, 2239 (1982)

33. Purcell K.F.
J. Amer. Chem. Soc., 89 (2), 247 (1967)

34. Purcell K.F.
J. Amer. Chem. Soc., 89 (24), 6139 (1967)

35. Purcell K.F. and Drago R.S.
J. Amer. Chem. Soc., 88, 919 (1966)

36. Sheng T.C. and Gay I.D.
J. Cat., 145, 10-15 (1994)

37. Baltusis L., Fryre J.S. and Maciel G.E.
J. Am. Chem. Soc., 109, 40-46 (1989)

38. Gay I.D.
J. Mag. Res., 58, 413 (1984)

39. Duncan T.M., Yates J.T. and Vaughan R.W.
J. Phys. Chem., 73, 975 (1980)

40. Morrow B.A. and McFarlan A.J.
Langmuir, 7, 1695 (1991)

CHAPTER 4

FLUORIDED ALUMINA CATALYSTS

4.1 INTRODUCTION

Alumina is an amphoteric oxide and for adsorption at the gas-solid interface its Brønsted acidity is very weak. However, the acid strength of Al_2O_3 can be modified by doping with halides, *e.g.* chloride or fluoride [1-6]. Treatment of the surface of Al_2O_3 with fluoride results in the replacement of surface hydroxyl groups by fluoride. The fluoride, having a higher electronegativity than the OH group, causes the residual H on the surface to be more acidic, *i.e.* the change in Al_2O_3 as a result of fluorine doping results in an increase in acid strength and in the number of acid sites capable of donating a proton. This transformation has been found to increase the activity for various acid-catalyzed reactions such as isomerization and catalytic cracking [6].

The fluorided alumina catalysts used in this work were γ-Al_2O_3 catalysts which contained 0.3 wt. % Pt and 1 wt. % fluoride ion. These were proprietary catalysts which were prepared by Exxon Corporation and appeared as grey-white extrudates; the catalysts are designated "ECx" where x refers to the temperature in degrees Celsius used to calcine the catalysts in air after preparation; the calcination temperatures were: 400, 450, 500 and 550°C.

The objective of this work was to see if the calcination temperature had an effect on the acidity of the catalyst; we were looking for small changes in acidity as in the case of the YSA catalysts. Whereas the addition of yttria to silica-alumina was designed to lower the acidity of

SA, in the present instant, the addition of fluoride to Al_2O_3 was intended to raise the acidity so that it would be useful as a skeletal isomerization catalyst.

All catalysts were prepared as self supporting discs (10 mg/cm^2). In the case of the ECx catalysts reduction in hydrogen was performed as part of the activation process; the catalysts were heated in H_2, 400 Torr was expanded into the cell from the vacuum manifold, at 150°C for 15 min. and were then evacuated for 5 min. This procedure was repeated three consecutive times at an elevated temperature of 450°C to ensure the complete reduction of platinum. Finally the catalyst was allowed to cool to room temperature in H_2 before evacuating once more prior to taking a background scan. The probe molecules used to investigate the surface acidity of these catalysts were CD_3CN and NH_3 both of which have already been discussed in Chapter 3 with respect to the surface acidity of YSA catalysts.

4.2 ACETONITRILE-d_3 (CD_3CN) ADSORPTION

As in section 3.4, of interest here is the C≡N spectral region, 2260-2350 cm^{-1}, which has been shown to be the most diagnostic in investigating the Lewis acidity of solid acids. Figure 4.1 shows IR spectra of various EC catalysts which have been activated at 450°C in H_2 and to which 5 Torr of CD_3CN had been added. Figure 4.2 shows the spectra which were recorded after 15 min. evacuation at room temperature. The spectra of CD_3CN adsorbed on the fluorided alumina catalysts are characterized by two major peaks at 2322 and 2268 cm^{-1}. The peak at 2268 cm^{-1} decreased considerably upon evacuation indicating that H-bonded or physisorbed species were present. However, unlike the YSA catalysts the peak was not removed indicating a stronger adsorption site. On pure γ-Al_2O_3 (see Figure 4.3) this peak, present at 2261 cm^{-1}, readily desorbed after 15 min. evacuation leaving a small residual peak. This residual peak is certainly only due to the antisymmetric CD_3 stretching mode (2258 cm^{-1} for gaseous CD_3CN) which is less intense than the symmetric mode at 2112 cm^{-1} in Figure 4.3.

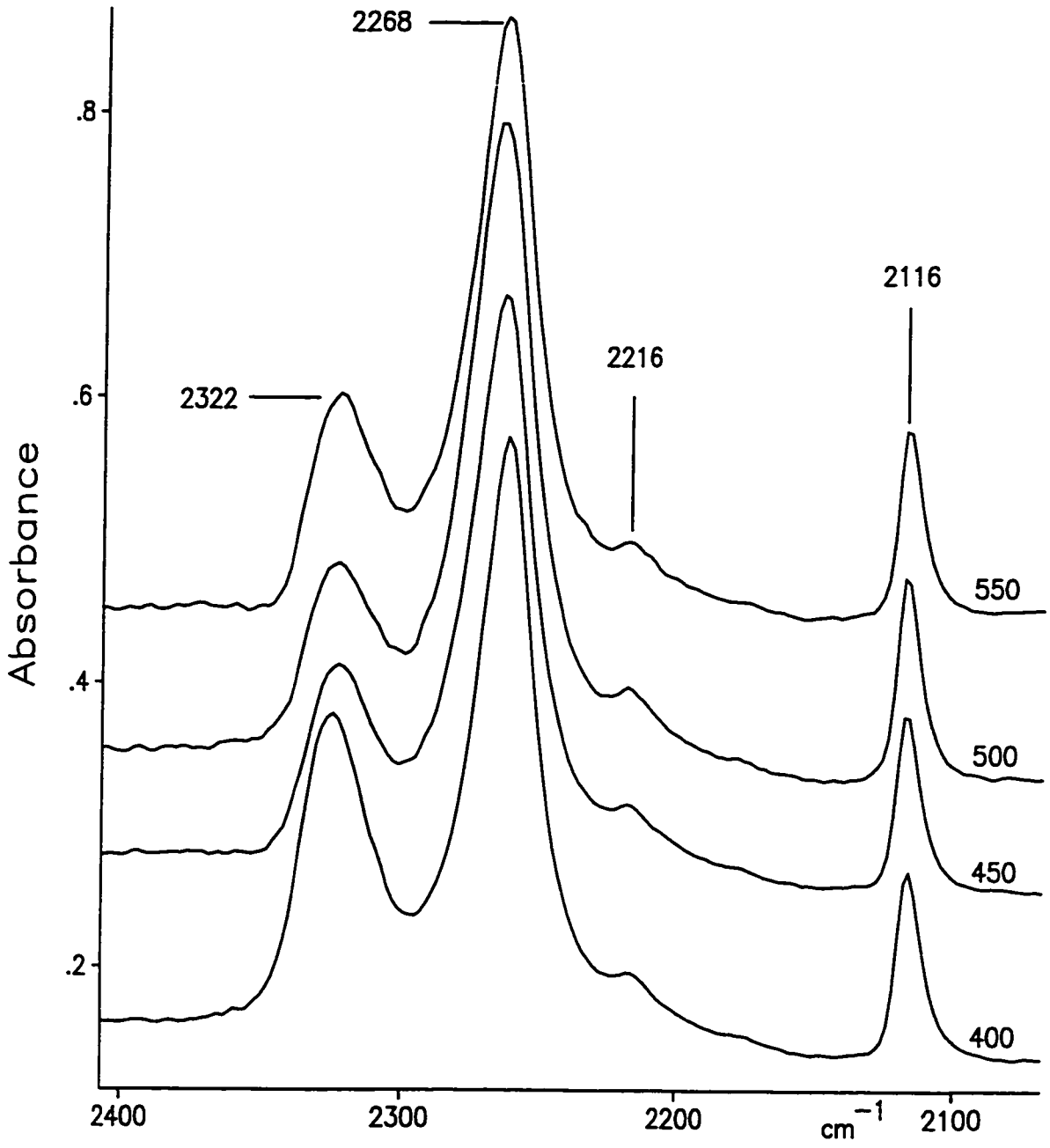

Figure 4.1 IR spectra of EC catalysts (calcination temperature at the side in degrees Celsius) activated at 450°C in H_2 to which 5 Torr of CD_3CN was added.

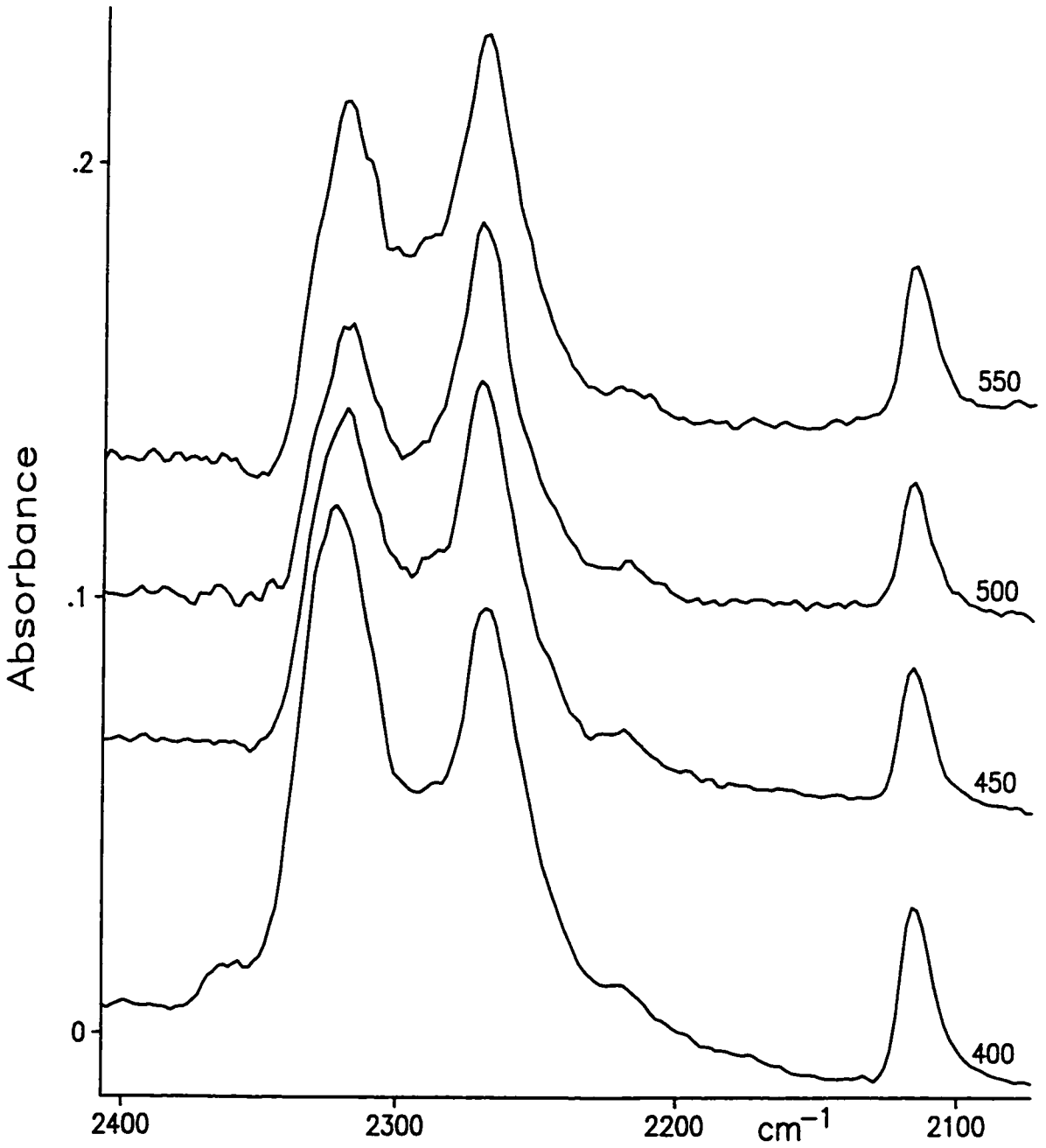

Figure 4.2 Spectra shown in Figure 4.1 after 15 min. evacuation at room temperature.

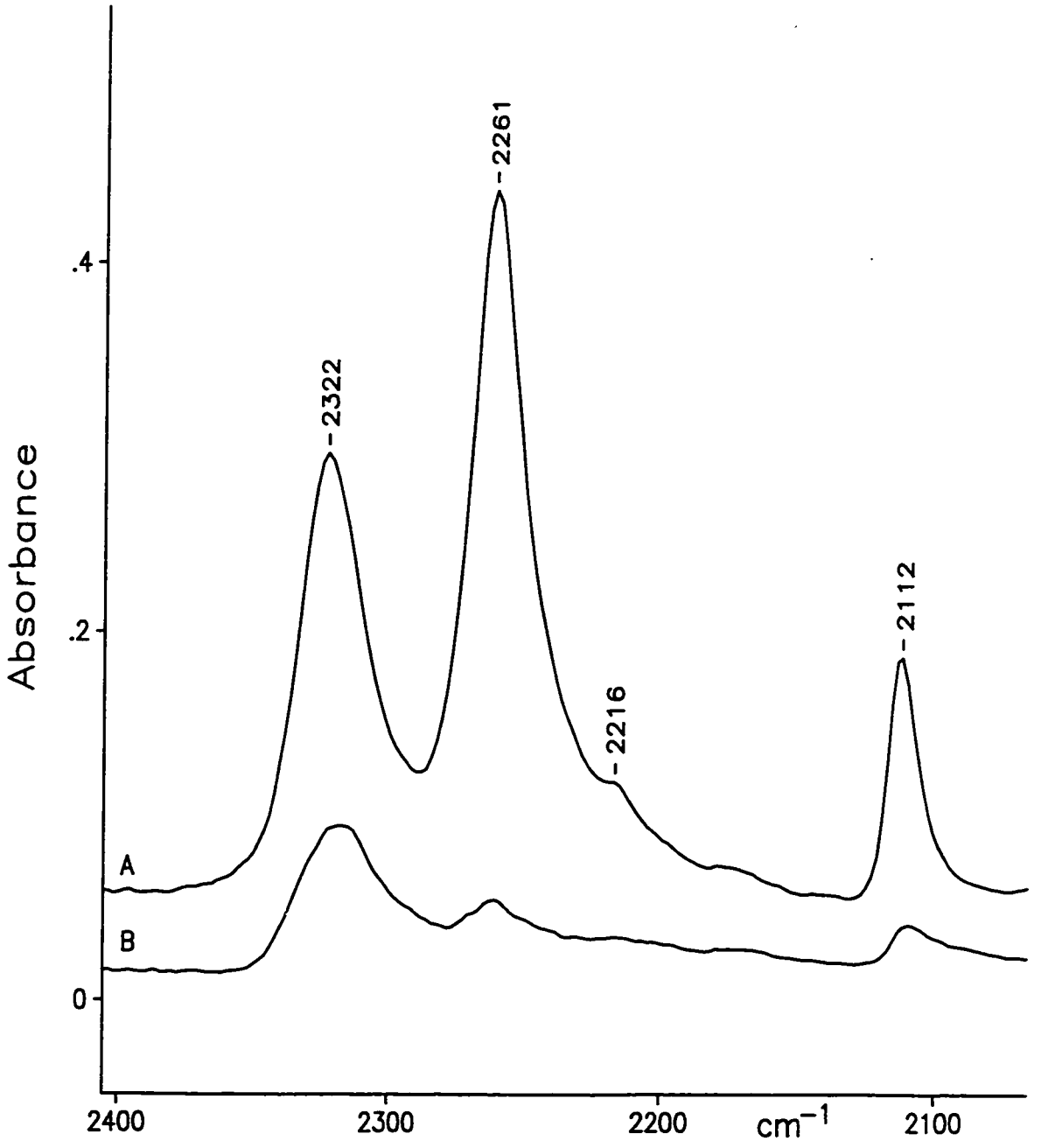

Figure 4.3 Exxon γ-Al_2O_3 activated at 450°C. **A** upon the addition of 5 Torr CD_3CN and **B** after 15 min. evacuation.

[The CD_3 stretching modes are far less intense than the CN stretching mode for adsorbed acetonitrile. Therefore, in Figures 4.1 and 4.2, there is a very weak contribution from the antisymmetric CD_3 stretch to the total intensity near 2268 cm^{-1}, but its intensity is expected to be less than that of the symmetric mode near 2116 cm^{-1} [7]. In the same context, in the spectra of CD_3CN on the YSA catalysts (section 3.4), there was a weak contribution near 2260 cm^{-1} which only manifests itself as a shoulder to low wavenumber of the main peaks after evacuation for 15 min. at room temperature, *e.g.* see Figure 3.24. Finally, the weak peak at about 2216 cm^{-1} in Figures 4.1-4.3 is due to the overtone of the CD_3 angle deformation mode which occurs at 1112 cm^{-1}]. Therefore, the peak at 2322 cm^{-1} is due to coordinated CD_3CN (near the same wavenumber as was found for coordination to Al on the YSA catalysts) and that at 2268 cm^{-1} is due to strongly physisorbed or H-bonded CD_3CN.

The absorbance scale in Figure 4.2 is expanded by a factor of three relative to that in Figure 4.1. Therefore, whereas there was an approximate halving of the intensity of the peak due to coordinated CD_3CN at 2322 cm^{-1} after evacuation (and a similar figure was found for adsorption of CD_3CN on the YSA catalysts) there was a five fold decrease in the intensity of the 2268 cm^{-1} peak upon evacuation. These changes were much greater after 15 min. evacuation (Figure 4.3) for pure γ-Al_2O_3. However, the pure γ-Al_2O_3 was activated in vacuum at 450°C whereas the fluorided catalysts were reduced in hydrogen and not subjected to a vacuum activation at 450°C. The hydrogen reduction has the effect of creating a much larger number of AlOH groups and fewer coordinatively saturated Lewis sites. Figure 4.4 shows the spectrum of EC450 which had been been vacuum activated at 450°C and not reduced in H_2. The initial intensity of the 2322 cm^{-1} peak is about five times greater than that which was observed for EC450 in Figure 4.1, clearly demonstrating that the hydrogen treatment reduces the number of Lewis acid sites. Finally, whether vacuum activated or reduced in H_2, there was significantly less reduction in the intensity of the peak due to coordinated CD_3CN after 15 minutes evacuation for the fluorided catalysts than for non-fluorided γ-Al_2O_3. This demonstrates the effect of fluorine on enhancing the strength of the Lewis acid sites.

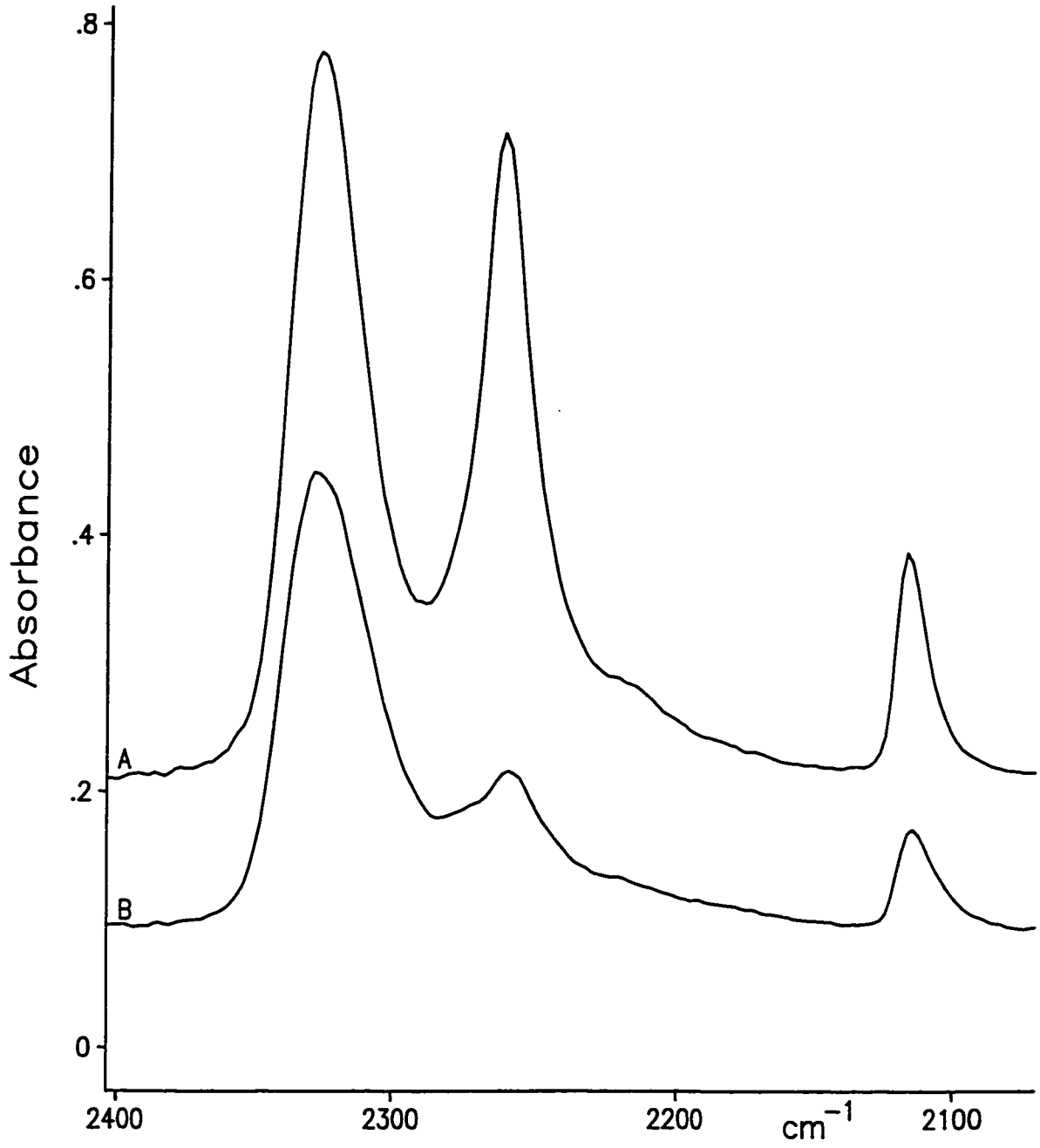

Figure 4.4 EC450 activated at 450°C. **A** upon the addition of 5 Torr CD_3CN and **B** after 15 min. evacuation.

4.3 *AMMONIA (NH_3) ADSORPTION*

The presence of Lewis or Brønsted acidity using ammonia as a probe molecule is characterized by the observation of specific angle deformation modes in the 1650-1400 cm^{-1} spectral region (see section 3.2). Figure 4.5 shows the IR spectra recorded after contacting the ECx catalysts with 5 Torr of NH_3 after each catalyst had been activated in hydrogen at 450°C; in each case, the NH_3 had been evacuated overnight (the spectra were virtually identical, about 5% more intense, if the evacuation was only for 5 min.). The same Figure also shows the IR spectrum of NH_3 which had been adsorbed on the Al_2O_3 base support, but in this instance the catalyst had been vacuum activated at 450°C. This latter spectrum is characteristic of chemisorbed ammonia adsorbed on all γ-Al_2O_3 catalysts [8-11]; IR spectra of several γ-Al_2O_3 catalysts from different preparations recorded in our laboratory have all shown these features for chemisorbed ammonia. The positions of the IR bands attributable to coordinated (Lewis) ammonia and protonated (Brønsted) ammonia are indicated. The IR bands due to NH_4^+ are different than those which were observed for the YSA catalysts; this is well understood and is related to the symmetry of the adsorbed species [12]. Briefly, the strong band near 1450 cm^{-1} is due to the triply degenerate antisymmetric NH_4^+ deformation mode, this splits into three components if the symmetry is lowered, and the band near 1680 cm^{-1} is due to the forbidden symmetric deformation mode in T_d symmetry which becomes allowed if the symmetry is reduced upon adsorption.

The spectral features noted for Al_2O_3 are also present for the EC catalysts although the relative intensities of the various peaks due to Brønsted versus Lewis species are different. There is a doublet in the 1490-1460 cm^{-1} spectral region for the EC catalysts. Figure 4.6 shows the IR spectrum for ammonia adsorbed on one of the EC catalysts which had *not* been subjected to the hydrogen treatment, but had been activated under vacuum at 450°C. This shows the evolution of the spectrum as increasing doses of NH_3 were added. All bands, including those due to the 1490-1460 cm^{-1} doublet grow in intensity to the same extent as the dosage of NH_3 increases. Although not shown, there was a very slight decrease in intensity of

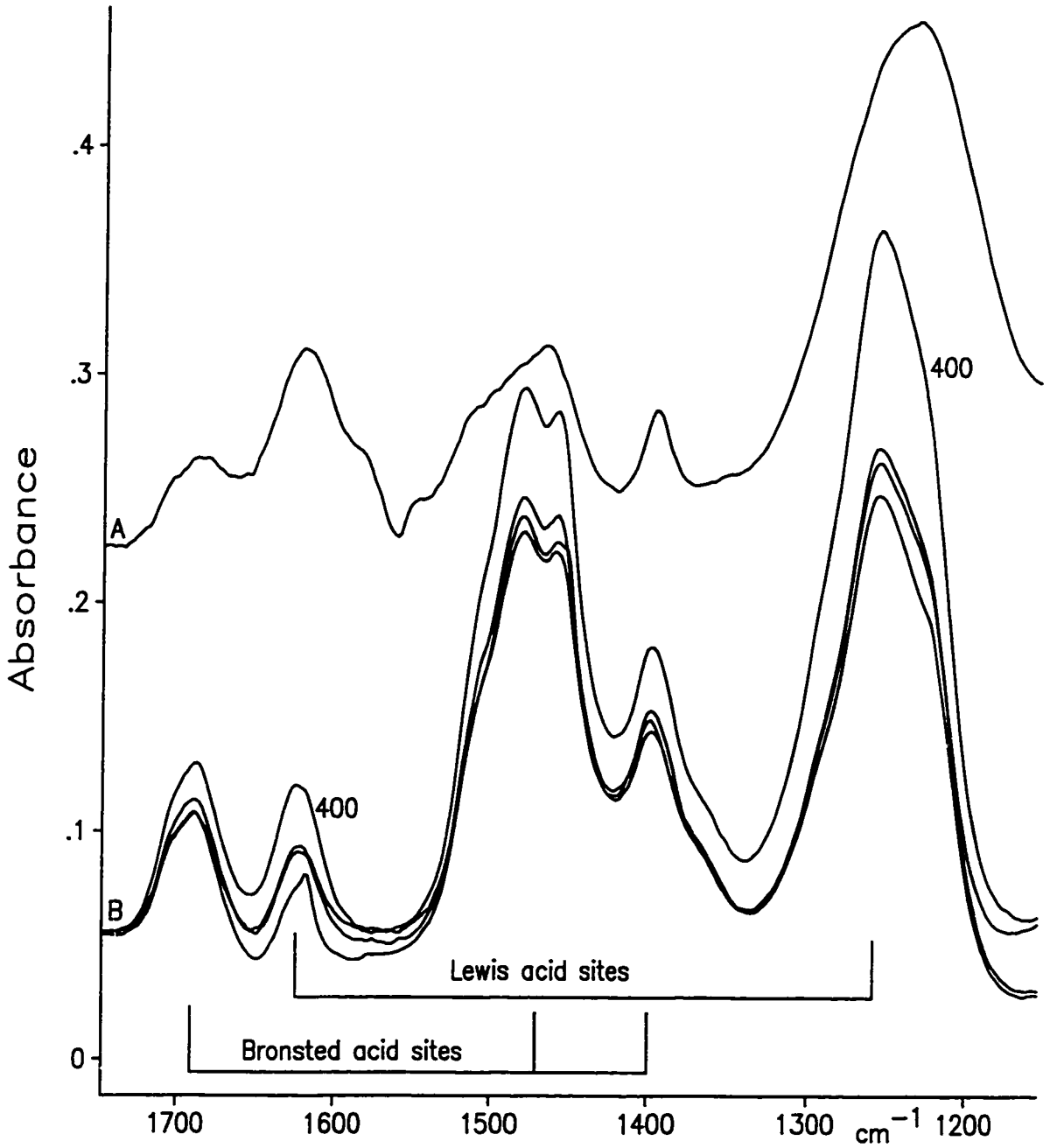

Figure 4.5 **A** Exxon γ-Al_2O_3 activated at 450°C, and **B** EC catalysts (400°C calcined sample indicated) activated at 450°C in H_2; spectra were recorded after 5 Torr NH_3 was added and then evacuated overnight.

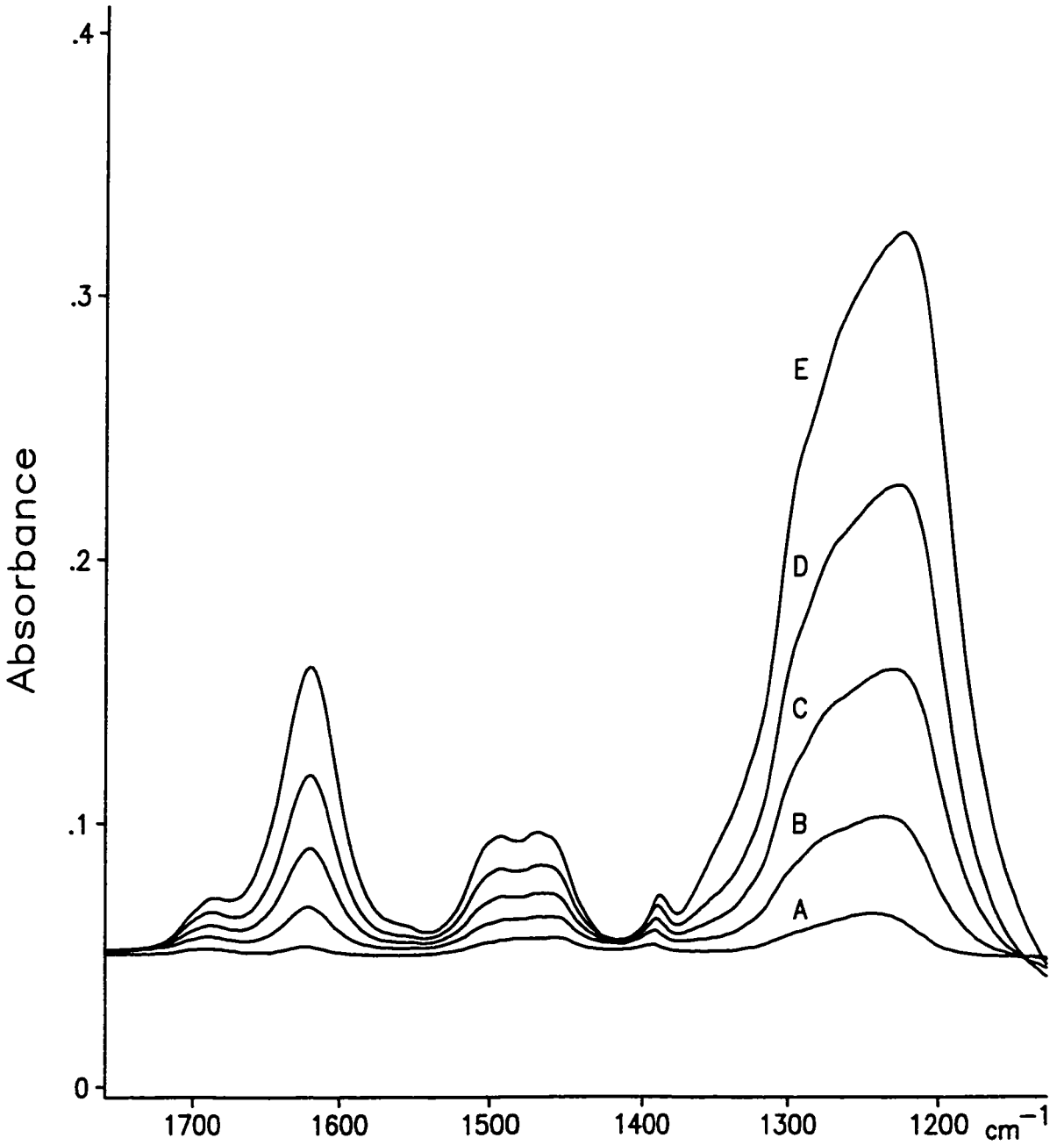

Figure 4.6 EC500 Al_2O_3 activated at 450°C upon the addition of NH_3: **A** 0.1 Torr, **B** 0.3 Torr, **C** 0.6 Torr and **D** 0.9 Torr, **E** 1.2 Torr.

all bands, uniformly, following evacuation overnight. Therefore, there is no clear evidence that the multiciplicity of IR bands is due to the adsorption of ammonia on sites of different acid strength, or at least all sites are filled to the same extent as NH_3 is added or removed by evacuation. This doublet was observed in the spectra of samples which were not subjected to a reduction in hydrogen (Figure 4.6) and is therefore not related to hydrogen spillover as a result of the presence of platinum in the catalyst. Further discussion is not warranted.

What is noteworthy in comparing the spectra in Figures 4.5 and 4.6 is that the peaks due to coordinated NH_3 are more intense relative to those due to NH_4^+ for the sample which did not contain platinum or which had not been 'reduced' in hydrogen. This is in accord with the results from the adsorption of acetonitrile; the number of sites capable of coordinating either molecule is greater for vacuum activated samples than for those containing Pt which had been reduced in hydrogen. Conversely, the intensity of the 'Brønsted doublet' at 1490-1460 cm^{-1} is much more intense, relatively, for the Pt containing EC samples which had been reduced in hydrogen (Figure 4.5). This again shows that the presence of Pt and the treatment in H_2 at 450°C reduces the number of Lewis acid sites and increases the number of Brønsted acid sites as compared to those catalysts which had been activated under vacuum at 450°C.

4.4 DISCUSSION

The objective of this work was to determine whether the calcination temperature used in catalyst preparation had any influence on the acidity of some platinum containing fluorided Al_2O_3 catalysts, all of which had been identically treated in hydrogen at 450°C and then cooled in hydrogen to room temperature. Fluorided Al_2O_3 has been extensively studied in other contexts and a more detailed investigation of this system would have been redundant.

The increase in the number of Brønsted acid sites relative to pure Al_2O_3 was expected and is well known [6]. There was not much change in the number of Lewis acid sites, but this

is more related to the hydrogen treatment which has the effect of diminishing the number of these sites relative to catalysts which had been vacuum activated at 450°C. Between the individual fluorided catalysts, there was not a striking difference in the numbers of either type of acid site. Based on peak intensities, the number of sites available for coordination and for protonation may be slightly greater for EC400 than for the others. Further discussion is unwarranted and a more detailed investigation of this system will not be undertaken.

REFERENCES

1. Satterfield C.N.
   "Heterogeneous Catalysis in Industrial Practice", 2nd ed., McGraw-Hill, Inc., N.Y. 1991

2. Scokart P.O., Selim S.A., Damon J.P. and Rouxhet P.G.
   *J. Colloid Int. Sci., **70** (2), 209-222 (1979)*

3. Hughes T.R., White H.M. and White R.J.
   *J. Cat., **13**, 58-64 (1969)*

4. Peri J.B.
   *J. Phys. Chem., **72** (8), 2917-2925 (1968)*

5. Kiselev A.V. and Lygin V.I.
   "Infrared spectra of Surface Compounds", Keter Publishing House Jerusalem Ltd. 1975

6. Ghosh A.K. and Kydd R.A.
   *Catal. Rev. Sci. Eng., **27**, 539 (1985)*

7. Pelmenschikov A.C., van Santen R.A., Janchen J. and Meijer E.
   *J. Phys. Chem., **97**, 11071 (1993)*

8. Shen J., Lochhead M.J., Bray K.L., Chen Y. and Dumesic J.A.
   *J. Phys. Chem., **99**, 2384-2392 (1995)*

9. Shen J., Cortright R.D., Chen Y. and Dumesic J.A.
   *J. Phys. Chem., **98**, 8067-8073 (1994)*

10. Lercher J.A., Grundling C. and Eder-Mirth G.
Cat. Today, 27, 353 (1996)

11. Morterra C. and Magnacca G.
Cat. Today, 27, 457 (1996)

12. Zecchina A., Marchese L., Bordiga S., Paze C. and Gianotti E.
*J. Phys. Chem. B, **101**, 10128 (1997)*

CHAPTER 5

CATALYST PERFORMANCE

5.1 INTRODUCTION

When work was started on this project it was with the intention of incorporating different instrumental techniques to characterize various practical oxide catalysts and to correlate this with catalyst performance using a suitable test reaction. The techniques involved in this study included temperature programmed desorption (TPD), infrared (IR) spectroscopy, gas chromatography (GC) and solid state nuclear magnetic resonance (NMR) spectroscopy. Our basic premise was to develop a routine which would:

1. Measure the strength of an acid site;
2. Determine whether the acid site was Lewis or Brønsted and determine the structure of the site;
3. Determine the numbers of acid sites of different types;
4. Correlate the results with a real catalytic reaction.

TPD can be used to show the relative strength of adsorption among surface active sites [1] and it can provide information on the absolute number of sites provided that peaks are well separated. In isolation however it does not provide information on the nature of the site (Lewis or Brønsted) or its structure.

IR spectroscopy can be used to clearly distinguish the type of surface acid sites under investigation and to gain a relative measure of Lewis and Brønsted acidity via the use of

suitable probe molecules. However, because the extinction coefficients are generally not known, it is not possible to obtain quantitative data, *i.e.* absolute numbers of sites, nor is it possible to determine the strength of the acid sites [2].

By combining the individual strengths of IR, TPD and a test reaction approach, and add to this solid state NMR with which acid site concentrations could be determined, a multifaceted approach to catalyst characterization can be developed. This approach would lead to a more comprehensive understanding of the role of acidity in heterogeneous catalysis. An *in situ* IR/TPD method was developed for this purpose which has been described previously (Chapter 3). In this chapter, we describe work related to using a test reaction to monitor catalyst acidity. The majority of the work went into modifying a stainless steel TPD/micro reactor and a Varian 3700 GC to which it was interfaced. In modifying this system it was with the intention of adapting it to study the isomerization of 2-methyl-2-pentene (2M2P) which was the chosen test reaction (see the next section). In order to determine the products of this reaction the GC had to be fitted with a capillary column and a split flow injector system.

5.2 ISOMERIZATION OF 2-METHYL-2-PENTENE (2M2P)

Acid catalysts are used in industry to manufacture a host of different products from petroleum feedstock [3]. Hence in developing and further optimizing catalysts for specific reactions, it is of paramount importance to have a method capable of correlating acid properties of a catalyst to performance.

In the presence of acidic catalysts, olefins can undergo *double bond migration* (**DBM**) as well as *skeletal isomerization* (**SKI**) [4,5,6]. In the former, a carbenium ion undergoes isomerization via H-transfer along the hydrocarbon chain; whereas in the latter, a methyl shift along the olefin chain leads to a highly branched carbenium ion. The rate of such a methyl

shift is 1000 times slower than that of a H-shift [4]. Hence, DBM is a relatively facile transformation, *i.e.* it requires only mild acidic and temperature conditions. Harsher conditions are required to bring about SKI which may also lead to side reactions such as polymerization or cracking; *i.e.* SKI requires higher temperatures and stronger acid catalysts than does DBM.

In this work, catalyst performance was investigated by studying the isomerzation of 2M2P. The isomerization of 2M2P is of interest because this olefin can isomerize into different products depending on the nature of the catalyst, thus providing information on the relative acidity of catalysts [7,8]. Of particular interest is the conversion of 2M2P to 4-methyl-2-pentene (4M2P) and 3-methyl-2-pentene (3M2P):

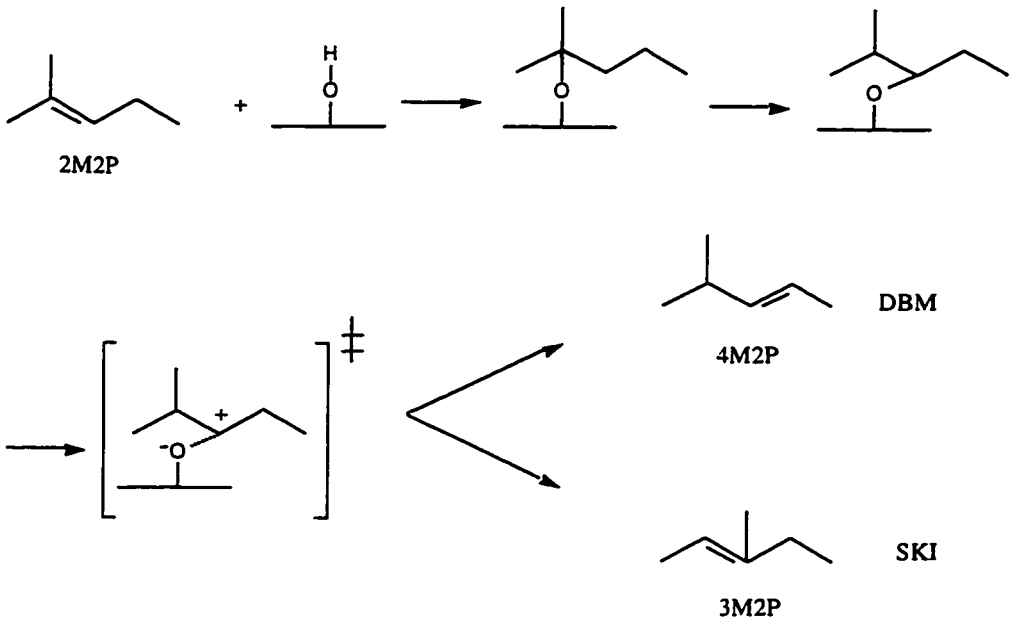

(5.1)

It has been proposed that the rearrangement of 2M2P in reaction (5.1) goes via protonation of the olefin followed by isomerization and eventual desorption from the surface [7,9]. Hence an intermediate alkoxy species bound to a surface hydroxyl group rearranges by a hydride shift to a cationic intermediate which undergoes a proton shift, DBM, or methyl migration, SKI. The selectivity ratio of skeletal isomerization to double bond migration (S_{SKI}/S_{DBM}) was determined for 2M2P conversion over various catalysts [7,10]. An increase in selectivity ratio indicates an increase in the cationic character of the rearranging intermediate, hence an increase in the acidity of the catalyst. A weak solid acid can easily catalyze the DBM during the conversion of 2M2P to 4M2P whereas the formation of 3M2P, which involved SKI, required stronger acids [7,10]. The use of selectivity ratios as opposed to individual selectivities was preferred since differences in acid site populations were thus normalized. In particular, selectivity ratios of *trans* 3M2P : *cis* 4M2P were determined in this work.

5.3 EXPERIMENTAL

There are two parts to this section: the flow system within which the micro reactor was located and the analysis system which consisted of a Varian 3700 GC both of which were customized for this work.

5.3.1 Flow System

The experiments were conducted using a stainless steel flow system with a fixed bed micro reactor. The system consisted of three segments: a gas delivery system through which hydrogen and helium were passed, an injection port where 2M2P entered the system, and a reactor/bypass segment, shown in Figure 5.1.

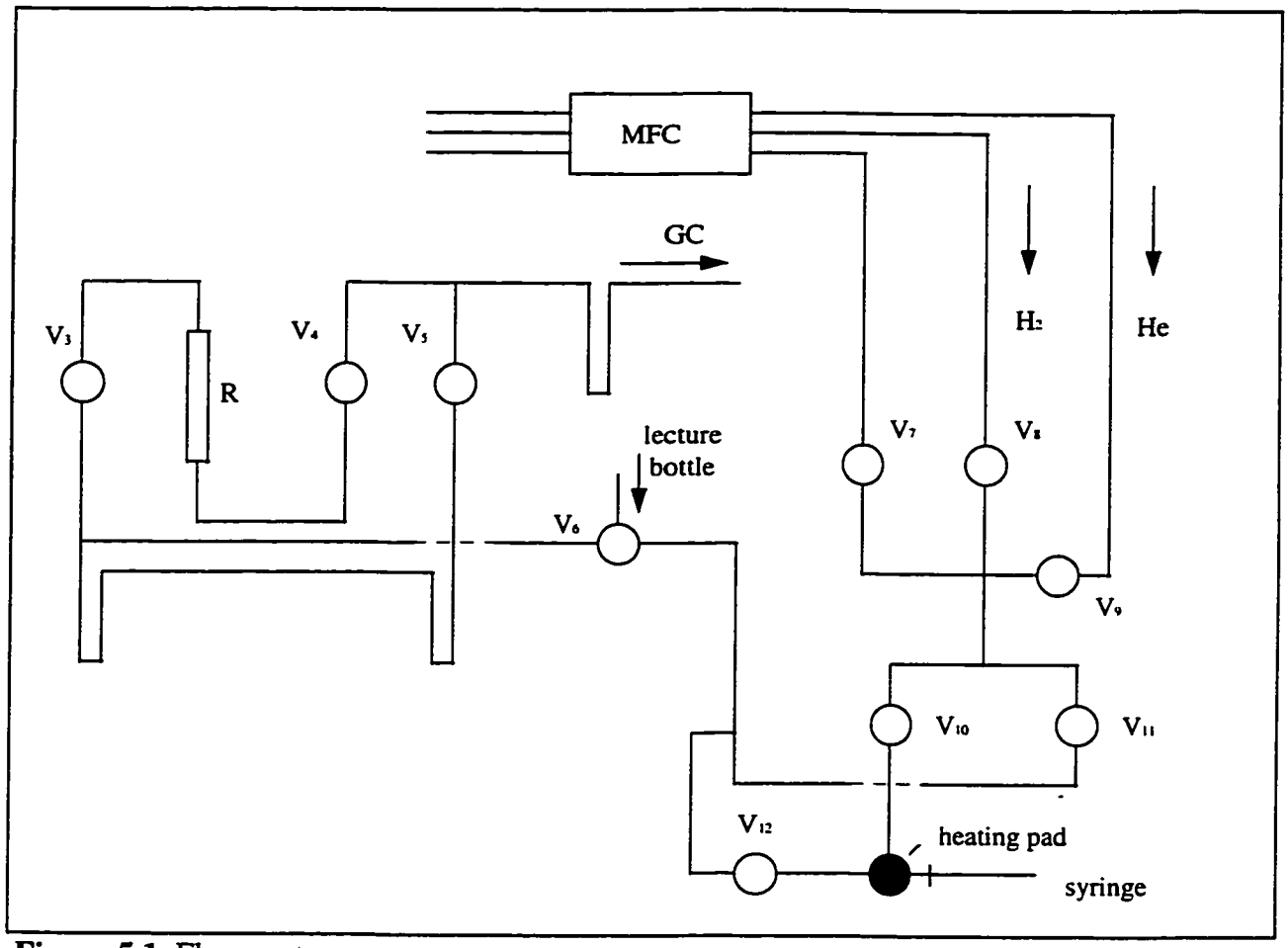

Figure 5.1 Flow system.

Hydrogen (Ultra-high purity, 99.995%) and helium (Ultra-pure carrier grade, <1 ppm O_2 and H_2O) were obtained from Air Products Ltd. The gas cylinders were equipped with two stage regulators to which 1/4" o.d. copper tubing with Swagelok fittings were attached. Gas flow rates were regulated by a Matheson model 8249 multiple mass flow controller (MFC) and valves V_7, V_8 and V_9 were brass Nupro B-4HK packless bellows sealed valves. Tubing which passed through valve V_7 was extra tubing and was not used in this work.

The injection port segment consisted of three valves (V_{10}, V_{11} and V_{12}) which were Nupro SS-2H bellows sealed valves. Injections into the flow system were made using a stainless steel syringe. The syringe resided on a Sage Instruments syringe pump model 341

(not shown in Figure 5.1) and it was attached to the flow system via a stainless steel bored-through Swagelok T fitting.

Attached to the GC is a 6-port stainless steel gas sampling valve. The reactor/bypass segment (like the injection port segment) consisted of 1/8" stainless steel tubing and valves V_3 and V_4 were stainless steel Hoke packless bellows whilst V_5 was a Nupro SS-2H bellows sealed valve. By closing V_3 and V_4 with V_5, open the reactor, R, could be bypassed and gas mixtures flowed directly towards the gas sampling valve of the GC. Conversely, if V_5 was closed and V_3 and V_4 were opened, gases would flow through the reactor prior to reaching the GC. Valve V_6 was a three way valve to which a gas from a lecture bottle could also be introduced into the system, *e.g.* in the determination of the retention times of *unretained* gases, such as methane or butane, from which column flows were determined.

The micro reactor, shown in Figure 5.2, was constructed from 3/8" o.d. stainless steel and connected to the flow system via Cajon VCR fittings using copper gaskets. A narrow 7 mm o.d., 8 cm length quartz tubing was placed inside the 8 mm i.d. (1 cm^3 in volume) reactor to position the catalyst which resided on quartz wool at the centre of the furnace. The furnace was constructed from 1.07 Ω/ft nichrome wire having a total resistance of 12 Ω and catalyst temperatures were measured by a sheathed Type K thermocouple the output of which was displayed on a digital Omega model 670 thermocouple thermometer.

All experiments were performed at atmospheric pressure with a helium carrier gas flow of 150 cc/min through the system and a hydrogen gas flow rate of 80 cc/min when needed for catalyst reduction. In the results presented in section 5.4 150 mg catalyst samples were activated at 500°C either under helium for an hour or under hydrogen for three hours if reduction was necessary. Reactions were then carried out by flowing 4.6 mol% olefin (2-methyl-2-pentene) in a helium stream at 250°C.

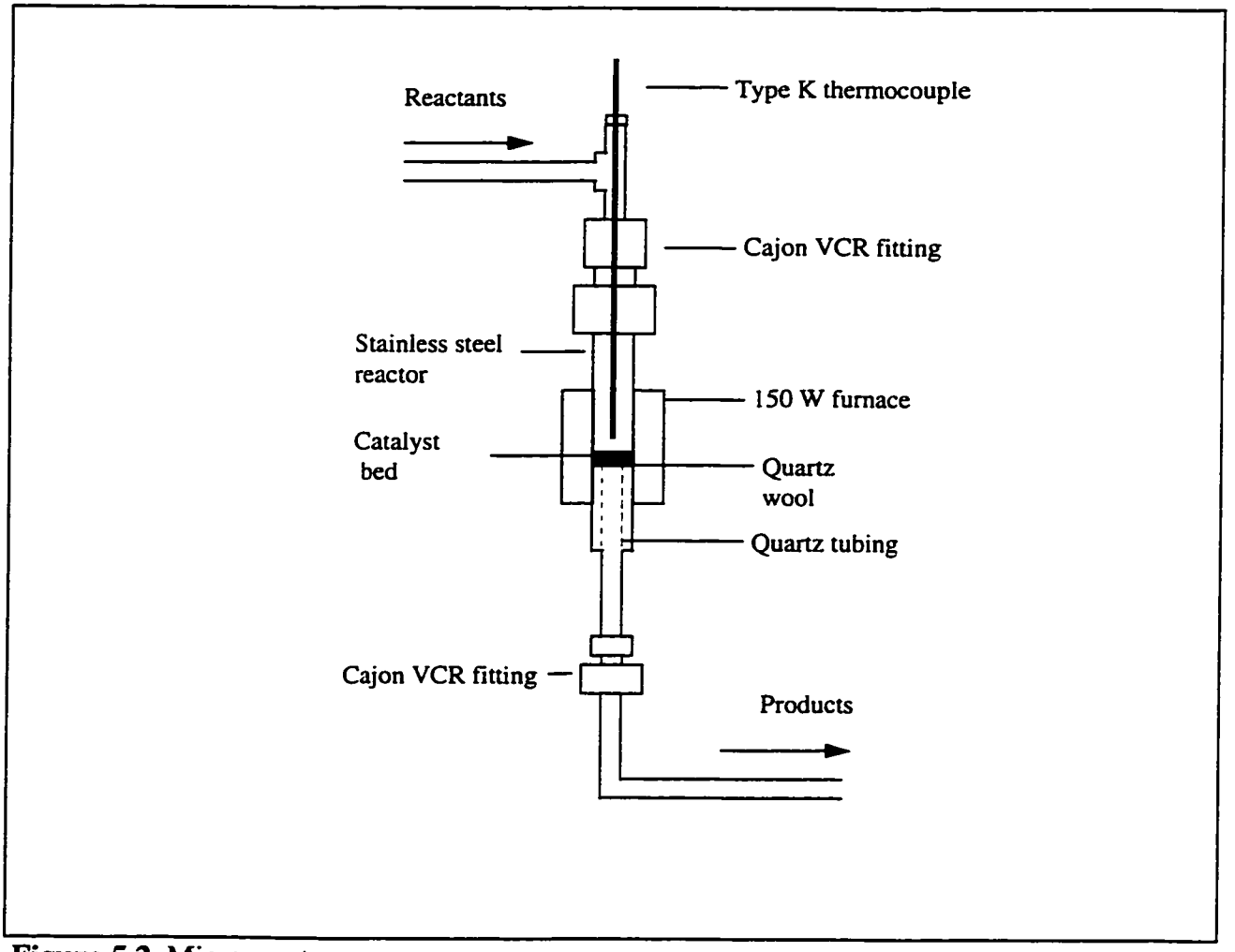

Figure 5.2 Micro reactor.

5.3.2 Gas Chromatograph

The GC was initially equipped with a conventional packed column, but because the separation of the isomers of 2M2P required a capillary column, it was necessary to modify the instrument to accept a J&W 60 m, 0.32 mm o.d. DB-1 fused silica capillary column. It was also necessary to install a J&W model II split injector system which was based on a flow controlled back pressure regulated pneumatic system; this allowed for the control of the injection port flow and the column flow. A flame ionization detector (FID) was used in this work, the signals of which were integrated using a Hewlett Packard 3390A integrator.

The majority of GC detectors are designed for packed column use where optimum performance is achieved when carrier gas flow rates lie in the range of 20-60 cc/min. However in the case of capillary columns, carrier gas flow rates are considerably less and typically lie between 0.5-4 cc/min [3,7]. As a result, these lower flow rates lead to a lower signal/noise at the detector. In order to circumvent this problem and to optimize the sensitivity of the detector, nitrogen *make up gas* was added at the column detector interface; thus the nitrogen flow rate was independent of carrier gas flow rates.

As noted previously, the MFC was used to regulate the total flow of carrier gas in the flow system up to the injection port of the split injector. The back pressure regulator in the split injector system was used to set the column head pressure, *i.e.* the average linear gas velocity through the column. The carrier gas flow rate through the column is simply determined by the head pressure assuming that the pressure of the column end is constant (atmospheric pressure). The two flows, column and inlet, were set using different devices and were independent of one another. The *split ratio* is the ratio of the split vent flow (measured at the split vent port or split flow exit) to the column flow. Physically it is the amount of sample transferred onto the column; for example, a split ratio of 100:1 indicates that for every sample taken, 100 parts is vented and 1 part enters the column. The split injector was an essential addition to the GC due to the smaller diameter of a capillary column relative to a packed column and the resulting differences in flow rates. In the case of capillary columns where flow rates are much lower an increase in split ratio would result in a quicker removal of sample material from its port of entry, narrower band widths and even sharper, but perhaps smaller peaks. Hence the split ratio can be readily changed depending on the type of sample and analysis required.

The following pneumatics, recommended by Varian and J&W Scientific were used:

Table 5.1 Pneumatics.

Gas	Gas cylinder regulatory pressure/psig	Flow rate/cc.min^{-1}
H_2 (FID)	40	30
air (FID)	60	300
N_2 (FID make up)	50	42
He (column carrier)	60	1

Carrier gas flow rates through a capillary column are usually expressed as linear velocities and can be measured by injecting a volatile non-retained compound, butane in this case (although methane would have also been suitable), and measuring its retention time, t_M. For a capillary column the linear velocity, u, is given as:

$$u(cm/s) = \frac{L}{t_M} \tag{5.2}$$

where L is the length of the column. The flow rate can then be determined from the relationship:

$$Flow(cc/min) = \frac{(\pi r^2 L)}{t_M} \tag{5.3}$$

where r is the radius of the column.

The auto linear temperature program used in this work is shown in table 5.2 and it was similar to that used by Stuart L. Soled of Exxon Research and Engineering Co.; Soled used a similar capillary column in his work with a 140:1 split ratio, whereas we used a split ratio of 90:1.

Table 5.2 Auto Linear Temperature Program.

T_1/°C	t_1/min	Program rate °C/min	T_2/°C	t_2/min
29	17	17	180	15

In order to correlate our results with those of Exxon, 2M2P and *trans* 4-methyl-2-pentene (*trans* 4M2P) were injected manually into the GC and the back pressure regulator was adjusted, the setting of which usually was in the 13-15 psi range, until matching retention times were obtained.

A list of retention times, provided by Soled, for various hexene isomers is given below in Table 5.3 and the results obtained in this section were referenced to this table.

Table 5.3 Hexene Isomer Retention Times (provided by Exxon; see Appendix I for the list of acronyms).

Retention time/min	Exxon peak assignment
4.831 - 8.405	C1 - C5
12.30	1H
10.127	4M1P
10.210	3M1P
10.717	23DM1B
10.808	***cis* 4M2P**
10.995	*trans* 4M2P
11.889	3MP
12.257	2M1P
13.173	2E1B
13.446	*cis and trans* 3H
13.668	*trans* 2H
13.928	2M2P
14.189	*cis* 3M2P
14.555	*cis* 2H
15.189	***trans* 3M2P**
16.355	23DMB
17.451 - 29.612	C7+

5.4 *SELECTED RESULTS*

In performing experiments using the gc/flow system numerous variables were encountered, and as a result, the majority of experiments consisted in ways in trying to optimize the efficiency of the tools in relation to the isomerization of 2M2P over various catalysts. The results presented in this section give insight into some of the work performed with yttria-silica-alumina catalysts, 4 and 16% (the same catalysts which were discussed in Chapter 3). Additional measurements were carried out on some γ-Al_2O_3 catalysts which contained 0.3 wt. % Pt and 1 wt. % fluoride ion. These were the same ECx catalysts which were discussed in Chapter 4. These results were chosen to illustrate the use of the GC/flow system to which more improvements still need to be made.

Table 5.4 Conversions and selectivities of 2M2P over YSA and EC catalysts*.

Catalyst	Q_1	Q_2	$S_{DBM\ 1}$	$S_{DBM\ 2}$	$S_{SKI\ 1}$	$S_{SKI\ 2}$	$(S_{SKI}/S_{DBM})_1$	$(S_{SKI}/S_{DBM})_2$
4% YSA	61.57	71.16	10.40	4.62	10.37	2.02	1.00	0.44
16% YSA	52.51	22.48	5.27	11.37	5.03	9.84	0.95	0.87
EC 400	34.95	0.91	5.61	0.28	2.65	0.51	0.47	1.82
EC 450	46.98	97.60	5.69	0.14	5.88	0.26	1.03	1.86
EC 550	40.05	36.51	8.18	4.00	7.86	5.12	0.96	1.28

*where DBM and SKI are the double bond migration (formation of *cis* 4M2P) and skeletal isomerization (formation of *trans* 3M2P) reactions for the two runs (1 and 2) performed on each of the catalysts; Q and S are their respective conversions and selectivities, shown in equations 5.4 and 5.5.

$$Q = \left(\frac{\sum (area) - (area)_{2M2P}}{\sum (area)} \right) * 100 \qquad (5.4)$$

$$S_{4M2P} = \left(\frac{(area)_{4M2P}}{\sum (area) - (area)_{2M2P}} \right) * 100 \qquad (5.5)$$

5.5 DISCUSSION

With both the YSA and EC catalysts it was observed that the baseline increased after 17 min., then settled, and that small peaks were eluted during the ramping of the temperature; the majority of the peaks came out after 25 min. (more so in the second runs). Hence not only were hexene isomers observed, but also higher molecular weight compounds, eluted at higher temperatures.

The skeletal isomerization to double bond migration selectivity ratios for YSA catalysts indicate a decrease in acidity in the first run from 4 to 16% YSA as was expected since 16% YSA is less acidic than 4% YSA. In the second run however the opposite was true; it is difficult to make comparisons between runs since catalyst activity varies over time on line as was indicated by the differences in selectivity ratio from trial 1 to 2. In the case of the EC catalysts the selectivity ratio increased from EC400 to EC450 then decreased from EC450 to EC550. Hence there exists a relationship between calcination temperature and catalyst activity with EC450 resulting in optimum activity. However, IR results show that EC400 is the most acidic catalyst and it was expected to have optimum activity, but this was not the case.

Conclusions based on these preliminary results are difficult to make as there are other variables which need to be optimized such as the sensitivity of the FID detector and the split ratio. The major source of error in this work was the method of 2M2P injection. Several experiments were performed to test the constancy of the flow of the reactant, from various

syringes using the Sage Instruments syringe pump, some of which lasted for over 6 hours with samples bypassing the reactor and sampled at 20 min. intervals. In all cases there was a large deviation in 2M2P areas over an entire experiment, up to 38% in some cases, not to mention that sample introduction from the flow system into the GC was performed manually which added to the overall uncertainty. One alternative would be to use a precision fluid delivery Isco syringe pump instead of the Sage Instruments syringe pump currently in use; the former instrument is a pulse free delivery pump capable of operating over a wide range of flow rates, 0.1 μl/min-200 ml/min, and pressures, 0-10 000 psi [11]. This instrument would alleviate many problems associated with constant flow deliveries including the presence of air-bubbles in syringes. However the cost of this instrument coupled with the cost of the large amounts of reactant 2M2P which would be necessary to fully carry out this type of work was not within the financial means at the time (≈ $20,000) and as a result the project was suspended.

REFERENCES

1. Cvetanovic R.J. and Amenomiya Y.
   *Adv. Catal., **17**, 103 (1967)*

2. Guillaume D., Gautier S., Despujol I., Alario F. and Beccat P.
   *Cat. Lett., **43**, 213-218 (1997)*

3. Pearce R. and Patterson W.R. *eds.*
   "Catalysis and Chemical Processes", Blackie and Son Ltd., Glasgow 1981

4. Wojciechowski B.W. and Corma A.
   "Catalytic Cracking Catalysts, Chemistry and Kinetics", Marcel Dekker, Inc., N.Y. 1986

5. Pines H.
   "The Chemistry of Catalytic Hydrocarbon Conversion", Academic Press, Inc., N.Y. 1981

6. Olah G.A. and Molnar A.
   "Hydrocarbon Chemistry", John Wiley & Sons, Inc., N.Y. 1995

7. Kramer G.M. and McVicker G.B.
   *Acc. Chem. Res., **19**, 78-784 (1986)*

8. Soled S.L., McVicker G.B., Murrell L.L., Sherman L.G., Dispenziere N.C., Hsu S.L. and Waldman D.
   *J. Cat., **111**, 286-295 (1988)*

9. Kramer G.M., McVicker G.B. and Ziemak J.J.
   *J. Cat., **92**, 355-363 (1985)*

10. Soled S. and McVicker G.B.
*Cat. Today, **14**, 189-194 (1992)*

11. *Chemical and Engineering News, **74** (20), p.35 May 13, 1996*

CHAPTER 6

THIN FILMS

6.1 INTRODUCTION

All oxides are strong absorbers of infrared radiation in the spectral regions associated with their lattice vibrations. Consequently, when using traditional self supporting discs which contain a minimum of about 2 to 10 mg of material per cm^2 (the exact quantity depends on the type of oxide and on its surface area), IR spectra of adsorbed species which have vibrations themselves in the lattice region cannot be observed. In particular, when an adsorbate containing a metal atom Z adsorbs on an metal oxide M_xO_y to give linkages M-O-Z or $(M\text{-}O)_2Z$, the stretching vibrations associated with these assemblies will generally lie in the spectral region where the oxide disc is itself opaque. This severely limits one's ability to determine the structure of adsorbed species.

The low wavenumber cutoff depends on the nature of the oxide. For silica, it is about 1300 cm^{-1} although there are two regions of partial transparency between 1000-850 cm^{-1} and between 750-600 cm^{-1}, as shown in Figure 1.1. For other oxides, cutoff is at or below 1000 cm^{-1}, and Figure 1.3 shows IR spectra of a self supporting disc of Al_2O_3 whose low wavenumber limit of transmission is 1000 cm^{-1}. The IR spectra of discs of TiO_2 and ZrO_2 are shown in Figure 1.5 and have low wavenumber limits of transmission at 900 and 800 cm^{-1} respectively.

To circumvent this problem of high background absorption in low wavenumber regions this laboratory developed in 1984 [1] what has been termed the *thin film* (TF) technique, at that

time for silica; the technique has also been used extensively by others [2-5]. In simple terms (further details are given in Chapter 1) the amount of silica is reduced to about 0.1 mg/cm^2 by forming a film of silica on an optically transparent support window, *e.g.* NaCl or ZnSe (see Figures 1.7 and 1.8). The infrared spectrum of adsorbed species in the regions where the background changes substantially is obtained via spectral subtraction, and an example of this was shown in Figure 1.9.

Considerable success has been achieved using the TF method with silica, and IR spectra of adsorbed species down to as low as 200 cm^{-1} have been obtained [1-3]. [To record spectra to 200 cm^{-1}, it is necessary to have a FTIR spectrometer with CsI optics, and the support window must be CsI, or silicon]. There are two limitations to this method. First, the sample can only be heated to about 450°C depending on the characteristics of the support window. Second, all experiments must be done *in situ* with the sample in a fixed position in the IR beam in order to avoid artefacts during spectral subtraction in regions where the background is rapidly changing. The latter limitations also mean that it is not possible to heat the sample after the experiment has begun, at least using the most common type of IR cell (shown in Figure 2.1).

Previous work in this laboratory has mainly been concerned with characterization of the surface of SiO_2. To this end, we have used a variety of so called hydrogen sequestering (HS) agents, that is, molecules which will react with surface SiOH groups to cleave the OH bond thus forming a SiOZ bond. The reaction between silica and $TiCl_4$ could be envisaged as follows:

SINGLE:

$$SiOH + TiCl_4 \longrightarrow SiOTiCl_3 + HCl \qquad (6.1)$$

H-BONDED:

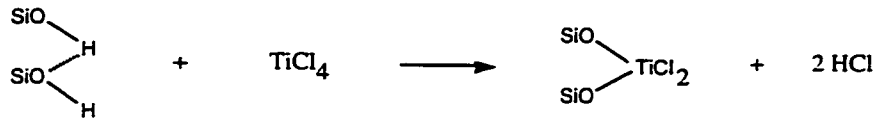

(6.2)

GEMINAL:

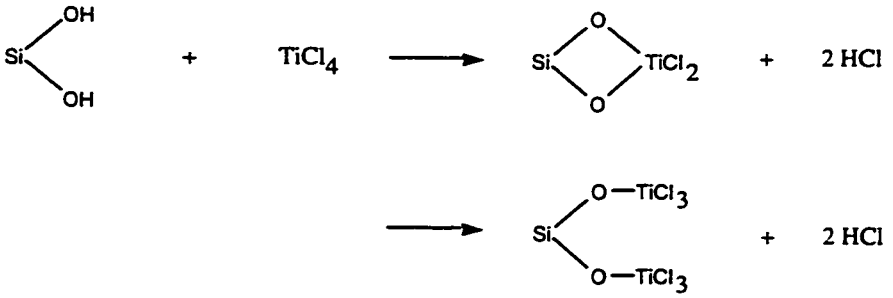

(6.3a) *top* and (6.3b) *bottom*

In addition, as has been previously found for $AlMe_3$, $TiCl_4$ might react with siloxane sites as follows:

(6.4)

Earlier studies [4] showed that $TiCl_4$ reacted with silica according to reactions (6.1), (6.2) and (6.3) [these results will be discussed in more detail later in this chapter]. Finally, the reactions of some other hydrogen sequestering agents with SiO_2 have been studied in our laboratory; these include, $GaMe_3$ [6], $AlMe_3$ [4], BF_3 [7,8], BCl_3 [8], $ZnMe_2$ [9], $CdMe_2$ [9], HMDS (hexamethyldisilazane, $Me_3SiNHSiMe_3$) [4], $SbMe_5$ [10], $PMe_{3-n}Cl_n$ (n = 0-3) [5,11,12], $P(OMe)_3$ [13], $POCl_3$ [11] and B_2H_6 [14]. As a result of these studies, a clear picture of the structure and reactivity of the silica surface has emerged.

Although the reactions of some of the above HS agents with self supporting discs of other oxides have been studied by us and by others, at the time this thesis work commenced there were no other published thin film studies of any oxide other than silica. Therefore, it was decided that this method might well be utilized to probe some simple oxides such as TiO_2, Al_2O_3 and ZrO_2. These oxides are more complex than silica by virtue of having multiple types of surface hydroxyl groups, and having Lewis acid sites, and weak Brønsted acidity in the case of TiO_2 and ZrO_2. Therefore, this was an uncharted area of research. As with silica, which has low wavenumber vibrational modes associated with Si-OH stretching and SiOH angle deformations, we anticipated that these oxides would also have such MOH modes which could render it difficult to interpret the spectrum of a new adsorbed species. This will be discussed further in Section 6.2.

The work described in this chapter is mainly concerned with studies of the TF spectra of SiO_2, Al_2O_3, TiO_2, and ZrO_2, and the reactions of the HS agents, HMDS, $TiCl_4$, $GaMe_3$ and BCl_3. The thin film spectra (4000-200 cm^{-1}) for all of these oxides were shown in Figures 1.6 and 1.7 and spectra on an expanded wavenumber scale, from 1400-200 cm^{-1}, are shown in Figures 6.1 and 6.2. Previous work with silica was limited to the spectral region above 500 cm^{-1} because of the use of a ZnSe support window, which in turn was dictated by the KBr optics of the Bomem FTIR spectrometer. During the course of this work the FTIR was fitted with CsI optics which would permit spectral studies down to 200 cm^{-1}; accordingly, using a CsI support window, we have re-examined the adsorption of these HS agents on silica. The importance of this is that MCl_x stretching modes generally lie in the spectral range from 500 to 350 cm^{-1}, and these could not have been observed with the ZnSe support window.

Although the surface area (m^2/g) for each of the oxides used is reported in Chapter 1, we repeat the data here: SiO_2 (200), Al_2O_3 (105), TiO_2 (55) and ZrO_2 (45).

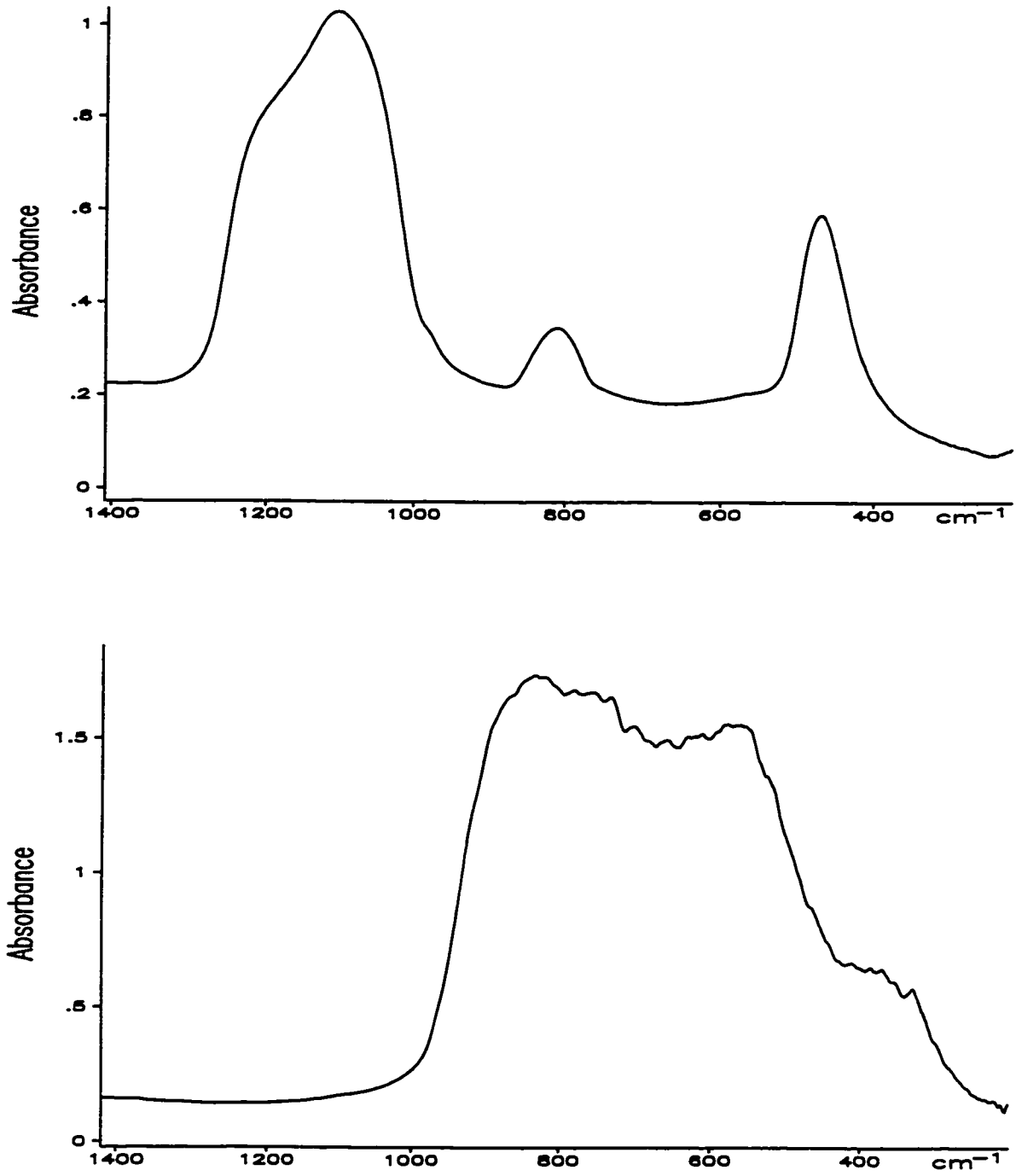

Figure 6.1 Infrared spectra of room temperature activated silica (top) and alumina (bottom) thin films.

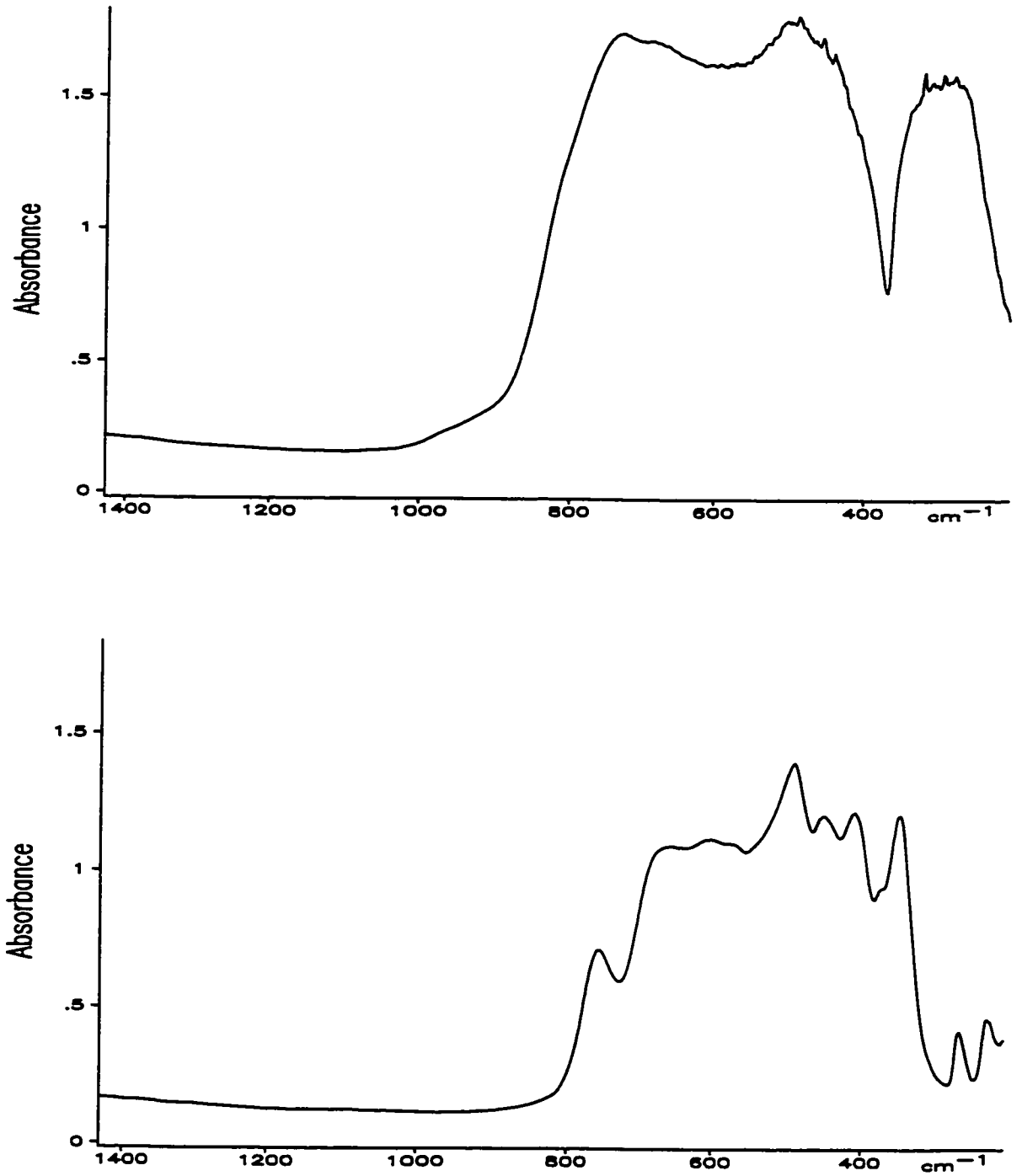

Figure 6.2 Infrared spectra of room temperature activated titania (top) and zirconia (bottom) thin films.

6.2 *LOW WAVENUMBER OH MODES*

The infrared spectrum of silica has bands below 1000 cm^{-1} which are due to Si-OH stretching modes at 984 cm^{-1} and due to SiOH angle deformation modes at 860 and 778 cm^{-1}. When SiO_2 reacts with an HS agent, the disappearance of these bands would be expected to appear as a negative feature in any spectrum which is derived from subtracting the background spectrum before reaction from that which is observed after reaction. The existance of these modes can be revealed by H/D exchange (treating the sample with D_2O) and subtracting the 'H' spectrum from the 'D' spectrum. An example of such an exercise is shown for silica in Figure 6.3. Peaks going down are due to the 'H' form, those going up are due to the 'D' form. The Si-OH stretch originally at 984 cm^{-1} shifts to 960 cm^{-1} upon deuteration, and the doublet at 860/778 cm^{-1} shifts to 620 cm^{-1}. [The reason for the doublet in the 'H' spectrum and a single peak in the 'D' spectrum has been discussed by Morrow and McFarlan in [15]]. Therefore, reaction with OH groups on silica with an HS agent would be expected to show negative features due to the disappearance of the sharp feature at 984 cm^{-1} and the broad 860/778 cm^{-1} doublet.

The features noted above for SiO_2 are well known. However, for the other oxides this is an unexplored area. Experiments involving H/D exchange were carried out for Al_2O_3, ZrO_2 and TiO_2, at either 150 or 450°C activation. For ZrO_2 and TiO_2, no features could be detected which could be attributable to OH features on the surface. Given the very low intensity of the OH stretching modes on these materials, we assume that these bands were below the detection limit, given the very high background absorption below 800 and 900 cm^{-1} respectively for ZrO_2 and TiO_2.

For Al_2O_3, which has a higher absorbance in the OH stretching region than the previous two oxides, features were detected. Figure 6.4 shows the spectrum observed after H/D exchange. There is a negative band at 943 cm^{-1} and a positive one at 707 cm^{-1}. The isotope shift is by a factor of 1.33 which certainly suggests that this is a mode associated with

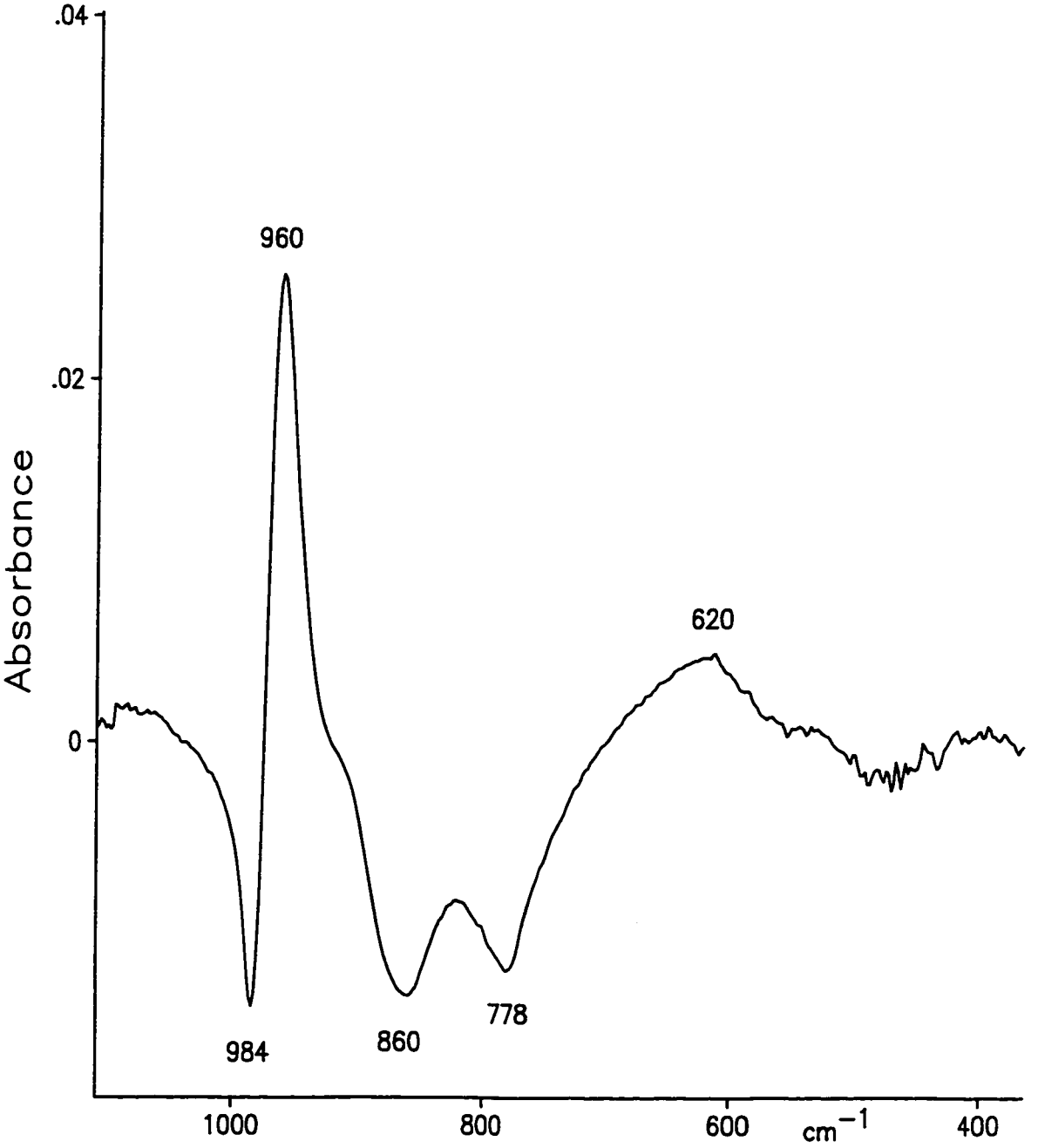

Figure 6.3 Silica thin film which has been subjected to H/D isotope exchange.

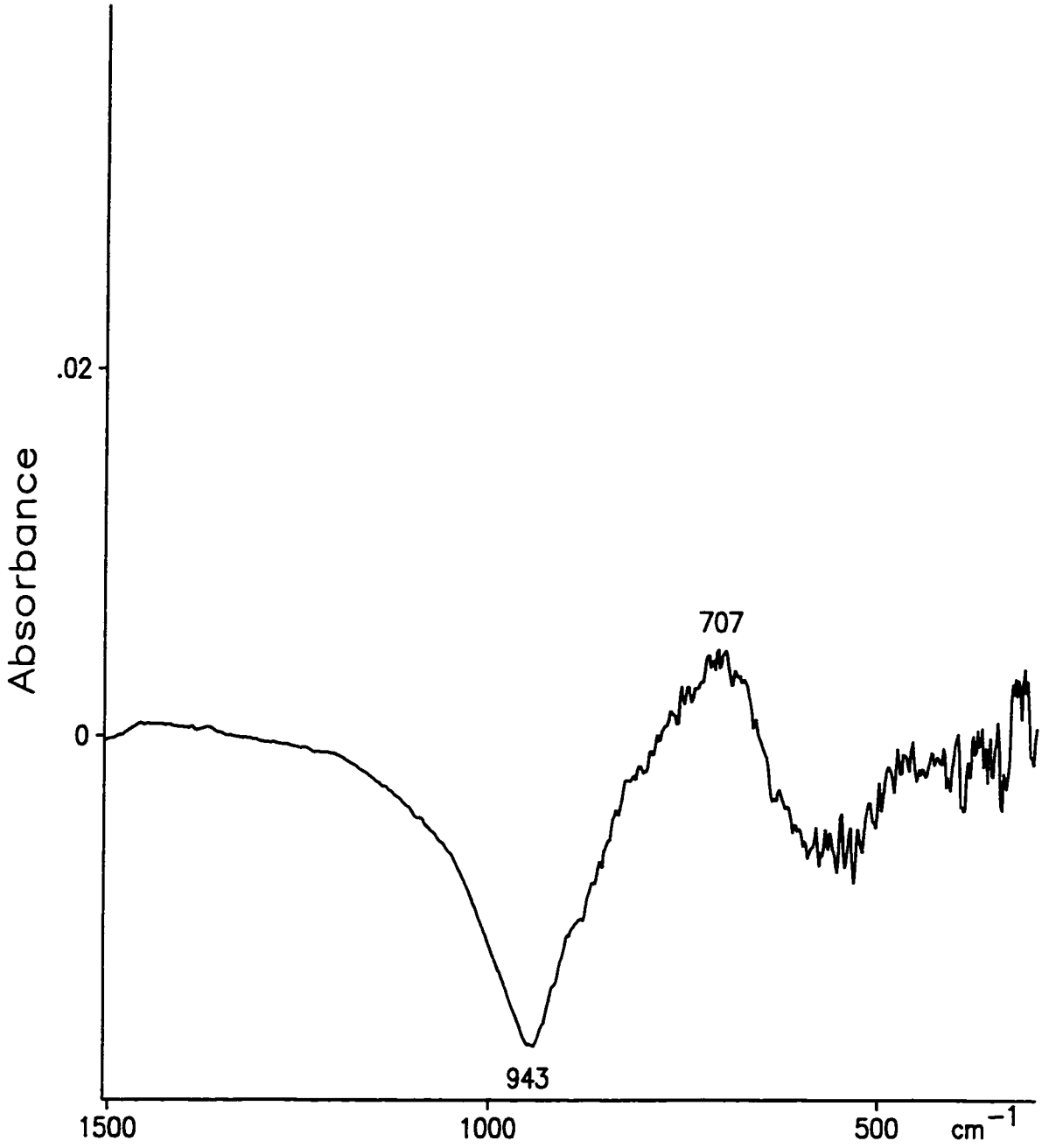

Figure 6.4 Alumina thin film which has been subjected to H/D isotope exchange.

an AlOH angle deformation vibration (the shift is about the same for the SiOH angle deformation mode). Although the spectrum shown in Figure 6.4 is applicable to Al_2O_3 which had been only subjected to room temperature evacuation, a similar 'negative' band at 943 cm^{-1} was found from H/D exchange for samples activated at 400°C. Therefore, we expect this negative feature to be present in the spectra of alumina after reaction with an HS agent.

6.3 HEXAMETHYLDISILAZANE (HMDS) ADSORPTION

HMDS ($Me_3SiNHSiMe_3$) is a well known silylating agent [4,16,17] and reacts with MOH groups to produce $MOSiMe_3$ with the liberation of NH_3. The reaction is extremely rapid at room temperature and on a self supporting disc the reaction is complete within about 60 seconds [17]. Figure 6.5 shows the IR spectra of HMDS and HMDS-d_{18} adsorbed on silica. The strong doublet near 850 cm^{-1} and a weaker band at 758 cm^{-1} are due to rocking modes of the methyl group and the band at 1260 cm^{-1} is due to the symmetric methyl deformation mode. In the spectrum of HMDS-d_{18} the pair of bands at 777 and 737 cm^{-1} are methyl rocking modes and the methyl angle deformation is at 1009 cm^{-1}.

The negative peak near 980 cm^{-1} is due to the replacement of the Si-OH stretching mode by the antisymmetric Si-O-Si stretching mode at 1022 cm^{-1}. In gas phase HMDSO or HMDSO-d_{18} the latter mode is near 1075 cm^{-1}, and the symmetric Si-O-Si mode is found as a very weak band near 520 cm^{-1}. The IR and Raman spectra of HMDS adsorbed on silica have been published previously [4], and this spectrum is shown here as a reference spectrum for HMDS adsorbed on the other oxides. The methyl rocking and deformation modes are expected to be insensitive to the nature of the oxide, whereas the M-O-Si modes would be expected to shift depending on the nature of M. There is a suggestion of a negative feature near 1240 cm^{-1}. This is frequently observed when a HS agent chemisorbs on silica unless there is a strong overlapping band due to the chemisorbed fragment. Its origin is presumed to be related to a surface siloxane mode which absorbs radiation at the high wavenumber end of the

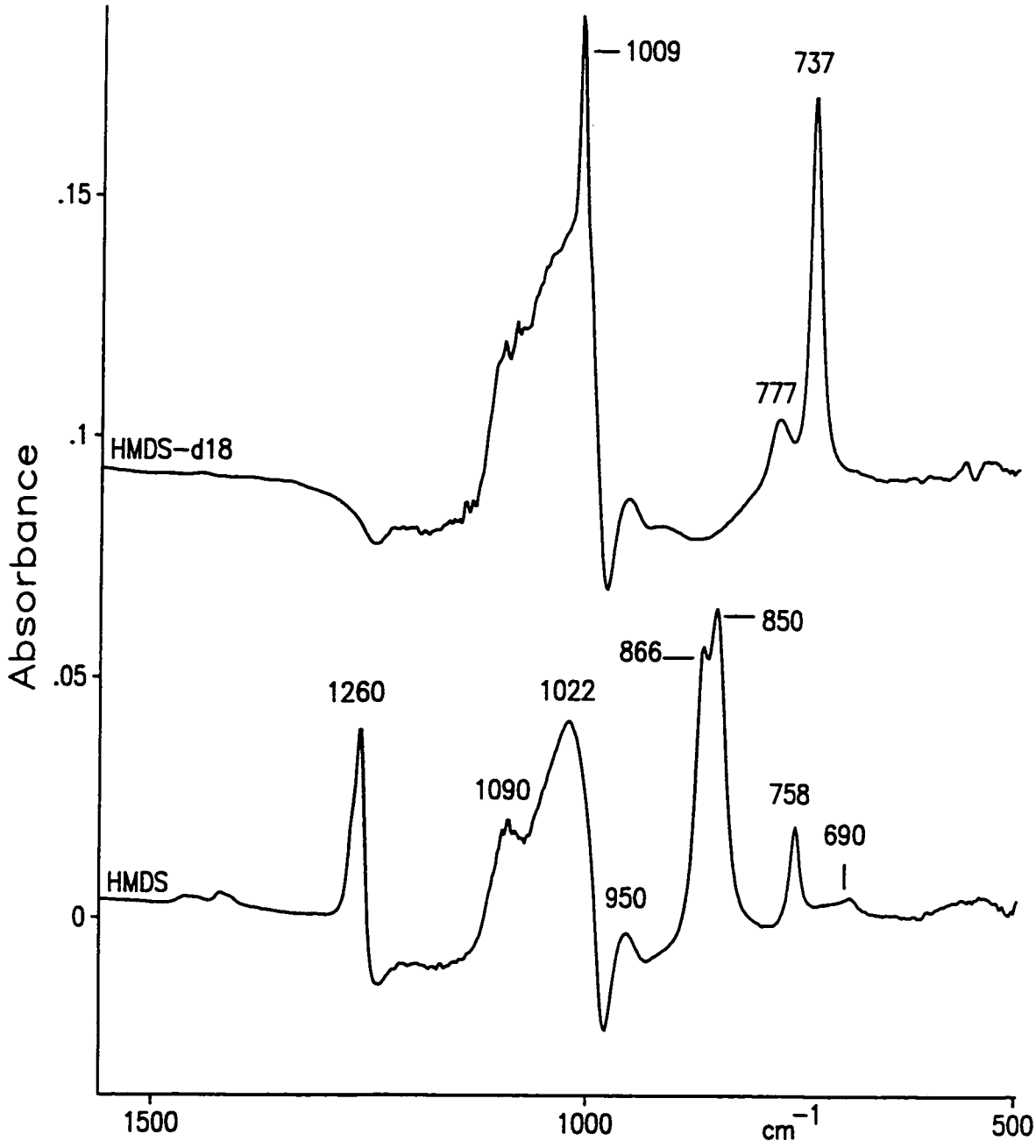

Figure 6.5 HMDS and HMDS-d_{18} chemisorbed on silica.

intense 1090 cm^{-1} band due to bulk SiOSi vibrations. In some examples to be discussed later, this negative feature is quite intense.

Figure 6.6 shows the spectra of HMDS chemisorbed on Al_2O_3, TiO_2 and ZrO_2 (for comparison the spectrum for SiO_2 is repeated). All spectra show the very distinct 1260 cm^{-1} methyl deformation mode (this band can be seen using discs of these oxides) and there is a band near 850 cm^{-1} which would correspond to the methyl rocking modes. For Al_2O_3 there is the expected negative feature near 940 cm^{-1} due to the elimination of the AlOH deformation modes, and there is a new broad feature at 1080 cm^{-1} which is known to be the expected position of an Al-O-Si stretching mode [18]. For ZrO_2 there is a relatively strong band at 838 cm^{-1} which would correspond to a methyl rocking mode. It is tempting to assign the sharp feature at 750 cm^{-1} to another rocking mode, but as will be discussed later in connection with the adsorption of other HS agents, this band is a common feature in most spectra of molecules chemisorbed on ZrO_2 and is a spectral artefact. In the spectrum of ZrO_2 there is a sharp strong band at 970 cm^{-1} which, from other work in this laboratory related to the preparation of zirconia-silica catalysts, is due to the Zr-O-Si stretching mode [19]. The weak bands below 700 cm^{-1} are unassigned, they may be due to SiC stretching modes [20], or to the symmetric Zr-O-Si stretching mode.

The spectrum of HMDS on TiO_2 will be briefly discussed because there were problems with this oxide in all of the studies which might be related to its unusual reactivity. The band at 850 cm^{-1} is the usual methyl rocking mode and the negative feature at 830 cm^{-1} is another spectral artefact which will be discussed further later. The strong broad band at 970 cm^{-1} is certainly due to the antisymmetric Ti-O-Si stretching mode [4,20]. A unique band was observed at 1190 cm^{-1} which was not observed for HMDS adsorbed on any of the other oxides. For HMDS itself, there is a unique IR band at 1186 cm^{-1} which is due to the NH deformation mode, and at first glance we considered that this band could be due to some retained, unreacted HMDS on TiO_2. However, no other IR bands which are unique to HMDS could be observed. It also was not an artefact due to the use of a thin film; the spectrum above 900 cm^{-1} was

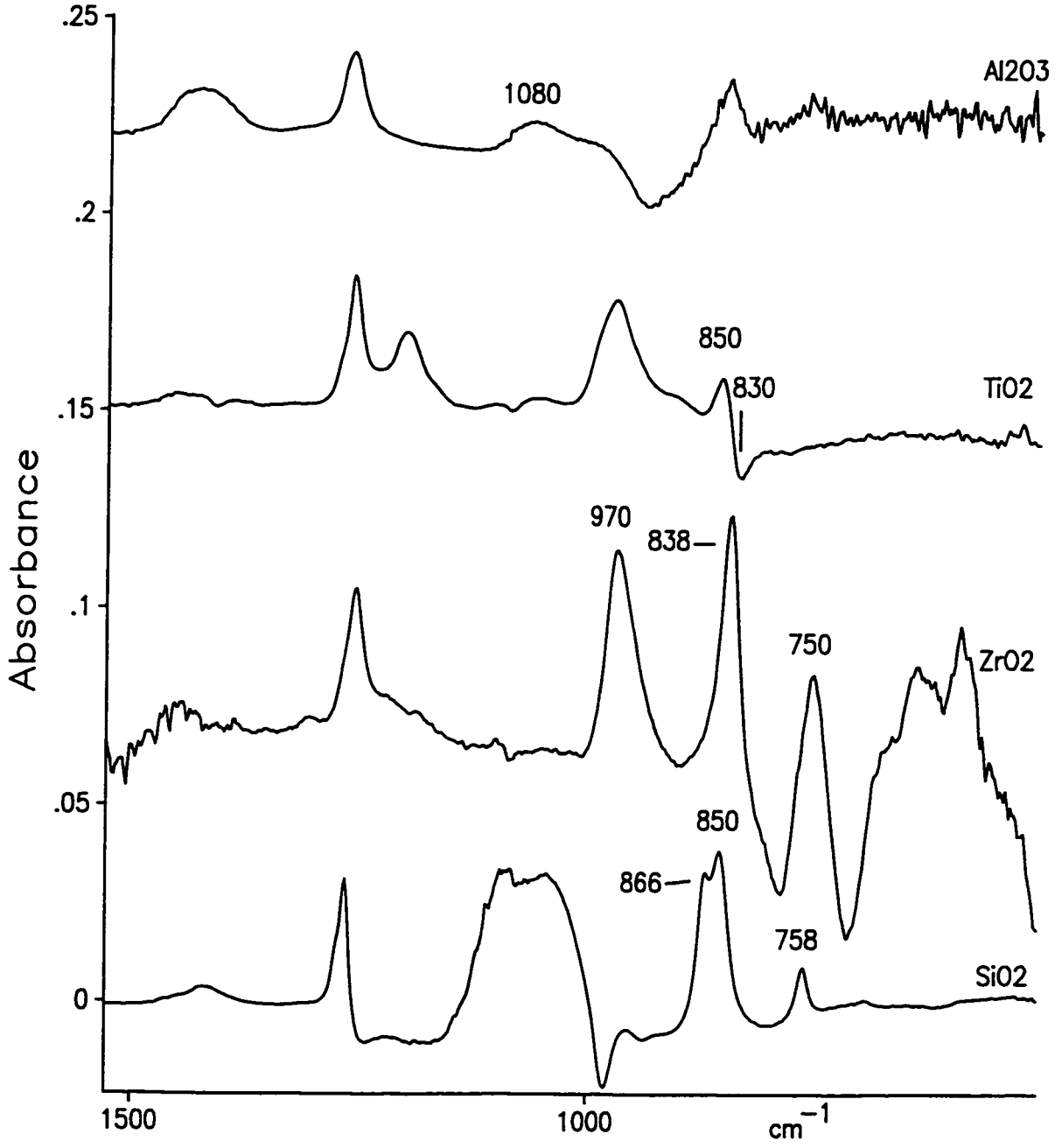

Figure 6.6 HMDS chemisorbed on Al_2O_3, TiO_2, ZrO_2, and SiO_2 (which was previously shown in Figure 6.5).

identical for HMDS chemisorbed on a TF or on a self supporting disc. However, the disc experiments revealed weak additional bands at 1600 and 1518 cm^{-1} which were not observed following the adsorption of HMDS on any of the other oxides. The latter bands are in regions known to be associated with NH_3 and NH_2 vibrations (see Chapter 3). Therefore, we adsorbed NH_3 on a TiO_2 disc to test this hypothesis, and characteristic IR bands were observed at 1518 cm^{-1} ($TiNH_2$ from the dissociative adsorption of NH_3) and at 1600 and 1182 cm^{-1} (coordinated NH_3). Evidently, the ammonia which is released during the trimethylsilation of TiO_2 by HMDS is capable of further reacting with this oxide.

6.4 TRIMETHYLGALLIUM (TMG) ADSORPTION

TMG, unlike HMDS, might be expected to react bifunctionally with OH groups (*e.g.* the equivalent of reactions 6.2 or 6.3), but previous studies of its reaction with silica have shown that the sole product of the reaction is $SiOGaMe_2$ and CH_4 [4]. Like HMDS, the low wavenumber modes associated with methyl deformation and rocking modes are not expected to be sensitive to the nature of the metal oxide; for gas phase $GaMe_3$ they occur at 1210 cm^{-1} and at 770/725 cm^{-1} [21] respectively. The M-O-Ga stretching mode would be expected to depend on the nature of M.

The IR spectrum of TMG chemisorbed on SiO_2 is shown in Figure 6.7A (and in Figure 6.7B). The bands near 740 and 700 cm^{-1} are due to methyl rocking modes and those at 600 and 540 cm^{-1} are due to the antisymmetric and symmetric GaC_2 stretching modes of $SiOGaMe_2$ [4,6]. The very strong band at 1003 cm^{-1} is due to the Si-O-Ga antisymmetric stretching mode and it is assumed that the apparent peak at 962 cm^{-1} is an artefact due to the disappearance of the Si-OH stretching mode at 980 cm^{-1} which appears as a 'negative' feature superimposed on the low wavenumber side of the 1003 cm^{-1} peak. It is to be noted that there is a very pronounced negative feature between 1250 and 1200 cm^{-1} with a sub-maximum at

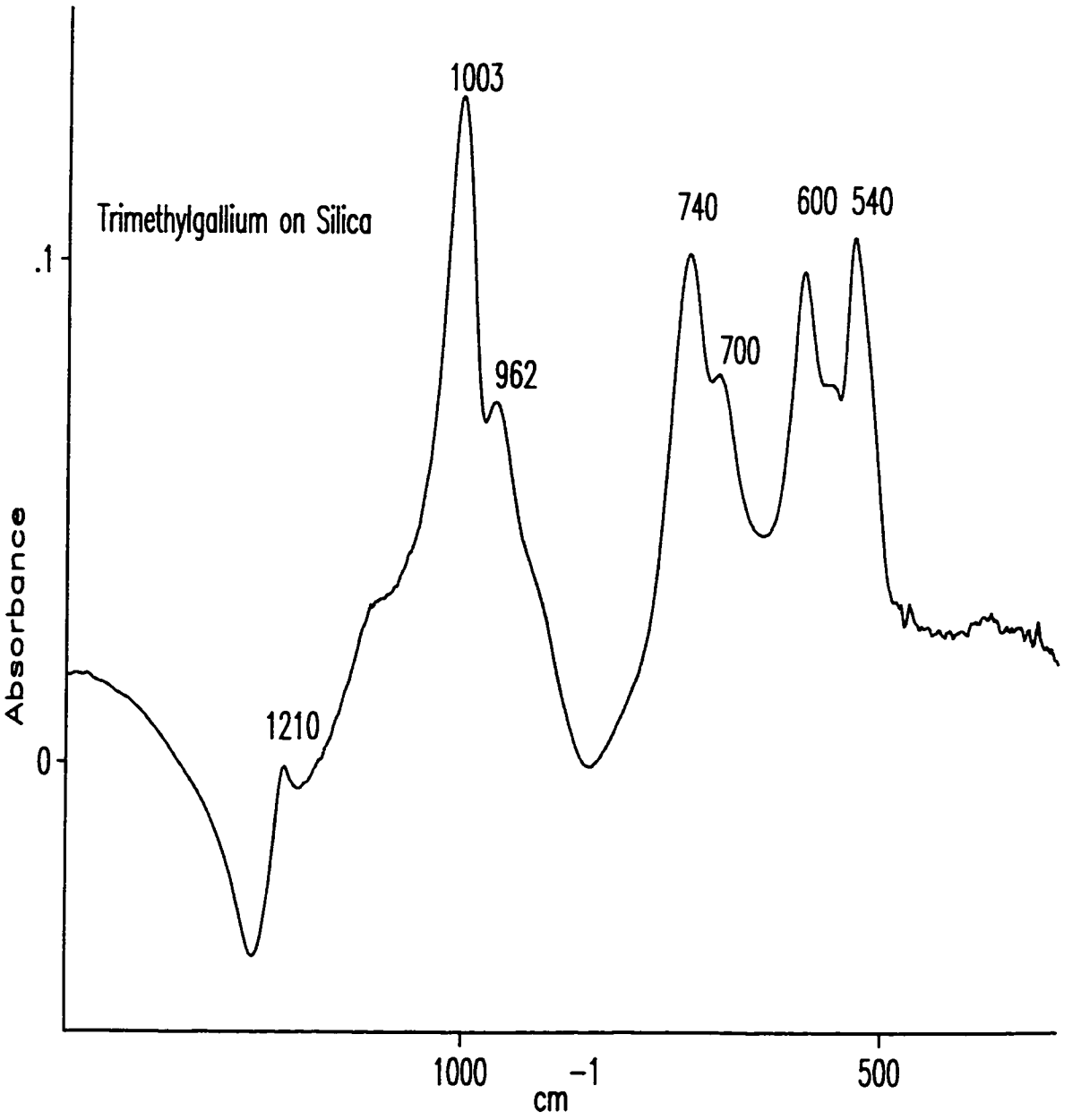

Figure 6.7A Trimethylgallium chemisorbed on silica.

1210 cm^{-1}; the latter is due to a symmetric methyl deformation mode. The negative feature is, as was found with HMDS chemisorption on SiO_2, associated with the disappearance of a surface mode of silica, and is a common feature in most TF spectra when there is not a strong overshadowing new spectral feature in this wavenumber region. The above features have been noted previously in IR and Raman studies of the chemisorption of TMG on SiO_2 which have been carried out in this laboratory [4,6]. A weak feature in the low wavenumber region appears at 560 cm^{-1}; this is possibly due to the symmetric SiOGa stretching mode which is expected to lie in this spectral region.

The spectrum of TMG chemisorbed on SiO_2 was the same regardless of the temperature of activation, room temperature, 150 or 400°C. This is consistent with the previous notion that TMG only reacts monofunctionally with SiOH groups [4]; that is, the degree of hydrogen bonding does not alter the structural form of the chemisorbed species. Moreover, the spectrum did not change when water or oxygen was added to the sample. Given that TMG is extremely pyrophoric and is extremely reactive with water, this would appear to be an anomaly. However, as with many chemisorbed metal alkyl compounds, sequestering of the first alkyl group is often very facile whereas removal of a second alkyl is often an activated process [6,9]. Therefore, although removal of the first methyl via reaction with SiOH occurs readily, even in the presence of water, removal of a second methyl is difficult and probably requires higher temperatures before this reaction proceeds at an appreciable rate. This behaviour has been postulated previously by this laboratory in a study of the reaction of TMG with silica discs, but in that case we only had access to the CH stretching region near 2900 cm^{-1}, a region which is not very structure sensitive. That there is no change in the low wavenumber region associated with GaC and SiOGa vibrations strongly supports the notion that $SiOGaMe_2$ is relatively unreactive with water at room temperature.

The spectrum of TMG chemisorbed on Al_2O_3 (Figure 6.7B) is very similar to that for TMG on SiO_2 with respect to the methyl rocking, deformation and Ga-C_2 stretching modes.

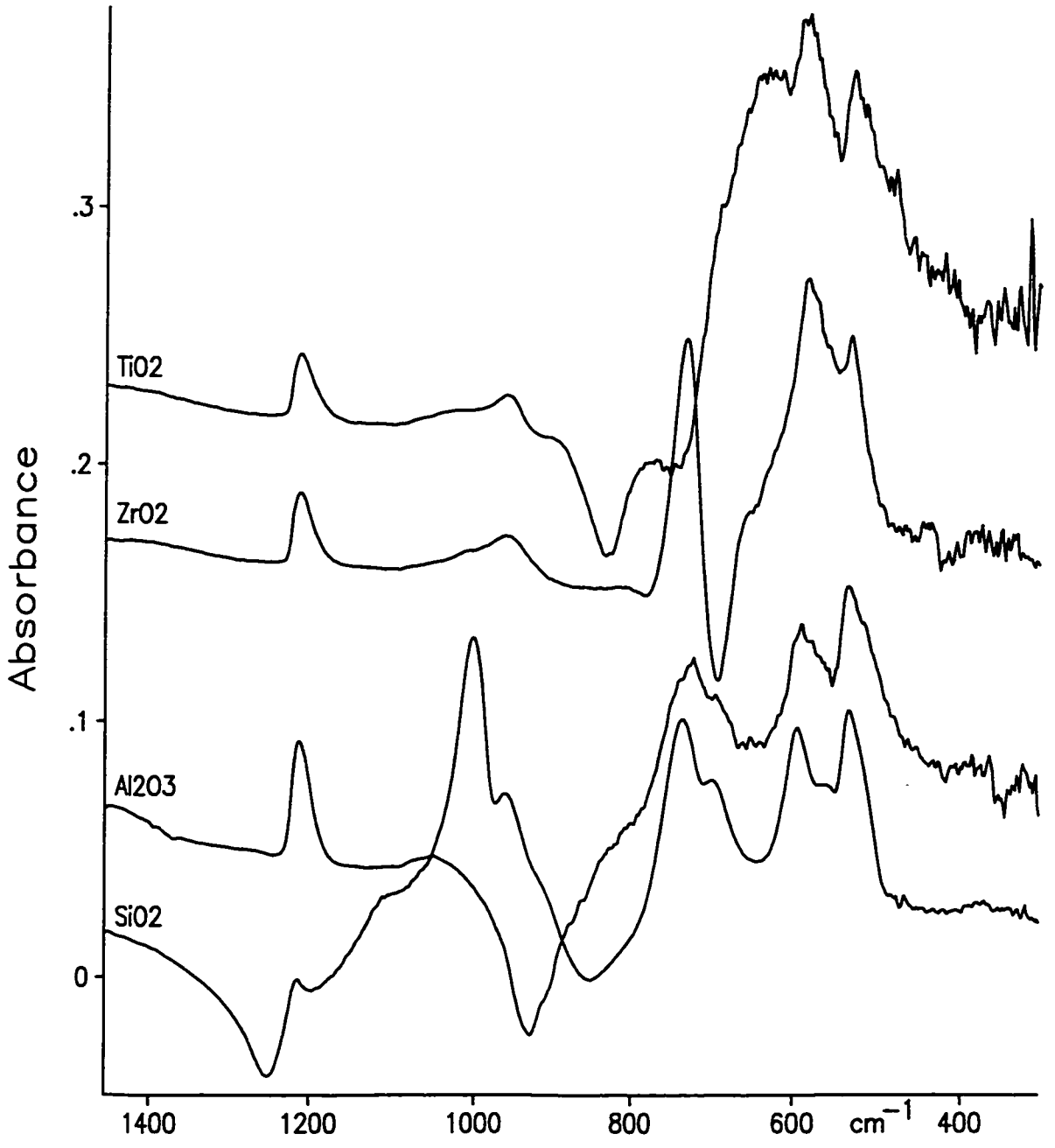

Figure 6.7B TMG chemisorbed on TiO_2, ZrO_2, Al_2O_3 and SiO_2 (which was previously shown in Figure 6.7A).

However, there is a very pronounced and expected negative peak at 940 cm^{-1} due to the disappearance of the AlOH deformation mode. This possibly masks a mode due to the antisymmetric Al-O-Ga stretching mode, expected to be in the 1000-900 cm^{-1} spectral region. There is a slight positive feature near 1000 cm^{-1} which might be attributable to this mode, but further speculation is not warranted. The symmetric deformation band at 1213 cm^{-1} is clearly seen and, unlike the situation for SiO_2, it is not partially masked by a negative surface mode.

The spectrum for TMG on ZrO_2 is shown in Figure 6.7B. Although there is clear evidence of the deformation mode at 1213 cm^{-1}, and of GaC stretching modes between 600 and 500 cm^{-1}, this spectrum is, otherwise, very different from those for TMG on SiO_2 or Al_2O_3. The broad band at 960 cm^{-1} is almost certainly attributable to the antisymmetric Zr-O-Ga stretching mode. The very strong peak at 735 cm^{-1} and the negative peak at 695 cm^{-1} are spectral artefacts, as will be discussed further in section 6.7.3. However, part of the contribution at 735 cm^{-1} might be due to an expected methyl rocking mode which was observed at this wavenumber for TMG adsorbed on SiO_2 and Al_2O_3. In the latter cases, the peak was not as intense and was not as sharp as on ZrO_2. This illustrates one of the continuing frustrations we have encountered in seeking low wavenumber spectral data in the unexplored domain of oxides other than silica.

Finally, TMG on TiO_2 is shown in Figure 6.7B. Although features at 1213 cm^{-1} are obviously attributable to the methyl deformation mode, and that at 960 cm^{-1} can be assigned to the antisymmetric TiOGa stretching mode, the lower wavenumber assignments are difficult because of the negative peak at 830 cm^{-1} which distorts spectral data in this region. However, the peaks at 590 and 530 cm^{-1} appear common to all spectra and can be attributed to the GaC stretching modes. It was very difficult to obtain reproducible low wavenumber spectra for TiO_2 with TMG and the other HS agents used, and for this reason, we will not discuss the results further for TiO_2 except in the general discussion where the problems will be dealt with.

6.5 *TITANIUM TETRACHLORIDE ($TiCl_4$) ADSORPTION*

Like trimethylgallium, $TiCl_4$ reacts very rapidly with the OH groups on silica [4,17], and thin film spectra have been published previously [4]. Of all of the probe molecules used, this is the only one which has shown evidence of a mono and bifunctional reaction with silica giving the products as depicted by reactions 6.1 and 6.2. Previously published spectra are shown in Figure 6.8. The lower wavenumber limit of the previous IR study was about 600 cm^{-1} due to the use of a NaCl support window, although that publication was also accompanied by Raman spectra which were recorded in the 1000 to 100 cm^{-1} spectral region. The initial assignments were based on the assumption that a doubly bonded surface species, $(SiO)_2TiCl_2$, (reaction 6.2) would only be formed on the 20°C activated silica which has SiOH groups which are close enough to hydrogen bond. The sharp IR band at 1030 cm^{-1} and broad band at 790 cm^{-1} for the 450°C activated sample were attributed to the antisymmetric and symmetric Si-O-Ti vibrations of $SiOTiCl_3$. Those at 920 and 725 cm^{-1} and the shoulder near 1000 cm^{-1} for the 150°C activated sample were attributed to vibrations of the cyclic $(SiO)_2TiCl_2$ unit. As will be discussed below, these assignments probably have to be reassessed. However, with the conversion of the FTIR to CsI optics, this investigation has been able to access the infrared spectral region associated with the $TiCl_x$ stretching modes which, for $TiCl_4$, are at 500 cm^{-1} (triply degenerate antisymmetric mode) and at 388 cm^{-1} (symmetric mode) [22]. The $TiCl_x$ stretching modes for $SiOTiCl_3$ or for $(SiO)_2TiCl_2$ would be expected to lie between 500 and 388 cm^{-1} [20].

New IR spectra of $TiCl_4$ adsorbed on SiO_2 which had been activated at 20°C or at 400°C are shown in Figure 6.9. These are spectra which were recorded immediately after introduction of about 5 Torr of $TiCl_4$ to the IR cell. The bands between 1050-900 cm^{-1} are similar to those recorded earlier, there are only weak features between 800-650 cm^{-1}, and there is a very strong band at 500 cm^{-1} due to the antisymmetric $TiCl_4$ stretching mode due to physically adsorbed and/or gaseous $TiCl_4$. There is an additional weak band near 405 cm^{-1}

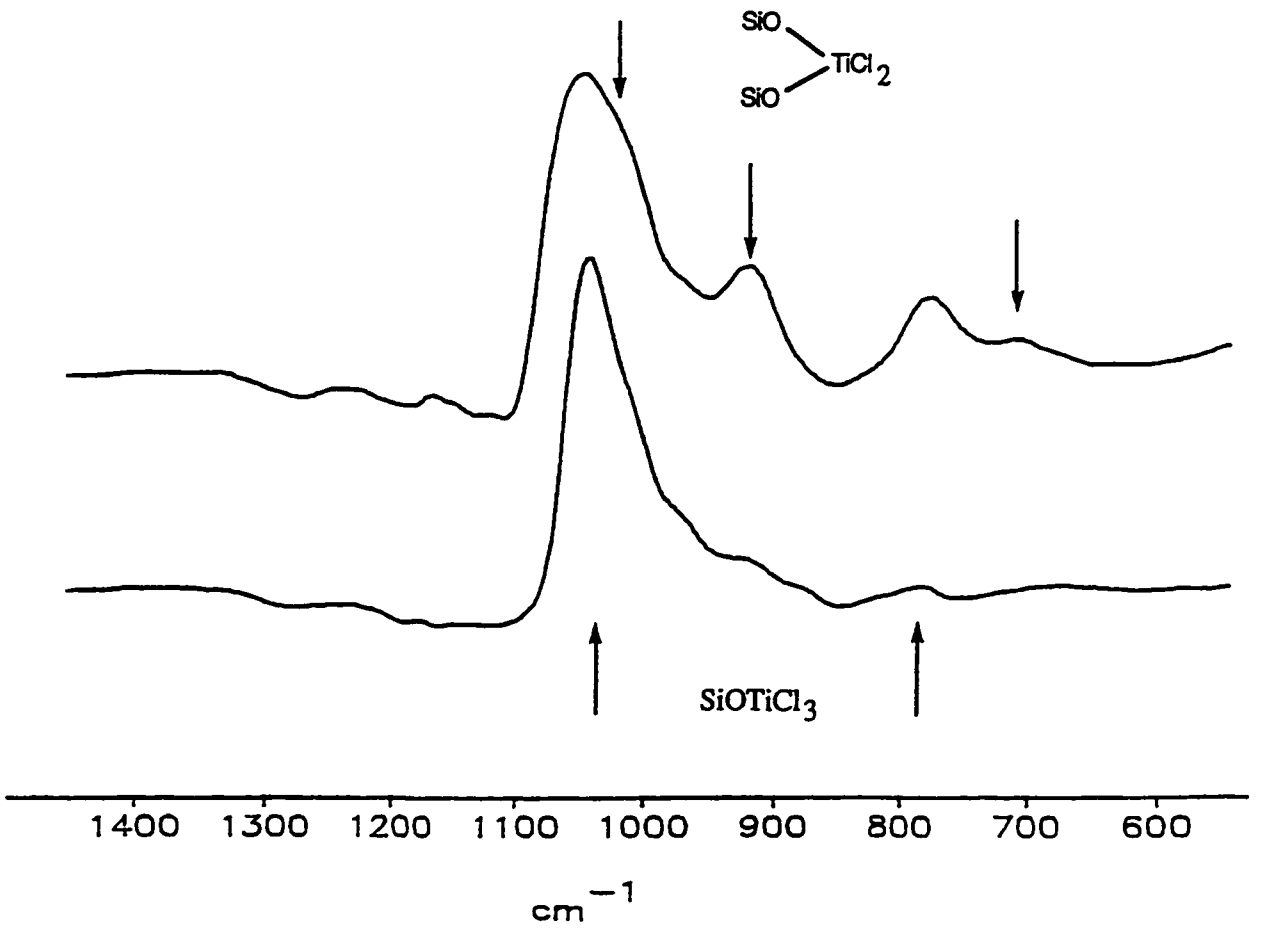

Figure 6.8 Aerosil silica activated at 150°C (top curve) and 450°C (bottom curve) after reaction with $TiCl_4$. The arrows for the top curve refer to the creation of new spectral features attributed to the $(SiO)_2TiCl_2$ species whereas those for the bottom curve refer to the formation of $SiOTiCl_3$ species.

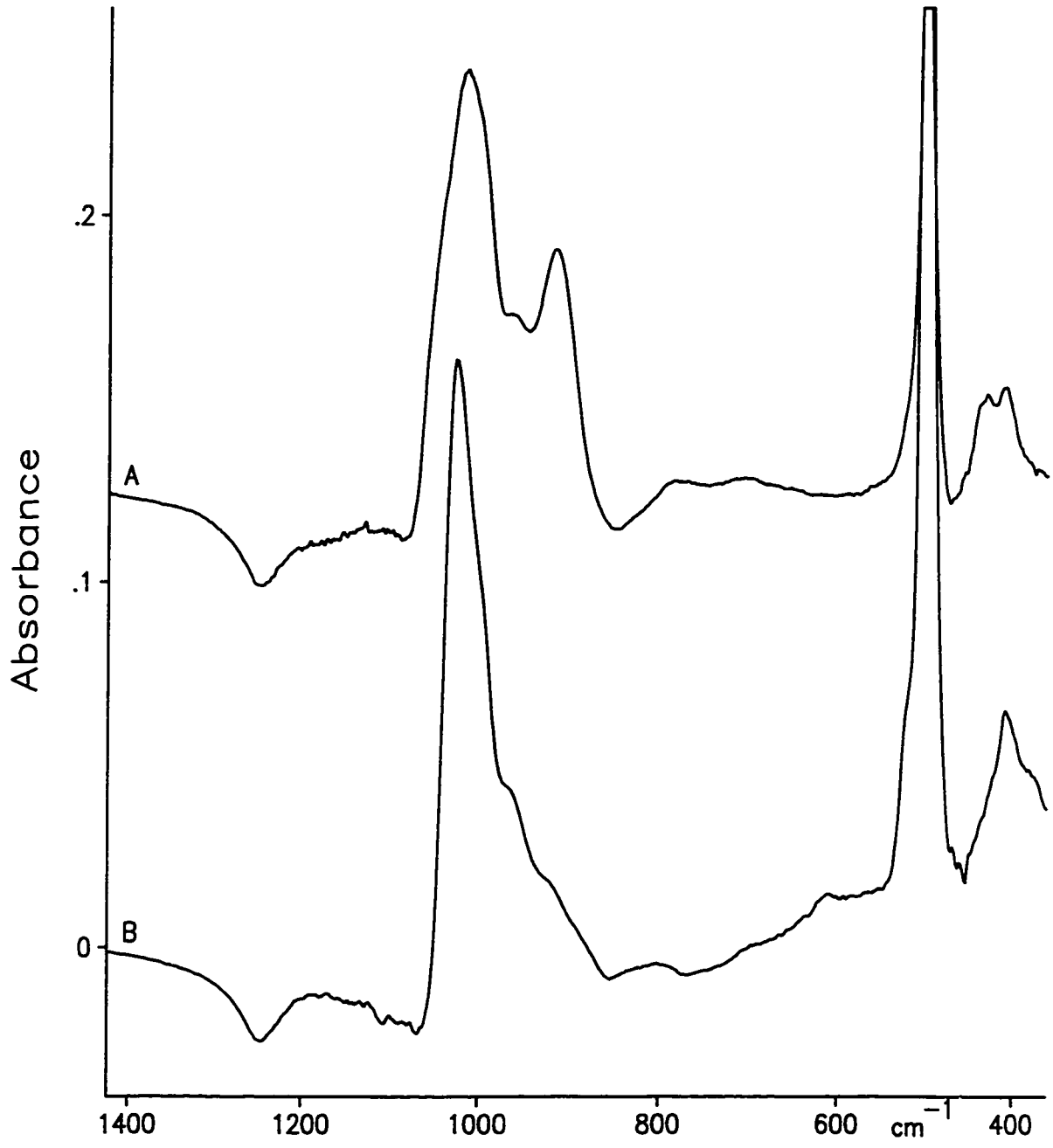

Figure 6.9 $TiCl_4$ adsorbed on SiO_2 activated at **A** 20°C and **B** 400°C.

which will be discussed further below (the symmetric stretching mode for tetrahedral $TiCl_4$ is forbidden in the infrared). The strongest band, at 1028 cm^{-1} for the 400°C activated sample is relatively sharp, whereas for the 20°C activated it has asymmetry and its peak maximum is at 1016 cm^{-1}.

The time evolution of the spectra are important. Figure 6.10 shows the spectral changes observed for the 400°C activated sample with increased time of contact with $TiCl_4$, or following evacuation of $TiCl_4$. The most striking and predictable effect is the rapid decrease in the intensity of the peak at 500 cm^{-1} due to removal of unreacted $TiCl_4$. More subtle, is the slow decrease over 15 h evacuation of the peaks at 1028, 960 (shoulder) and the growth of a weak peak near 785 cm^{-1}. The lower wavenumber region will be discussed later. Figure 6.11 shows the spectral changes for the 20°C activated sample. Here, the spectral changes are much more dramatic. Arrows indicate the direction of spectral change with time, but the most important feature is the dramatic increase in intensity in the 800-650 cm^{-1} spectral region. These changes appear to be correlated with a decrease in the intensity of the peak near 500 cm^{-1}, and the changes below 500 cm^{-1} are even more complex.

Figure 6.12 shows, on an expanded wavenumber scale, the spectral region from 550 to 350 cm^{-1} from Figure 6.11. Apart from a steady decrease in the intensity of the peak at near 500 cm^{-1}, there is a complex change in the region from 450 to 400 cm^{-1}. For the first spectrum observed immediately after the addition of $TiCl_4$ there is a weak peak at 410 cm^{-1} with a shoulder to high wavenumber (these and other positions of peak maxima are shown on the Figure). With increasing time, the maximum appears at 436 cm^{-1} and by the last spectrum after 15 h evacuation there is a slight appearance of a secondary shoulder at 457 cm^{-1}.

The behaviour is suggestive of a process whereby chlorine atoms are sequentially eliminated from a $SiOTiCl_3$ fragment, giving ...$TiCl_2$ and, finally ...TiCl. In general the antisymmetric stretching mode is not expected to change in wavenumber significantly during

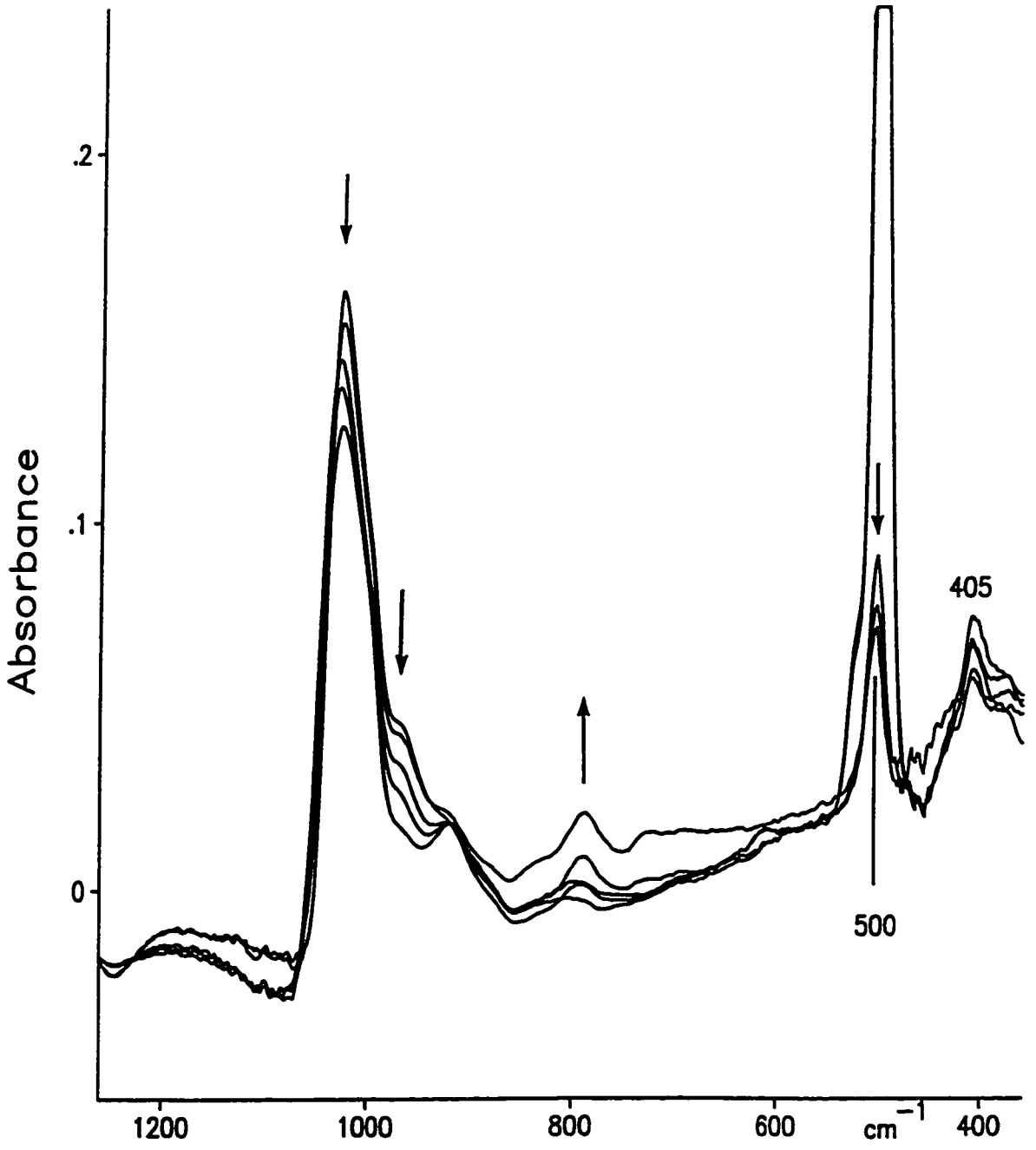

Figure 6.10 $TiCl_4$ adsorbed on 400°C activated SiO_2 for 5 and 30 min., and subsequently evacuated for 5 min., 30 min. and 15 h. The arrows indicate the direction of the spectral changes with increasing time.

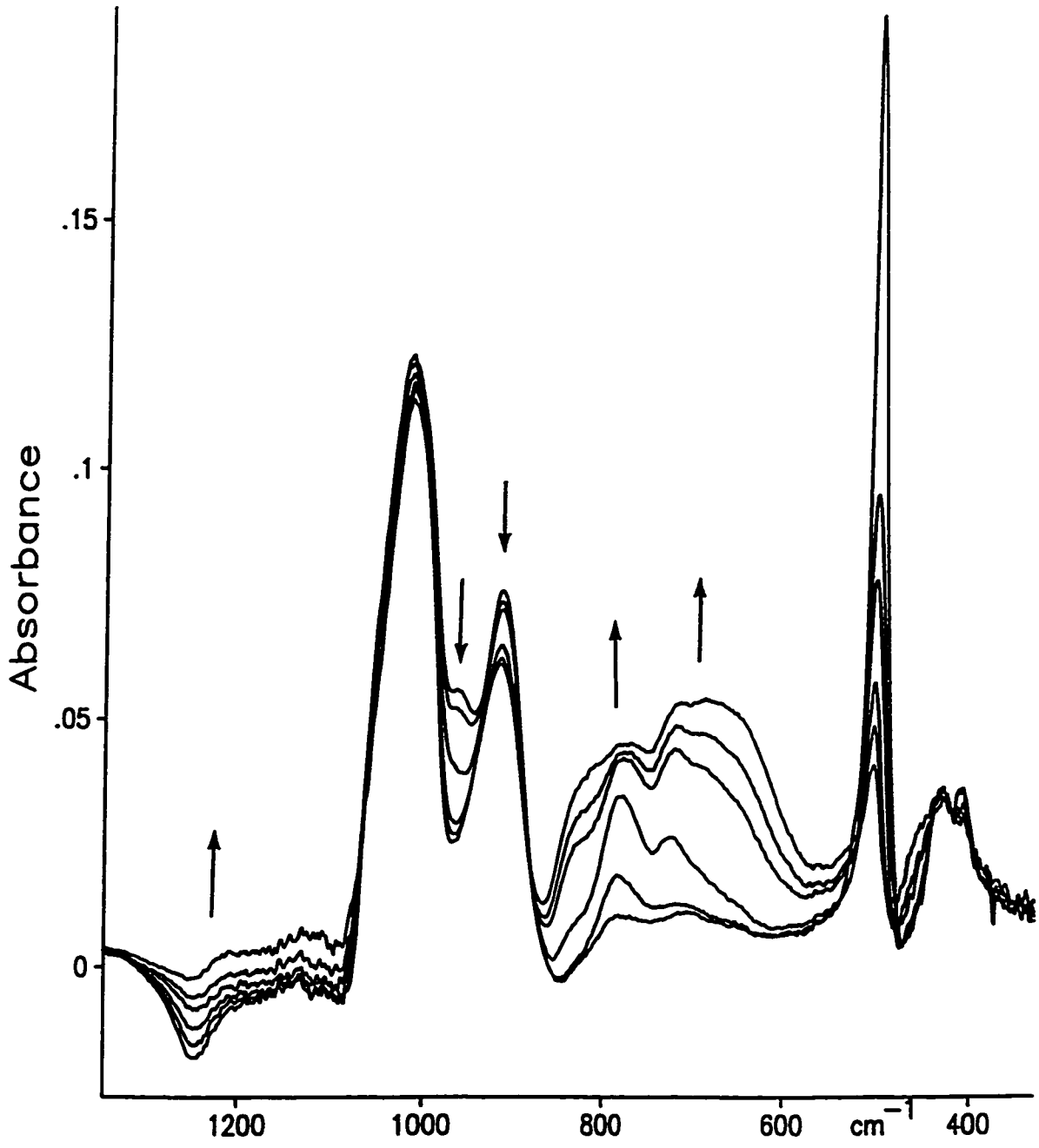

Figure 6.11 $TiCl_4$ adsorbed on 20°C activated SiO_2 and subsequently evacuated for 5 s, 15 min., 90 min., 6 h and 15 h. The arrows indicate the direction of the spectral changes with increasing time.

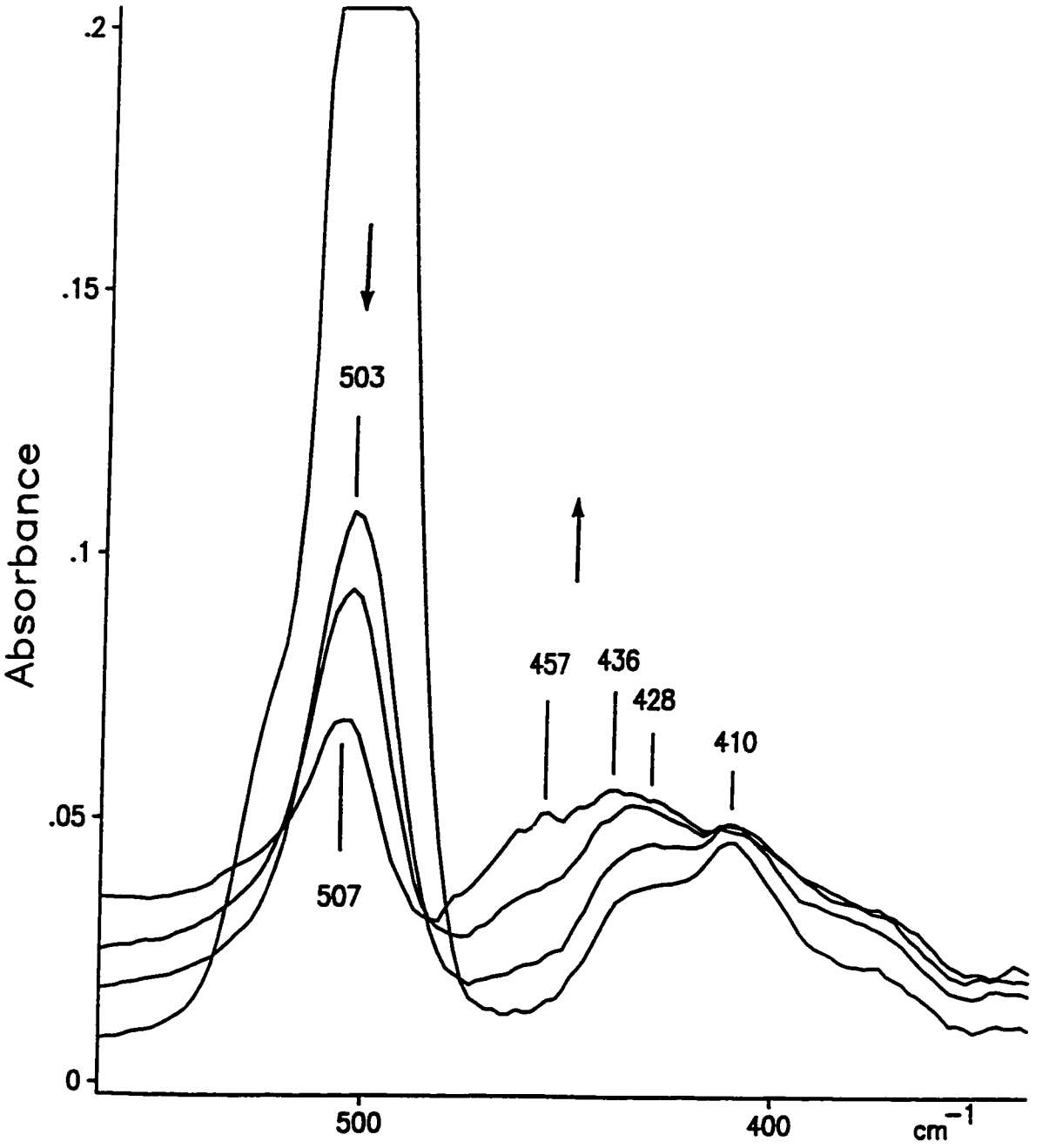

Figure 6.12 $TiCl_4$ adsorbed on 20°C activated SiO_2 and subsequently evacuated for 5 s, 15 min., 90 min., 6 h and 15 h (as in Figure 6.11, but on an expanded wavenumber scale). The arrows indicate the direction of the spectral changes with increasing time.

this process and the average $TiCl_x$ frequency remains approximately constant. For example, for $TiCl_4$, the average of the triply degenerate stretching mode at 500 cm^{-1} and the non-degenerate symmetric mode at 388 cm^{-1} is 472 cm^{-1}. This average does not change significantly as the number of halogen atoms is reduced (similar correlations exist for M-carbon and M-chlorine stretching modes, *e.g.* in GeMeCl and SiMeCl compounds [20]). This being accepted, we can calculate (see Appendix II) the expected position of the symmetric $TiCl_x$ stretching mode for other fragments, it being assumed that the antisymmetric mode is at 500 cm^{-1}. For ...$TiCl_3$ it is 416 cm^{-1}, for ...$TiCl_2$ it is 444 cm^{-1}, and for ...TiCl it is the average, 472 cm^{-1}.

Therefore, assuming that the adsorption of $TiCl_4$ initially gives $SiOTiCl_3$ we expect a band near 416 cm^{-1} (observed 410 cm^{-1}). A species $(SiO)_2TiCl_2$ would be expected to have its symmetric stretch at 444 cm^{-1} (there is a shoulder at 428 cm^{-1}). With time, the 428 cm^{-1} shoulder becomes a peak at 436 cm^{-1} which suggests conversion of the trichlorinated species to the dichlorinated species (little apparent decrease at 410 cm^{-1} is due to overlap by the much broader 436 cm^{-1} feature). Finally, a higher wavenumber shoulder grows at 457 cm^{-1}; the calculated wavenumber for the single chlorinated species is 472 cm^{-1}. Although we stress that the calculated wavenumbers are not to be considered more than a guide of the expected shifts during this process (replacement of Cl by O would have more complicated effects on the exact wavenumber of the remaining TiCl vibrations), it is clear that such a successive substitution is probably responsible for the observations.

There is an overall decrease in the intensities of the $TiCl_x$ modes with time and a considerable increase in the intensities of bands in the 800-650 cm^{-1} spectral region. The overall effect suggests that as the number of chlorine atoms bound to Ti decreases, additional SiOTi bonds are formed. Schematically, we might have:

$$SiOTiCl_3 \rightarrow (SiO)_2TiCl_2 \rightarrow (SiO)_3TiCl \rightarrow (SiO)_4Ti \qquad (6.5)$$

the latter species corresponding to insertion of titanium into the silica lattice. Before discussing this effect further, we will consider the chemisorption of $TiCl_4$ on the other oxides, and then we will consider the chemisorption of some other chlorine containing HS agents on silica in order to see whether this is a general feature of the chemisorption of these molecules on oxides or on specific oxides.

The spectra observed after reacting Al_2O_3, TiO_2 and ZrO_2 with $TiCl_4$ are shown in Figure 6.13. All spectra were recorded after 30 minutes evacuation at room temperature. Unlike $TiCl_4$ on silica, there was no change depending on the time of contact with the reactant or with increasing time of evacuation. Indeed, the spectra are very undistinguished, the bands are broad, and, most significantly, there are no IR bands near 500 cm^{-1} which would be expected for an antisymmetric $TiCl_x$ stretching mode. Finally, there were no significant spectral differences which depended on whether the temperature of activation was 20°C or 400°C.

There is a broad band centred at 750 cm^{-1} for Al_2O_3, it is near 820 cm^{-1} for ZrO_2 and near 875 cm^{-1} for TiO_2 (the very sharp feature at 739 cm^{-1} for ZrO_2 will be discussed later). In the case of ZrO_2 and TiO_2 these bands would also be observed using self supporting discs. These bands are likely due to MOTi stretching modes, as may some of the lower wavenumber features. The lack of distinct $TiCl_x$ stretching modes makes it difficult to speculate further. Either these are too low in intensity to be detected due to the lower surface area of these oxides as compared to SiO_2, or $TiCl_4$ rapidly and completely becomes dechlorinated and is incorporated into the oxide lattice giving a mixed oxide surface. In the latter case, one would expect direct chlorination of the surface to yield MCl species. There is no spectroscopic evidence for this but, as with silica, where the SiCl bands are so weak that they are barely detectable [23], even for self supporting discs, we would not expect these bands to be strong for other oxides and, for a thin film, their intensities would probably be below the limit of detection.

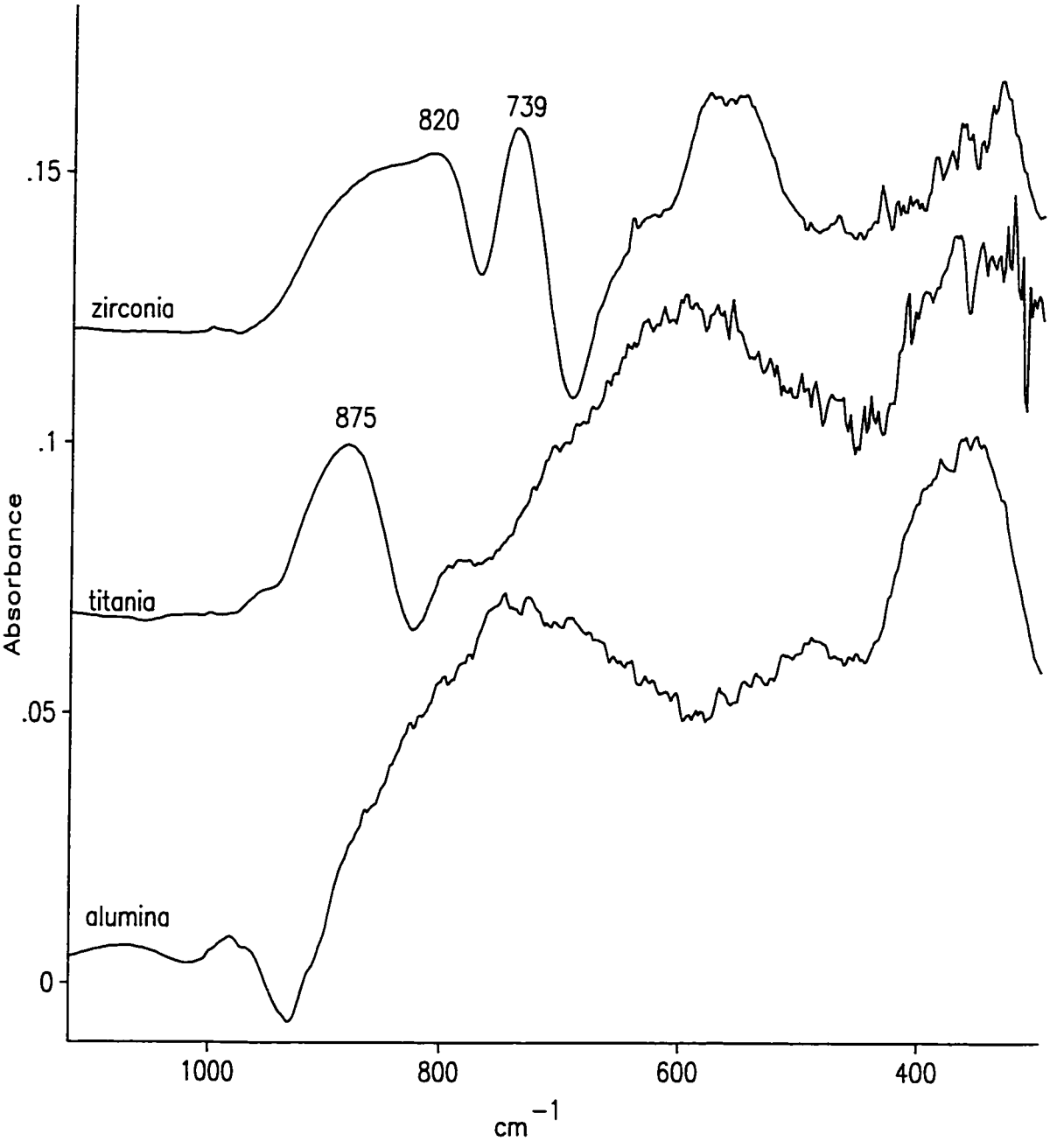

Figure 6.13 $TiCl_4$ chemisorbed on Al_2O_3, TiO_2 and ZrO_2.

6.6 *OTHER PROBES*

The unusual behaviour of $TiCl_4$ on SiO_2 has prompted an examination of the reactivity of some other chlorine containing probe molecules in order to determine if the reactivity of $TiCl_4$ is unique or whether it is a general characteristic of any Cl containing species. These molecules, the chemisorption of which on silica discs has previously been studied, are $VOCl_3$ [24,25], BCl_3 [8] and $GeCl_4$ [20].

6.6.1 *Vanadyl Trichloride ($VOCl_3$)*

Infrared spectra of $VOCl_3$ adsorbed on room temperature activated SiO_2 are shown in Figure 6.14. The most intense bands in the presence of $VOCl_3$ are the very sharp band at 1043 cm^{-1} and the broader band at 508 cm^{-1} which are due to the V=O and antisymmetric VCl_3 stretching modes respectively [22]. The other $VOCl_3$ mode in this spectral region is the very weak symmetric VCl_3 stretching mode at 410 cm^{-1} which is shown on an expanded wavenumber scale in Figure 6.15. The reaction of $VOCl_3$ with a single SiOH group is expected to yield a $SiOV(=O)Cl_2$ species which should also have a V=O stretching vibration near 1000 cm^{-1}, in addition to two low wavenumber VCl_2 stretching vibrations between 508 and 410 cm^{-1}. In addition, the SiOV stretching mode should probably lie near 1000 cm^{-1}. As was found for $TiCl_4$ on SiO_2, there is the progressive growth of new bands in the 800 to 700 cm^{-1} spectral region with increasing reaction time.

The sharp band which remains at 1043 cm^{-1} after evacuation of the reactant is the V=O stretching mode of $SiOV(=O)Cl_2$ and the 955 cm^{-1} band is the antisymmetric SiOV stretching mode [24,25]. The origin of the bands at 1005 and 912 cm^{-1} is somewhat obscure at present and is under investigation in the laboratory of Dr. S. Scott (University of Ottawa, Department of Chemistry). The IR band at 912 cm^{-1} was very weak when the reactant was adsorbed on 400°C activated silica (the other bands were about the same), and this behaviour was found with respect to the 920 cm^{-1} from the adsorption of $TiCl_4$ on room temperature versus 400°C

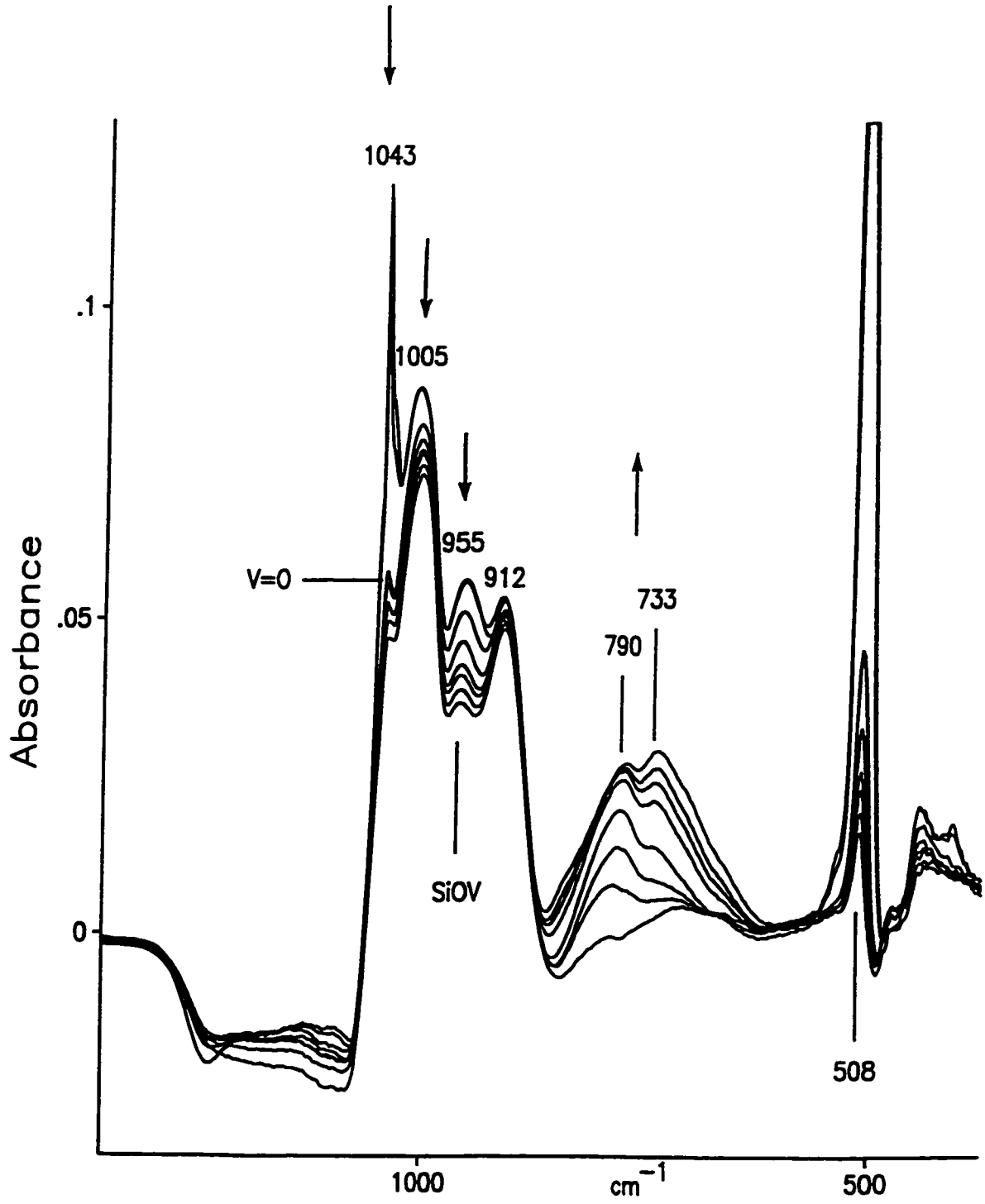

Figure 6.14 Vanadyl trichloride adsorbed on room temperature activated SiO_2. The arrows indicate the direction of the spectral changes with increasing reaction time; *i.e.* reaction cell was evacuated for 5 min., 30 min., 3h, 6h, 9h, 12h, and 15h.

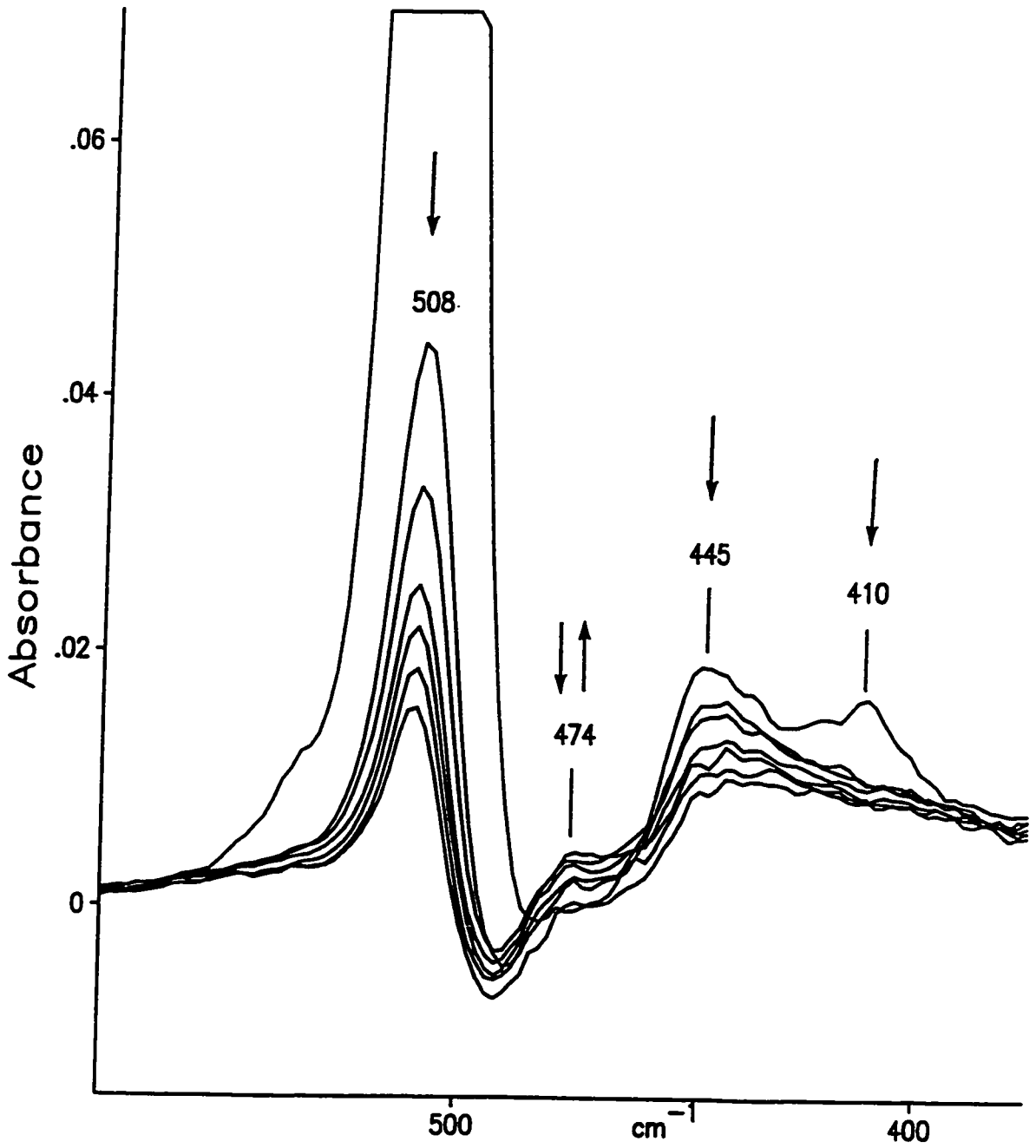

Figure 6.15 Vanadyl trichloride adsorbed on room temperature activated SiO_2 (as in Figure 6.14, but on an expanded wavenumber scale). The arrows indicate the direction of the spectral changes with increasing reaction time. The peak at 474 cm^{-1} grows initially and then decreases in intensity.

activated silica.

In the VCl_x stretching region, after evacuation of excess $VOCl_3$ the weak band at 410 cm^{-1} virtually disappears but there remains a sharp band at 508 cm^{-1}. There is also initially a band at 445 cm^{-1} whose intensity steadily decreases with time. Finally, there is a very weak feature at 474 cm^{-1}; this feature was not present initially and its intensity in fact reached a maximum half way through the series of spectra which are shown, and then it decreased in intensity (this feature cannot be clearly seen in the monochrome spectra shown in Figure 6.15). Using the same arguments which were used to justify the assignments for chemisorbed $TiCl_4$, assuming that the antisymmetric VCl_x stretching mode remains constant near 508 cm^{-1}, the symmetric mode for a $SiOV(=O)Cl_2$ would be expected to be at 445 cm^{-1} (there is a band at this wavenumber) and for $(SiO)_2V(=O)Cl$ it would be at 476 cm^{-1} (there is a band at 474 cm^{-1}). All of this suggests that there is a progressive change with time which results in the conversion of the initial product of the reaction, $SiOV(=O)Cl_2$, into the monochloro derivative (decrease in intensity of the 445 cm^{-1} band and increase in intensity of the 474 cm^{-1} band with time) and finally, the monochloro species loses its last Cl atom (eventual decrease in the intensity of the 474 cm^{-1} band). All of this is accompanied by complex changes in the 1000 to 900 cm^{-1} spectral region, and, most significantly in the 800 to 700 cm^{-1} spectral region, the latter being associated with vibrations of ring structures which contain SiOV linkages as in, for example, $(SiO)_2V(=O)Cl$. Regardless of the exact assignments in the 1000 to 700 cm^{-1} spectral region, it is apparent that $VOCl_3$ progressively loses its chlorine atoms to yield a mixed vanadium-silicon oxide surface. This behaviour is remarkably similar to that which was observed following the adsorption of $TiCl_4$ on SiO_2.

6.6.2 Boron Trichloride (BCl_3)

Boron trichloride is an extremely reactive molecule and its reaction with silica discs is not understood. The BCl_3 stretching mode in the gas phase is at 955 cm^{-1} for the ^{11}B isotope (80% natural abundance) and at 993 cm^{-1} for ^{10}B (20% natural abundance). A SiOB stretching

mode is expected in the 1500 to 1200 cm^{-1} spectral region [7,8]. Because of the isotopic distribution for boron, any absorption band due to the predominant isotope will have a weaker component to higher wavenumber due to the minor isotope. This usually gives rise to IR bands which are asymmetric to high wavenumber.

The IR spectrum of BCl_3 in contact with 400°C activated silica is shown in Figure 6.16. There is a broad band centred at 1360 cm^{-1} and a pair of bands at 955 and 993 cm^{-1} due to the BCl stretching mode of physically adsorbed or gaseous BCl_3 (both boron isotopes), and a weak peak at 723 cm^{-1}. A virtually identical spectrum was observed for room temperature activated silica. Evacuation greatly reduced the intensity of the IR bands due to the BCl_3 stretching modes and causes the appearance of a low wavenumber shoulder at 1280 cm^{-1}. The latter grows with time at the expense of the BCl_3 stretching mode. After 30 min. evacuation, the stretching modes have virtually disappeared and the 1280 cm^{-1} spectral feature dominates. Previous studies using self supporting discs [26] have shown that this reaction is extremely complex, there are more IR bands than can be detected when using a thin film, but that there is also a progressive disappearance of the BCl modes with time and that multiple bands appear in 1400-1250 cm^{-1} spectral region. The band at 1360 cm^{-1} must be due to the antisymmetric SiOB stretching mode and that at 1290 cm^{-1} is almost certainly due to an SiOB mode in a more complex structure. Boric oxide itself has strong BO stretching modes in the 1400 to 1200 cm^{-1} stretching region [7]. Therefore, BCl_3 appears to behave like the Ti and V derivatives in that complex dechlorination reactions occur leading to a mixed surface oxide.

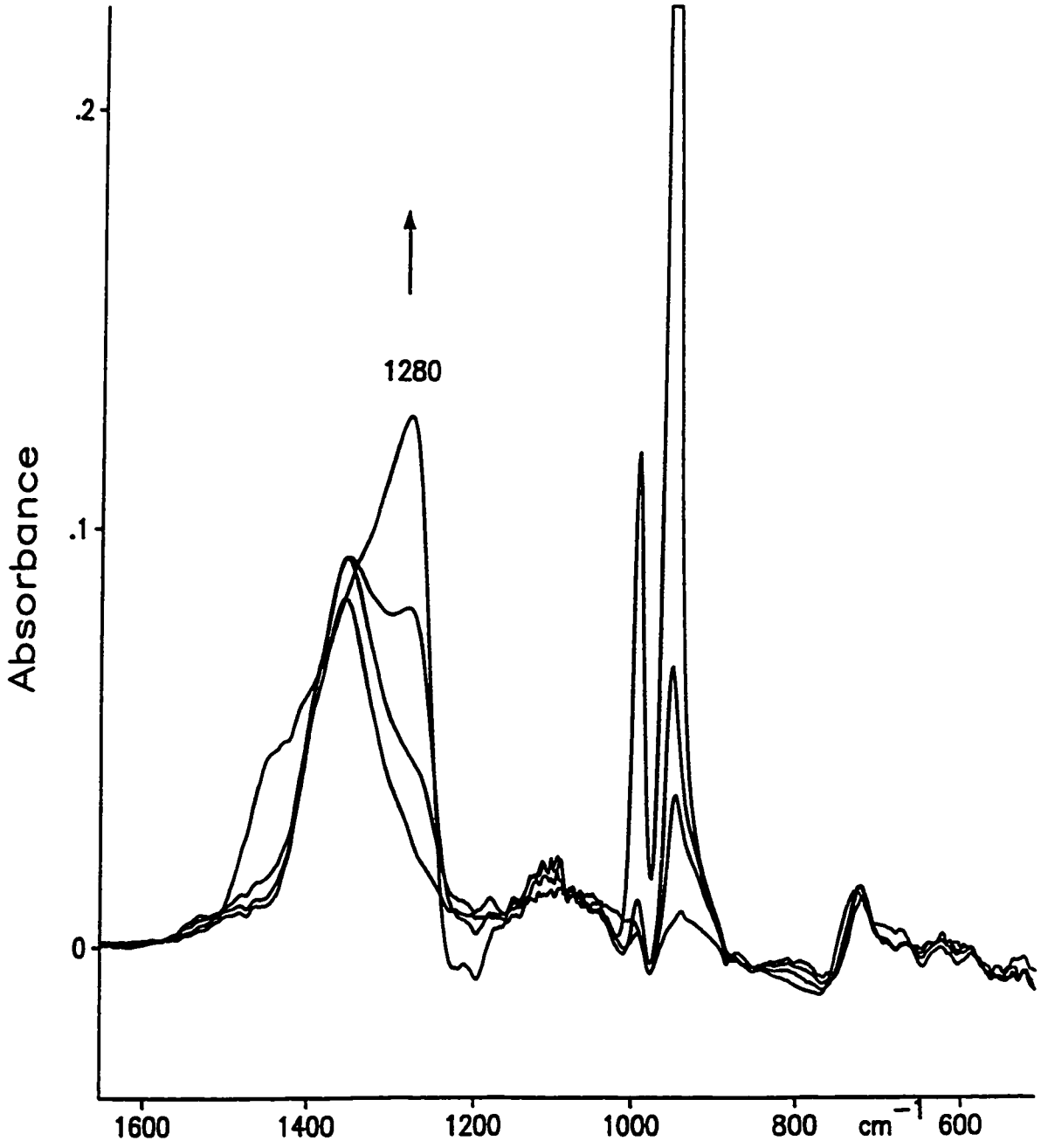

Figure 6.16 Boron trichloride adsorbed on 400°C activated SiO_2. The arrow indicates the direction of spectral changes with increasing time of evacuation: 10s, 5 min. and 30 min.

6.6.3 *Germanium tetrachloride ($GeCl_4$)*

$GeCl_4$ is relatively unreactive insofar as heating to about 300°C is required before it will react from the gas phase with SiO_2 discs [20]. The infrared spectrum of this molecule adsorbed on a TF of SiO_2 resembled that which has been previously observed for molecules which strongly physically adsorbed on the SiOH groups [15,27]. There was a perturbation of the SiOH modes [15] and the antisymmetric $GeCl_4$ stretching mode at 480 cm^{-1} was observed [22]. There were no spectral changes with time and the physically adsorbed material could not be pumped off at room temperature even after 15 hours of evacuation. Therefore, there was no dechlorination of $GeCl_4$ on silica.

6.7 *DISCUSSION*

This discussion will be divided into three parts. We will first discuss the results relative to the reactions of HMDS and $GaMe_3$ on the oxides, then we will discuss the results relative to the chlorine containing HS agents, and, finally, we will discuss the question of the general utility of the thin film method and the problem of spectral artefacts.

6.7.1 *Methyl Containing HS Agents*

The infrared spectra of the trimethylsilated oxides from the chemisorption of HMDS showed few surprises insofar as most of the low wavenumber IR bands associated with methyl rocking and deformation modes were detected. As in earlier studies [4,9,20] we were unable to detect the expected SiC_3 stretching modes which are expected in the 700 to 600 cm^{-1} region; these, however, are known to be very weak [20]. Tripp and Hair [1] were also unable to detect these modes in a TF spectrum of the adsorption of chlorotrimethylsilane on silica.

The spectrum of trimethylgallium on silica was similar to that which had been observed previously and there was again no evidence for a bifunctional reaction [4]. No additional features were observed in the 500-200 cm^{-1} spectral region, and none are expected for a $SiOGaMe_2$ species; the GaC_2 angle deformation modes are expected to lie below 200 cm^{-1} [20]. The GaC_2 stretching modes were readily detected at 600 and 540 cm^{-1} and there was an additional weak band at 560 cm^{-1} which was tentatively attributed to the symmetric SiOGa mode. The same IR bands (except for that at 560 cm^{-1}) in the low wavenumber spectra on the other oxides was less well resolved than those for SiO_2, but the same spectral features were generally detected.

To summarize, the chemisorption of HMDS and TMG on silica was well understood before this study began and these two systems were used to probe the feasibility of obtaining low wavenumber spectral data on other oxides. To this end, the experiment was a success.

6.7.2 Chlorine Containing HS Agents

In contrast to the results for the methyl containing HS agents, the results for the chlorine derivatives were quite unexpected and revealed hitherto unexpected features. In the spectral region associated with MCl stretching vibrations there was the clear and expected observation of the symmetric and antisymmetric MCl_x stretching vibrations of $SiOTiCl_3$ and of $SiOV(=O)Cl_2$. This is the first time these vibrations have been observed for these molecules using IR spectroscopy, and to our knowledge, the only other IR example of the observation of MCl_x vibrations is from the work of Tripp and Hair [1,2] which reported spectra from the chemisorption of dichlorodimethylsilane and trichloromethylsilane on silica.

The unexpected result was the progressive apparent dechlorination of $SiOTiCl_3$ and $SiOV(=O)Cl_2$ with increasing time after the initial chemisorption, accompanied by the growth of new IR bands in the 800 to 700 cm^{-1} spectral region which have been attributed to 'ring' modes of new multiply bonded Ti and V species (*e.g.*, $(SiO)_2TiCl_2$). In the experiments

described above, the samples were contacted with the reactant for a short time and then the samples were evacuated for a prolonged period. In order to determine whether the evacuation was essential for this process to occur, some supplementary experiments were carried out using $TiCl_4$.

The region between 1000 and 550 cm^{-1} is accessible using self supporting discs of silica if the quantity of silica is in the 2.5 to 3 mg/cm^2. Therefore, the growth of the IR bands between 800 and 650 cm^{-1} can be observed following the adsorption of $TiCl_4$ on such discs. Three experimental situations were followed: (1) following the adsorption of $TiCl_4$, spectra were recorded over several hours without evacuation of the excess $TiCl_4$; (2) the adsorption of $TiCl_4$, followed by evacuation of $TiCl_4$ so as to remove excess, then leaving the reaction cell under static vacuum for several hours; (3) the experiment was carried out under identical conditions to that used to produce Figure 6.11, that is, continuous dynamic evacuation after brief contact with $TiCl_4$. In all cases, the spectral changes were virtually identical and representative spectra are shown in Figure 6.17 for the static vacuum situation (2) above. There was a continuous growth of the IR bands in the 800 to 650 cm^{-1} spectral region due to SiOM modes which we attribute to multiply bonded surface species.

It appears that the results for $TiCl_4$ on silica are, therefore, not related to the presence or absence of $TiCl_4$ either physically adsorbed or in the gas phase. The dechlorination of $TiCl_4$ on silica and its eventual incorporation as a mixed metal surface oxide is probably thermodynamically driven. That is, the formation of a strong TiO bond in place of a weaker TiCl bond is an energetically favourable process. Further, if there is eventual diffusion of Ti into the bulk of the silica lattice there would be an increase in entropy. Similar entropy arguments were invoked in Chapter 3 in order to account for the diffusion of yttrium into the bulk of silica-alumina catalysts. As for the other oxides, the absence of spectral changes with increasing time after chemisorption coupled with the failure to detect $TiCl_x$ stretching modes might be an indication that the dechlorination is almost instantaneous. However, we acknowledge that the signal-to-noise ratio was poor in these cases, and that the surface area is

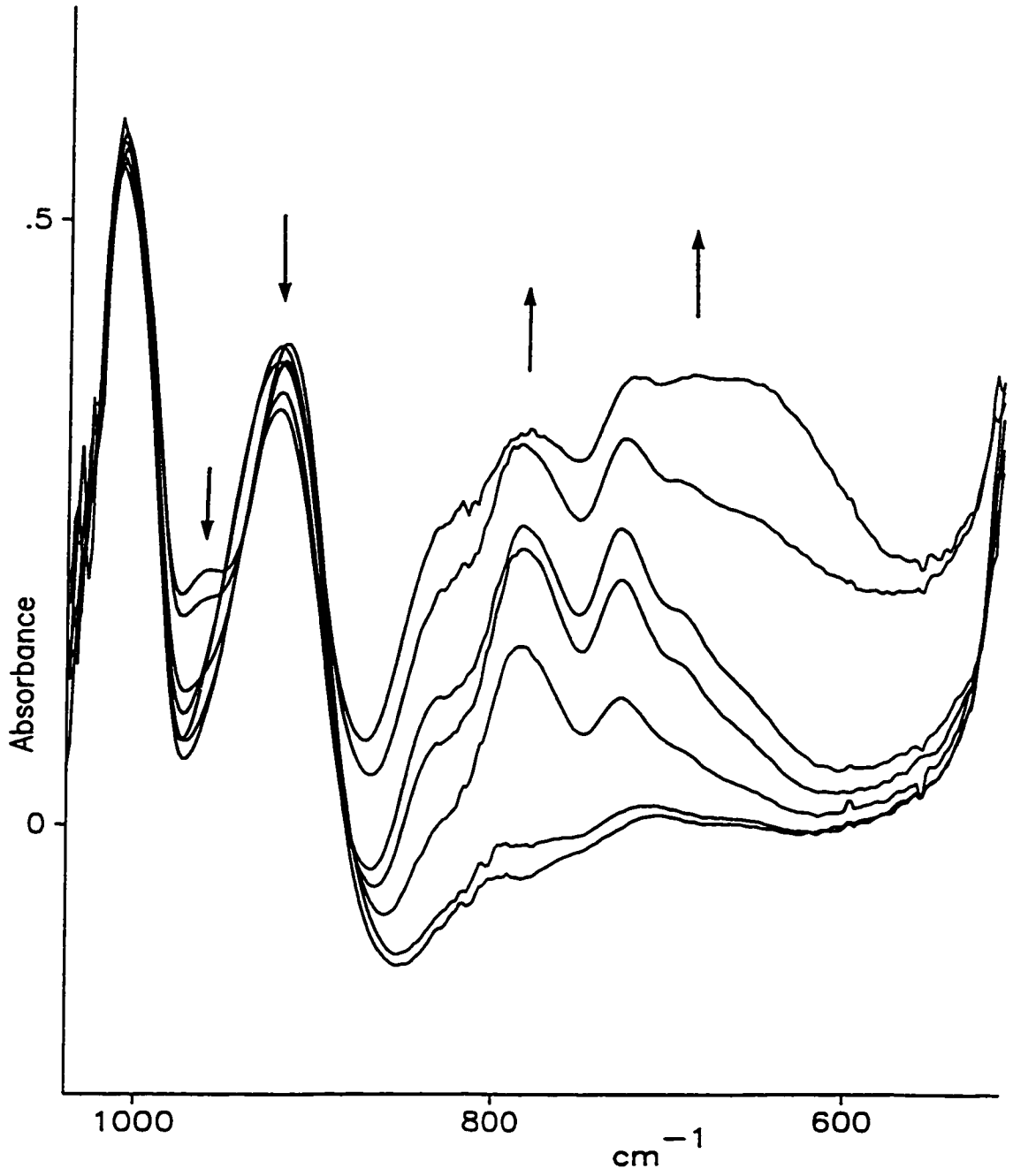

Figure 6.17 $TiCl_4$ chemisorbed on SiO_2 followed by evacuation at room temperature for 1 min. and 10 min. The reaction cell was then left under static vacuum for 2 h, 3 h, 6 h and 15 h. Arrows indicate the direction of spectral changes with increasing time.

lower than that of silica, hence our ability to detect a MCl_x stretching mode may have been hampered.

The important result of this study, as it applies to silica, is that previously assumed mechanisms of the reactions of various chlorine containing molecules with silica may have to be modified. It has been widely assumed [16,28-31] that $TiCl_4$ and BCl_3 only react with OH groups via the simple reactions depicted by scheme 6.1 to 6.3. This work has shown that the reactions might be that straight forward for the initially chemisorbed species, but that other surface species will have to be considered for longer times of contact with the reactant. This can have important consequences with respect to the preparations of mixed oxide catalysts from these materials for catalytic purposes.

6.7.3 Spectral Artefacts

Several times reference was made to 'spectral artefacts', that is, anomalous spectral features which did not appear to be related to the nature of the chemisorbed surface species. This does not refer to spectral features which appear as negative peaks as a result of the elimination of MOH modes during reaction, such as the 980 cm^{-1} band due to the Si-OH stretching mode. Rather, this refers to spectral changes which appear not to be related to elimination of surface OH groups.

We have noted that there is frequently a 'negative' peak near 1250 cm^{-1} when HS agents react with silica (Figures 6.5, 6.7A, 6.9, 6.10, 6.11 and 6.14). This band is in a region where the background spectrum is rapidly changing and is to the high wavenumber side of the strongest band due to SiOSi modes which has its maximum at 1100 cm^{-1}, see Figure 6.1. Although the appearance of this band is a common feature, it is not linked to surface SiOH modes. We have suggested, without proof, that this is probably due to an alteration in the network or assembly of SiOSi bands which constitute the broad and dominant spectral feature of silica in the 1300 to 1000 cm^{-1} spectral region. That is, the formation of a new SiOMX

species possibly alters some of the 'bulk like' SiOSi modes such that a weak negative feature appears at 1250 cm^{-1}. A similar problem occurred with TiO_2 in that a 'negative' band sometimes was observed near 830 cm^{-1} after chemisorption (Figures 6.6 and 6.13). This band was only clearly evident in one case in this thesis (Figure 6.6), but it was apparent in other unpublished spectra, for example, for BCl_3 adsorbed on TiO_2. As with silica, 830 cm^{-1} is just to high wavenumber of the spectral region where the background absorption of titania starts to rise rapidly (Figure 6.2).

A similar but more serious problem arose in the case of zirconia. A common feature of most spectra of chemisorbed species on ZrO_2 was a sharp band near 735 cm^{-1} which was often accompanied by a slight negative feature near 690 cm^{-1}. Figure 6.18 shows spectra for $TiCl_4$, $GaMe_3$ and BCl_3 adsorbed on a thin film of ZrO_2 (the spectra for the $TiCl_4$ and $GaMe_3$ are plotted on an expanded wavenumber scale from Figures 6.13 and 6.7B respectively). Chemisorbed BCl_3 is not expected to have a vibration in the 735 cm^{-1} spectral region and Figure 6.19a shows the background spectrum before reaction, 6.19b is the spectrum after reaction and evacuation of excess BCl_3 and 6.19c is the difference spectrum plotted on an expanded absorbance scale relative to the curves a and b. Although three examples of this phenomenon are illustrated in Figure 6.18, the spurious peak at 735 cm^{-1} and the negative one at 690 cm^{-1} arose in many instances not discussed in this thesis where, like BCl_3, a mode is not expected at this wavenumber. It almost certainly arises because of a change in the scattering characteristics of the substrate because of a change in the index of refraction once a chemisorbed layer is formed. As seen in Figure 6.19, this results in an apparent shift of the original background peak at 760 cm^{-1} to lower wavenumber which creates the artefact at 735 cm^{-1} and is accompanied by the negative 'dips' in the spectrum to high and low wavenumber of 735 cm^{-1}. Such spectral artefacts may limit the useful information which may be obtained in this spectral region in future studies of adsorption on zirconia.

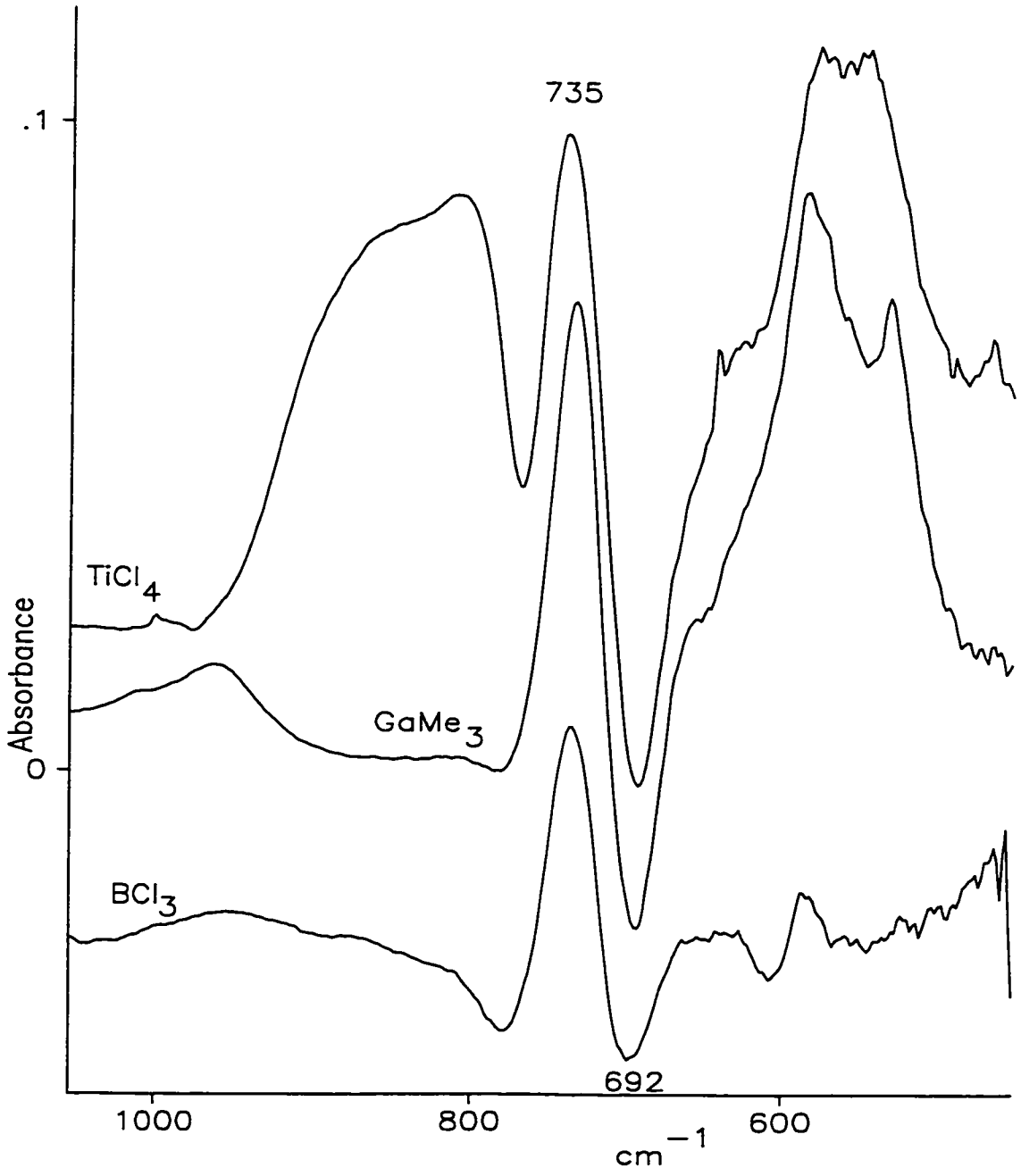

Figure 6.18 Spectra of $TiCl_4$, $GaMe_3$ and BCl_3 adsorbed on ZrO_2.

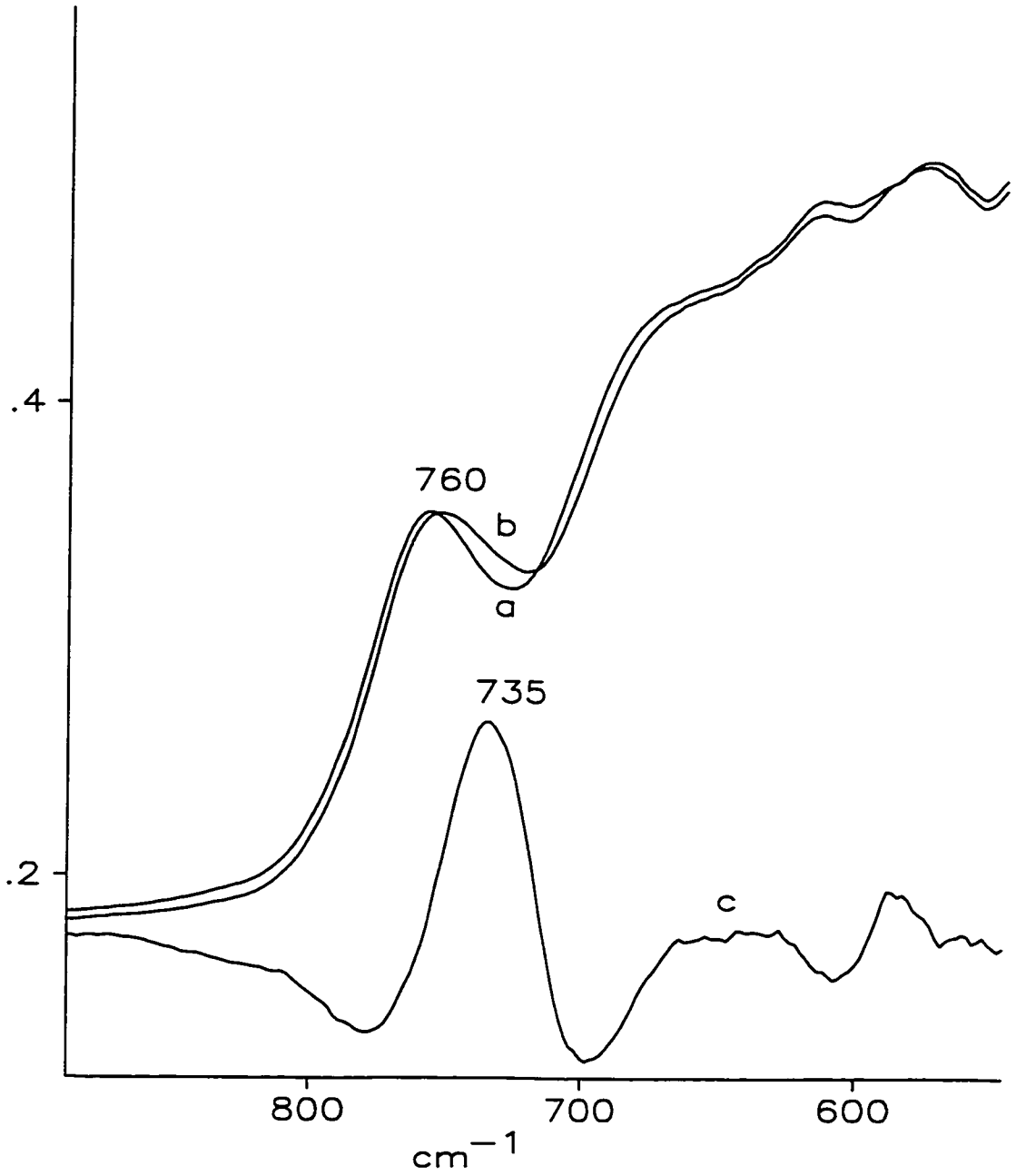

Figure 6.19 BCl_3 adsorbed on ZrO_2. **a** background spectrum before reaction, **b** spectrum after reaction and evacuation of excess BCl_3 and **c** difference spectrum plotted on expanded scale relative to **a** and **b**.

REFERENCES

1. Morrow B.A., Tripp C.P. and McFarlane R.A.
   J. Chem. Soc. Chem. Commun., 1282 (1984)

2. Tripp C.P and Hair M.L.
   Langmuir, 7, 923 (1991)

3. Tripp C.P and Hair M.L.
   Langmuir, 8, 1961 (1992)

4. Morrow B.A. and McFarlan A.J.
   *J. Non-Cryst. Solids, **120,** 61 (1990)*

5. Morrow B.A. and Lang S.J.
   *J. Phys. Chem., **98,** 13319 (1994)*

6. Morrow B.A. and McFarlane R.A.
   *J. Phys. Chem., **90,** 3192 (1986)*

7. Morrow B.A. and Devi A.
   *J. Chem. Soc. Faraday Trans. 1, **68,** 403 (1972)*

8. Morrow B.A. and Devi A.
   Chem. Comm., 1237 (1971)

9. McFarlan A.J.
   Ph. D. Thesis, University of Ottawa, 1991

10. Wang Y. and Morrow B.A.
    *Langmuir, **12,** 4153 (1996)*

11. Morrow B.A., Lang S.J. and Gay I.D.
Langmuir, ***10,*** *756 (1994)*

12. Lang S.J., Gay I.D. and Morrow B.A.
Langmuir, ***11,*** *2534 (1995)*

13. Gay I.D., McFarlan A.J. and Morrow B.A.
J. Phys. Chem., ***95,*** *1360 (1991)*

14. Morrow B.A. and McFarlane R.A.
Langmuir, ***2,*** *315 (1986)*

15. Morrow B.A. and McFarlan A.J.
J. Phys. Chem., ***96,*** *1395 (1992)*

16. Morrow B.A.
Stud. in Surf. Sci. Catal., ***57A,*** *A161 (1990)*

17. Morrow B.A. and McFarlan A.J.
Langmuir, ***7,*** *1695 (1991)*

18. Sheng T.C., Lang S., Morrow B.A. and Gay I.D.
J. Catal., ***148,*** *341 (1994)*

19. Dang Z., Anderson B.G., Amenomiya Y. and Morrow B.A.
J. Phys. Chem., ***99,*** *14437 (1995)*

20. Morrow B.A. and Hardin A.H.
J. Phys. Chem., ***83,*** *3135 (1979)*

21. Kvisle S. and Rytter E.
Spectrochim. Acta, ***40A,*** *939 (1984)*

22. Nakamoto K.
"Infrared spectra of Inorganic and Coordination Compounds", 2nd Edition, Wiley-Interscience, New York, 1970

23. Lang S.J. and Morrow B.A.
J. Phys. Chem., 98, 13314 (1994)

24. Rice G.L. and Scott S.L.
Langmuir, 13, 1545 (1997)

25. Rice G.L. and Scott S.L.
J. Molec. Catal. A: Chem., 125, 73 (1997)

26. Devi A.
M. Sc. Thesis, University of Ottawa, 1971

27. Denning D.
B. Sc. Thesis, University of Ottawa, 1996

28. Haukka S., Lakomaa E. -L. and Root A.
J. Phys. Chem., 97, 5085 (1993)

29. Haukka S., Lakomaa E. -L. and Suntola T.
Thin Solid Films, 225, 280 (1993)

30. Kytokivi A., Lakomaa E.-L. and Root A.
Langmuir, 12, 4395 (1996)

31. Kytokivi A., Lakomaa E.-L., Root A., Osterholm H., Jacobs J.-P. and Brongersma H.H.
Langmuir, 13, 2717 (1997)

GENERAL CONCLUSIONS

This thesis consisted of two major areas of research: (1) the modification of the acidity of oxide and mixed oxide catalysts and (2) the acquisition of low wavenumber vibrational data from thin films of oxides.

The first major area of research was concerned with the infared (IR) characterization of yttria-silica-alumina catalysts (Y_2O_3-SiO_2-Al_2O_3, YSA) and, to a lesser extent, fluorided alumina catalysts (F-Al_2O_3, FA) using the basic probe molecules: pyridine (Py), ammonia (NH_3) and deuterated acetonitrile (CD_3CN). In the YSA catalysts the addition of well dispersed weakly basic yttria (4-16 wt. percent) lowered the overall acidity of SiO_2-Al_2O_3 (SA) to levels shown by FA catalysts. In the case of FA catalysts, fluoride, 1 wt. percent, was added to increase the acidity of alumina.

The adsorption of Py on YSA clearly indicated that the number of Brønsted acid sites, confirmed by the characteristic peak at 1547 cm^{-1}, decreased with increased Y_2O_3 loading. Furthermore, protonated Py was very strongly adsorbed and evacuation at room temperature (RT) or 100°C did not significantly reduce the numbers of PyH^+ species. The number of Brønsted sites was greater on catalysts which had been activated at 150°C than at 450°C.

Py also displayed the unique ability to quantitatively determine the ratio of Y^{3+} and Al^{3+} sites available for coordination. As expected the Y^{3+}:Al^{3+} ratio increased with Y_2O_3 loading. However, the overall intensity of the Y^{3+}/Al^{3+} (1446 cm^{-1}/1456 cm^{-1}) doublet for coordinated Py did not change significantly upon Y_2O_3 loading which indicated that the overall number of Lewis sites remained more or less constant on YSA catalysts.

In the case of the adsorption of NH_3 on YSA catalysts the intensity of the IR band due to coordinated NH_3 was lower for pure SA than for YSA for either activation temperature, *i.e.*

150 or 450°C. Ignoring any differences in the extinction coefficient of NH_3 coordinated to either Y^{3+} or Al^{3+} this would suggest that there were fewer coordination sites available on SA than on any of the YSA catalysts.

The number of Brønsted acid sites for protonated NH_3 (indicated by the presence of a peak at about 1450 cm^{-1}) was greater for 150°C activation than for 450°C activation (as was the case for protonated Py). In both cases this was attributed to the greater hydroxyl content on YSA catalysts at lower activation temperatures capable of protonating the probe molecules. The only data relative to the strength of the Brønsted sites for the same probe came from the ammonia TPD experiments. These suggested that there was a small decrease in acid strength as the yttria content increased.

Temperature programmed desorption (TPD) results of coordinated NH_3 showed that there was an insignificant difference in the temperature at which NH_3 desorbed from any catalysts. This was also true for adsorbed CD_3CN, but these experiments did show differences in the ratio of the peak heights of CD_3CN coordinated to either Al^{3+} (2330 cm^{-1}) or Y^{3+} (2294 cm^{-1}) Lewis sites. The peak for CD_3CN coordinated to Y^{3+} sites appeared to decrease to a greater extent than that for coordinated to Al^{3+} sites at increasing temperatures. Hence Al^{3+} Lewis acid sites were more thermally stable than Y^{3+} Lewis acid sites.

The objective of the YSA work was to determine whether the addition of the weakly basic oxide yttria would lower the acidity of silica-alumina catalysts to that of fluorided alumina. To this end, this thesis has shown that both the numbers and the strength of the Brønsted acid sites decreased as the yttria content increased. With respect to the Lewis acid sites, there was not a significant difference in the total number of these sites with increasing yttria content, although electron deficient aluminum sites were replaced by yttrium sites as the yttria content increased.

Alumina has insignificant Brønsted acidity (it does have Lewis acidity) but the addition of a halide, particularly fluoride, is know to induce the creation of Brønsted acid sites. The objective of the work described in Chapter 4 was to determine whether the initial calcining temperature (400 to 550°C) of a 1.0 weight percent fluorided alumina catalyst containing 0.3 weight percent platinum had any influence on the acidity. These catalysts were reduced in hydrogen prior to adsorbing a probe molecule (NH_3 and CD_3CN) and we confirmed that this had the effect of increasing the number of Bronsted acid sites by virtue of creating a larger number of AlOH groups and decreasing the number of Lewis acid sites.

The catalysts had been calcined at 400, 450, 500 and 550°C for one hour prior to reduction in hydorgen. This thesis showed that there was not a striking difference between any of the cataysts regarding the number and strength of the acid sites, with the possible exception of that which was calcined at 400°C, which had a slightly greater number of both Lewis and Brønsted acid sites.

The second major area of research dealt with the acquistion of low wavenmuber vibrational data from thin films (TF) of the oxides SiO_2, Al_2O_3, TiO_2 and ZrO_2. When the TF technique was first developed it was for studying adsorbed species on silica in regions where it was normally opaque to IR radiation (1300 to 500 cm^{-1}). The work in this thesis had two objectives. First, to explore the possibility for the first time of studying thin films of oxides other than silica. Second, the KBr optics in the FTIR spectrometer were replaced by CsI so that the spectral range was extended down to 200 cm^{-1}, and this gave access for the first time (for silica and the other oxides) to the low wavenumber spectral region associated with the $TiCl_x$ and $VOCl_x$ stretching modes from the chemisorption of $TiCl_4$ or $VOCl_3$ on SiO_2 (and on the other oxides).

The characterization of the pure oxides was carried out with the following hydrogen sequestering (HS) agents: hexamethyldisilazane (HMDS), trimethylgallium (TMG), and $TiCl_4$. The use of HMDS is well understood (a trimethyl silating agent) and we were able to observe

most of the low wavenumber IR bands associated with methyl rocking and deformation modes. As in earlier studies we were unable to detect SiC_3 stretching modes, which are known to be very weak in the 700-600 cm^{-1} region.

In the case of TMG, the low wavenumber spectra on the other oxides were less well resolved than for the spectra of TMG on SiO_2, but the same spectral features were generally detected. No additional features were observed in the 500-200 cm^{-1} region and none were expected for $SiOGaMe_2$. There was no evidence of a bifunctional reaction to give $(SiO)_2GaMe$.

For the chlorine containing HS agents we were able to observe the progressive dechlorinaiton of $SiOTiCl_3$ and $SiOV(=O)Cl_2$ surface moeities with increasing time of contact after initial chemisorption on SiO_2. These conclusions were based on the observation of the progressive elimination of various MCl_x stretching modes which were accompanied by the growth of new IR bands in the 800-700 cm^{-1} spectral region which were attributed to 'ring' modes of new multiply bonded Ti and V species.

The adsorption of $TiCl_4$ on Al_2O_3, TiO_2 and ZrO_2 did not show any $TiCl_x$ stretching modes, even after initial chemisorption, nor was there any change in the TiO modes depending on the time of contact with the reactant or with increasing evacuation. We have concluded that rapid declorination occurs. Rapid dechlorination of BCl_3 also occurred on these oxides. However, $GeCl_4$ was unreactive on these oxides, as it is on silica (reaction at 400°C is necessary before $GeCl_4$ will graft on to silica) and no dechlorination resulted.

This work has confirmed the utility of the TF method for studying adsorption on oxides other than silica, and the ability to extend the spectral range to 200 cm^{-1} has provided new and revealing information regarding the dechlorination of reactive chlorine containing HS agents. This process had not been anticipated at the start of this work, its origin is probably thermodynamic, and it may have important implications regarding the nature of grafted

halogen containing species on oxides, and of the structure of the catalysts which are prepared by chemical vapor deposition methods from these precursors.

Appendix I

List of Hexene Isomers.

Name	Exxon peak assignment
C_1 - C_5 hydrocarbons	C1 - C5
1-hexene	1H
4-methyl-1-pentene	4M1P
3-methyl-1-pentene	3M1P
2,3-dimethyl-1-butene	23DM1B
cis 4-methyl-2-pentene	*cis* 4M2P
trans 4-methyl-2-pentene	*trans* 4M2P
3-methyl-pentene	3MP
2-methyl-1-pentene	2M1P
2-ethyl-1-butene	2E1B
cis and trans 3-hexene	*cis and trans* 3H
trans 2-hexene	*trans* 2H
2-methyl-2-pentene	2M2P
cis 3-methyl-2-pentene	*cis* 3M2P
cis 2-hexene	*cis* 2H
trans 3-methyl-2-pentene	*trans* 3M2P
2,3 dimethyl-butene	23DMB
C_7 & higher hydrocarbons	C7+

Appendix II

$TiCl_x$ Stretching Mode Calculations.

$TiCl_4$ $\quad \frac{1}{4}\nu_{as} + \frac{1}{4}\nu_s = 472\ cm^{-1}$

$\frac{1}{4}[3(500\ cm^{-1})] + \frac{1}{4}(388\ cm^{-1}) = 472\ cm^{-1}$

$TiCl_3$ $\quad \frac{1}{3}[2(500\ cm^{-1})] + \frac{1}{3}\nu_s = 472\ cm^{-1}$

$TiCl_2$ $\quad \frac{1}{2}[1(500\ cm^{-1})] + \frac{1}{2}\nu_s = 472\ cm^{-1}$

IMAGE EVALUATION TEST TARGET (QA-3)

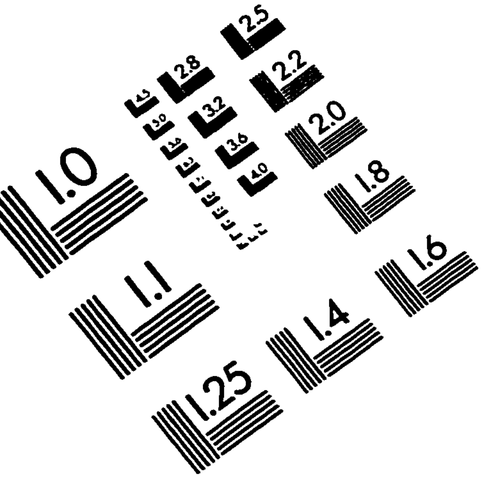
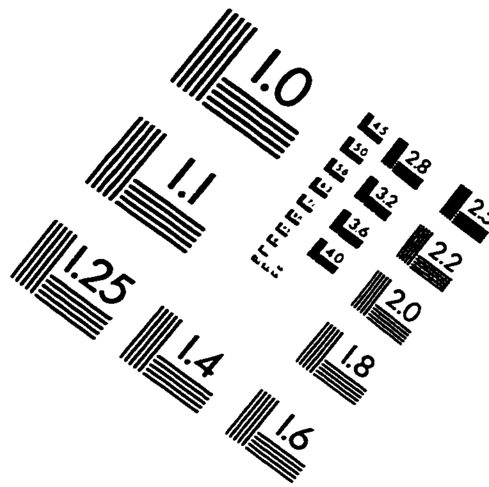
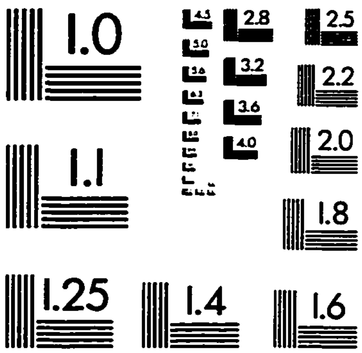

150mm

6″

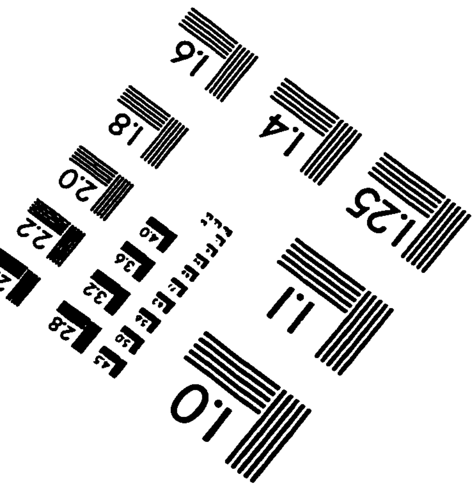
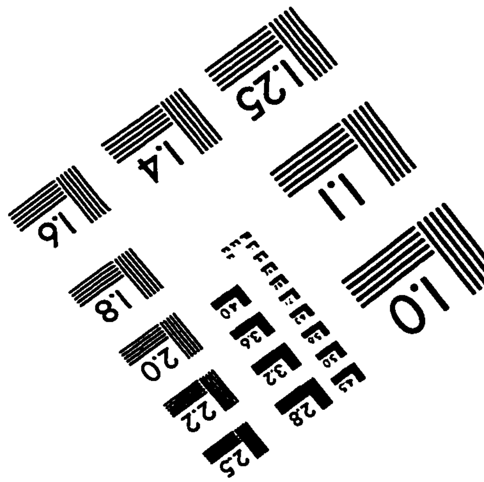

APPLIED IMAGE, Inc
1653 East Main Street
Rochester, NY 14609 USA
Phone: 716/482-0300
Fax: 716/288-5989